2009-01-01

Earth Field Magnetic Resonance Imaging And Paramagnetic Contrast Agents

Saideh Sadat Mortazavi
University of Texas at El Paso, ssmortazavi@miners.utep.edu

EARTH FIELD MAGNETIC RESONANCE IMAGING
AND PARAMAGNETIC CONTRAST AGENTS

SAIDEH SADAT MORTAZAVI

Department of Chemistry

APPROVED

_____
James M. Salvador, Ph.D., Chair

_____
Jorge Gardea-Torresdey, Ph.D.

_____
Katja Michael, Ph.D.

_____
Miguel Castro-Colin, Ph.D.

_____
Patricia D. Witherspoon, Ph.D.
Dean of the Graduate School

DEDICATION

I dedicate this work to THE ONE and THE ONLY ONE whom we are all from him, and we all return to him.

I also dedicate this work to my dear MOTHER.

EARTH FIELD MAGNETIC RESONANCE IMAGING AND PARAMAGNETIC CONTRAST AGENTS

by

SAIDEH SADAT MORTAZAVI

THESIS

Presented to the Faculty of the Graduate School of

The University of Texas at El Paso

in partial fulfillment

of the requirements

for the degree of

MASTER OF SCIENCE

Department of Chemistry

THE UNIVERSITY OF TEXAS AT EL PASO

December 2009

ACKNOWLEDGEMENTS

First and for the most, I would like to express my sincerest gratitude to my dear mentor, Dr. James M. Salvador, whom throughout his precious life has either educated himself or others. He is very knowledgeable yet humble and is always available for his students. Not only did he guide me through this research project, but I also managed to appreciate and further learn from his vast knowledge. His support, patience, fairness, honesty, trustworthiness, intelligence, and logical behavior are outstanding and always will remain with us. He is the best advisor I could have ever had.

I would like to thank Dr. Jorge Gardea-Torresdey and his research group, Dr. Jose Peralta who was a great help on this project, Dr. Martha Lopez-Moreno, Dr. Guadalupe De La Rosa, and graduate student Jose Angel Hernandez for their help, advice, and kindness.

I appreciate the effort of my committee members, Dr. James M. Salvador, Dr. Jorge Gardea-Torresdey, Dr. Katja Michael, and Dr. Miguel Castro-Colin to improve my thesis.

Also, I appreciate the great assistance of Dr. Evan Mccarney and the Magritek Corporation for answering my questions about the EFMRI instrument.

I appreciate Dr. Bonnie Gunn for all the assistance she provided.

I am thankful of my peers, Christina Alvarado, David Chavez, and Arturo Montes, for creating a friendly environment in our lab as well as their help.

Next, I acknowledge the financial support of The University of Texas at El Paso and the department chair Dr. Gardea-Torresdey.

I thank Grace Awad and Lucema Armenta for their assistance.

Finally, I would like to thank my family (Jalal, Hosna, and Amir Mohammad Rastegray) for cooperating with me during this time.

ABSTRACT

The goal of this research was to visualize the uptake of copper by plants to aid phyto-remediation research. The hypothesis was that regions of the plant with more copper will have an enhanced NMR signal using copper as a paramagnetic contrast agent.

As the name implies, Earth Field Magnetic Resonance Imaging (EFMRI) spectrometry uses a magnetic field 300,000 times weaker than a 600 MHz Nuclear Magnetic Resonance (NMR) spectrometer. Just like in conventional human MRI, this portable instrument is capable of recording one, two and three dimensional images though the sample size is much smaller.

The enhancement of signal was first demonstrated recording the 2D images of different concentrations of aqueous copper sulfate solutions.

The last research focused on growing soybean and mesquite plants in hydroponic media containing 0.25 mM copper nitrate for four weeks and recording their EFMRI images alongside plants grown without copper nitrate.

Results showed EFMRI to have the advantage of probing the plant absorption of copper without having to dissect the specimen and therefore will take less sample preparation and time than current analysis techniques. This technique could be beneficial to aid phyto-remediation technology by using plants that are capable of absorbing copper as a heavy metal pollutant and imaging the plants to assure copper accumulation in them.

TABLE OF CONTENTS

LIST OF TABLES

LIST OF EQUATIONS

LIST OF FIGURES

CHAPTER I (INTRODUCTION)

1.1 Basic Concepts of MRI and its Advantages

Magnetic Resonance Imaging (MRI) is one of the tomographic imaging techniques that has the capability to produce an internal image of an object from externally measured Nuclear Magnetic Resonance (NMR) signals. MRI imaging works in the radio frequency range of the electromagnetic radiations which is an advantage compared to Computed Tomography (CT) scan or X-ray that use ionizing radiation. Consequently MRI does not have much harmful effect, yet is rich in information. Also, acquiring an image depends on three factors as follow: nuclear spin density, T_1 (a spin lattice relaxation time constant), and T_2 (a spin-spin relaxation time constant). These parameters could be suppressed or enhanced to cause a different looking image (Zhi-Pei and L. 2000).

In an imaging process, magnetic moments are converted to bulk magnetization by the use of a static magnetic field called B_o. The magnitude of this magnetization is proportional to the strength of the magnetic field. Then by using a radio frequency (RF) excitation the bulk magnetization is switched to transverse magnetization which by returning to equilibrium, and based on Faraday's law of induction, a signal is produced (Zhi-Pei and L. 2000). The frequency of precession for every nucleus is different because its gyro-magnetic ratio (proportionality constant, γ) for every nucleus is different. When the system reaches equilibrium, the X-Y magnetization, also called transverse magnetization, has decayed as time has gone by due to some field in-homogeneity which causes some of the nuclei to precess faster than others. This means the magnetization has grown in the Z direction as thermal equilibrium is established (Fukushima and Roeder 1981). In NMR, slow relaxation is beneficial because it means transverse magnetization survives and could be observed, and as a result free induction decay

(FID) is persistent to obtain a high resolution spectrum which means a narrow line-width is achieved (Keeler 2005). Moreover, the core of MRI deals with the use of gradients to encode spatial information upon RF excitations, and finally image construction is obtained (Zhi-Pei and L. 2000). The magnetic field gradient is a non-uniform magnetic field because it is weaker than the static magnetic field. In the imaging phase the NMR signal is important, and phase instability is caused by temporal fluctuations of the Earth's magnetic field while field uniformity allows the use of large samples (Mohoric, et al. 2004).

There are many advantages to MRI applications in comparison to other methods:

a) Beside the vast utilization of MRI in the medical field, there are nonmedical applications of NMR imaging relevant to material science such as plant imaging.
b) Chemical composition of a sample can be imaged by analyzing signal intensities.
c) Unlike other methods that are destructive or sometimes inaccurate, NMR imaging is nondestructive yet more accurate.
d) MRI deals with non-ionizing radiation which is an advantage of employing this method.
e) MRI facilitates determining the distribution of chemical components of plants as well as localizing them spatially such as localization of water, fat, and carbohydrates.

Further elaborations on the latter include experimental techniques, in vivo examination of plant morphology and development, and noninvasive plant histo-chemistry (Blumich 2000).

1.2 Terranova Earth Field Nuclear Magnetic Resonance (EFNMR) and Earth Field Magnetic Resonance Imaging (EFMRI)

As the name implies, Earth Field Magnetic Resonance Imaging (EFMRI) spectrometry uses the Earth Magnetic field which is around 50 μT. The Earth magnetic field varies in direction as well as magnitude according to our location on Earth. For example, on the second floor of the Physical Science Building at UTEP, the effective Earth magnetic field is 43 μT

where as on the third floor it is 53 μT. Also, the Earth magnetic field is 300,000 times weaker than a 600 MHz NMR spectrometer. For example, in the case of the hydrogen nuclei in a sample of water and in the absence of an external magnetic field (meaning in the presence of the Earth magnetic field) the spins are spread in all directions. Therefore the total magnetic field of the sample is zero. However, in the case of EFNMR/EFMRI and in the presence of a polarizing field (375 times larger than the Earth magnetic field, 18.8 mT) the spins start Larmor precession around the field, meaning that each proton spins almost 2000 cycles per second (Hz). And for comparison, in the presence of a14 T static magnetic field the spins start Larmor precession around the field at 600 MHz (Levitt 2008).

For the Terranova EFNMR/MRI purchased from Magritek Company in New Zealand, the low detection field is the Earth's magnetic field while the spins are polarized at a high magnetic field relative to detection, which is the act of acquiring signal. The higher polarization field is 18.8 mT while the low detection field is 50 μT. For a 600 MHz NMR, the polarization and detection are both at a magnetic field strength of 14 T.

The Terranova EFNMR/MRI consists of a probe made of three concentric tubes each wound with a coil and a spectrometer. The coils are called the B_1 coil (used for exciting and detecting of the precessing magnetization), Gradient coils (used for providing a linear magnetic field across the sample), and the Polarization coil (used for providing polarized spins via applying a large current to establish a polarized nuclear magnetization in a sample) also called B_p (Figure 1.1). The spectrometer (Figure 1.2) consists of a digital signal processor (DSP), which is controlled by a personal computer (PC), which runs the data processing software called Prospa.

In an experiment, Prospa sends a pulse to the spectrometer's DSP via a USB port. Prospa also controls NMR experiments by sending pulses to the B_p, Gradient, and B_1 coils to

acquire data (Magritek, Terranova-MRI User Manual 2005). Although EFNMR is more practical in outdoor locations where in-homogeneity is not present since ferrous objects are absent and low frequency noise sources are minimized, a Gradient coil in three dimensions is implemented to provide shimming in order to combat the effect of noise as well as in-homogeneities in indoor locations (Coy, et al. 2006).

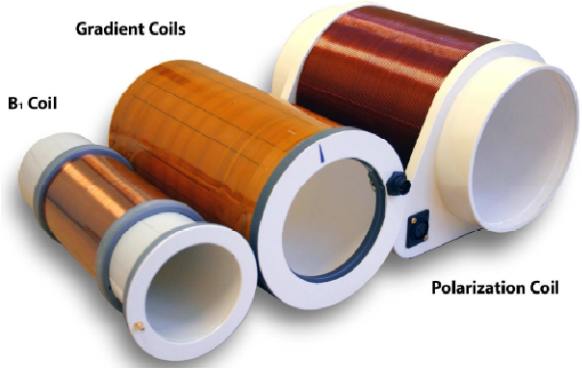

Figure 1.1 EFNMR/MRI coils

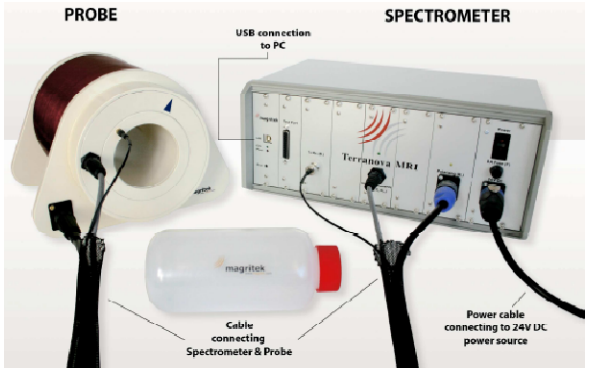

Figure 1.2 EFNMR/MRI apparatus: Spectrometer and Probe

The B_p coil is used to produce a polarizing field by applying a 6 ampere current for four seconds duration to provide a bulk polarized nuclear magnetization across the sample. The Gradient coil is made of two coils: one for pulsed gradient and the other for X, Y, and Z gradients for imaging and shimming. Its task is to produce linear magnetic field gradients across the sample. The B_1 coil is used to excite and detect the NMR signal. A short pulse of electromagnetic energy, called the RF or 90° pulse at the resonant or Larmor frequency of the nuclei in the local Earth's field (2 kHz-2.5 kHz), is applied to the coil which surrounds the sample in order to tip the bulk magnetization from the Z direction, which is the Earth's field direction, to the X-Y or transverse plane. The transverse magnetization will be detected by the B_1 coil as an induced electromotive force because the magnetization precesses about the Earth's magnetic field ($\boldsymbol{B\epsilon}$) at the Larmor frequency ($\boldsymbol{\omega}$) according to Equation 1.1 (Larmor Equation).

Equation 1.1 (Larmor Equation): $\boldsymbol{\omega = \gamma \cdot B\epsilon}$

A 500 ml plastic bottle is used for any liquid sample and is placed in the center of the cylindrical hole inside the probe. A large sample size should be used to compensate for the low detection field since smaller samples produce weaker signals (Magritek, Terranova-MRI User Manual 2005). Any solid sample should resemble the size and shape of the plastic bottle as much as possible in order to acquire a strong NMR signal. Liquid samples with low viscosity (such as water) generate a high amplitude spectrum whereas samples with high viscosity (such as honey) generate a low amplitude spectrum (Fukushima and Roeder 1981). In clinical MRI, although macromolecules contain protons, their spins cannot be seen by MRI because of their short relaxation times, so only the spins of water molecules are detectable (living tissues contain 60-80% water) (Vlaardingerbroek and A. 2003).

EFNMR/MRI can be used to detect the NMR signal strength of many different samples using a pulse and collect macro as well as producing 1, 2, and 3 dimensional images by using Spin echo or Gradient echo imaging. Appendix A describes the details of how to work with EFNMR/MRI and how to acquire images in 1D, 2D, and 3D, which was the first step in conducting the research described in this thesis.

1.3 Spin Lattice Relaxation (T_1) and Spin-spin Relaxation (T_2)

At equilibrium a longitudinal magnetization is established, and no magnetization in the transverse plain exits. The longitudinal magnetization depends on the number of spins, the size of the static field, and gyro-magnetic ratio. Each spin is a vector quantity, meaning that it has a magnitude and a direction. The magnitude is determined by γ of any nucleus, so each magnetic moment has an X, Y, and Z component. The bulk magnetization is built up by adding the Z components of the magnetic moment of all nuclei. In the case when an RF pulse is applied to the

equilibrium magnetization, the longitudinal magnetization rotates to the X-Y plane causing a decrease in the Z component of the magnetization. The transverse magnetization precesses about the Z axis, and this precession is what we detect in the form of an FID signal. The process in which the longitudinal magnetization is reached to its equilibrium value is called longitudinal relaxation or spin lattice relaxation. The reason it is called lattice is because this relaxation involves the flow of energy from the spins to the surroundings (Keeler 2005). Spin lattice relaxation converts the excess energy to translational, rotational, and vibrational energy in the surrounding atoms (lattice). The spin lattice relaxation time, T_1, is the timed required for this excess energy to drop to 37% of its original value. In other words, T_1 is the time required for the longitudinal magnetization to recover 63% of its longitudinal equilibrium value (DatabaseMRI, T_1 2003-2009). Moreover, in order for the longitudinal magnetization to recover to 99% of its equilibrium value, it takes 5 T_1 where as recovery to 95% takes 3 T_1. The closer the spins are to the equilibrium, the slower the rate of change of longitudinal magnetization (Keeler 2005).

The process in which transverse magnetization decays to an equilibrium value of zero is called spin-spin relaxation or transverse relaxation. "In the dipolar mechanism, the source of the local field is the magnetic moment of other nuclear spins in the sample" (Keeler 2005). T_2 is the time required for the transverse magnetization to decay to 63% of its original value (DatabaseMRI, T_2 2003-2009).

T_2 is not related to energy exchange with the surrounding where as T_1 is related to accepting energy from the spins so that the spins relax and thermal equilibrium is reached. T_1 could be weak in the absence of molecular motion or paramagnetic agents or rigid solids, but it could be strong in different solutions. In addition, $T_1 > T_2$ in most solids while $T_1 = T_2$ in liquids. When molecular motions are fast as it is in non-viscous liquid, $T_1 = T_2$ (Fukushima and

Roeder 1981). The more mobile the molecules, the less intermolecular contact are present between them. Therefore, T_1 and T_2 become longer. T_1 at lower temperature is less than T_1 at higher temperatures. For example, T_1 at 280 K is less than T_1 at 340 K.

Also, unpaired electrons could generate local fields in the same way as described above, and are a source of relaxation because the magnetic moment of electrons is greater than protons. Therefore, the local field created by electron is much higher compared to protons (Keeler 2005).

In summary: 1) T_1 is the time required for the excess energy to drop to 1/e (0.37) of its original value. 2) Starting from zero magnetization in the Z direction, the Z magnetization will grow after excitation from zero to a value of about 63% of its final value in a time of T_1.
3) T_2 characterizes the rate at which the X-Y component of the magnetization vector decays in the transverse magnetic plane. It is the time it takes for the transverse signal to reach 37% (1/e) of its initial value after flipping into the magnetic transverse plane. 4) The transverse magnetization value drops from maximum to a value of 37% of its original value in a time of T_2.

1.4 Magnetism and Paramagnetic Relaxation Time Contrast Agents

Magnetism comes from: a) circulation of electric currents, b) magnetic moments of electrons, c) magnetic moments of atomic nuclei, the first two being much greater than the third one (Levitt 2008).

Materials could be classified into two main categories:

a) Diamagnetic materials with a non-permanent magnetic dipole moment
b) Paramagnetic, ferromagnetic, anti-ferromagnetic or ferrimagnetic materials with a permanent magnetic moment

Paramagnetic materials consist of atoms containing permanent dipole moments while neighboring magnetic moments do not interact. The magnetic moments are located in random

directions in the absence of a magnetic field. However, in the presence of a magnetic field a small magnetization develops, so the susceptibility (the extent of a material to become magnetized in the presence of a magnetic field) is small yet positive. An unpaired electron is required for paramagnetic substances. For example copper has an unpaired electron which enhances the local magnetic field (Jakubovics 1994).

Electrons in orbitals as pairs cancel the generated magnetic fields, but the direction of magnetism in materials with an unpaired electron when placed in an external magnetic field is aligned with the magnetic field. Therefore, paramagnetic agents have the capability of augmenting the magnetic field strength (Bushberg, et al. 2002). Metal ions such as Co, Fe, Gd, Ni, Mg, Li, Cu, Cr, and Mn, diatomic gases such as O_2 and NO, and salts of transition metals are paramagnetic. These substances with unpaired electrons have strong magnetic moments and could be used as paramagnetic contrast agents, meaning they could increase the intensity of a signal and consequently an image. In the case of clinical MRI, paramagnetic contrast agents are gadolinium chelates, manganese, and iron compounds (Weishaupt, Kochli and Marincek 2006).

Therefore, paramagnetic contrast agents enhance magnetic resonance (MR) image contrast by changing T_1 and T_2 relaxation times. Paramagnetic contrast agents in MR imaging change the image intensity because of change in T_1 and T_2. In clinical MRI these agents are used to detect any malignancy and must have low toxicity while being excreted easily from the body (Kuperman 2000).

In other words, contrast in NMR provides distinguishable images between regions within a sample. Positive contrast means that the signal intensity is higher in the region of interest, while negative contrast means that the signal is weaker in the region. The magnitude of data in NMR imaging presents the number of spins in a region of a sample. Therefore NMR images

display contrast between regions with different spin densities. This is useful in imaging applications; however, the regions of interest within a sample sometimes contain similar spin densities. Therefore, contrast agents need to be used in imaging to distinguish between these homogeneous regions.

Contrast in imaging is based on the existing differences in NMR properties of a sample known as relaxation times. Relaxation times are used to achieve contrast in an image by highlighting the differences between the regions of interest. Also, if regions of sample are homogeneous, contrast agents are used to achieve contrast in these regions via changing the relaxation times.

A contrast agent is a substance capable of altering the spins relaxation times when they are in contact with the agent. Contrast agents can augment the sensitivity of an NMR imaging experiment while creating positive or negative contrast.

Paramagnetic contrast agents, which are a class of contrast agents, possess unpaired electrons and have a positive magnetic susceptibility. The magnetic fields generated by the paramagnetic contrast agent decrease the T_1 and T_2 relaxation times of neighbor spins. A decrease in T_2 causes a decrease in the signal whereas a decrease in T_1 results in an increase in the signal. Also, for low concentrations of the contrast agent the T_1 effects dominate to produce positive contrast. Larger concentrations of the contrast agent create negative contrast. The extent of positive or negative contrast is controlled by adjusting MRI parameters (Magritek, Terranova-MRI Student Guide 2006).

1.5 Phyto-remediation

Soil, water, and air heavy metal contamination is one of the serious ecological problems in the world (Sias 1998). Water contaminations are a result of the contaminants present in soil

and air which gradually reach living organisms (Gardea, et al. 2005). Within the last century, great amounts of toxic metals and chemicals have been disposed into soil and water from various sources including industry (Senthilkumar, et al. 2005). Therefore, cleaning up the contaminated sites has become a major issue in this century. Fortunately, a method called phyto-remediation recently has been introduced to the society. Phyto-remediation is the use of plants to remove contaminants from polluted water or soil. This technology can be used to clean up heavy metal contaminated soil or water (Haque 2008). Plants for phyto-extraction have to be metal hyper-accumulator meaning tolerant to the target metal (Gardea-Torresdey, et al. 2005). In addition, phyto-extraction can be used for the recovery of precious metals such as gold, silver, platinum, and palladium (Gardea, et al. 2005).

1.6 Plants

Readily bio-available metals for plant uptake consist of cadmium, nickel, zinc, arsenic, and copper; moderately bio-available metals are cobalt, manganese, and iron while lead, chromium, and uranium are not very bio-available (Health 2003).

Some plants are capable of tolerating toxic metals through the use of several mechanisms such as developing metal-tolerant enzymes or retaining metal in the roots and preventing metal translocation to the shoots (Fernandes and Henriques 1991).

1.6.1 Mesquite

One of the important exploited trees of deserts is mesquite (Haque 2008). The plant can uptake Cr, Ni, Cu, As, Au, and Se easily (Gardea, et al. 2005). Mesquite is tolerant to drought meaning it can draw water from the water table through its long root into soil as deep as 190 ft (Figure 1.3). On the other hand, it can use available water in the upper part of the ground as well (Haque 2008). Mesquite is the pioneer of several heavy metal hyper-accumulating plants

(Senthilkumar, et al. 2005). For example, velvet mesquite (Prosopis juliflora) is capable of germinating in copper concentrations ranging from 10-1280 ppm (Victor, Pillay and Al-Minj 2007).

Figure 1.3 A mesquite tree at UTEP

Some common species of mesquite are honey mesquite (Prosopis glandulosa), velvet mesquite (Prosopis juliflora also called Prosopis velutina), creeping mesquite (Prosopis strombulifera) and screwbean mesquite (Prosopis pubescens) (Haque 2008).

In a study in the state of Arizona, Prosopis juliflora was investigated as a bio-indicator of industrial pollution. The results showed that Cu and Cd content were much higher in plant components compared to the level in the soil. Therefore, the plant could be used to decontaminate heavy metal polluted soils containing Cd, Cu, Ni, Cr and Al several times higher than the existing level in the soil (Senthilkumar, et al. 2005).

In another study, seedling height decreased exponentially with increase in copper concentrations (seedlings grown in 10, 20, 40, 80, 160, 320, 640 and 1280 ppm of Cu concentration while control seedlings were 2.4 ppm). Even though the seedlings showed symptoms of toxicity, they accumulated high levels of copper. Therefore, mesquite seedlings as well as the plant served as a sink for copper in contaminated soils (Victor, Pillay and Al-Minj 2007).

1.6.2 Soybean (Glycine max)

Soybean, cultivated in East Asia for 5,000 years, has been consumed as cooking oils, margarine, flour, soya milk, soy sauce, and tofu. The dried bean contains 18–22% fat, 35% carbohydrate. One hectare of soybeans yields 162 kg of protein in comparison with 9 kg per hectare for beef which reveals that soybean is one of the richest and cheapest sources of protein (Research 2009).

Soybean provides a complete protein for vegetarian diets low in lipids. Biochemists have isolated a component in soybean which prevents cancer (Jurgonski and Smart 1997).

According to an analysis on soybean seeds a concentration of 0.5 mM Cu induced a significant reduction in carbohydrates and protein contents of the seeds (El-Mashad 2003).

A study on the effect of excess Cu applied through leaves and roots in soybean plants was done. The application of 50µM $CuSO_4$ on leaves increased chlorophyll. In contrast, soybean plants grown in hydroponic medium (plants growth via nutrient solution rather than soil) with the same concentration of Cu showed lower chlorophyll (Bernal, Cases, et al. 2007).

Finally, in another study, copper content in soybean seed exhibited higher amount than its shoot. Shoot and seed phosphorus content and their uptake significantly increased with 2.5 kg Cu/hectare application (Barik and Chandel 2001).

1.7 Copper

Copper sulfate is known as a herbicide and its effect on seed germination is likely to be more severe when compared to copper nitrate (Victor, Pillay and Al-Minj 2007).

Copper is present in I and II oxidation states in plant tissues (Sias 1998). Cu gets absorbed and transported through mesquite as Cu (II). However, in the leaves Cu was present in the (I) and (II) oxidation states (Gardea, et al. 2005).

Cu concentration in non-contaminated soils is 20-30 ppm and in natural waters is less than 2 ppb while more than 2000 ppm of Cu level in soils has been recorded in mining areas and in the vicinity of Cu smelters (Fernandes and Henriques 1991). On the other hand, the normal Cu concentration in plant biomass is 12 ppm where as in marine plants it is 3.5 ppm while Cu concentrations in hyper-accumulating plants vary from 6.6 to 2117.4 ppm (Haque 2008). Due to its strong binding by soil components, only a limited fraction of the total amount of Cu present in the soil is available for plant uptake (Fernandes and Henriques 1991).

Copper (Cu) is a nutrient essential for organisms that utilize photosynthesis (i.e. cyanobacteria, algae and plants). Also, copper plays an important role in metabolic processes. For example, Cu is a cofactor of enzymes and metalo-proteins that catalyze redox reactions in chloroplasts (Bernal, Ramiroa, et al. 2006).

Cu in Elodea is an example of active transport mechanisms while a study has shown that Cu entered soybean through passive flux. In fact, when Cu concentrations in the environment are low, active absorption dominates. Passive uptake takes place when Cu level in the medium increases because of damage to the membrane, so the plant loses its uptake selectivity (Fernandes and Henriques 1991).

1.8 Literature Review

Based on a literature review [(Planinsic, Stepisink and Kos 1994), (Coy, et al. 2006), (Mohoric, et al. 2004), (Melton and Poliak 1971), (Callaghan, Eccles and Seymoura 1997), (Halse and Callaghan 2008), (Xu, et al. 2008), (Robinson, et al. 2006), (Thiele 2007), (Qui, et al. 2007), …] no work is reported investigating the presence or absence of copper in plants using MRI.

CHAPTER II (MATERIALS, EQUIPMETS, AND EXPERIMENTAL)

2.1 Materials

A 500 ml plastic bottle and 2 plastic phantom tubes (or centrifuge tubes presented in figures 2.33-2.34) were provided within the EFNMR/MRI package.

The following items were purchased from the corresponding companies:

a) Velvet mesquite, *Prosopis juliflora velutina*, seeds from Granite Seed Company
b) Soybean seeds from Howe Seeds Inc.
c) Mason jars from Sam's Club
d) Plastic tubing, connectors, and air pumps from VWR International Company
e) Germination paper from Nasco Fort Atkinson Company
f) Antibiotic antimycotic solutions, glass pipettes, disposable transfer pipettes, and copper salts from Sigma Aldrich Chemical Company

2.2 Equipments

a) Pulse and collect, 1D, 2D, and 3D MRI images were recorded on a Terranova EFNMR/MRI purchased from the Magritek Company in New Zealand, http://www.magritek.com.
b) The pH meter (model 420 A) was used to adjust the pH of nutrient solutions.

2.3 Experimental

2.3.1 Doped Water

Water doped with cupric sulfate of concentrations 0.25, 0.5, 1, 2, 3, and 4 mM in 500 ml bottles was prepared. For each sample, T_1 and T_2 relaxation times were measured. For T_1 the measurement was performed in both polarizing and Earth fields. Appendix A, T_1 and T_2 sections, provides instructions of these procedures. The relaxation times for each sample were recorded. The concentration of $CuSO_4$ versus the three measured relaxation times was plotted

separately. Also, various prepared samples were used to acquire 1, 2 and 3D MRI images for demonstrating image contrast by adjusting the polarization time. Instructions on how to acquire an image are given in Appendix A.

2.3.2 Plant Preparation (Hydroponic Media)

Hydroponic media was prepared as described by the reference (Peralta-Videab, et al. 2002). In this method germination papers and de-ionized water were sterilized using an autoclave. Soybean and mesquite seeds were stirred in a 1 liter beaker containing 4% Clorox solution for 30 minutes to avoid fungal contamination, then washed with sterilized DI water 3 times. Soybean seeds were ready for rolling after eight hours where as mesquite seeds were kept in DI water for one day to soak before rolling. The seeds were arranged on wet sterilized germination papers under a laminar air flow hood and sterile conditions (Figure 2.1). 10 drops of antibiotic- antimycotic solution was added on top of the seeds. The paper was rolled and placed upright in a glass jar filled with 2 centimeters in height of sterilized DI water. Each roll contained 20 seeds of mesquite or 15 seeds of soybean. A plastic bag was used to cover the rolls, and the jar was placed in the germination chamber (Figure 2.2 presents 80 rolls of soybean, the last two bottom rows, and 100 rolls of mesquite, the last two top rows) at room temperature to exclude light.

Figure 2.1 Soybean (yellow) and mesquite (red) seeds

Figure 2.2 Germination chamber

Figure 2.3 Germinated seeds

The seeds germinated after 5 days (Figure 2.3) and were removed from the dark and placed under fluorescent light (two 34-W) for one day in order for photosynthesis to take place (Figures 2.4 and 2.5). The next day, when the color of the leaves changed from yellow to green (Figures 2.6 and 2.7), the seedlings of the same height were arranged in groups of 3 in the case of soybean and in groups of 5 in the case of mesquite on a piece of a plastic disposable transfer pipette to hold the plants in place in order to be transferred to 400 ml mason jars or other suitable containers by using a polystyrene base fitting on top of the containers (Figures 2.8 and 2.9). Glass pipettes, plastic tubing, connectors, and air pumps were used to oxygenate the roots.

Figure 2.4 Soybean germinated seeds after removal from dark

Figure 2.5 Mesquite germinated seeds after removal from dark

Figure 2.6 Soybean after one day being kept under fluorescent light

Figure 2.7 Mesquite after one day being kept under fluorescent light

Figure 2.8 Arrangement of mesquite seedlings

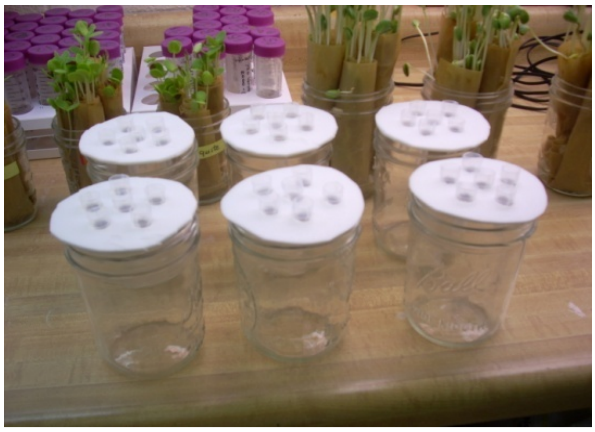

Figure 2.9 Mason jars, pipettes, and polystyrene base fitting

As described by (De La Rosa, Peralta-Videa and L. 2005), for 180 rolls of the plants nutrient solution was prepared by mixing 200 ml of each salt plus 18 liters of DI water. The solution was pH balanced to 4.8 using a pH meter to provide nutrients for the seedlings. A lower pH diminishes precipitation of Cu in the solution. Containers that were considered as controls only contained nutrient solution where as containers considered as treated contained sufficient amounts of copper salts. Three growth experiments were conducted.

2.3.3 First Experiments

The purpose of the first growth experiments was to find out the amount of Cu each plant could tolerate. Therefore, 300 mesquite and 150 soybean seeds were planted as explained in section 2.3.b. The plants were divided into control and treated with 4 mM (0.4g/400ml) cupric sulfate (Figures 2.10 to 2.12). After one day, all the treated plants died due to the high level of copper concentration poisoning the plants (Figure 2.13). A layer of bluish precipitate was observed at the bottom of the treated plants (Figure 2.13).

Figure 2.10 Transfer of seedlings to hydroponic

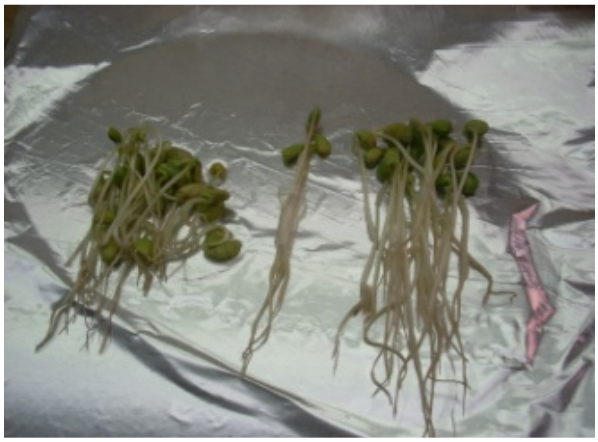

Figure 2.11 Transfer of seedlings to hydroponic

Figure 2.12 Plants before adding 4mM Cu

Figure 2.13 Plants after adding 4 mM Cu

The control plants were divided into different solutions containing 0.25, 0.5, 0.75, 1, and 2 mM cupric sulfate (Figures 2.14 and 2.15). Plants containing a 0.25 and 0.5 mM concentration of cupric sulfate survived up to two weeks, but plants with 0.75, 1, and 2 mM started to die after 5 days (Figures 2.16 and 2.17). However, a few mesquite plants containing 0.75 and 1 mM copper did survive up to two weeks.

Figure 2.14 Mesquite plants

Figure 2.15 Soybean plants

Figure 2.16 Dead soybeans

Figure 2.17 Dead mesquites

2.3.4 Second Experiments

The purpose of the second experiments was to determine how many plants were needed to fit packed into phantom tubes in order to acquire 2D MRI images. Soybean and mesquite seeds were planted (Figures 2.18 and 2.19) and the seedlings were transferred to nutrient solution. In the case of mesquite, 4 days after transferring, the plants were kept in 0.4 mM and 0.6 mM of cupric nitrate solution for 3days. In the case of soybean, 4 days after transferring, the plants were kept in 0.25 and 0.5 mM of cupric nitrate solution for 6 days. Then the images were acquired. Also in the case of soybean, 10 days after transferring, the plants were kept in 2 and 4 mM of cupric nitrate solution for 42 hours. And finally, in the case of mesquite, 11 days after transferring, the plants were kept in 2, 4, and 6 mM of cupric nitrate solution for 52 hours. Then

the images were acquired. The purpose of the last two experiments was to observe the effect of copper in the plants in a short period of time. Approximately, in the case of mesquite, 200 plants (equal to 40 grams) were needed to fit packed in a phantom tube, so 400 plants were needed to pack the treated and control tubes in order to acquire a 2D MRI image. And in the case of soybean, 80 plants (equal to 40 grams) were needed to fit packed in a phantom tube, so 160 plants were needed to pack the treated and control tubes in an experiment.

Figure 2.18 Mesquite, second run

Figure 2.19 Soybean, second run

2.3.5 Third Experiments

Based on the established experiences, in the third run 600 mesquite and 250 soybean seeds were planted. The plants were divided into control and treated ones with nutrient solutions containing a concentration of 0.25 mM cupric nitrate for three weeks in the case of soybean and four weeks in the case of mesquite. Then the 2D MRI images were acquired. It should be noted that due to change in seasons there was some difficulty to germinate soybean seeds. Therefore, it took three more runs of soybean germination in order to get sufficient amount of the plant. Figures 2.20-2.27 demonstrate the sixth run of the soybean germination and growth and figures 2.28-2.32 demonstrate the third run of the mesquite growth.

Figure 2.20 Soybean germination

Figure 2.21 Soybean transfer

Figure 2.22 Soybean transfer

Figure 2.23 Soybean growth

Figure 2.24 Soybean seedlings right after transfer to hydroponic (left treated, right control)

Figure 2.25 Soybean plants after 3 weeks (middle treated, left and right control)

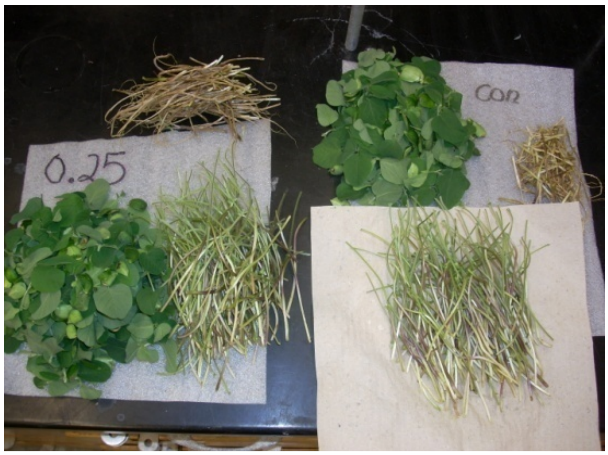

Figure 2.26 Soybean plants' parts

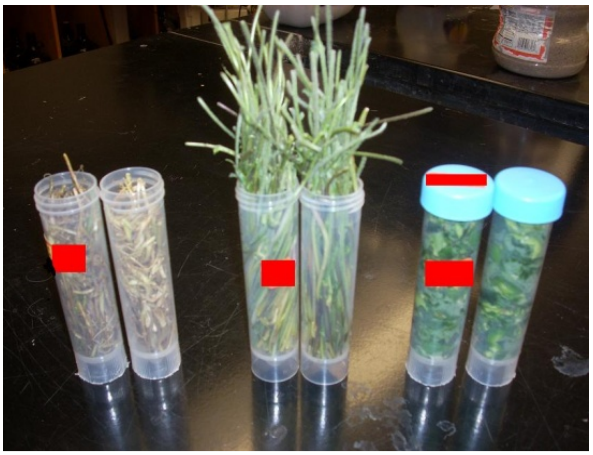

Figure 2.27 Soybean roots, stems, and leaves ready for MRI imaging

Figure 2.28 Mesquite seedlings right after transfer

Figure 2.29 Mesquite 3 days after transfer

Figure 2.30 Comparing treated and control

Figure 2.31 Mesquite 3 weeks after transfer

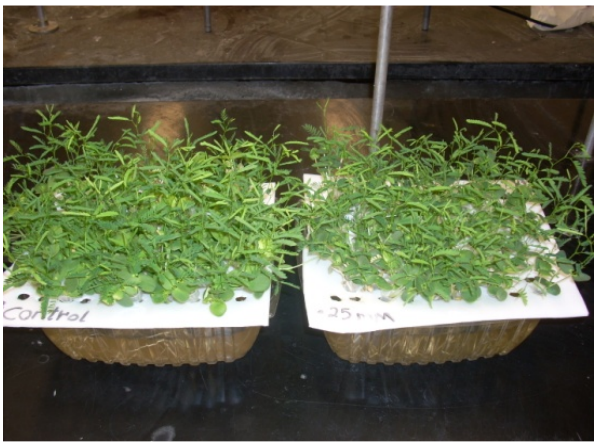

Figure 2.32 Mesquite 4 weeks after transfer

2.3.6 Parsley, Cilantro, and Celery

Parsley and cilantro were separated from the leaves since acquiring an image of the leaves was impossible. A bunch of the arranged stems were packed into two phantom tubes as control and treated samples (Figure 2.34). Then the 2D MRI images were acquired.

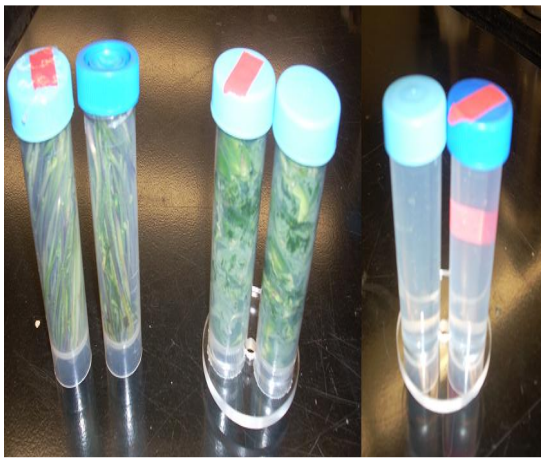

Figure 2.33 Soybean stems, soybean leaves and doped water in phantom tubes

Figure 2.34 Parsley, cilantro, and celery in phantom tubes

30 grams of cilantro stems were completely immersed in a 4mM cupric sulfate solution inside a phantom tube for 20 hours. In another tube 30 grams of cilantro stems were immersed in a phantom tube half filled with a 4 mM cupric sulfate solution for 20 hours. 2D MRI images were recorded of both samples along with 30 grams of cilantro stems in their own tube as a control.

50 grams of parsley stems immersed in a full amount of 3 mM cupric sulfate solution were kept for 6 hours inside a phantom tube. 2D MRI images were acquired of the sample along with 50 grams of parsley stems in a separate tube as a control.

In another series of trials, three samples of 35 grams of parsley stems were immersed in 0.5, 2, and 4 mM cupric sulfate solutions, respectively, inside phantom tubes for 20 hours. 2D MRI images were acquired of the samples along with 35 grams of parsley stems in a separate tube as a control.

Three samples of 50 grams of celery stems were immersed in 4mM cupric sulfate solution in three separate phantom tubes for 17 hours, 1 day, and 3 days, respectively. 2D MRI images were acquired of the samples along with 50 grams of celery stems in a separate tube as a control.

In another series of trials, two samples of 38 grams of celery stems were immersed in 4 mM cupric sulfate solution inside phantom tubes for 3 and 6 hours, respectively. 2D MRI images were acquired of the samples along with 38 grams of celery stems in a separate tube as a control.

CHAPTER III (RESULTS AND DISCUSSION)

3.1 Relaxation Time Contrast

The objective of these experiments was to understand the impact of $CuSO_4$ contrast agent on NMR of H_2O. Three 500 ml samples of water and water doped with 3000 and 4000 μM of $CuSO_4$ were prepared. NMR experiments were run on the samples using all the optimized parameters chosen during the instrument setup. An FID and spectrum from the three samples were acquired, and the sample peaks in the spectrum were integrated. The limits of the integration and the results were recorded. The same experiment for the three samples with a short polarization time of 500 ms was repeated. The spectrum over the indicated frequency range was integrated, and the results were recorded in Table 3.1.

Table 3.1 Copper (II) Concentration and Polarization Duration versus Signal Parameters

Sample type $CuSO_4$ (μM)	Polarization duration (ms)	FID amplitude (μv)	Signal Height (μV/Hz)	Signal Width (Hz)	Signal Integration
pure water	4000	97	132	2	97
pure water	500	30	28	2	30
4000	4000	80	17.5	2	25
4000	500	80	17.5	2	25
3000	4000	90	28	6	90
3000	500	85	26	6	86

Based on Table 3.1, in the case of the pure water sample decreasing the polarization time from 4000 to 500 ms decreased the signal intensity both in the FID and spectrum. However, in the case of doped waters with 3 and 4 mM $CuSO_4$, the FID and spectrum signals did not decrease deeply from the long and the short polarizing time. Interestingly, at the 500 ms polarization time the FID signals from the doped samples are greater than that of the pure water sample. This is because the contrast agent ($CuSO_4$) shortens T_1 in the doped water sample. As a result, the doped water sample becomes polarized more quickly, so it requires a shorter time to become

polarized. This phenomenon is due to the existing unpaired electron in the d orbital of copper which helps the sample to gain its longitudinal magnetization (polarized state) much faster. There is also a T_2 change between the pure water and the doped water samples. In case of pure water, the FID signal persists for much longer than the FID from the doped water sample. This was an indication that $CuSO_4$ decreased T_2 as well as decreasing T_1. Also, despite the decrease in T_2, the decrease in T_1 resulted in an increase in the signal intensity.

In order to understand the impact of $CuSO_4$ contrast agent on the H^1 NMR signal better, quantitative measurements of relaxation times were obtained. Six $CuSO_4$ solutions with concentrations of 250, 500, 1000, 2000, 3000, and 4000 μM were prepared in 500 ml plastic bottles. For each sample T_1-B_p, T_1-B_e, and T_2 relaxation times were measured and recorded in Table 3.2 (for instruction on how to acquire T_1 and T_2 refer to Appendix A).

Table 3.2 Relaxation times of water samples doped with $CuSO_4$

Sample	[$CuSO_4$] (μM)	T_1-B_p (ms)	T_1-B_e (ms)	T_2 (ms)
1	4000	(171 ± 8)	(189 ± 5)	(182 ± 10)
2	3000	(210 ± 30)	(210 ± 30)	(210 ± 40)
3	2000	(320 ± 30)	(290 ± 20)	(370 ± 20)
4	1000	(560 ± 10)	(530 ± 20)	(590 ± 30)
5	500	(860 ± 30)	(840 ± 40)	(870 ± 30)
6	250	(1360 ± 30)	(1320 ± 30)	(1270 ± 30)

Based on Table 3.2, values for T_1-B_p, T_1-B_e, and T_2 decreased as the concentration of $CuSO_4$ solutions increased in the samples. The relationship between the concentration of $CuSO_4$ and the relaxation times was plotted and depicted in Figures 3.1 to 3.3. These plots demonstrate an exponential decrease in T_1-B_p, T_1-B_e, and T_2 as the concentration of the contrast agent increases. The results were consistent with the results in the first experiment. Therefore, paramagnetic contrast agents decrease both T_1 and T_2 time constants.

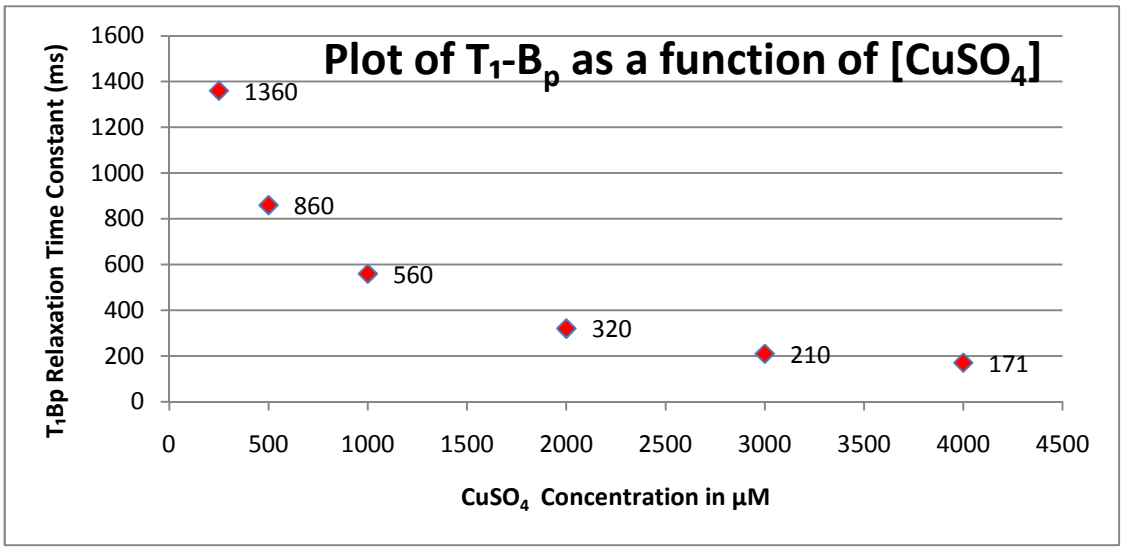

Figure 3.1 Plot of T_1-B_p as a function of $CuSO_4$ concentration

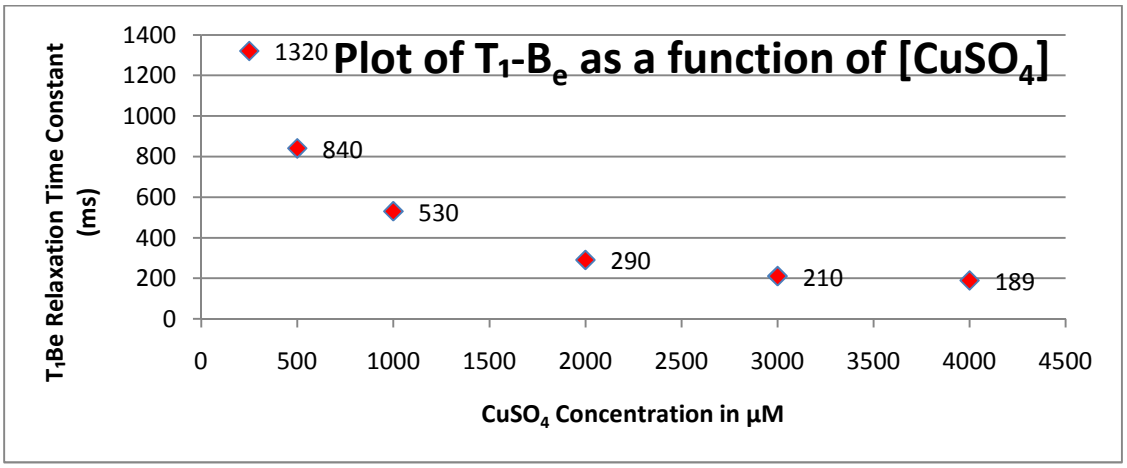

Figure 3.2 Plot of T_1-Be as a function of CuSO4 concentration

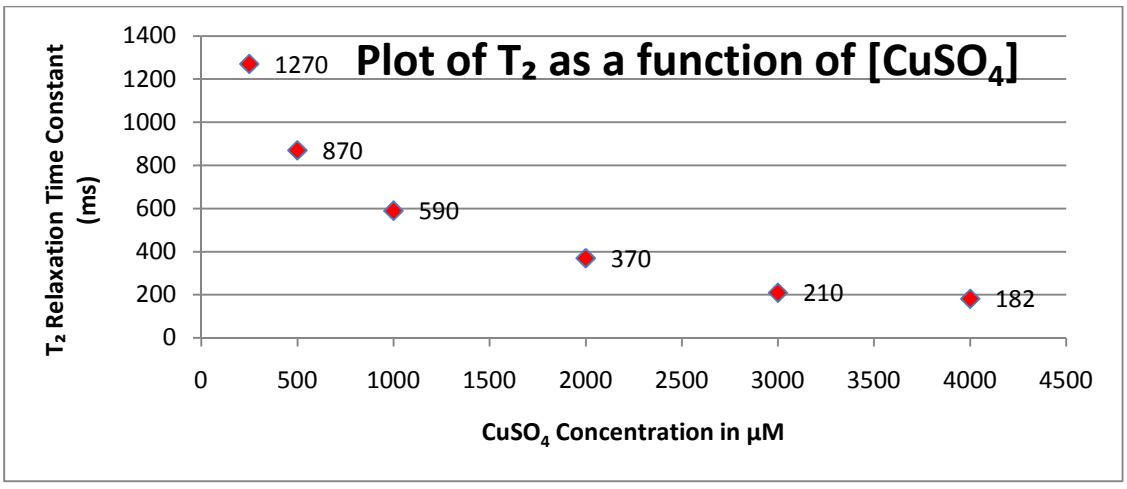

Figure 3.3 Plot of T_2 as a function of $CuSO_4$ concentration

3.2 Relaxation Contrast Imaging

The objective of the following experiments was acquiring T_1 and T_2 weighted 2D images of two compartment phantom tubes to display relaxation contrast. So, two types of contrast based on T_1 and T_2 relaxation time constants were investigated.

3.2.1 T_1 Weighted Imaging

An EFMRI sample made of two phantom tubes in which one tube filled with just distilled water and the other with water doped with 3 mM $CuSO_4$ was used for T_1 weighted imaging. So, the samples contained a short T_1 (doped water) and a long T_1 (plain water). Prior to imaging, T_1 and T_2 of both the pure water and the doped water were measured by using a 500 ml volume of the samples, meaning that T_1 and T_2 should not be measured with phantom tubes as the applied sample. The two-compartment sample was inserted in the center of the probe and a 2D-Gradient Echo image (2D GE) in the YZ orientation along with parameters depicted in Figure 3.4 was chosen. A repetition time of more than twice the polarization was chosen to insure a coil duty cycle of less than 50%. An echo time as short as possible was chosen in order to minimize any T_2 contrast effects, and images at several encoding times were acquired (4 scans). Four 2D GE in the YZ planes of 2 tubes of 3 mM doped water and plain water as T_1 weighted images were acquired by choosing polarizing times equal to 600 (three times greater than the shortest T_1 of the sample), 1200, 2000, and 4000 ms (twice as much as the longest T_1 of the sample) as depicted on the top part of Figure 3.5.

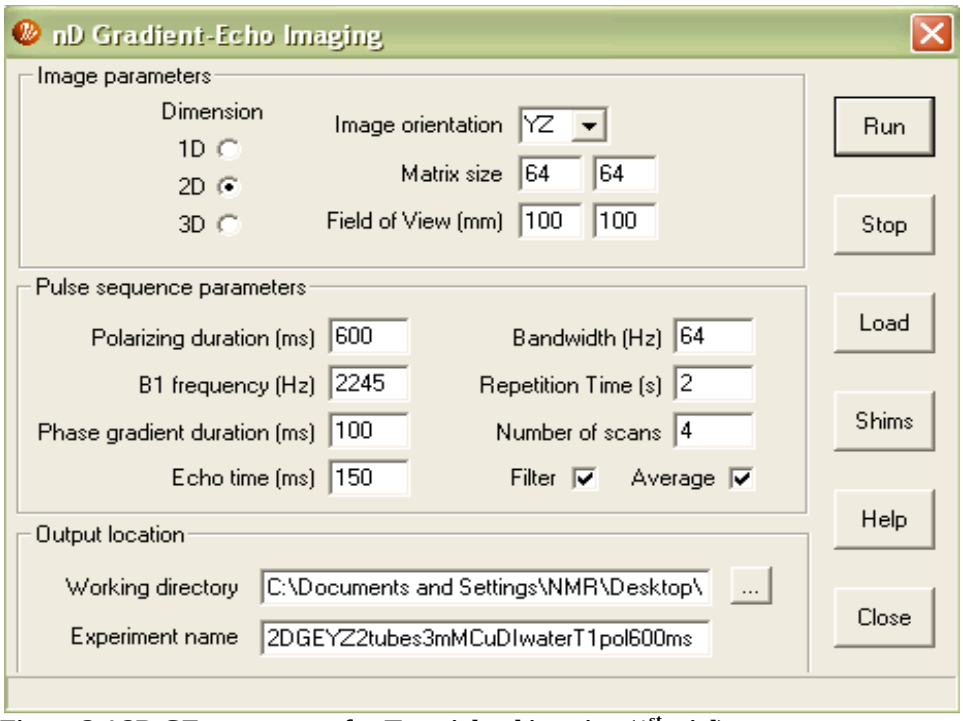

Figure 3.4 2D GE parameters for T_1 weighted imaging (1st trial)

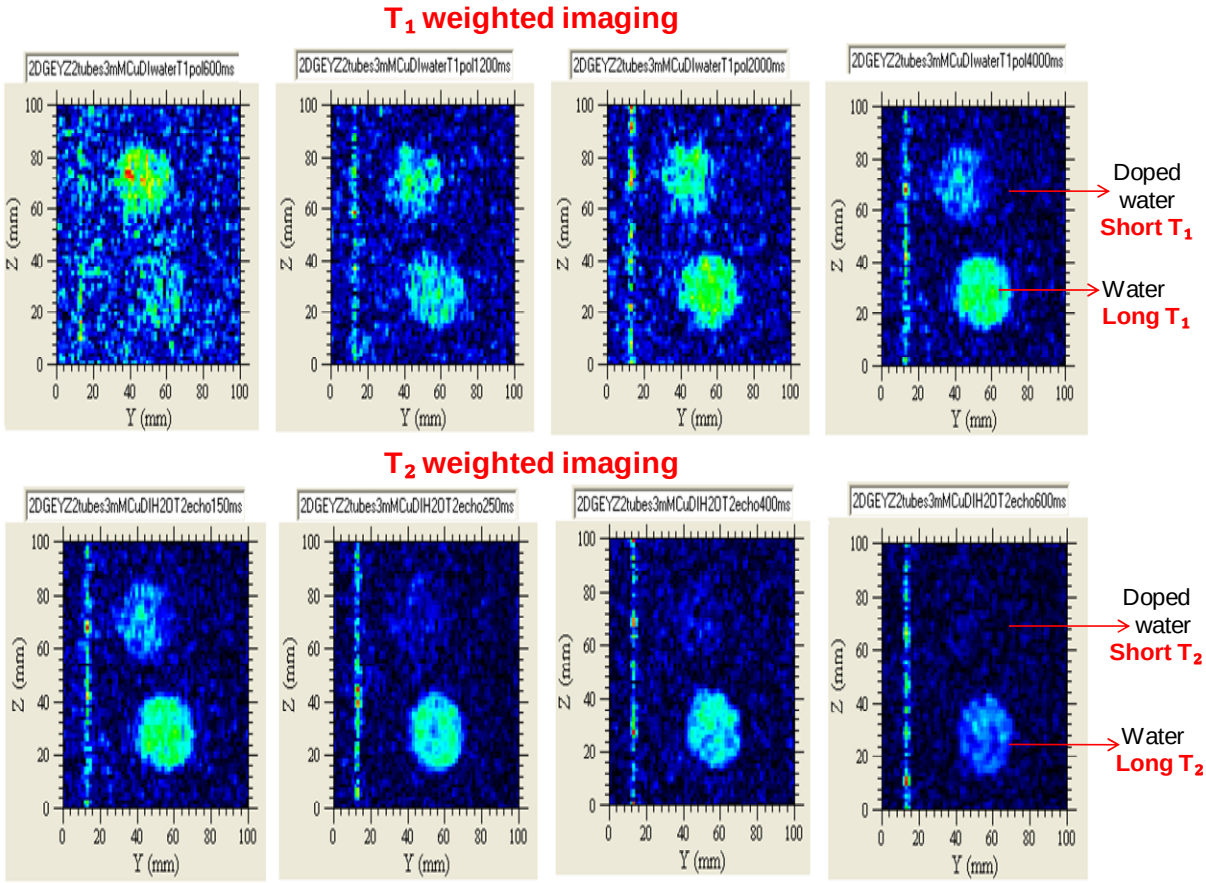

Figure 3.5 First trial of T_1 and T_2 weighted contrast imaging for doped and plain water

T_1 plays its role on the signal to noise ratio (SNR) of an image via the polarization pulse parameter of the imaging experiment. The correlation between the T_1 of a sample, its polarizing time, and the SNR of the corresponding image is expressed by Equation 3.1.

Equation 3.1: $$\text{SNR} \propto [1 - \exp(-T_{pol}/T_1)]$$

According to the equation, in order to increase the SNR of an image either polarization time must increase or the T_1 of the sample must be low. So, if two regions of the sample have different T_1 values, the polarization time can be chosen such that the SNR of the two regions show a difference as depicted on the top part of Figure 3.5. It is worth mentioning that plain water has T_1 and T_2 values of 2 seconds while the doped water (with 3 mM $CuSO_4$) has T_1 and T_2 values of almost 200 ms.

Based on Figure 3.5, a short polarization time (600 ms) made the short T_1 region (doped water tube) to appear brighter than the long T_1 region (plain water tube). And a long polarization times ideally should result in no contrast between the regions. As illustrated by Equation 3.1, the short T_1 species (doped water tube) requires a short polarization time to become fully polarized, whereas the long T_1 species (plain water tube) requires a long polarization time to become fully polarized. Therefore, the short T_1 region got polarized in a shorter time creating a stronger signal and so appeared brighter (top far left of Figure 3.5), whereas the long T_1 region got partially polarized within the same time period creating a weaker signal and so appeared darker as depicted on top far left of Figure 3.4. As the polarization time increased (top section of Figure 3.4), the long T_1 region (plain water tube) became more polarized creating a stronger signal and so appeared brighter and brighter. Finally on the top far right of Figure 3.5, which indicates a polarization time (4s) of twice the long T_1 sample (2 s), the contrast between the long and short T_1 regions ideally should become less until there should be no T_1 contrast in the image.

However, due to the effect of T_2 contrast the top image on the far right of Figure 3.5 shows this type of contrast. Note there is a noise streak along the Z dimension at 16 mm which is repeated in every single image.

3.2.2 T_2 Weighted Imaging

The same sample and procedure used for section 3.2.1 was applied for these experiments. So, four 2D GE in the YZ plane of 2 tubes of 3 mM doped water and plain water as T_2 weighted images were acquired by choosing the parameters depicted in Figure 3.6 and echo times equal to 150, 250, 400, and 600 ms (from the shortest possible echo time to the longest) as depicted on the bottom part of Figure 3.5. The polarization time was set to twice the long T_1 value of the sample (4s) so that there would be minimum T_1 contrast in the image.

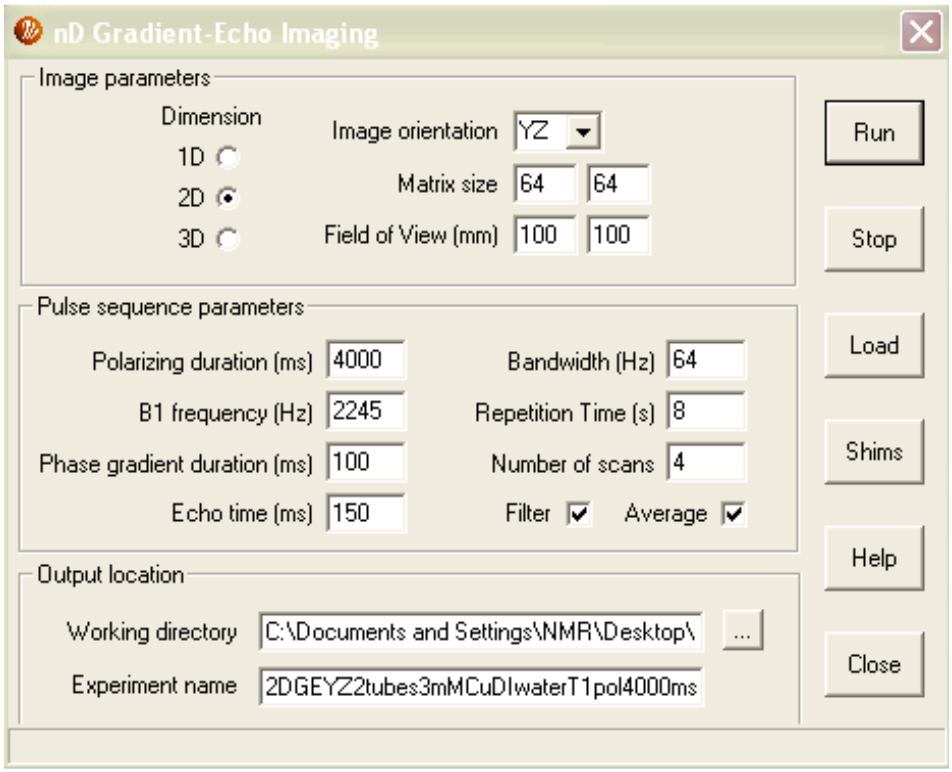

Figure 3.6 2D GE parameters for T_2 weighted imaging (1st trial)

The other type of contrast is T_2 contrast where the relationship between T_2 and the SNR of an image is given by Equation 3.2. By choosing an appropriate echo time, the SNR of two

regions with different T_2 values will be different.

Equation 3.2: $$\text{SNR} \propto \exp\left(-T_{echo}/T_2\right)$$

T_2 contrast is the opposite of T_1 contrast in which at short echo times compared to the short T_2 value (doped water tube), there should be little contrast between regions since neither the signal from the short T_2 region (doped water tube) nor the long T_2 region (plain water tube) has had sufficient time to decay significantly between the RF excitation and the center of the echo. However, at long echo times the signal from the short T_2 region has decayed more between the excitation pulse and the center of the echo than the long T_2 region, so the short T_2 region appeared darker than the long T_2 region (the bottom part of Figure 3.5). Therefore, the longer the echo time, the more pronounced T_2 contrast is.

Figures 3.7 illustrates the parameters for the 2D Spin Echo imaging (2D SE) experiment in the YZ orientation for the same sample with a polarization time of 600 ms as the second trial of the T_1 weighted imaging experiment. Similarly, Figure 3.8 presents the parameters for 2D SE in the YZ direction for the same sample with the minimum echo time of 100 ms as the second trial of the T_2 weighted imaging experiment. Note that there is a difference between the first trial parameters versus the second trial parameters in the T_1 and T_2 weighted contrast imaging. Figure 3.9 illustrates the corresponding images of the second trial T_1 and T_2 weighted contrast imaging for doped and plain water tubes. The top images from left to right correspond to Polarization durations of 600, 2300, and 4000 ms within the T_1 weighted imaging experiments while the bottom images from left to right correspond to echo times of 100, 200, 300, and 500 ms within the T_2 weighted imaging.

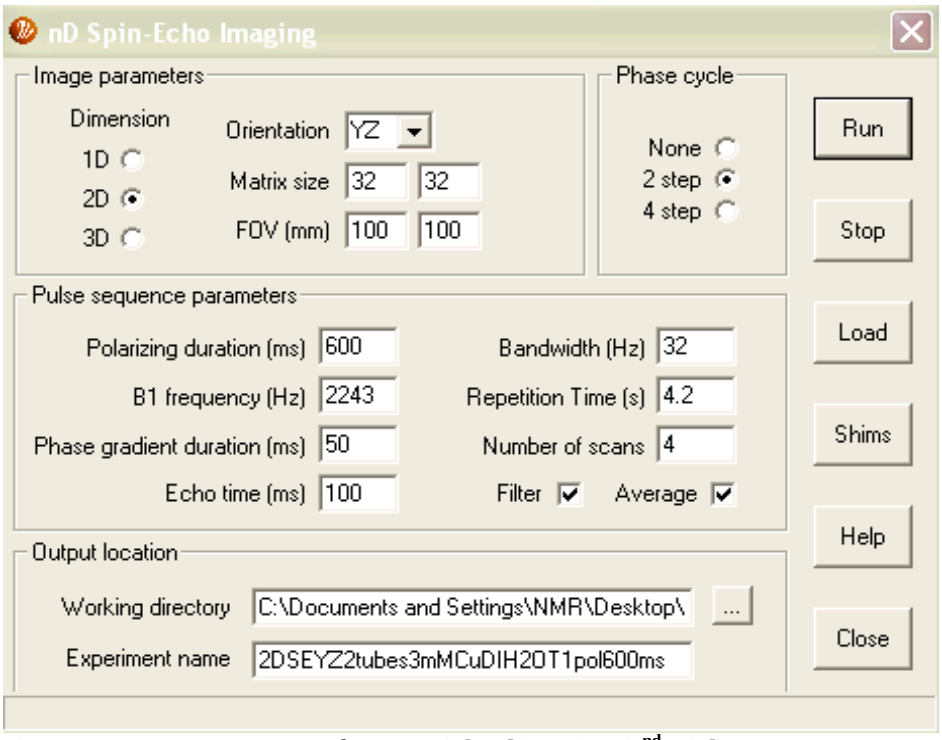

Figure 3.7 2D SE parameters for T_1 weighted imaging (2nd trial)

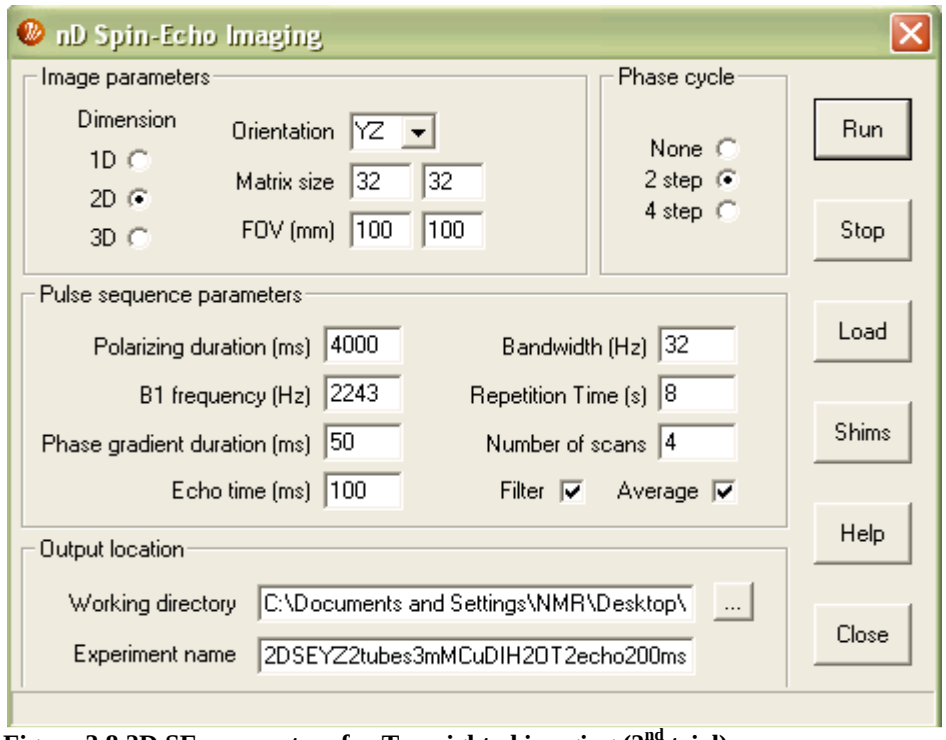

Figure 3.8 2D SE parameters for T_2 weighted imaging (2nd trial)

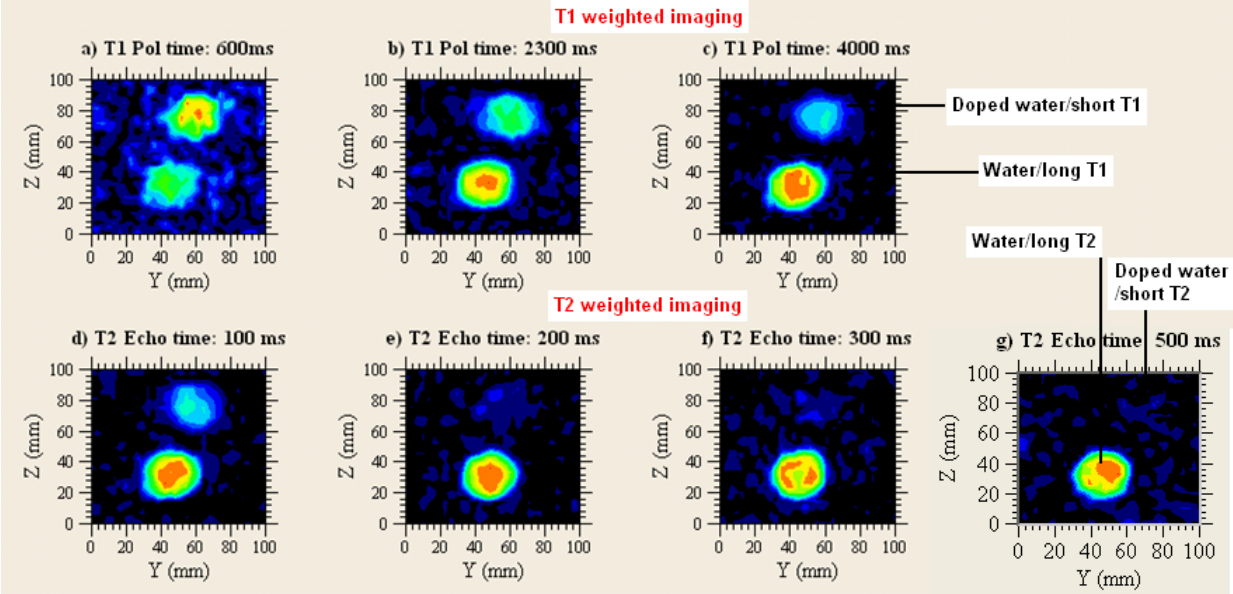

Figure 3.9 T_1 and T_2 weighted contrast imaging of doped and plain water (2nd trial)

As depicted on part a) of Figure 3.9, at the lowest polarization time (600 ms) only one sample is strongly visible in the image, and that was the short T_1 sample. At a longer polarizing time (2300 ms, part b of Figure 3.9) both samples are visible, but the short T_1 sample should be brighter in the image to illustrate the positive contrast. However, in both trials one and two this is not the case, meaning that the long T_1 region is brighter. This means that the long T_1 region at polarization duration of 2300 ms got polarized almost fully and appeared brighter that the short T_1 region and the short T_1 region appeared darker due to the T_2 contrast effect. Also, in the final image (part c) the short T_1 sample is not as bright as the long T_1 region again due to T_2 contrast, meaning that the minimum echo time (100 ms) did not completely remove T_2 contrast.

Also, Figure 3.9 presents four 2D SE images at four different echo times. At the shortest echo time (100 ms, part d) both samples are visible in the image but the long T_2 region is quite brighter; because of the limits on the minimum echo time, it was not possible to obtain an image with no T_2 contrast. At longer echo times (parts e and f) both samples are visible but the long T_2 region is much brighter (positive contrast). In the final image (part g), the short T_2 is invisible

while the long T_2 region is fully bright. Figure 3.10 demonstrates the second trail of T_1 and T_2 weighted contrast imaging for doped water and plain water demonstrating 2D surface plot feature available in the 2D plot menu under the view submenu. By selecting this option, the surface plot in the 3D plot window appears which represents the surface of the displayed image (Magritek, Prospa Software Manual 2004-2006).

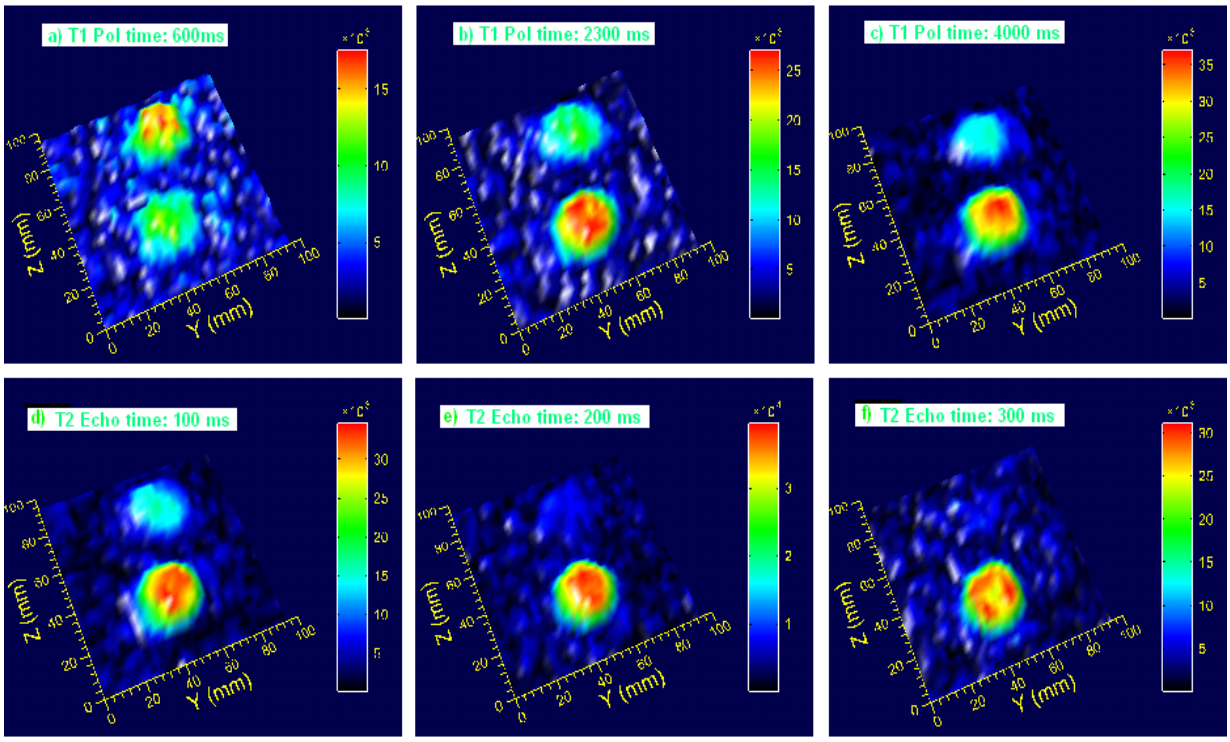

Figure 3.10 2D surface plot of Figure 3.9

There is another T_1 contrast method which is using a long polarization time and introducing a delay between the polarizing pulse and the excitation pulse. This results in the opposite type of contrast to that demonstrated above because the enhanced polarization of the short T_1 region will decay faster than that of the long T_1 region and so the short T_1 region appears darker for long delay times. At short delay times there is no contrast.

In addition, in most liquids T_1 is almost equal to T_2. So, if a liquid has a short T_2, it is more likely to have a short T_1 as well.

Furthermore, for target liquids that have short T_1 and T_2 values, T_1 contrast imaging is used to obtain positive contrast. And if the target liquid has long T_1 and T_2 values, T_2 contrast imaging is used to obtain positive contrast.

3.3 Contrast Imaging of various Concentrations of Doped Water

A sample made of two phantom tubes in which one tube filled with distilled water and the other with water doped with $CuSO_4$ of various concentrations as 250, 500, 1000, 2000, 3000, and 4000 μM was prepared. NMR experiments were run on all the samples using the optimized parameters. Figure 3.11 illustrates the Pulse and Collect macro for the two tubes: 0.25 mM doped water and the plain water. The rest of the macros are all the same as the depicted macro. FID and spectrum from all the samples were acquired and displayed in Figure 3.12 and 3.13.

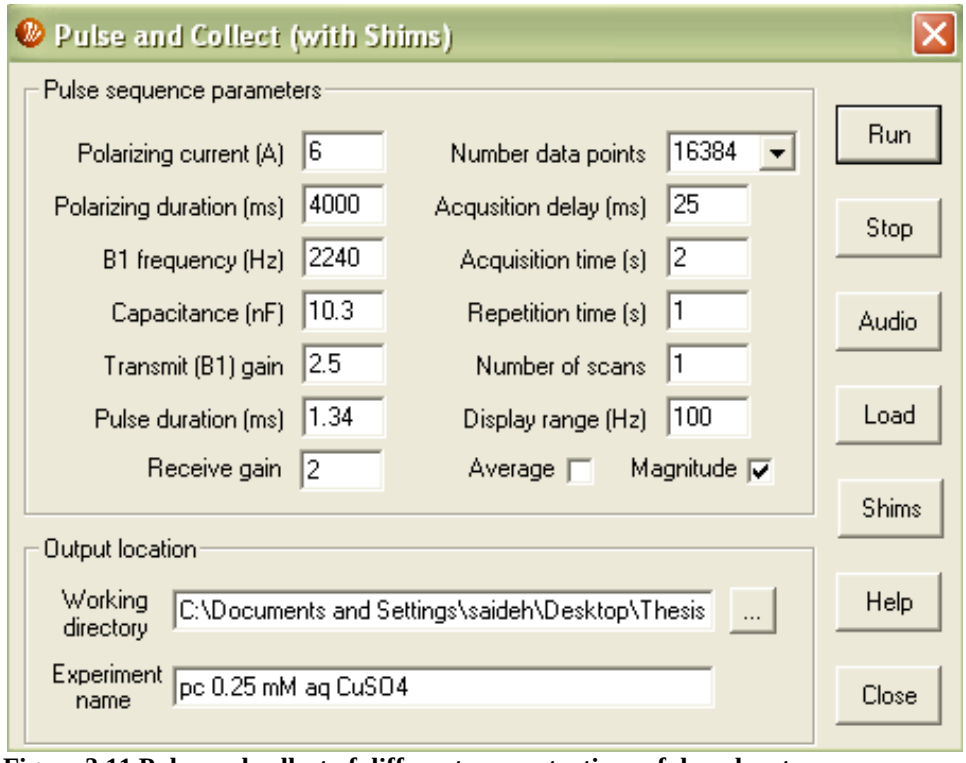

Figure 3.11 Pulse and collect of different concentrations of doped water

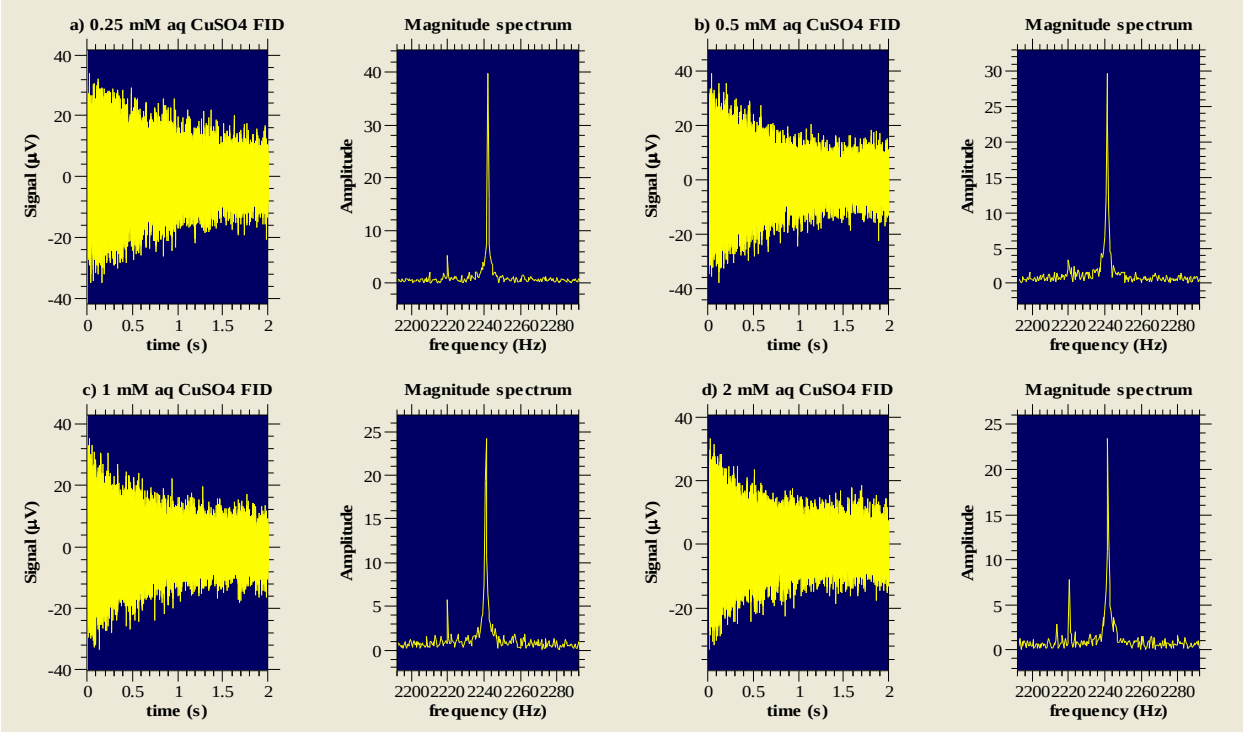

Figure 3.12 Plots of Pulse and collect of different concentrations of doped water

Table 3.3 demonstrates the obtained results from Figures 3.12 as well as parts a) and b) of Figure 3.13 within an acquisition time of 2 seconds.

Table 3.3 Signal strength of various cupric sulfate solutions

	FID (µV)	Spectrum (µV/Hz)
Figure 3.12, part a)	30	40
Figure 3.12, part b)	32	30
Figure 3.12, part c)	36	25
Figure 3.12, part d)	28	23
Figure 3.13, part a)	28	18
Figure 3.13, part b)	28	18

This means that as the concentration of doped water increases in one of the phantom tubes the spectrum amplitude decreases whereas the FID does not change much. The decrease in the spectrum amplitude is evidence of a decrease in T_2.

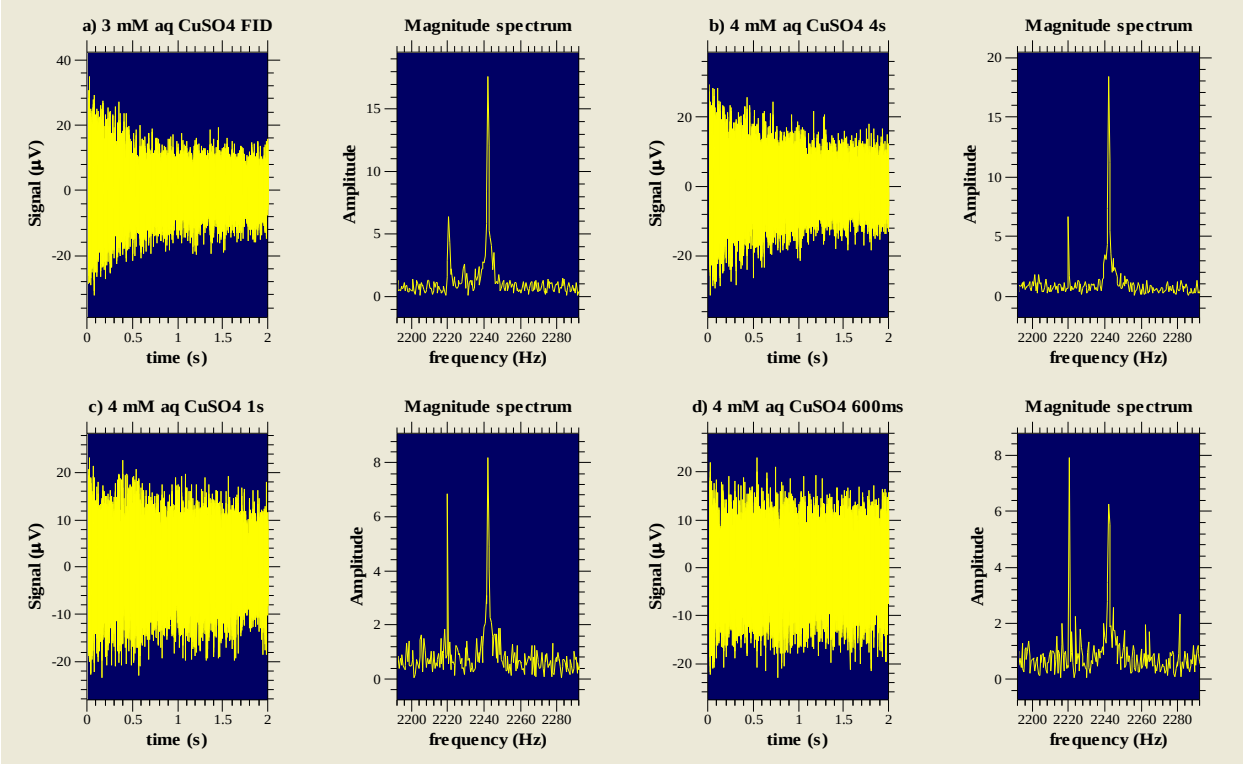

Figure 3.13 Plots of pulse and collect of different concentration of doped water

In part c) and d) of Figure 3.13, the polarization time was decreased from 4 s to 1 s and 600 ms, respectively, so the FID signals show a slight reduction in amplitude from 28 to 20 µV and lower, due to the presence of plain water tube and not the doped water tube. The corresponding spectrums show a peak at 2220 Hz which is a noise peak and the other peak at 2240 Hz being the sample peak of height 8 and 6 µV/Hz. The two spectrum amplitudes are reduced from 18 to 8 and 6 µV/Hz due to the presence of the plain water tube.

In the next set of experiments 2D SE imaging of different concentrations of doped water was done (same samples as above) as T_1 weighted imaging, and plots were obtained as shown in Figure 3.15. Figure 3.14 illustrates the macro for the 0.25 mM tube along with the plain water tube. Other macros of this set of experiments contained different polarization time according to the sample type.

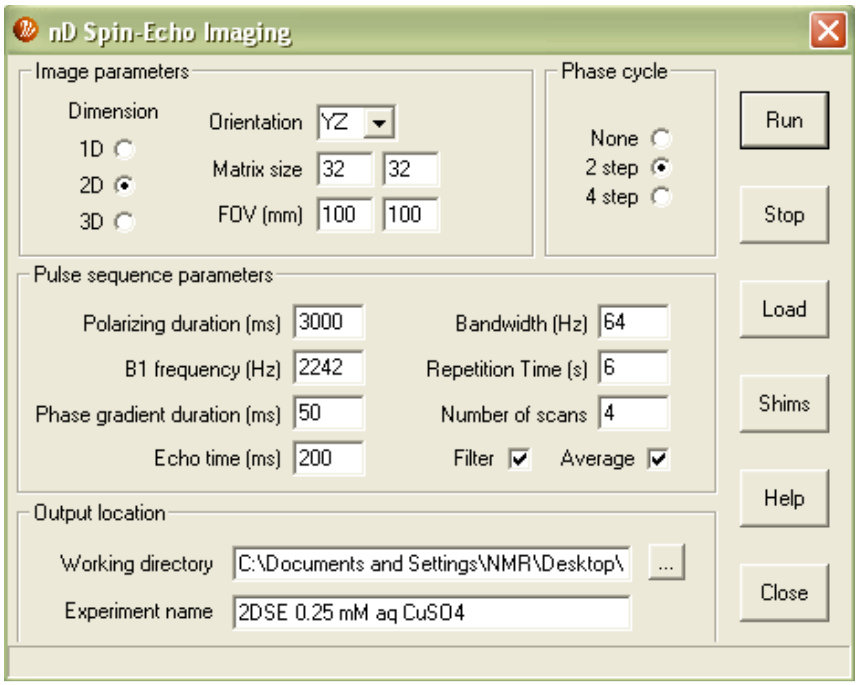

Figure 3.14 2D SE imaging macro of different concentrations of doped water

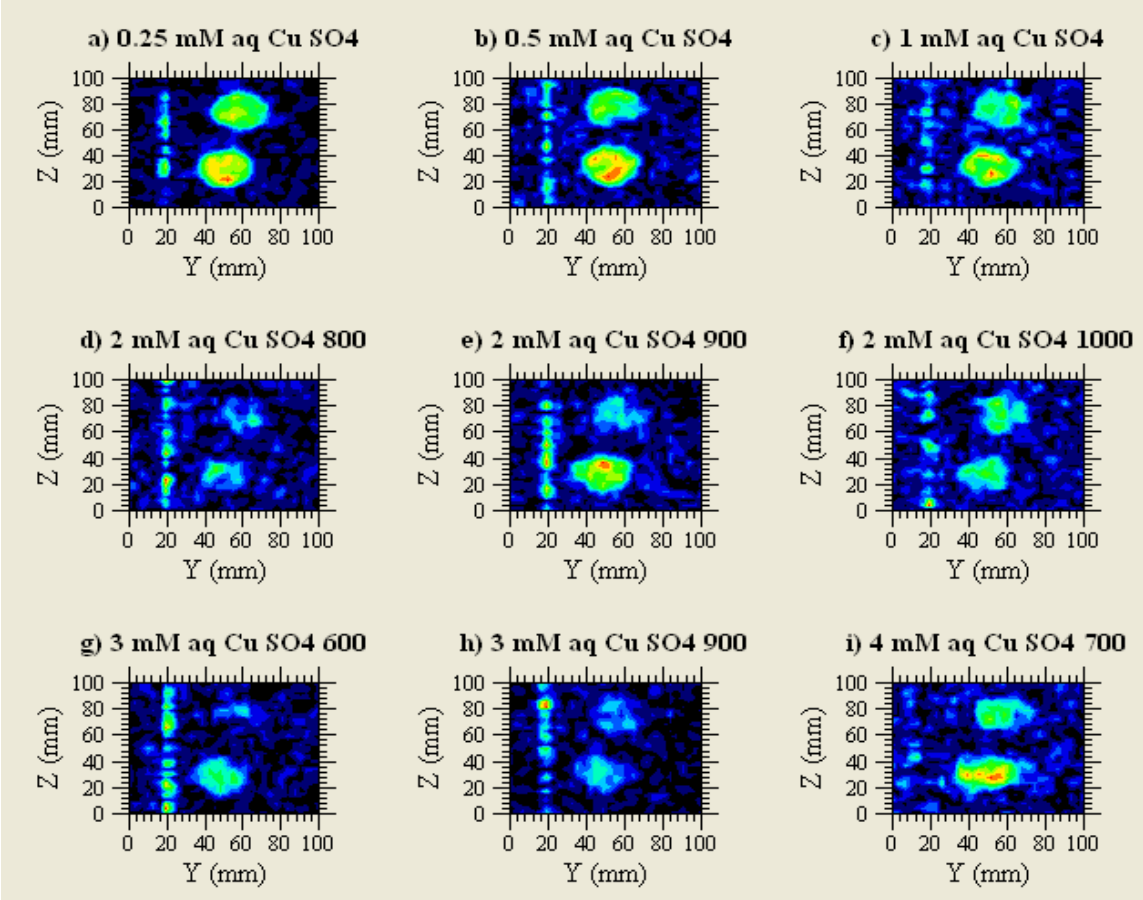

Figure 3.15 2D SE imaging plots of different concentrations of doped water

According to part a), b), and c) of Figure 3.15 as the concentration of the doped water tube increases, the corresponding images which are the bottom ones having a short T_1 values confirm an increase in signal intensity while contrast with the plain water images is visible. In parts d), e), and f) the concentration is kept the same while the polarization duration has changed from 800 to 900 and 1000 ms. Again the contrast is visible in each image while the 900 ms polarization duration is the appropriate duration to illustrate an obvious contrast in the image. In part d), the image is missing sufficient polarization duration while in part f) contrast has become less visible. In parts g) and h), contrast between the images is visible and 600 ms is sufficient polarization duration. Part f also indicates a visible contrast between the 4 mM tube and the plain water. A noise streak along the Z dimension at 20 mm in all the images is present.

Figure 3.16 demonstrates 2D SE and 3D SE acquired images of 2 phantom tubes, one filled with 3 mM doped water and the other with plain water.

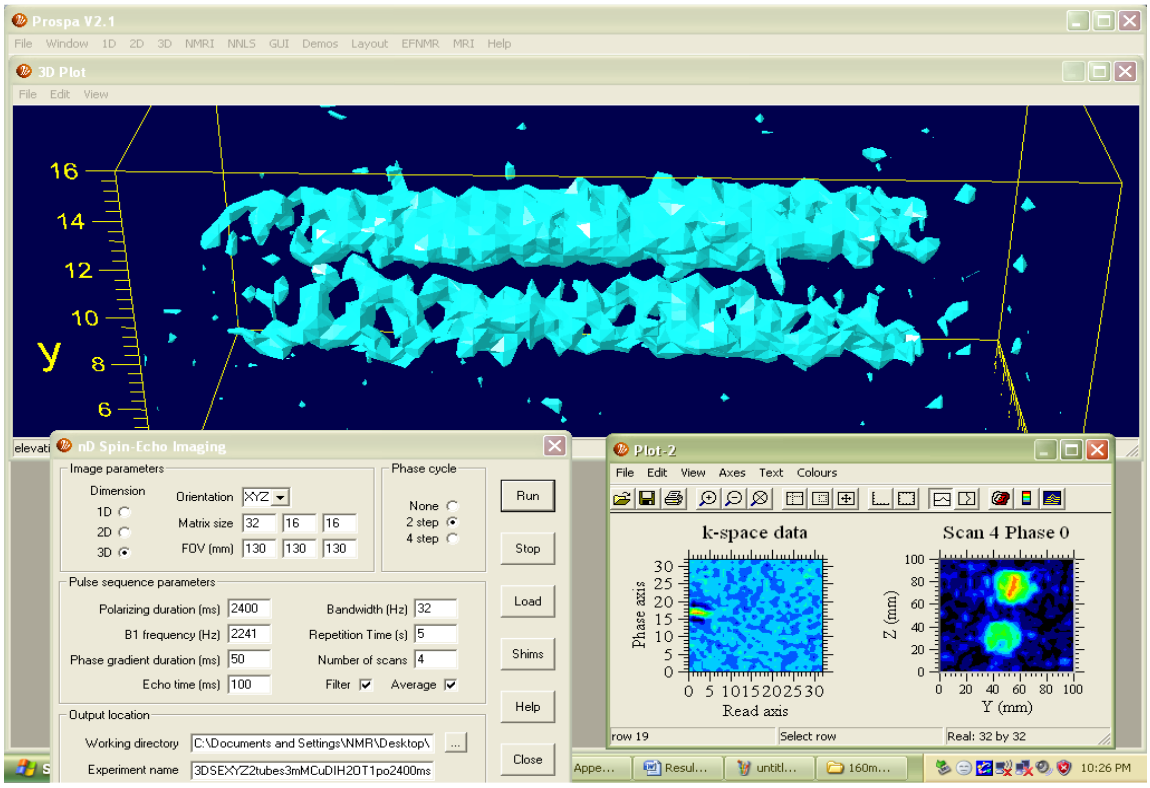

Figure 3.16 2D and 3D of 2 tubes, one filled with doped and the other with plain water

As depicted in Figure 3.16, a minimum echo time was applied to diminish any T_2 contrast. Clearly in the 2D as well as the 3D T_1 weighted imaging, the contrast is obvious for the doped water tube leading to a brighter image in the 2D case and a thicker cylinder in the 3D image. The polarization duration was neither 600 being twice the short T_1 tube nor 4000 ms being twice the long T_1 tube. Figure 3.17 illustrates the same sample, the same type of experiment, and the same parameters as above. The difference was in polarization duration being 600 ms and no filter was applied.

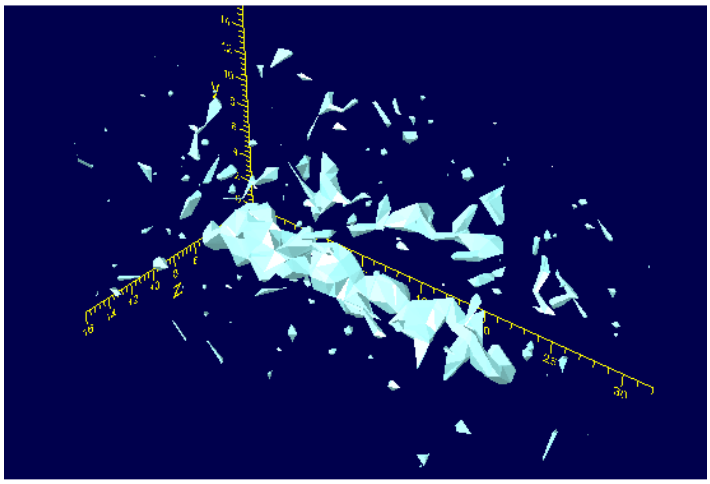

Figure 3.17 3D image of two phantom tubes: plain and 3mM

As depicted in Figure 3.17, another example of contrast for T_1 weighted imaging has been done. Since the polarization duration was short (600 ms), the nuclei in the long T_1 tube (plain water) did not get polarized enough, and so the image has appeared weak while for the short T_1 tube (3 mM doped water) the image appeared much stronger. Also, due to the absence of a filter, the image contains noise.

3.4 Contrast Imaging of Vegetables

Parsley stems and leaves were packed into a 500 ml plastic bottle. A PC was run followed by 2D SE imaging of the sample. Figures 3.18 and 3.19 demonstrate the macro and the acquired image for this sample.

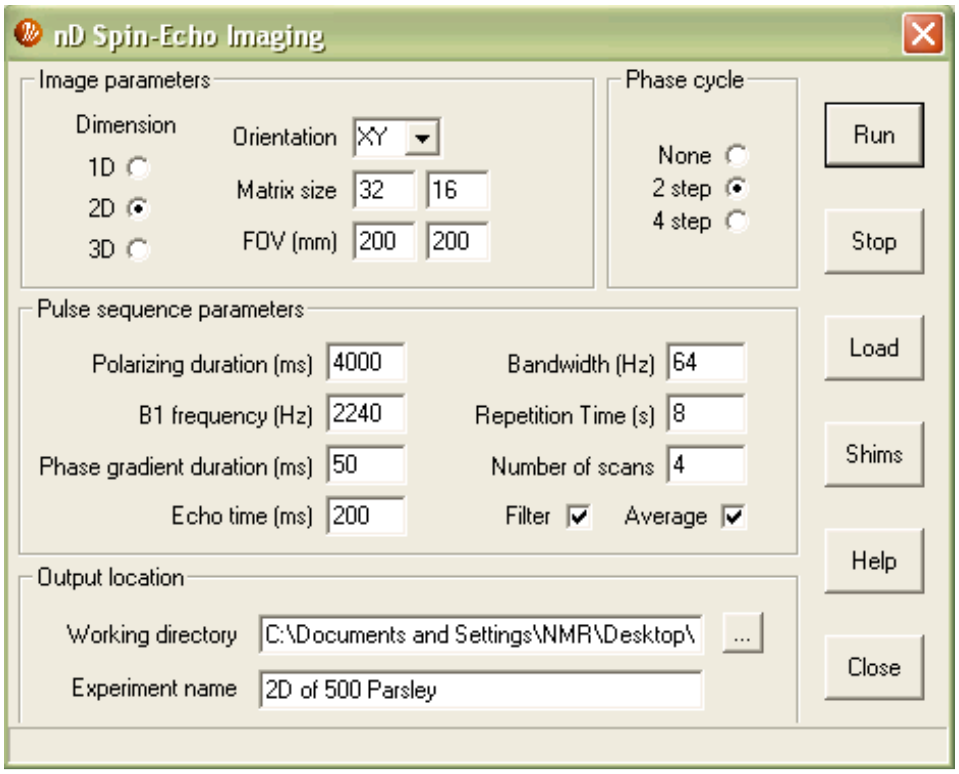

Figure 3.18 2D SE of 500 ml parsley

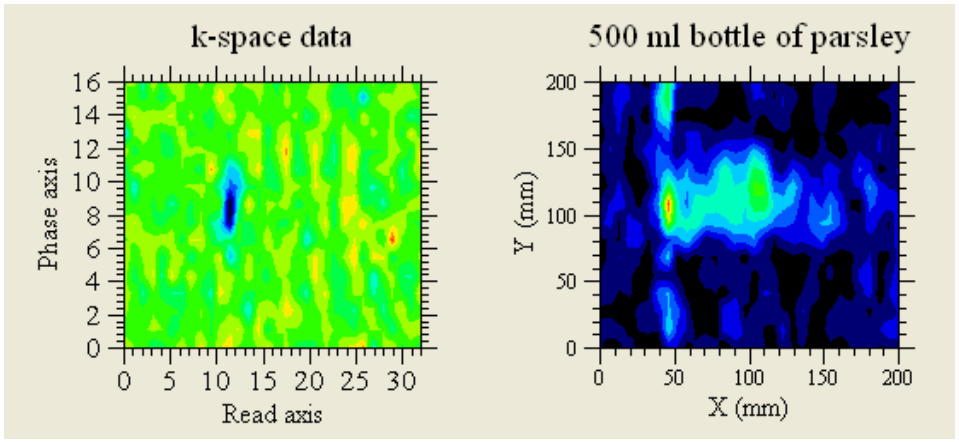

Figure 3.19 Plot of 2D SE image of 500 ml parsley

Figure 3.19 illustrates a noise streak and a brighter image in the region the stems were accumulated whereas in the region the leaves were accumulated the image is darker. This confirms the presence of more water (hydrogen nuclei) in the stems versus the leaves. Also, the obtained spectrum amplitude for this sample was very low in the range of 2 μV/Hz which proves the lack of hydrogen nuclei in this sample.

In the next experiment, imaging of two phantom tubes, one filled with parsley and the other with 3 mM doped water, was performed. The macro for this experiment is demonstrated in Figure 3.20 and the plots are presented in Figure 3.21 as an interpolated plot and in Figure 3.22 as a contour plot (available in "view" submenu of 2D plot).

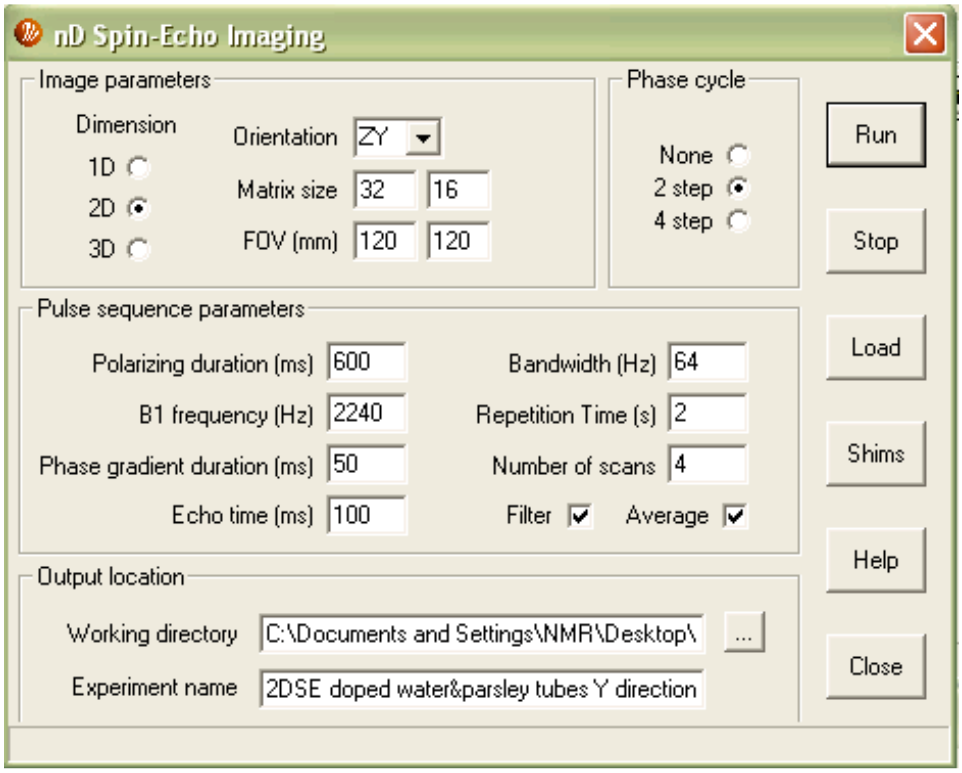

Figure 3.20 2D imaging of parsley tube versus another tube filled with doped water

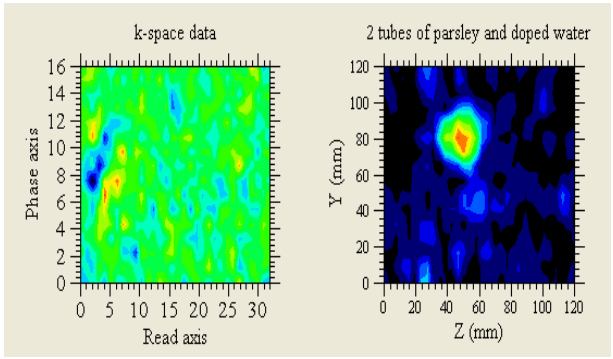

Figure 3.21 Interpolated 2D plot of parsley tube versus another tube filled with doped water

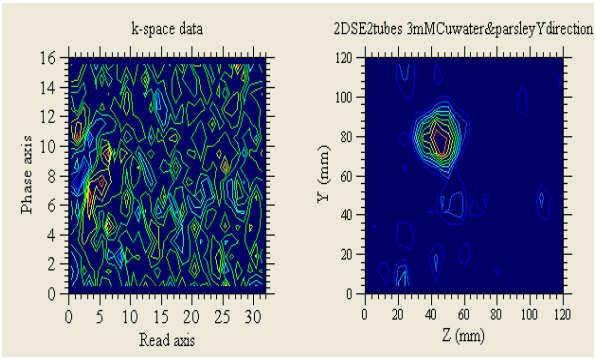

Figure 3.22 Same plot display as figure 3.21 in contour mode

As depicted on both Figures 3.21 and 3.22, the doped water tube shows a much stronger SNR and a brighter image versus the parsley tube to confirm the absence of significant amount

of water in the parsley tube. Although, the polarization duration in this experiment was 600 ms, greater polarization duration of 4000 ms would not have created a stronger image for parsley.

The next experiment was a comparison between parsley stems versus cucumber stems. Therefore, a 2D SE was run with a sample of two tubes, one filled with parsley stems and the other with cucumber stems along with polarization duration of 4 s. Figures 3.23 and 3.24 illustrate the macro and the acquired image for this experiment. In order to confirm the accuracy of this set of experiments, a second run was done. So, two magnitude images of the same sample were acquired while the orientation of the tubes has changed 180°.

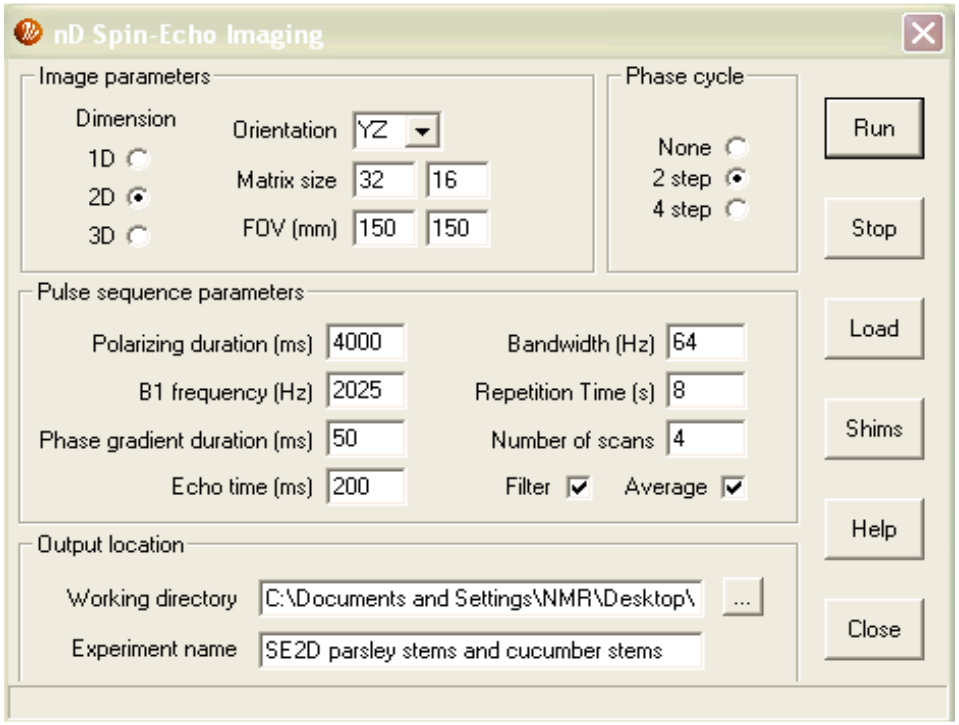

Figure 3.23 2D imaging of parsley stems versus cucumber stems

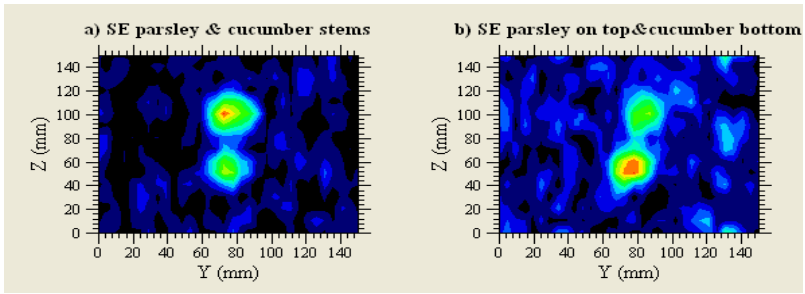

Figure 3.24 Plot of 2D imaging of parsley stems versus cucumber stems

In Figure 3.24 a) the cucumber plant is on top of the window whereas in part b) the cucumber is at the bottom. As illustrated in this figure, the region that belongs to a cucumber is brighter and has a stronger SNR. This means that cucumber plants contain significantly more water compared to parsley stems.

The last experiment of this set was a comparison between cucumber plants as a whole and parsley leaves. So, a 2D SE was run with a sample of two tubes, one filled with parsley leaves and the other with whole cucumber plants along with a polarization duration of 4 s. Figures 3.25 and 3.26 illustrate the macro and the acquired image for this experiment.

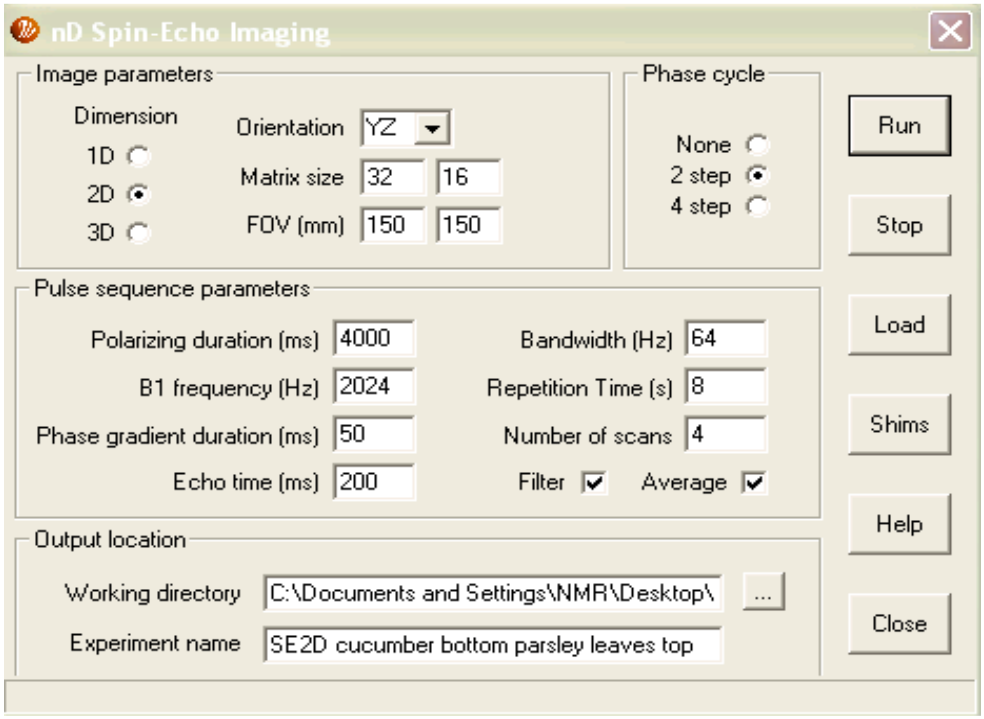

Figure 3.25 Macro for 2D imaging of two tubes: cucumber plants versus parsley leaves

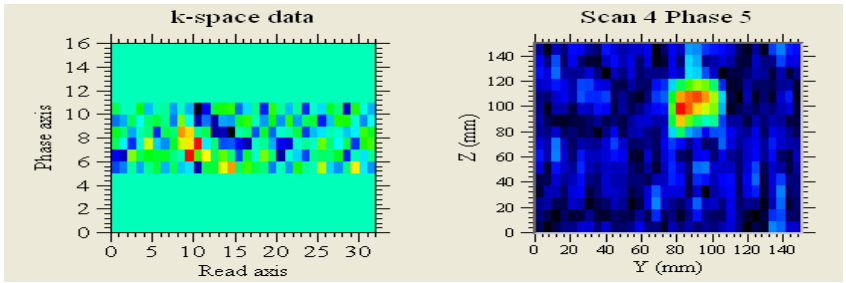

Figure 3.26 Plots of 2D imaging of cucumber plants versus parsley leaves

In this experiment the important lines of k-space were scanned, and the obtained image is equivalent to the final image. According to Figure 3.26 the only visible region belongs to the cucumber plant whereas the image of parsley leaves did not appear in the window. This experiment confirmed the accuracy of the previous experiments in which due to the absence of water in parsley leaves no image could be observed.

3.5 Contrast Imaging of plants grown in Paramagnetic Contrast Agents

This set of imaging experiments demonstrates the contrast between control plants grown in nutrient solutions versus treated plants grown in nutrient solutions doped with cupric nitrate as a paramagnetic contrast agent. As depicted in Figure 3.27, the average length of five mesquite plants grown as control mesquite was 17 cm while the average length of five plants grown as treated mesquite (nutrient solution of cupric nitrate with concentration of 0.25 mM) was 14 cm. The PC experiment was done on the sample containing one tube filled with control mesquite versus the other tube filled with the treated mesquite. The weight of each tube was 55 grams.

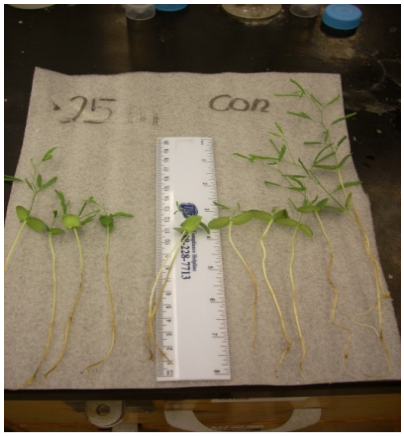

Figure 3.27 A comparison of control and treated mesquites

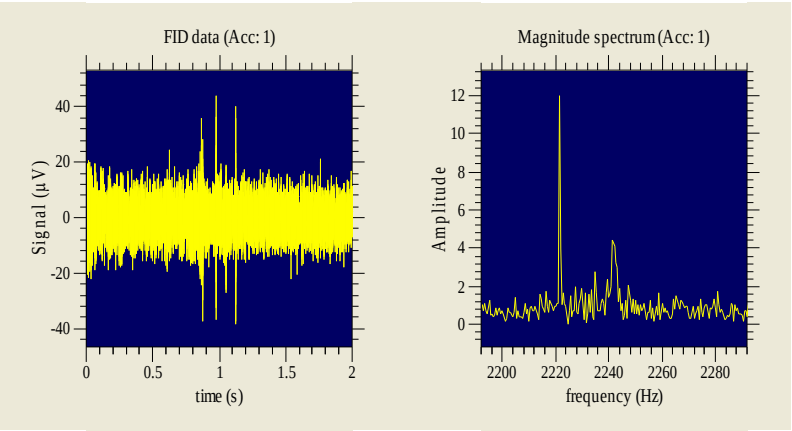

Figure 3.28Pulse and collect of 0.25 mM mesquite

As depicted in Figure 3.28, the FID and the spectrum signals obtained for this sample is very weak. There is a noise peak at 2220 Hz and the sample peak is at 2240 Hz meaning that in general the SNR for either a 500 ml sample or two phantom tubes of mesquite is weak.

Figure 3.29 is the macro for 2D SE imaging of this sample with polarization time of 600 ms followed by its plot in Figure 3.30 as well as the second plot for the same sample and experiment with 800 ms polarization time.

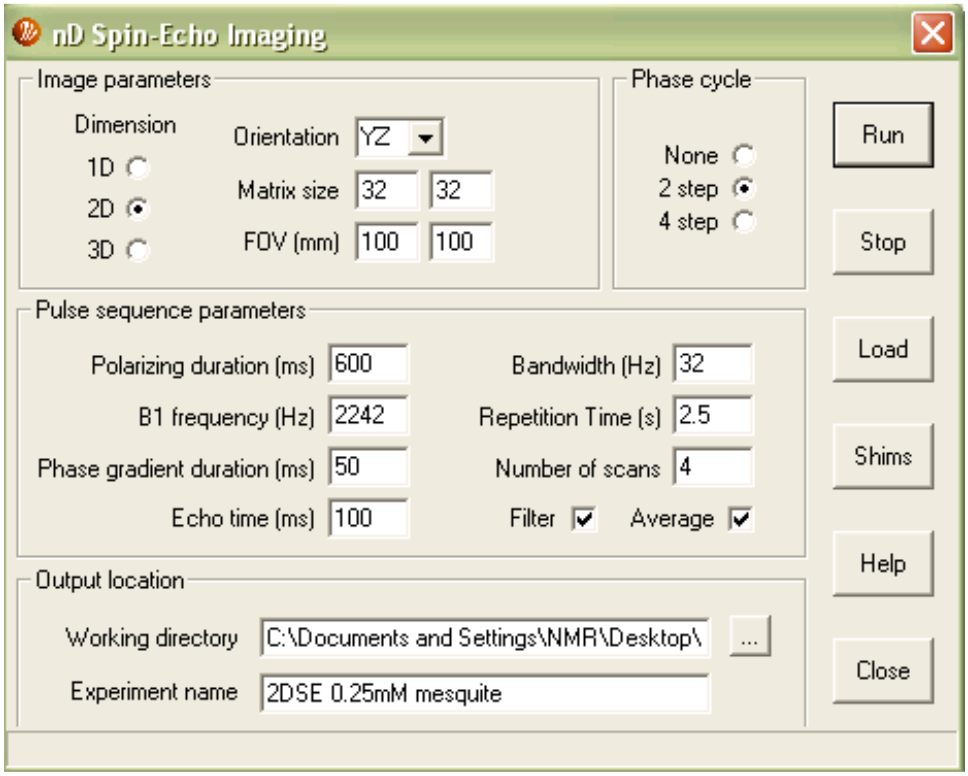

Figure 3.29 2D SE imaging of 0.25 mM mesquite versus control

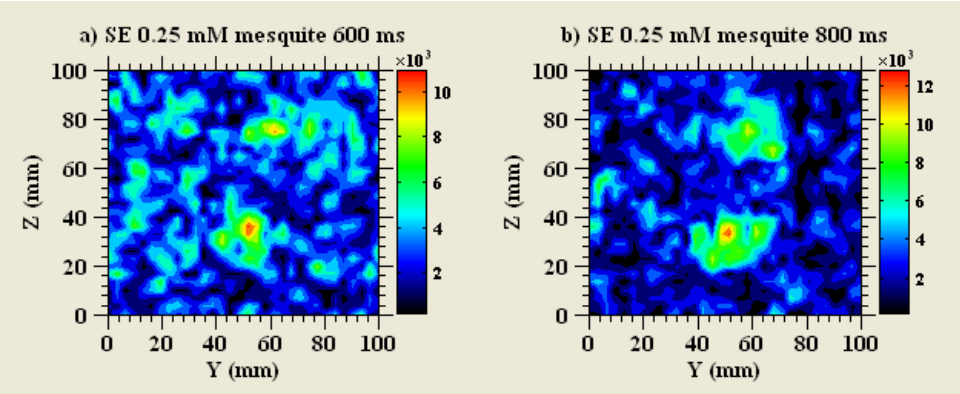

Figure 3.30 2D SE plots, 0.25 mM mesquite versus control (600 and 800 ms polarization time)

In both windows of Figure 3.30, the image of the treated plant is illustrated at the bottom of the window while the actual treated plant tube inside the probe was oriented at top. By applying polarization times of 600 and 800 ms the contrast between the controls versus the

treated plants is visible. This proves that plants grown in solution doped with paramagnetic contrasting agents do absorb copper and this absorption could be confirmed by contrast imaging techniques via EFMRI.

The following set of images was the first trial for soybean experiments which demonstrates the difference between control plants grown in nutrient solutions versus treated plants grown in nutrient solutions doped with cupric nitrate as a contrast agent. Prior to imaging PC was run on each sample. Table 3.4 demonstrates the acquired spectrum amplitude for parts a), b), c), and d) of Figure 3.32. The polarization duration for all the performed experiments was 600 ms except for part d) which was 1 s.

Table 3.4 EFNMR signals of soybean samples

Figure 3.32	Spectrum amplitude (μV/Hz)
part a)	3.5
part b)	4
part c)	6
part d)	7

For all parts of Figure 3.32, the sample contained two phantom tubes. In part a), one tube filled with treated soybean leaves grown in 2 mM cupric nitrate nutrient solution, and the other tube filled with treated soybean leaves grown in 4 mM cupric nitrate nutrient solution. In part b), one tube was filled with treated soybean stems grown in 0.5 mM cupric nitrate nutrient solution, and the other tube filled with control soybean stems. In part c), one tube was filled with combined treated soybean leaves and roots grown in 0.5 mM nutrient solution, and the other tube filled with combined control soybean leaves and roots. In part d), one tube was filled with treated soybean stems grown in 0.5 mM cupric nitrate nutrient solution, and the other tube filled with control soybean stems by applying polarization duration of 1 s. In part e), the same sample was used as in part d) with polarization duration of 600 ms. Part f) is the same image as part e); only in different color mode (spectrum color mode under “color” submenu of 2D plot).

Figure 3.31 demonstrates the macro for part a) of this set of experiment, and Figure 3.32 illustrates the acquired images for different soybean experiments.

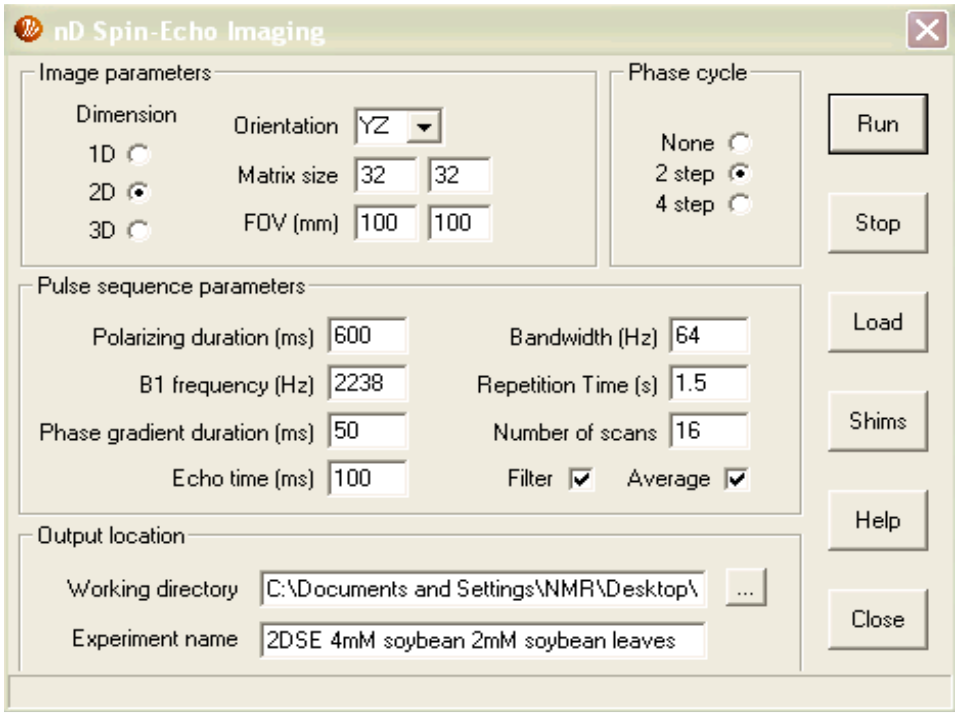

Figure 3.31 2D SE imaging of 4mM and 2mM soybean leaves

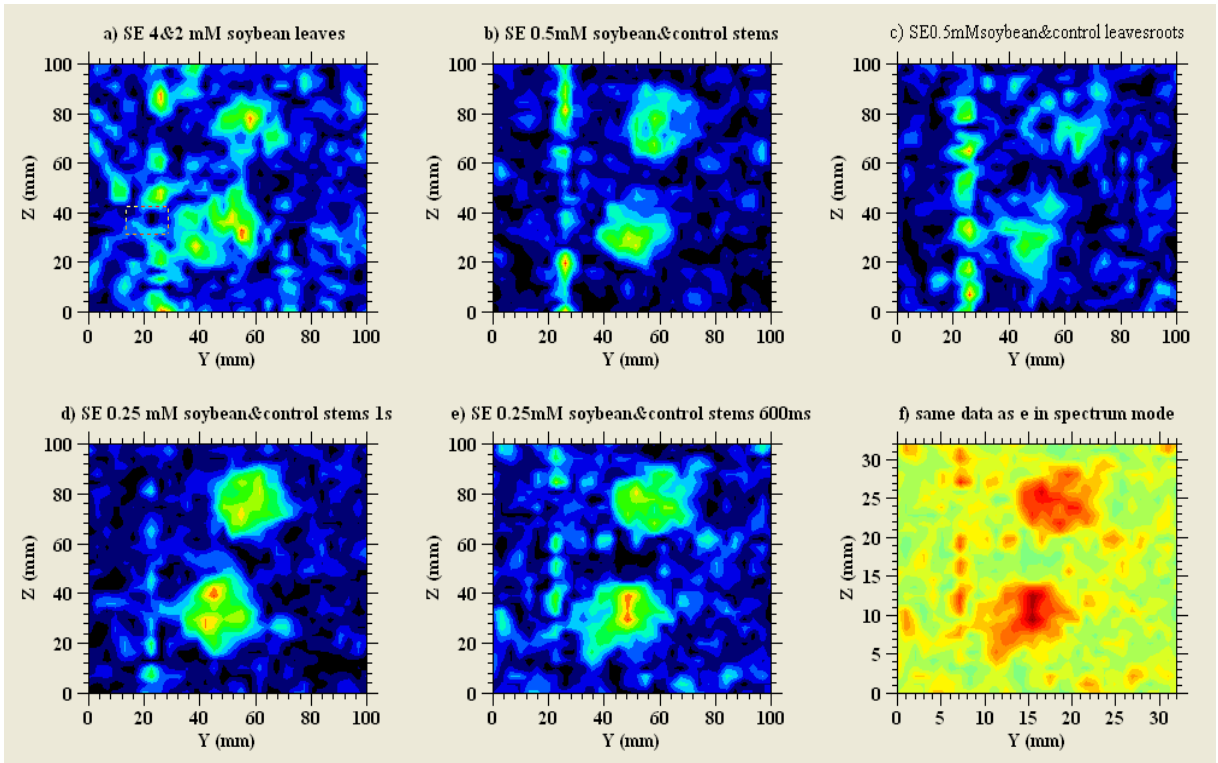

Figure 3.32 Plots of 2D SE imaging of soybean

As illustrated in part a) of Figure 3.32, the bottom region corresponding to the 4 mM sample posses a stronger SNR, and so a brighter image was obtained compared to the tube containing the 2 mM sample located on top of the image. The 4 mM sample is the short T_1 region compared to the 2 mM sample. In part b) of Figure 3.32, the bottom image corresponds to the treated soybean stems and is brighter compared to the control sample located on the top of the window. In part c), again the bottom region containing the treated roots and leaves showed a brighter image indicating that the treated sample contained copper and is the short T_1 region. In part d) the bottom region contained the treated sample and is brighter compared to the control tube located on top. The polarization time is 1s indicating a good polarized sample, and so a good SNR is obtained in both regions. Part e) demonstrates that even with lower polarization duration a good contrast was obtained. Therefore in all the experiments, the bottom regions of the windows, confirms the presence of copper proving that soybean plant up took copper since these regions appeared brighter indicating the short T_1 region. In all windows there is a streak of noise at 20 mm along the Z direction.

The following set of images was the last trial for soybean experiments which demonstrates the difference between control plants grown in nutrient solutions versus treated plants grown in nutrient solutions doped with cupric nitrate. As depicted in Figure 3.33, the average length of five plants grown as control soybean was 28.5 cm while the average length of five plants grown as treated soybean (nutrient solution with concentration of 0.25 mM cupric nitrate) was 26 cm. The PC experiment was run on the sample containing one tube filled with control soybean versus the other tube filled with the treated soybeans (35 grams each).

Figure 3.33 A comparison of control and treated mesquites

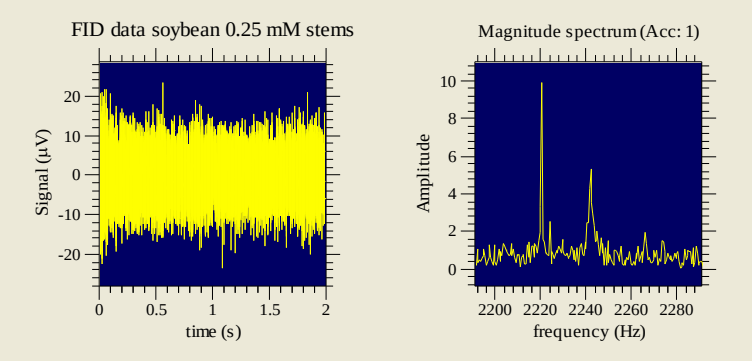

Figure 3.34 Pulse and collect of 0.25 mM Soybean

For all parts of Figure 3.36, the sample contained two phantom tubes; one tube full of treated soybean stems grown in 0.25 mM cupric nitrate nutrient solution, and the other tube full of control soybean stems. The only variant was polarization duration as depicted on Table 3.5.

Table 3.5 Various Polarization Duration for the soybean sample

Figure 3.36	Polarization duration (ms)
Part a)	600
Part b)	1000
Part c)	2000
Part d)	4000

Figure 3.35 demonstrates the macro for part a) of this set of experiment, and Figure 3.36 illustrates the acquired images for different soybean experiments.

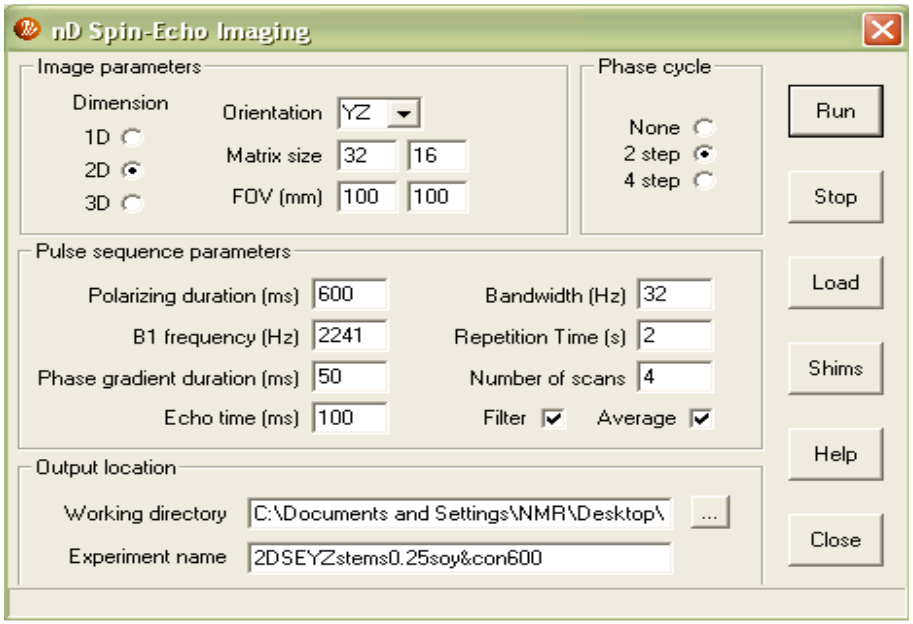

Figure 3.35 2D SE imaging of 0.25 mM Soybean versus control

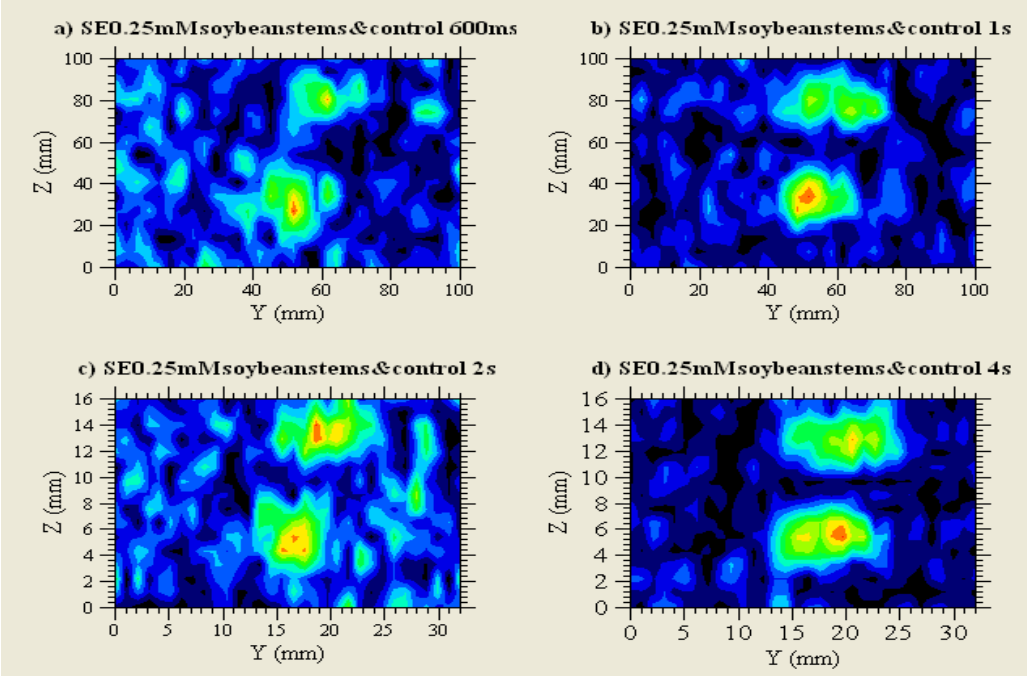

Figure 3.36 Plots of SE images of 0.25 mM Soybean versus control (different B_p durations)

As depicted in Figure 3.36, all cases clearly confirm the difference between the control tubes versus the treated ones. Again the treated plants were the short T_1 regions located at the bottom of the window. Also, it was proven that paramagnetic contrasting agents such as copper salts absorbed by soybean or mesquite plants could enhance SNR to create a brighter image.

3.6 Imaging of Vegetables Immersed in Solutions of Contrast Agents

This set of images demonstrates the difference between control vegetables immersed in water versus treated ones immersed in solutions doped with cupric nitrate as the contrast agent.

PC experiments were run on the sample containing one tube filled with celery immersed in water versus the other tube filled with celery immersed in 4 mM cupric sulfate solution for one day and for the next experiment for one day plus 6 hours. The amplitude of the acquired spectrums was 18 μV/Hz for part a) of Figure 3.38 while for part b) it was 12 μV/Hz. The average weight of each tube was 45 grams. Figure 3.37 illustrates the macro for this experiment and the corresponding plots are presented in Figure 3.38.

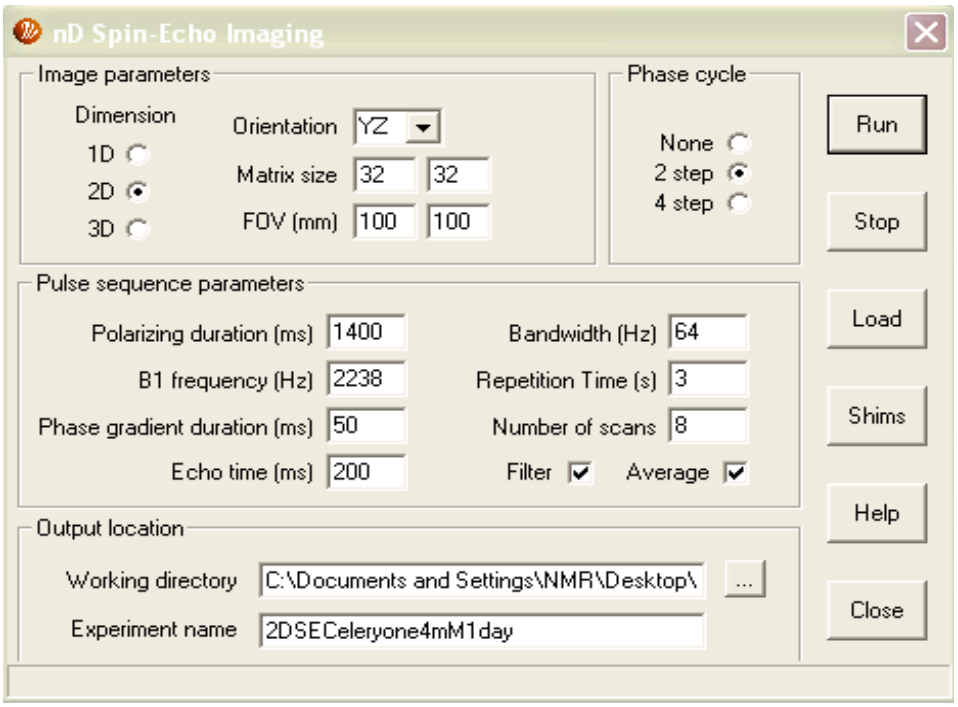

Figure 3.37 2D SE imaging of celery doped with 4 mM $CuSO_4$ for one day

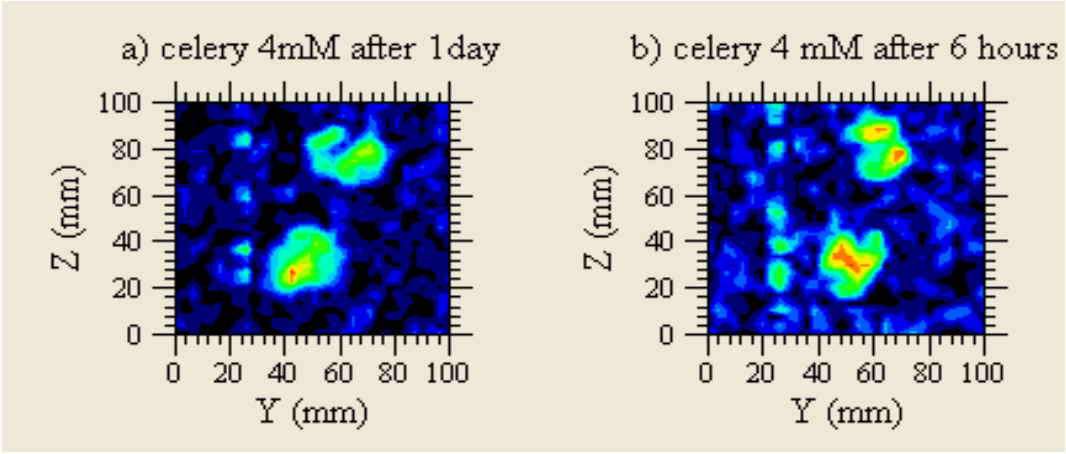

Figure 3.38 Plots of 2D imaging of celery doped with 4 mM $CuSO_4$ for one day and six hours

Parts a) and b) of Figure 3.38 demonstrates the brighter images located at the bottom of the window (compared to the control celeries located on top) of celery sticks treated with 4 mM $CuSO_4$ solution. Therefore, celery also absorbs copper through passive transport and could be used to demonstrate contrast imaging via EFMRI.

Finally in the last set of experiments, PC and imaging were run on three set of parsley samples. One sample contained one tube filled with parsley immersed in water versus the other

tube filled with parsley immersed in 3 mM cupric sulfate solution for six hours (part c of Figure 3.40). For the second experiment the same sample was kept in a refrigerator for one day (part a of Figure 3.40). Also, the only difference between part a) and b) of Figure 3.40 was the polarization duration of 600 and 1000 ms. For the third sample, one tube was filled with parsley immersed in water versus the other tube filled with parsley immersed in 0.5 mM cupric sulfate solution for 20 hours (part d of Figure 3.40). The amplitude of the acquired spectrums for parts a) and b) of Figure 3.40 was 7.5 µV/Hz and 6.5 µV/Hz respectively. The average weight of each tube was 35 grams. Figure 3.39 illustrates the macro for this experiment and the corresponding plots are presented in Figure 3.40.

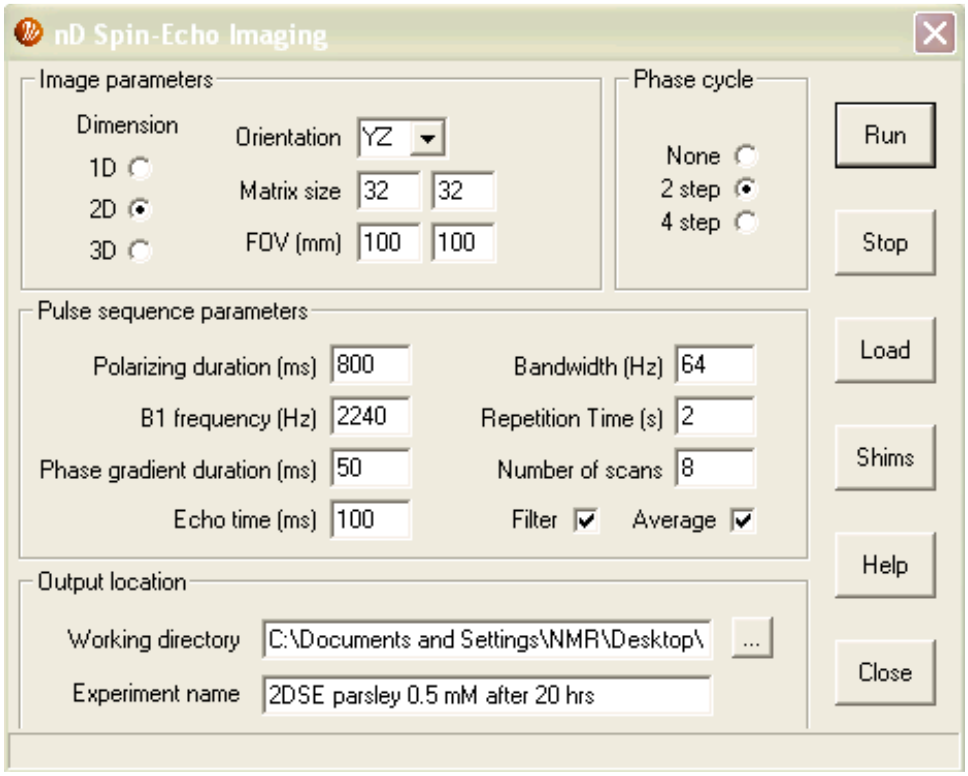

Figure 3.39 2D SE imaging of parsley kept in 0.5 mM of CuSO4 for 20 hours

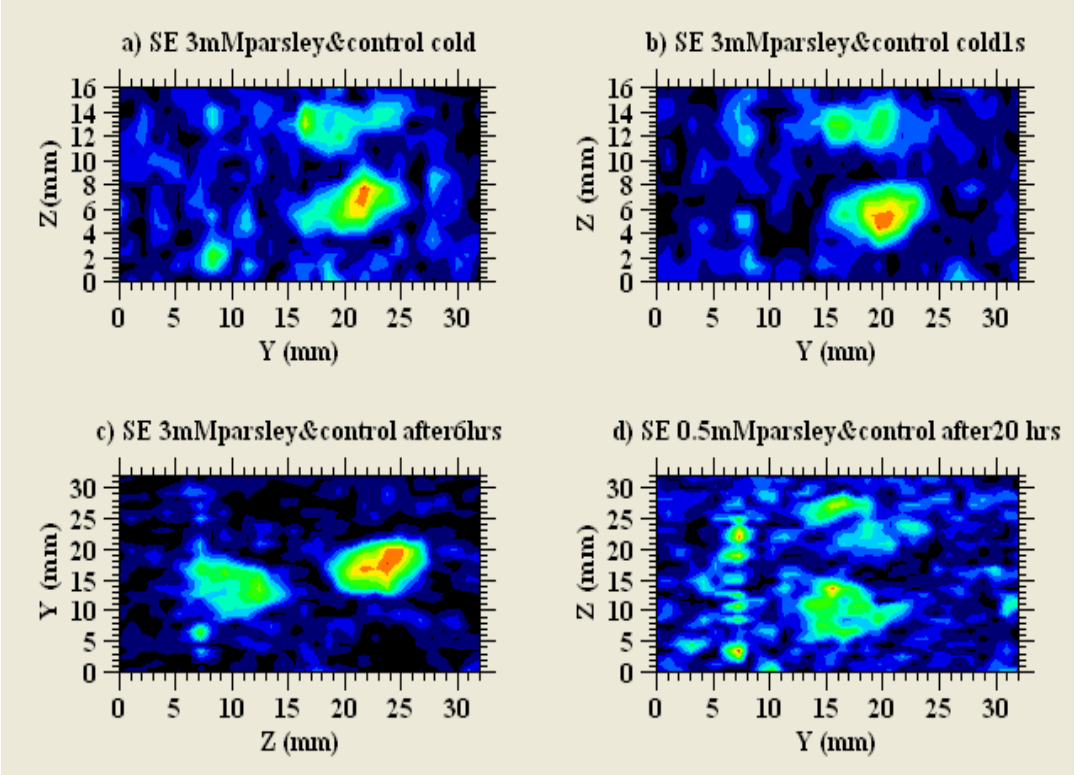

Figure 3.40 Plot of 2D image of parsley kept in 0.5 mM Cu for 20 hours and 3mM for 6 hours

In Figure 3.40, the bottom region of the window corresponds to the treated parsley while the top is the control. Also, in part c) of Figure 3.40, the right region corresponds to the treated parsley. As depicted in part a) and b) of Figure 3.40, by applying polarization durations of 600 and 1000 ms to the cold sample, an enhancement in signal is observed in both cases. In part c), the orientation is in ZY plane and is different than other parts, but the contrast is clear. Finally, in part d) again contrast is observed. Although the FID and the spectrum signals intensity were low as depicted in most cases, it was possible to acquire a reasonable contrast image in all experiments.

CHAPTER IV (CONCLUSION)

Although the Magritek Corporation demonstrated that the EFMRI instrument is capable of recording T_1 and T_2 weighted images as well as the application of paramagnetic contrast agents in solution, this work demonstrates that not only can EFMRI image a moisture difference in plants but that copper as a paramagnetic contrast agent can enhance the water signal in plant tissues and hence, copper uptake by plants can be monitored.

In the course of demonstrating that EFMRI can be used to image copper update by plants, several new observations were made. First, both mesquite and soybean seedlings formed precipitates from cupric sulfate but not much from cupric nitrate solutions. Second, although mesquite is reported to be a hyper-accumulator of copper in their natural environment, under hydroponic conditions most plants could not survive growing in copper (II) solutions with a concentration above 0.5 mM. Third, plants grown in treated solutions appeared smaller in size and shorter in length relative to the plants grown in control solutions. Fourth, the uptake of copper as paramagnetic contrast agent was observed by EFMRI for both plants grown in nutrient solution and cut vegetables immersed in cupric sulfate solution.

This technique has the advantage of probing the plant absorption of copper without destroying the plant. Furthermore, in comparison with other techniques like Inductively Coupled Plasma Atomic Emission Spectroscopy (ICP-AES[1]), it takes less sample preparation and is less time consuming since ICP-AES requires plant separation into roots, stems, and leaves, drying of

[1] ICP-AES is an analytical technique used for detecting trace metals. It is a type of emission spectroscopy that uses the inductively coupled plasma to produce excited atoms and ions that emit electromagnetic radiation at wavelengths characteristic to a particular element. The intensity of the emission indicates the concentration of the element within the sample.

the obtained plant parts, and microwave acid digestion (EPA 3051 method). Nevertheless, both techniques could be used to demonstrate the presence or absence of copper in plants.

The hypothesis of this research was that regions of the plant with more copper should have an enhanced NMR signal using copper as a paramagnetic MRI contrast agent. Although the technique can be well illustrated with solutions of known copper concentrations, it has been more difficult to demonstrate in hyper-accumulating plants such as mesquite and soybean. Different polarization duration and echo time were approximated since it was not possible to measure T_1 and T_2 values for all plant samples due to low signal. For example, it was not possible to get a signal from 30 grams of cilantro. Hence, negative contrast was sometimes observed, which could be due to incorrectly set parameters or too much contrast agent (Magritek, Terranova-MRI Student Guide 2006). Individual plants could not be imaged due to the low resolution of the EFMRI instrument. It was not possible to resolve the presence of copper in different parts of the plants (roots, stems, leaves). The signal intensity was not correlated to the amount of copper in either solution or in plant tissues, which would require measurements with other techniques like ICP-AES. Yet the goal of this research, which was visualizing the uptake of copper by plants to aid phyto-remediation research, was partially achieved.

Therefore, in order to confirm and improve this technique, it is suggested to use a high resolution commercial MRI or possibly a high field NMR to be able to resolve the uptake of copper in different plant parts such as roots, stems, and leaves with less amount of sample and at different stages of plant growth. Furthermore, in future studies a way must be found to correlate the NMR signal intensity to the concentration of accumulated copper inside the plants and by using another technique such as ICP-AES to interpret different signal intensities.

APPENDIX A

A.1 Instrument Setup

The first requirement for running an EFNMR experiment is to choose a suitable location in order to acquire a strong signal. The probe must be at least a few meters away from any ferrous object (to eliminate magnetic field in-homogeneity that would result from their presence) or any source of low frequency electrical noise including the computer and the spectrometer plus all the wires accompanying them. Not only the location but also the orientation of the probe is of great concern due to their effects on the noise magnitude. A compass as well as a Magnaprobe are used to orient the probe properly so that its longitudinal (X) axis is orthogonal to the Z direction of the probe which is also the Earth's field direction (the blue arrow on the side of the probe). This will optimize the 90° and 180° pulses as well as imaging. Therefore, the arrow on the probe, indicating the axis of the Z-imaging gradient, should be directed along the Earth's field axis via using a Magnaprobe. Next, the system must be connected properly and the Prospa software should be installed on the computer. Also, experiments are run from dialog windows (also called macros or GUIs standing for Graphic User Inter-phase) which allow the user to control an experiment by choosing values for different parameters. The Prospa window contains a list of menus each explained on pages 2-3and2-4 of the USER MANUAL. The EFNMR and MRI menus are covered in the USER MANUAL and STUDENT GUIDE while the Prospa program features are explained in the PROSPA MANUAL.

A.2 Preliminary Experiments

At this point basic experiments (under EFNMR menu) are run to evaluate the system as well as the chosen location.

A.2.1 Analyzing B_1 Coil

In order to coarsely tune the B_1 transmit/receive coil by applying an impulse to the B_1 coil and detecting the response so that the system can be tuned to the resonant frequency of the nuclei, Analyze Coil is run (Figure A.1). The B_1 coil and the spectrometer create a parallel circuit in which the coil is an inductor with an inductance, L, and a resistance, R, connected in parallel to a capacitance, C, within the spectrometer. When the system is in detection or receive mode, this circuit is used to detect the signal. The circuit resonates at a frequency according to Equation A.1. The coil L and C is used to determine the frequency at which the coil resonates which is designated as ω_0.

Equation A.1: $$\omega_0 = \frac{1}{\sqrt{LC}}$$

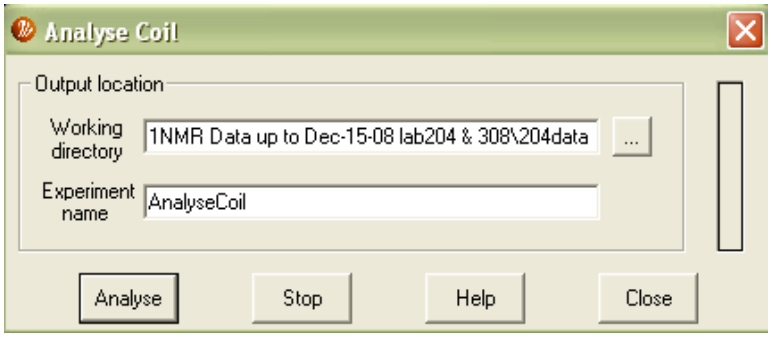

Figure A.1 Analyzing Coil

This procedure is repeated over a range of capacitance values to determine the parameters of the coil (L and R). At each value of capacitance (C), the resonance response is measured as a function of time (Figure A.2, first plot). The time domain signal is Fourier transformed to produce the frequency domain plot (Figure A.2, second plot). A plot of resonant frequency for the LCR circuit as a function of capacitance (Figure A.2, third plot) could be used to estimate the capacitance of the coil. Also by using Equation A.1 the coil capacitance for resonance at Larmor frequency could be calculated as follow: $\omega = \frac{1}{\sqrt{LC}} \Rightarrow C = \frac{1}{\omega^2 \cdot L} = \frac{1}{(2\pi \times 2230\ \text{Hz})^2 \times 0.5\ \text{H}} = 9.6\text{nF}$

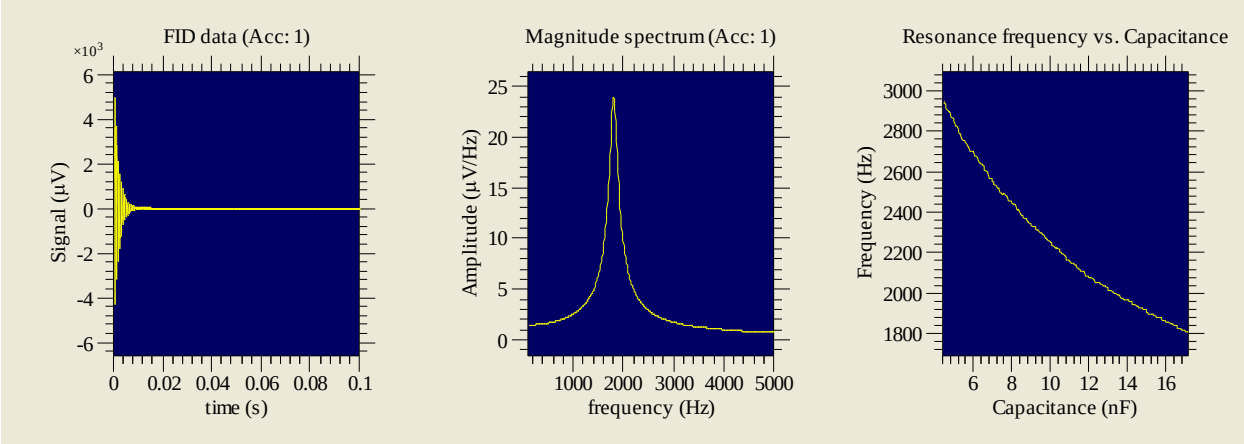

Figure A.2 Plots of Analyzing Coil

A.2.2 Monitoring Noise

The next step is measuring the external noise detected by the B_1 coil. The noise level is environmentally sensitive and is dependent on the location and orientation of the probe. By selecting the Monitor Noise experiment (Figure A.3) data are acquired in the absence of any NMR signal excitation and so only noise level is recorded.

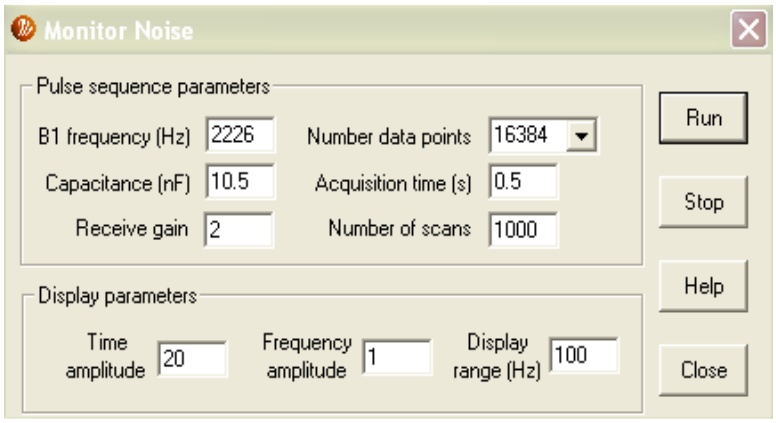

Figure A.3 Monitoring Noise

Any root-mean-square (RMS located on top of the time domain data, Figure A.4) value below 10 µV is acceptable; a noise level less than 5 µV is good (a spectrum with 150 µV/Hz was acquired with 5.4 µV noise level) while a noise level less than 3 µV is ideal. Noise levels above 10 µV makes acquiring NMR signals challenging and MRI is impossible. So upon having high noise levels the location should be changed.

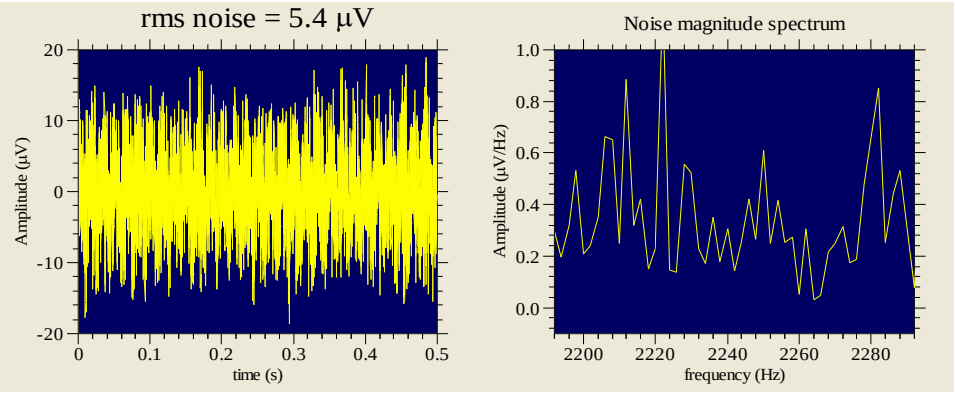

Figure A.4 Plots of Monitoring Noise

A.2.3 Signal Acquisition (Pulse and Collect Experiment, PC)

The next step is obtaining a free induction decay (FID). Acquiring the first FID through the application of a Pulse and Collect experiment (PC) to set up the system parameters is very time consuming and requires a great deal of trial and error. By applying a polarization pulse (Figure A.5), an enhanced bulk nuclear magnetization in the sample oriented in the Earth's field direction is established. After polarizing the sample via B_p, the net magnetization vector precessing at the Larmor frequency (ω) about the Earth's magnetic field (B_e) according to the Larmor Equation A.2 is rotated into the transverse plane by a RF excitation pulse (also called 90° pulse or B_1 pulse), and it precesses about the Earth's field direction and produces an induced electro motive force (emf) in the detection coil.

Equation A.2: $$\omega = \gamma \cdot B_e$$

The induced electromotive force in the detection coil is measured as a voltage and that is the signal displayed in the time domain window as free induction decay (FID). The magnitude of the induced emf (the NMR signal) is proportional to the magnitude of the net magnetization in the transverse plane which is in turn dependent on the net magnetization established in the sample by the polarization pulse. So the NMR signal intensity depends on polarization current and duration. The relationship between the signal and polarizing pulse duration (T_p) is

exponential (not linear) due to T_1 relaxation as follows: $1 - \exp\ (-Tp/T_1)$.

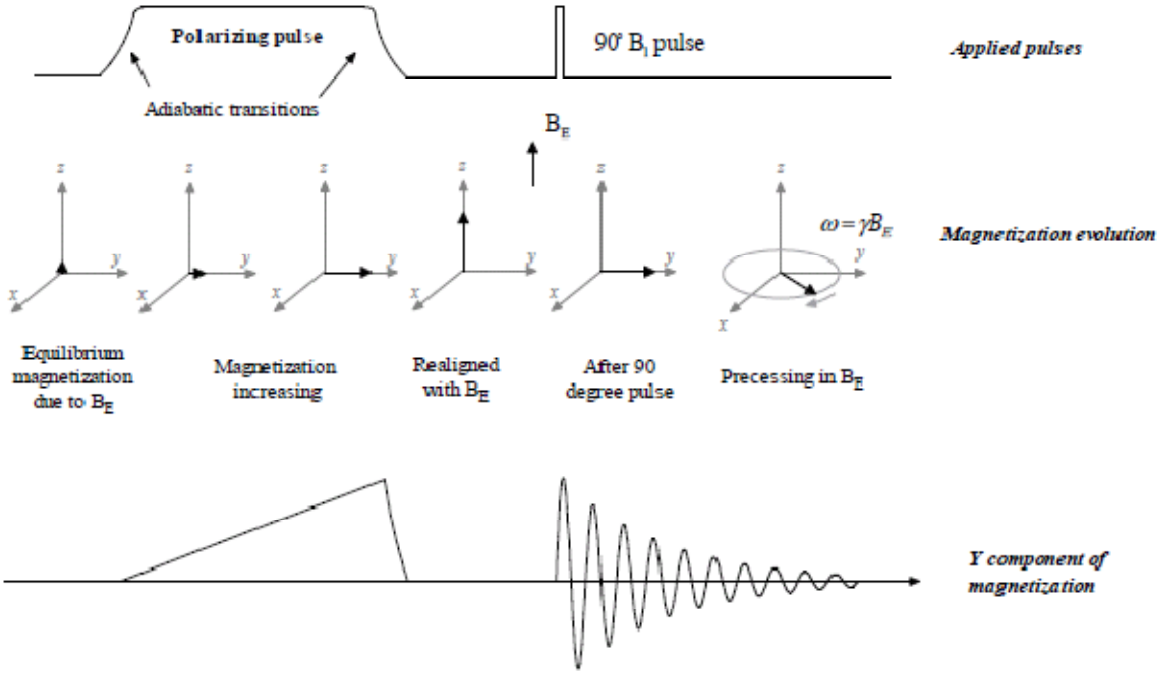

Figure A.5 The pulse sequence diagram for pulse and collect experiment (Magritek, Terranova-MRI User Manual 2005)

FID is an exponentially decaying sinusoidal signal and after Fourier transform is converted to a spectrum (a strong narrow peak). Averaging FIDs increases the SNR by coherently adding the signal and incoherently adding the random noise. The SNR can be estimated upon dividing the FID peak at the beginning by the FID peak at the end of the signal. Also, the SNR improvement equals the square root of the number of accumulated scans. For example if an experiment is repeated 16 times, the SNR improves by a factor of four. In general, adjusting sample size, back ground noise, probe tuning, B_1 pulse duration optimization, polarization length, and sample position improve SNR. In the frequency domain, the field homogeneity increases SNR, and this can be optimized by shimming.

Most of the FID window should contain signal not noise. Usually noise peaks are narrow while sample peaks have a width depending on the rate of decay of the FID. The faster the FID

decays, 10s to 100s of ms, the broader the peak is. Again ferrous objects disrupt the local Earth's magnetic field which causes a faster decay of the FID. One good way to check whether a peak is an NMR signal or noise is to acquire a signal in the presence of the sample and compare it with a signal in the absence of the sample. If the peak is an NMR peak, it will disappear when the experiment is done with the sample removed. And if it is a noise peak, it will not change in the absence of the sample.

Various parameters as listed on Figure A.6 control signal acquisition including: number of data points, acquisition time, acquisition delay, number of scans, and display range. The number of data points and acquisition time determine the time spacing of the FID. If the FID does not decay completely by the end of the acquisition time, then the acquisition time must be increased. So, an appropriate acquisition time is a duration in which the signal decays to just below the noise within the FID window. The B_1 pulse duration and transmit gain determine the tip angle of the RF pulse. The RF pulse duration could be used as a mean of finding an NMR signal by altering this value. A clear explanation of the pulse and collect experiment is available on section 1.4.2 of the STUDENT GUIDE. Also, section 2.4.3 of the USER MANUAL goes over the task of each parameter listed in the PC macro. All these parameters should be optimized at a new chosen location.

Figure A.7 presents an excellent acquired FID for a 500 ml bottle of water while Figure A.8 demonstrates an extra ordinary FID with higher amplitude than usual for the same sample.

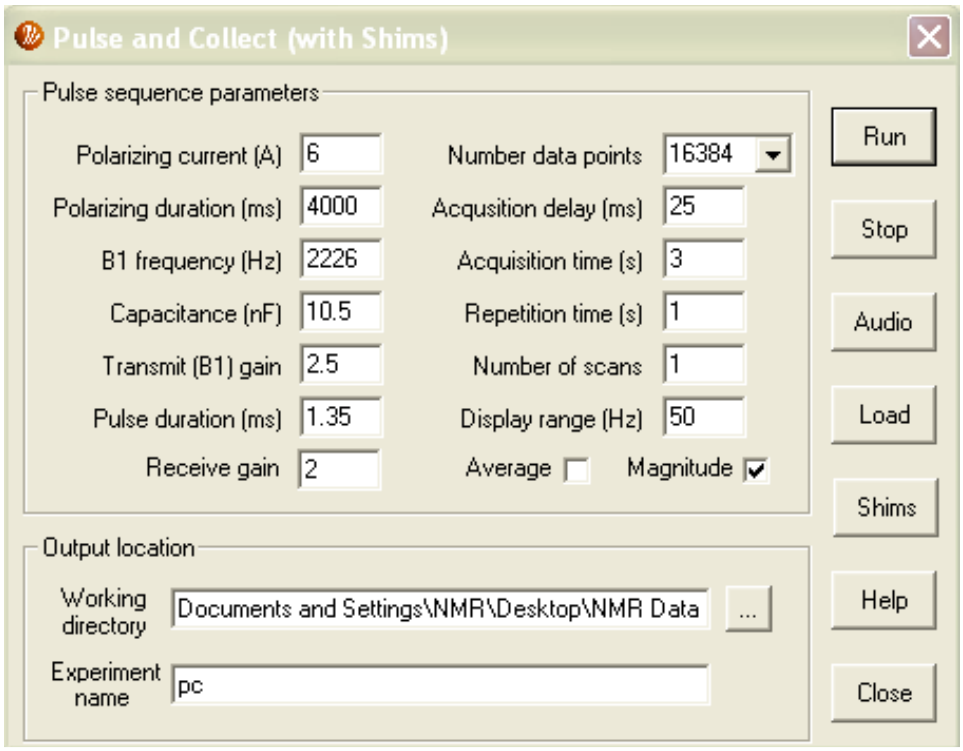

Figure A.6 Pulse and collect parameters of a 500 ml bottle of water

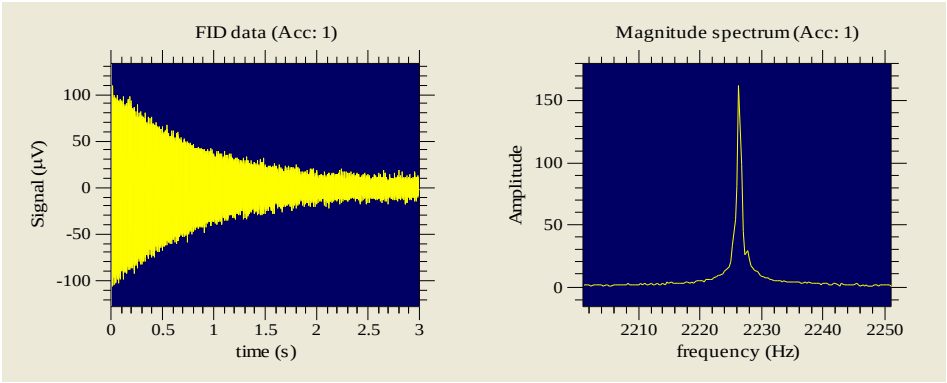

Figure A.7 An excellent plot of pulse and collect of a 500 ml bottle of water

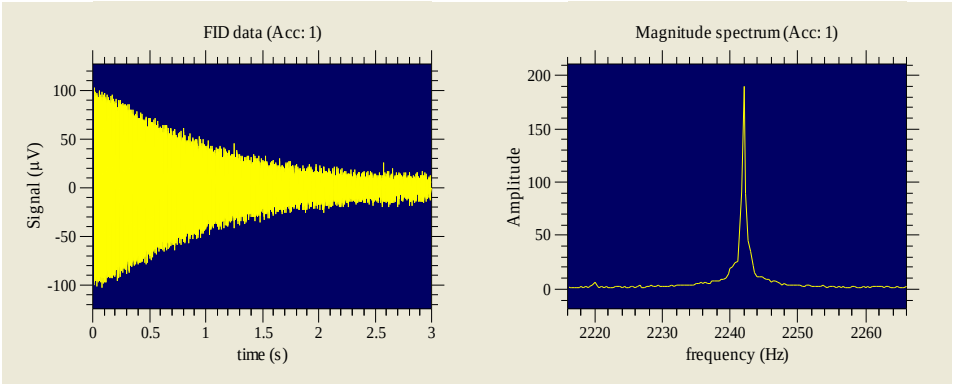

Figure A.8 An extraordinary FID and spectrum of a 500 ml bottle of water

Figure A.9 demonstrates the situation where receive gain is at its maximum value (10), so clipping has occurred. Normally this value should be around 2.5. This parameter amplifies the signal and the noise, so it does not improve the SNR.

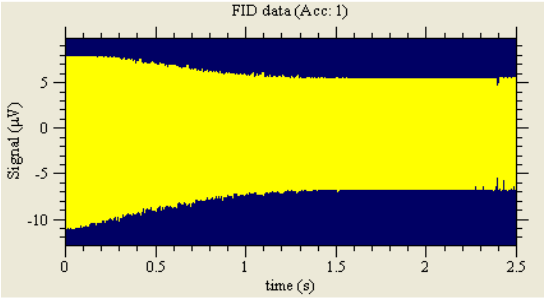

Figure A.9 A clipped FID

After Fourier transform is done on an FID, by default the NMR signal is a complex spectrum as depicted on Figure A.10. This requires a phase shift to bring the NMR peak into absorption mode. The phase of the spectrum can be altered so that the real part also called the magnitude displays the absorption peak and the imaginary part (the pale spectrum) displays the dispersion spectrum. However, if the signal to noise ratio in the frequency domain is poor, this routine could fail. To overcome this problem the magnitude of the spectrum is taken which has the disadvantage of producing broad peaks.

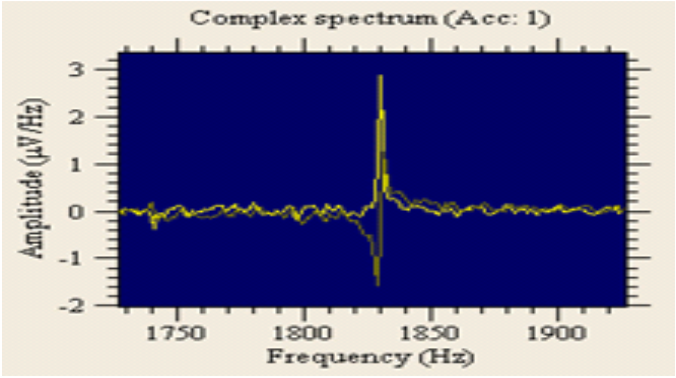

.

Figure A.10 A complex spectrum

At this point the goal is to acquire an FID that persists for at least 100 ms. In case if this signal is acquired then auto shim followed by optimization of the signal could be done. However, if no signal is acquired, a Spin Echo experiment could be used to find the signal.

A.2.4 Spin Echo

The goal of the Spin Echo is to reverse the de-phased spins due to magnetic field in-homogeneity. The 180° pulse (or Spin Echo pulse) generated by the B_1 coil flips the de-phased magnetic field vectors on the Y-axis. Section 2.4.4 of the USER MANUAL explains about the Spin Echo experiment and how an NMR signal could be detected. Based on Figure A.11, all the parameters are the same as the PC experiment except a 180° pulse duration and Echo time. An echo (Figure A.12, first plot) and a broad spectrum (Figure A.12, second plot) with low amplitude (8 µV/Hz) are acquired. Although the NMR signal is not strong, the center of the broad spectrum could be used as the B_1 (resonance) frequency for the sample.

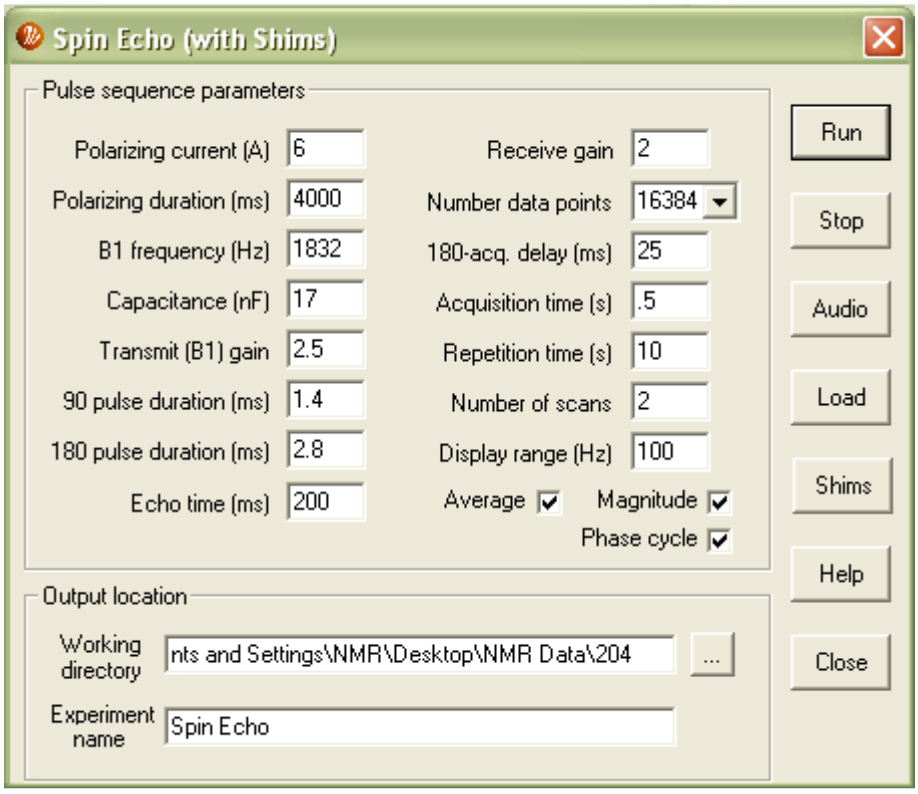

Figure A.11 The macro for Spin Echo experiment

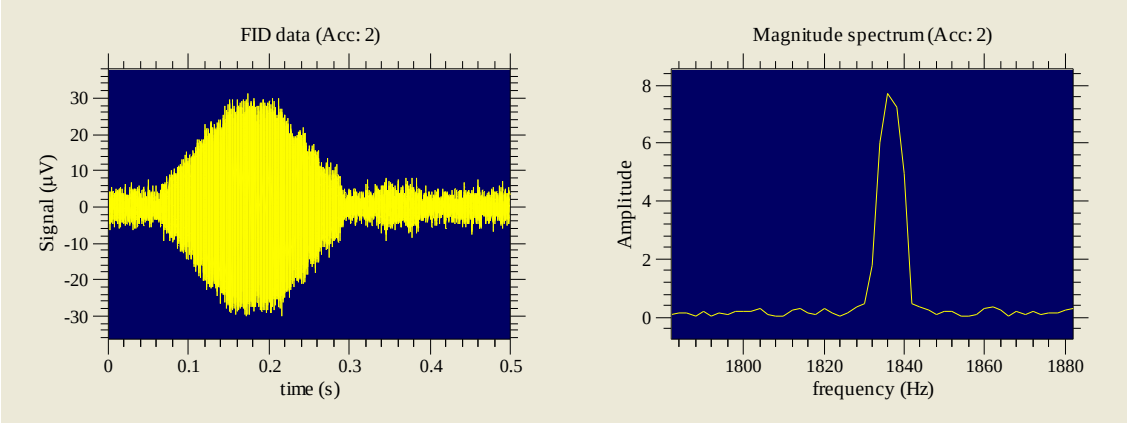

Figure A.12 Echo signal in the time domain (re-phasing/de-phasing) and spectrum

A.2.5 Autoshim

Once a resonance peak is detected, shimming is applied to improve the peak extensively. Shim coils provide a small current to create auxiliary magnetic field to compensate for in-homogeneity in the static magnetic field. So, shimming is correcting the in-homogeneity in the static magnetic field (Zhi-Pei and L. 2000). Section 2.4.2, pages 2-6 of the USER MANUAL introduces the T_2* concept which is the consequence of magnetic field in-homogeneity over the volume of the sample. So, whenever in-homogeneity is present, the FID signal decays rapidly because T_2*is the dominant source of decay. As a result a wide spectrum with a fast decayed FID is acquired. In general: $T_2^* < T_2 \leq T_1$. Section 2.4.5 of the USER MANUAL covers the shimming process. Also, section 2.4.3 of the STUDENT GUIDE explains the auto-shimming.

Figure A.13 contains all the parameters determining the shim quality. If the probe is moved to a new location or if a metal object is placed in the vicinity of the probe, the shimming must be repeated because the shimming parameters are sensitive to changes in the environment. Figure A.14 demonstrates the FID and spectrum for each step of the Auto-shim process. These plots are updated for each step of shimming and are presented as the iteration or history in the third plot of this figure. A good signal persists for 100s of ms or seconds and has a narrow line width along with high amplitude in the frequency domain.

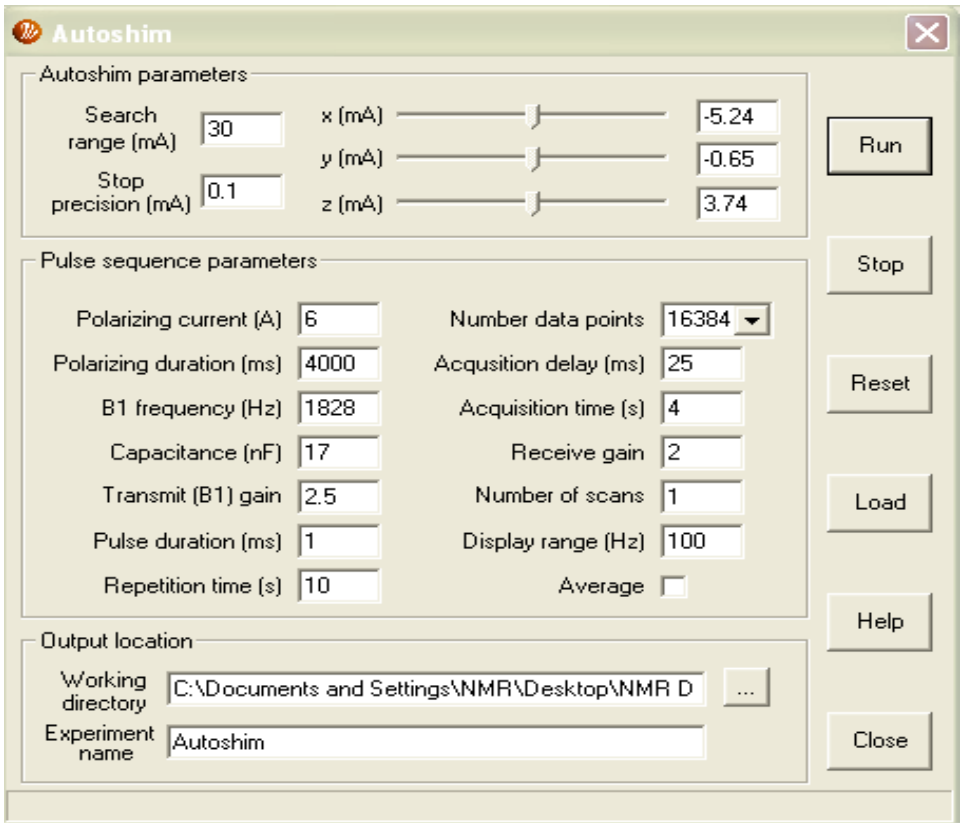

Figure A.13 Autoshim dialog window

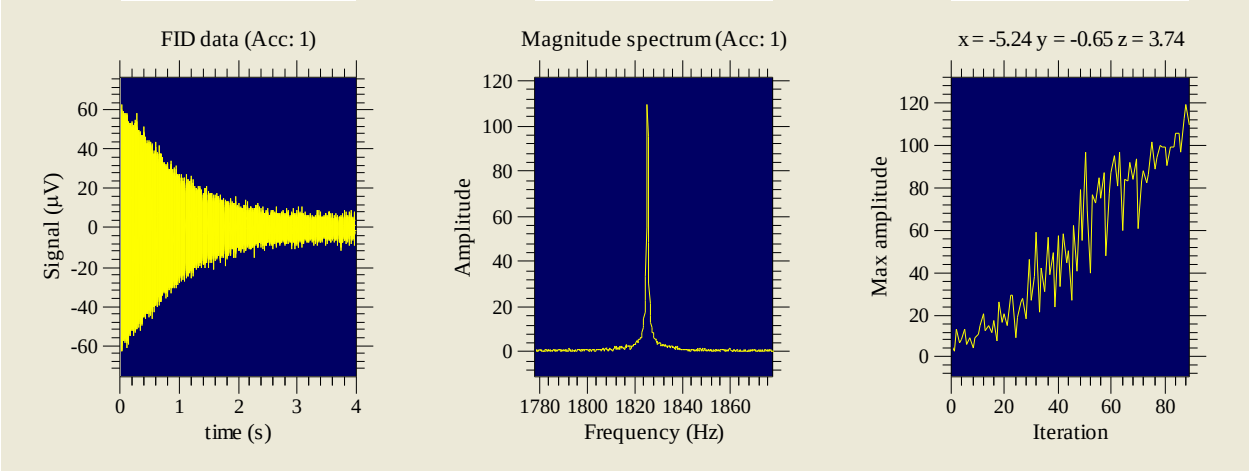

Figure A.14 Plots of Autoshim

A.2.6 Optimizing NMR Signal (FID)

Once a good magnetic homogeneity and reasonable signal are acquired, shimming helps a great deal to improve the signal. However there is more that could be done to improve the

signal amplitude and this is achieved through optimizing the FID. The first experiment performed was coarsely tuning the B_1 coil while here the coil is going to be tuned more accurately. These steps include tuning the B_1 coil, setting the B_1 frequency, calibrating the B_1 pulse duration, and minimizing the noise; the latter is done through signal averaging.

A.2.6.1 Tuning B_1 Coil

In order to tune the probe to the Larmor frequency of the sample, the resonance of the tuned B_1 coil must be observed. After a B_1 excitation pulse, the B_1 coil resonance decays in time and is called the coil ring-down. In order to obtain an NMR signal without observing the coil ring-down, a 25 ms acquisition delay between the excitation pulse and acquisition of the first data point is introduced. If this delay is shortened, the coil ring-down will be observed. Further, the Fourier transform of the ring-down signal will appear as a "sink-type" in the spectrum. The display range must be 1000 to observe the sinc-type peak when tuning the probe. The center of the peak is the resonance frequency of the coil.

Figure A.15 shows the broad sinc-type peak which is the coil response to the B_1 pulse, and the narrow spike is the NMR signal. In order to tune the probe, the capacitance of the system should be adjusted until the center of the peak coincides with the center of the resonance peak (Figure A.16). For example, according to Equation A.1, if the coil resonance is too low, the resonance frequency of the coil should be increased which means the capacitance should be decreased. The opposite is true in case of observing a high resonance frequency for the B_1 coil. Figure A.17 demonstrates that the higher the polarization duration and current, the thicker the FID will be obtained. Section 2.5 of the USER MANUAL covers more on the FID optimization while section 3.9 of the same manual explains about the B_1 coil ring-down.

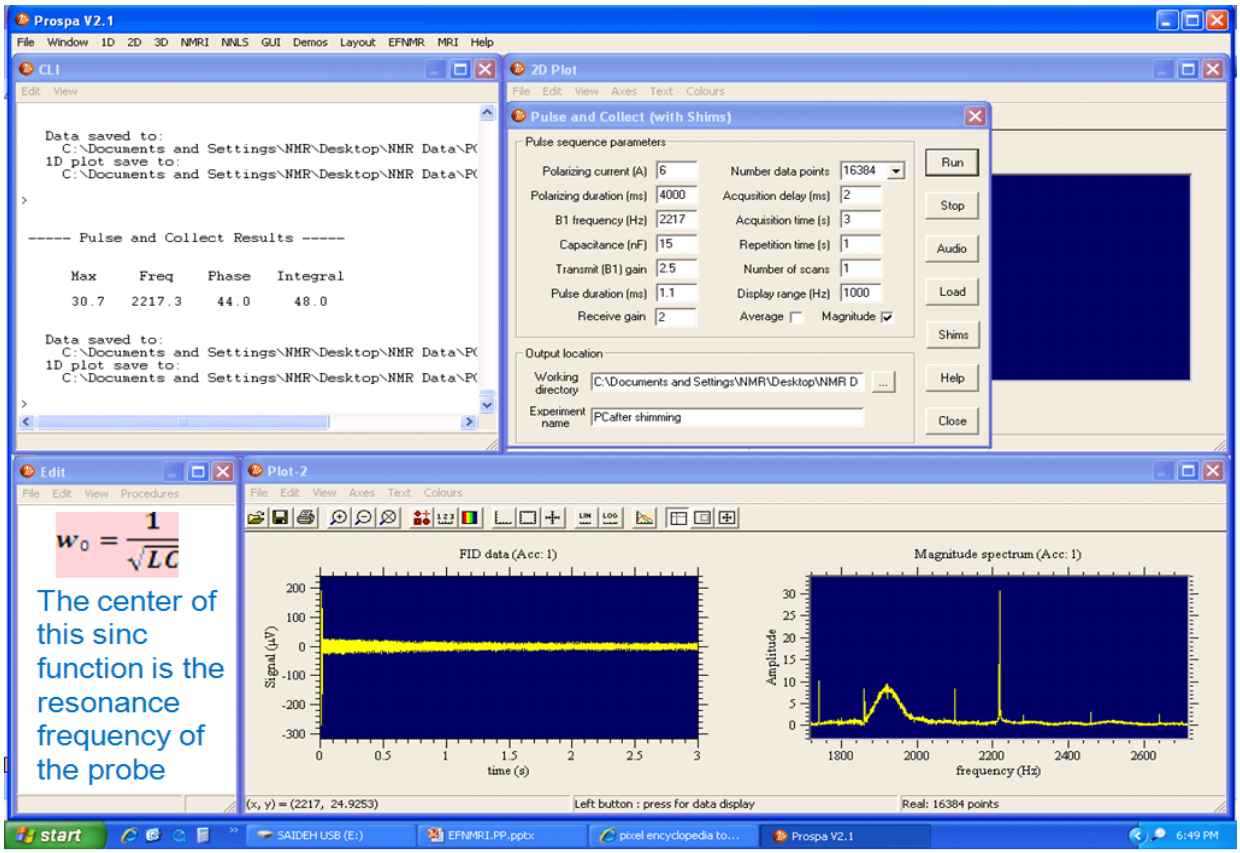

Figure A.15 An incorrectly tuned coil with acquisition delay of 2 ms

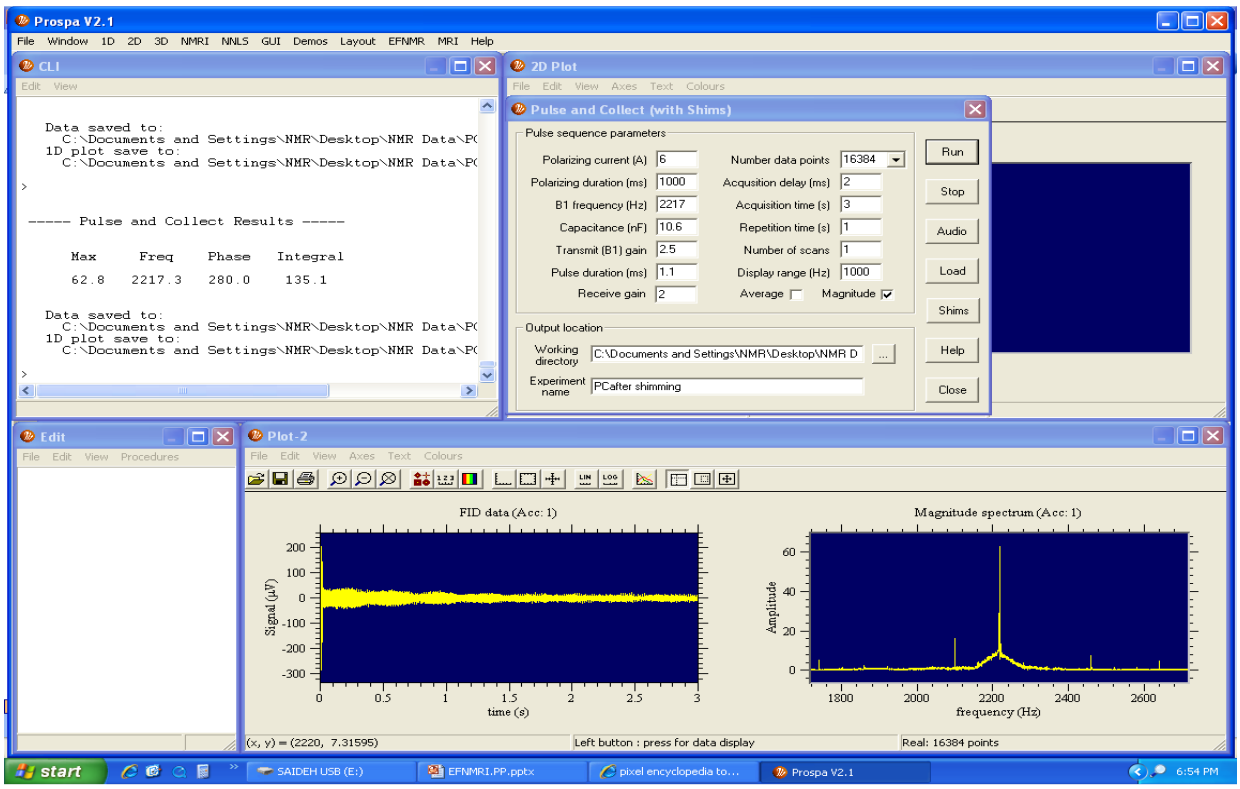

Figure A.16 A correctly tuned coil with acquisition delay of 2 ms

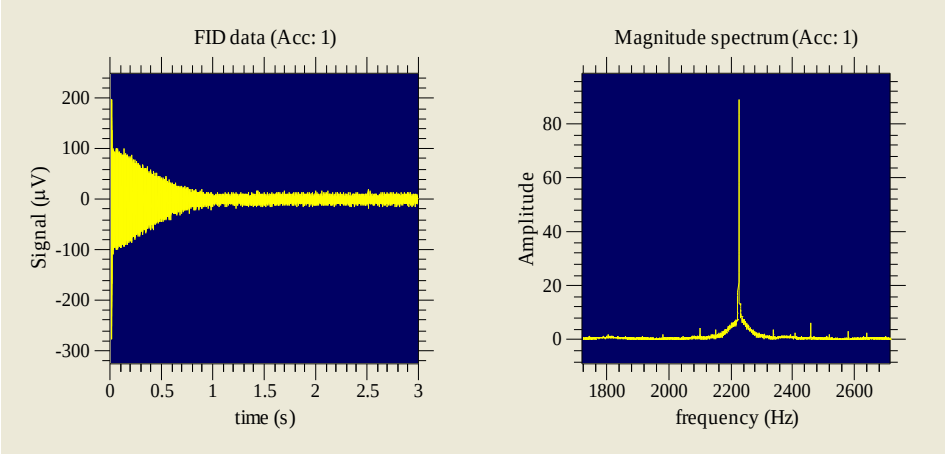

Figure A.17 A correctly tuned coil with 2ms acqu-delay (a thicker FID & stronger spectrum)

A.2.6.2 Calibrating B_1 Pulse Duration

For the B_1 Duration experiment, a series of PC with an array of B_1 pulse duration is obtained. The signal intensity produced by this macro is acquired by integrating the spectrum over the range of frequency values that defines the resonance peak. The integration width is obtained by inspecting a single spectrum of a PC. In general, a tip angle of 90° should yield the maximum signal while a tip angle of 180° should produce no signal. However in reality it yields a minimum signal because of B_1 in-homogeneity effects as depicted in the third 1D plot of Figure A.18. The plot demonstrates the signal amplitude versus B_1 pulse duration in which the maximum of the peak corresponds to the 90° pulse duration and the minimum of the peak to the 180° pulse duration. For B_1 pulse duration, half the reciprocal of the frequency should be used for minimum B_1 duration as well as the B_1 step size. For example, for B_1 frequency of 2217 Hz, B_1 duration and step size should be: $\frac{1 \div 2217}{2} = 0.226\, ms$. All other parameters are the same.

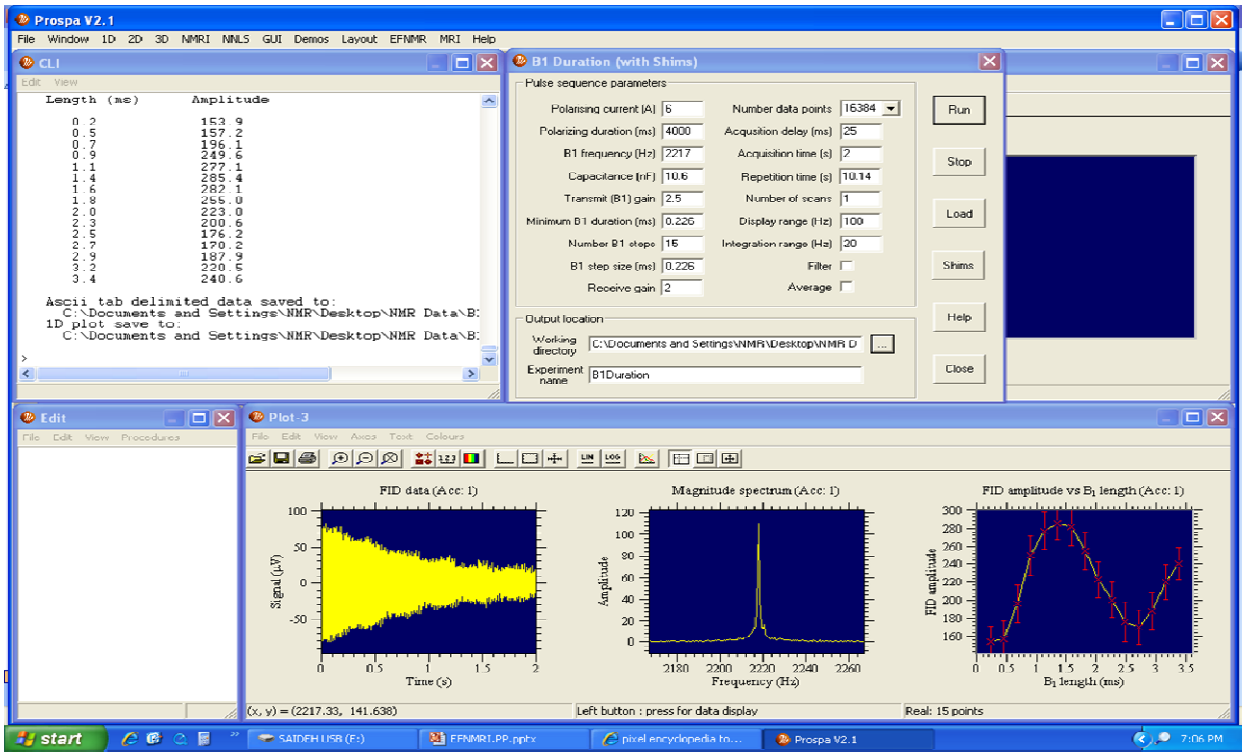

Figure A.18 A B_1 Duration Experiment

At this point optimizing the FID and spectrum signals is accomplished.

A.3 Spin-Lattice (Longitudinal) Relaxation: T_1

T_1 is the interaction of the spins with the environment that perturbs their momentum and realigns the spins with the magnetic field.

The T_1 time constant depends on molecular dynamics and the strength of the static magnetic field meaning the stronger the static magnetic field, the longer the relaxation times becomes. Also, the more mobile the molecules are the less intermolecular contact between them, so relaxation times become longer. Further, T_1 at higher temperatures is longer than T_1 at lower temperatures. During an EFNMR experiment, the dominant magnetic field is either the polarizing field (B_p) during the polarization pulse or the Earth's magnetic field (B_e) during signal excitation and detection. Therefore in case of EFNMR, T_1 can be measured in the Earth's field as well as in the polarizing field.

T_1 in the Earth's field (T_1-B_e) is obtained by applying the polarization pulse causing the evolution[2] of the longitudinal magnetization. After the polarization field is switched off adiabatically, meaning slowly within the course of 50 ms, an enhanced magnetization vector is aligned with the direction of the Earth's magnetic field. However, the dominant static magnetic field is now the Earth's field rather than the polarizing field, and the equilibrium magnetization now is proportional to the B_e which is much smaller. In other words, the net magnetization relaxes from the enhanced value (obtained from B_p) to the equilibrium value proportional to the B_e and thus is zero. The cause of this relaxation is spin-lattice relaxation. The time constant in this case depends on the B_e and might differ from T_1 value obtained in the polarization field for some samples.

To measure T_1 in the Earth's field, the PC with added delay between the polarization pulse and the RF excitation pulse is used. During this delay the longitudinal magnetization

[2] Evolution is the time after a pulse that allows the spins to get to the state one wants to probe. NMR is a time dependent measurement meaning the complex signal (intensity and phase) is a function of time. If two sine functions are present that start in phase but with different frequencies, at time zero they are the same. We must wait a certain amount of time before they look different. In an image this is the time that is waited for the spins to separate in phase due to a field gradient. At time zero the spins are lined up and cannot be differentiated, but over an evolution time they will separate out into their field dependent frequencies. When an echo is collected, information about what happened during this time is collected. For a specific local environment a certain state at the end of the evolution time is expected. Evolution is a term for what the spins do while waiting to pulse again on them or collect data (echo or FID).

decays according to Equation A.3.

Equation A.3: $E = E_0 [\exp(-t/T_1)]$

The amount of signal excited by the RF pulse will be directly proportional to the amount of available magnetization, so the signal magnitude will decay as a function of this delay time called, t. The relative signal amplitude (E/E_0 equivalent to the area under the spectral peak) is plotted as a function of this time, t, on the far right in Figures A.20 and A.21. It should be kept in mind that even with a zero pre-RF delay there is a hidden pre-pulse delay of 50 ms for allowing the magnetization to slowly align to the B_e direction. In addition, there is the 25 ms delay of the RF pulse which makes it hard to measure T_1 values below 100 ms. For the best results the maximum delay should be several T_1 values (Figure A.19). Since the T_1 value for a water sample is 2 seconds, a reasonable range of pre-RF delay is 500 ms to 5 seconds at 500 ms intervals. As depicted in Figures A.20 and A.21, the higher the concentration of copper in the solution the lower the T_1-B_e value becomes due to the effect of copper as a paramagnetic contrasting agent (T_1-B_e of 3 mM Cu solution was 189±5 ms). Also T_1-B_e of oil has a low value of 190 ms due to the reduced mobility of the hydrogen nuclei of the oil sample in comparison with a water sample.

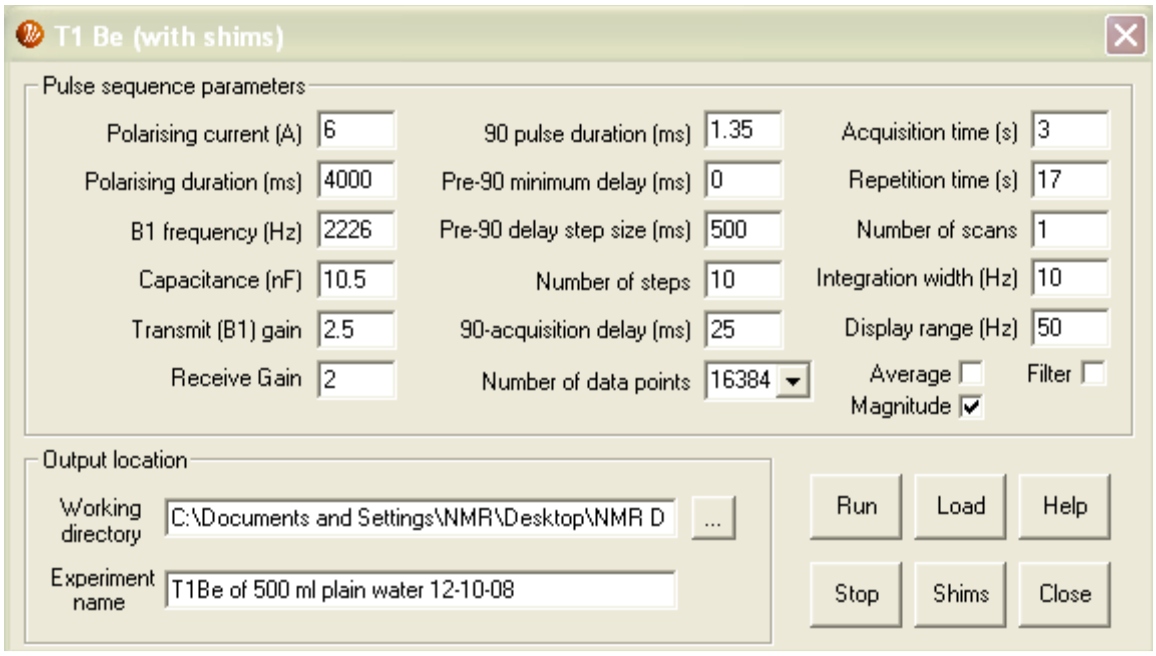

Figure A.19 T_1-B_e of a 500 ml bottle of water (The Gui is related to the first series of T_1)

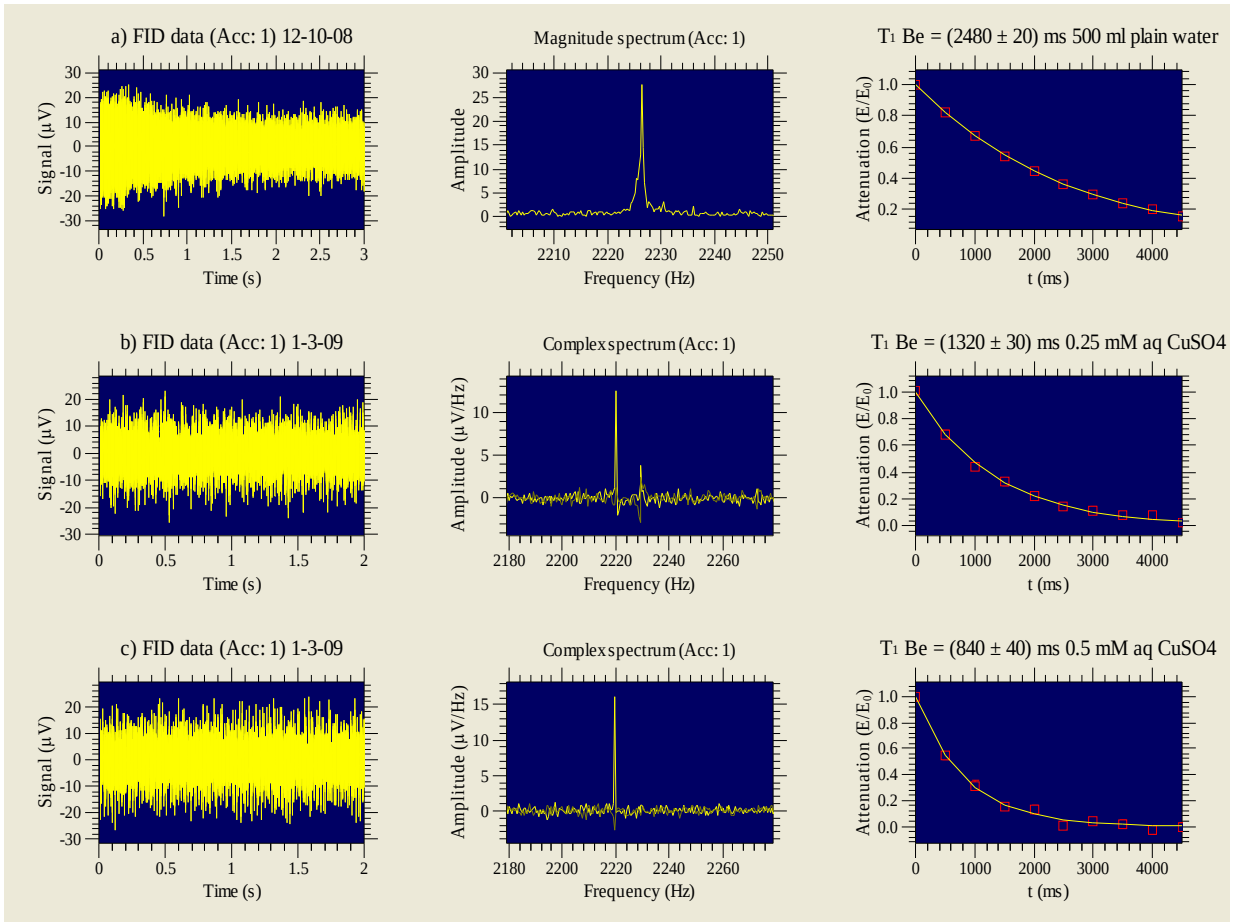

Figure A.20 T_1-B_e plots of 500 ml water doped with various concentrations of cupric sulfate

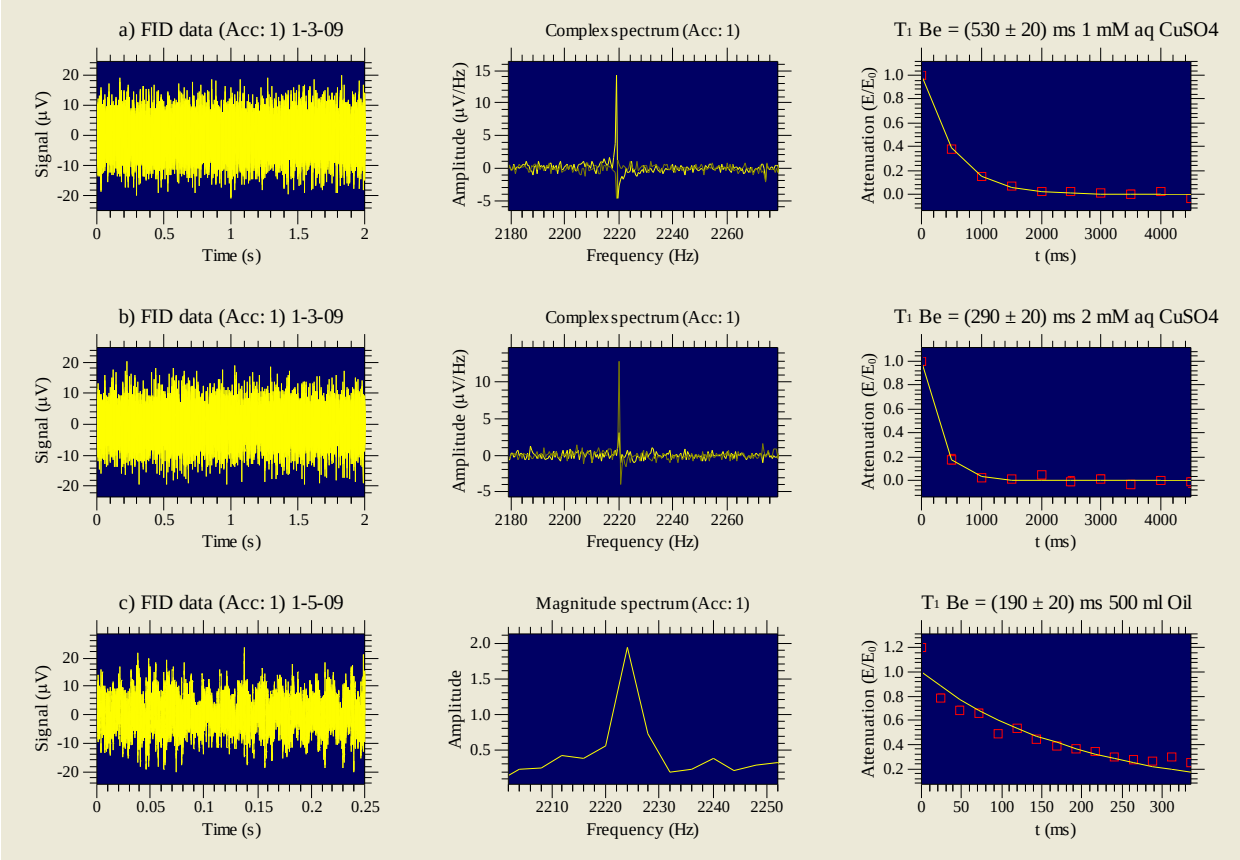

Figure A.21 T_1-B_e of 500 ml water doped with various concentrations of cupric sulfate and oil

T_1 in the polarizing field (T_1-B_p) is obtained by applying the polarization pulse on the sample. This time dependence signal during the polarization pulse is defined by Equation A.4 where E_0 is the signal magnitude at equilibrium in the polarizing field as the T_p increases.

Equation A.4: $E = E_0 [1 - \exp(-T_p/T_1)]$

T_1-B_p in the polarizing field can be measured by applying an array of 10 steps of polarizing pulse durations starting at 500 ms with a range of 500 ms to 5 second being the upper limit for several T_1 values (Figure A.22). A list of polarization duration values and the corresponding signal magnitude was obtained, and the relative signal amplitude (E/E_0) was plotted as a function of polarization pulse duration (T_p) on the far right in Figures A.23 and A.24. As depicted in Figures A.23 and A.24 the higher the concentration of copper in the solution, the lower the T_1-B_p value due to the effect of copper as a paramagnetic contrasting agent.

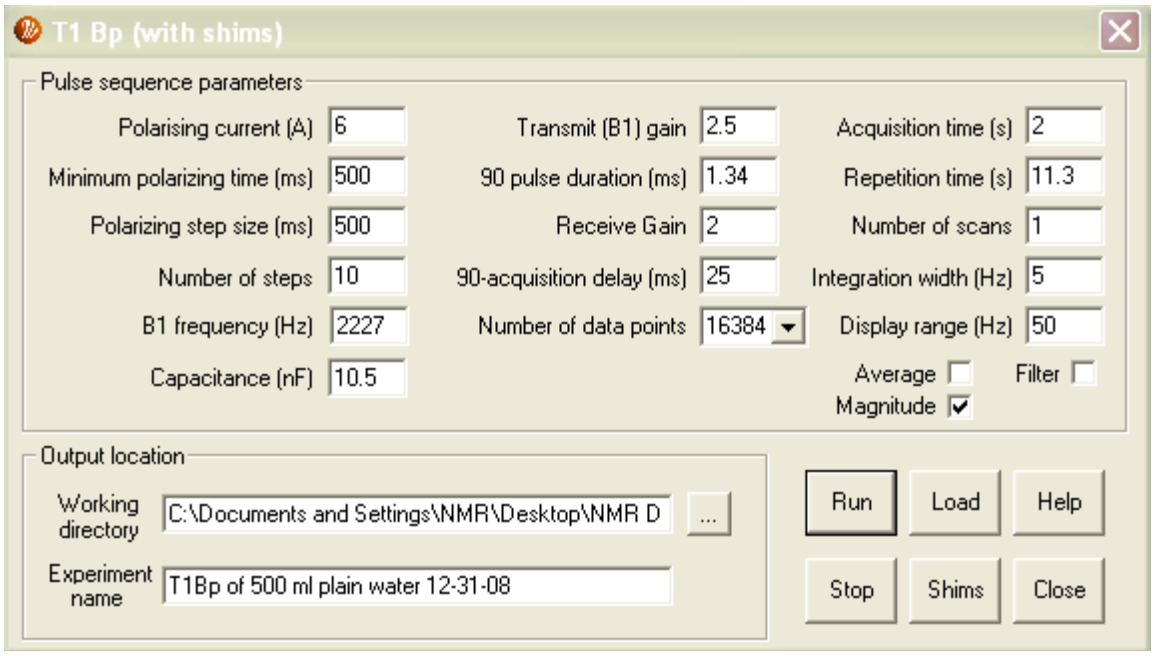

Figure A.22 T_1-B_p of a 500 ml bottle of water (The Gui is related to the first series of T_1)

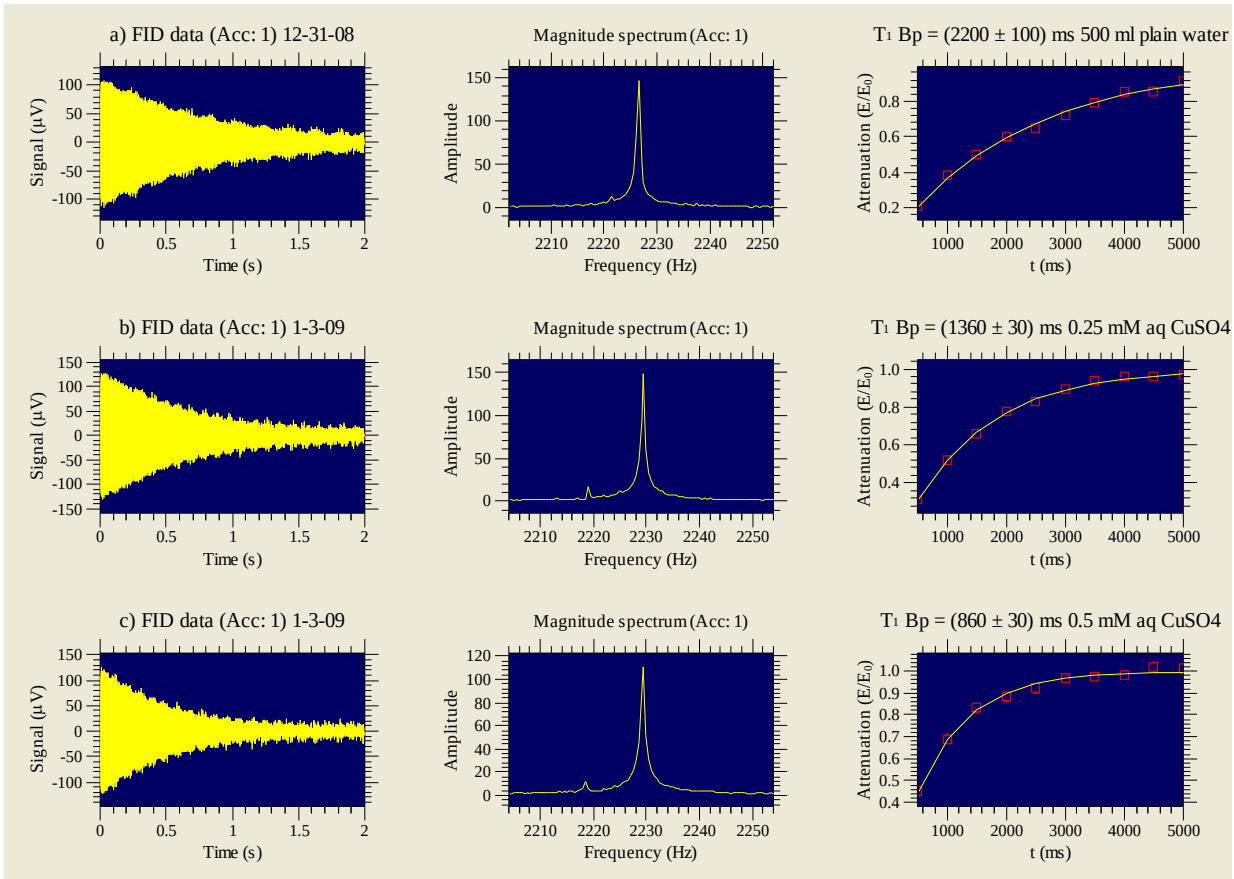

Figure A.23 T_1-B_p plots of 500 ml water doped with various concentrations of cupric sulfate

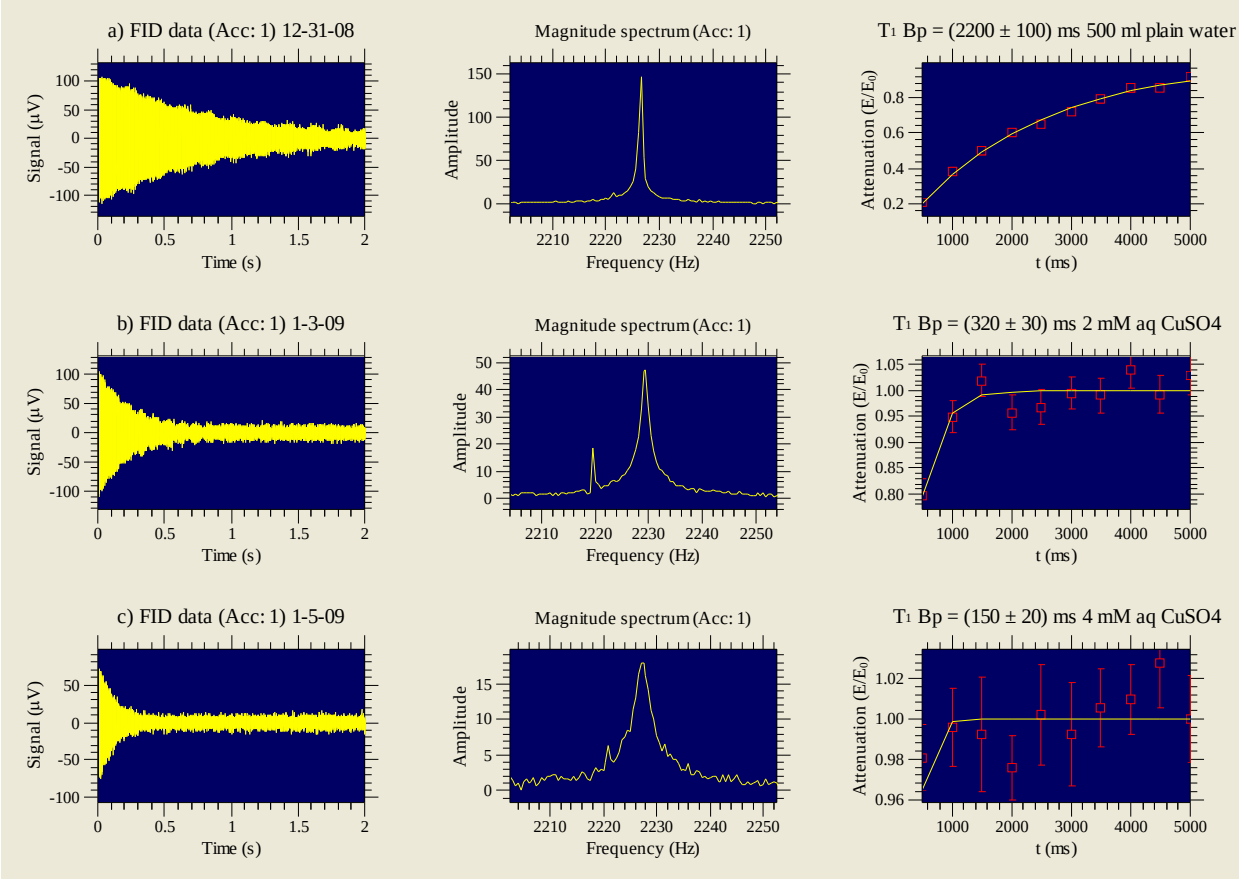

Figure A.24 T_1-B_p plots of 500 ml water doped with various concentrations of cupric sulfate

Again as shown in Figures A.26, T_1-B_p of oil has a low value due to the less mobility of the hydrogen nuclei present in the oil sample. The step size in the T_1-B_p macro is 50 ms in Figure A.25. Appendix C illustrates PC spectral values, T_1-B_e, T_1-B_p, and T_2 values for various tested samples.

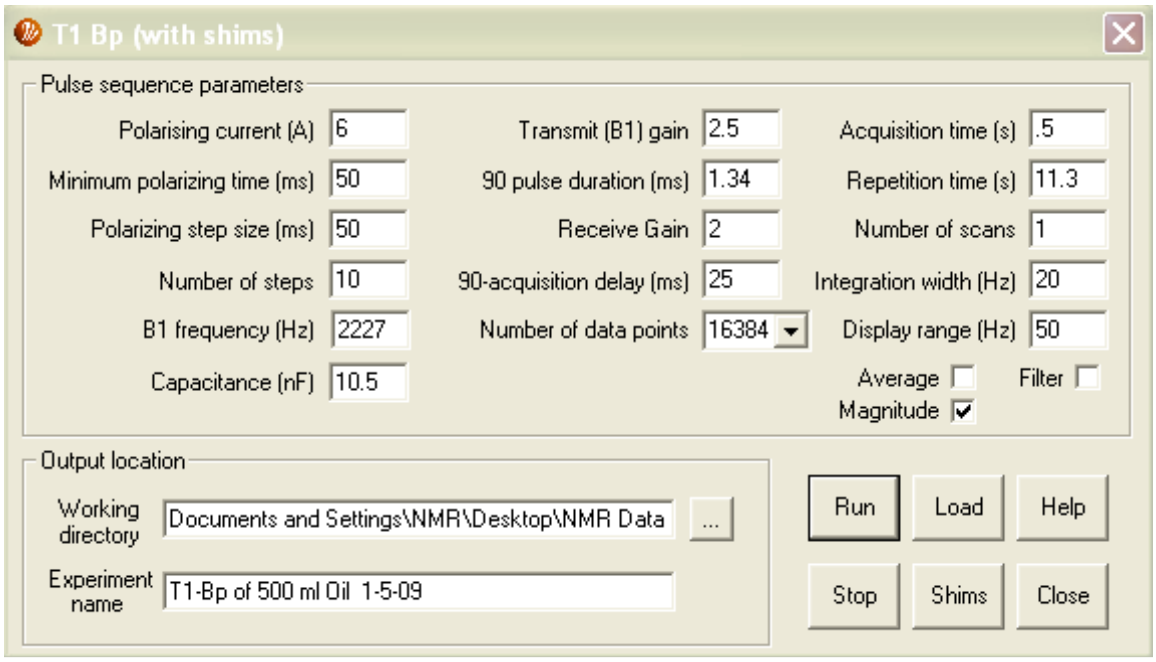

Figure A.25 T_1-B_p macro of a 500 ml bottle of oil

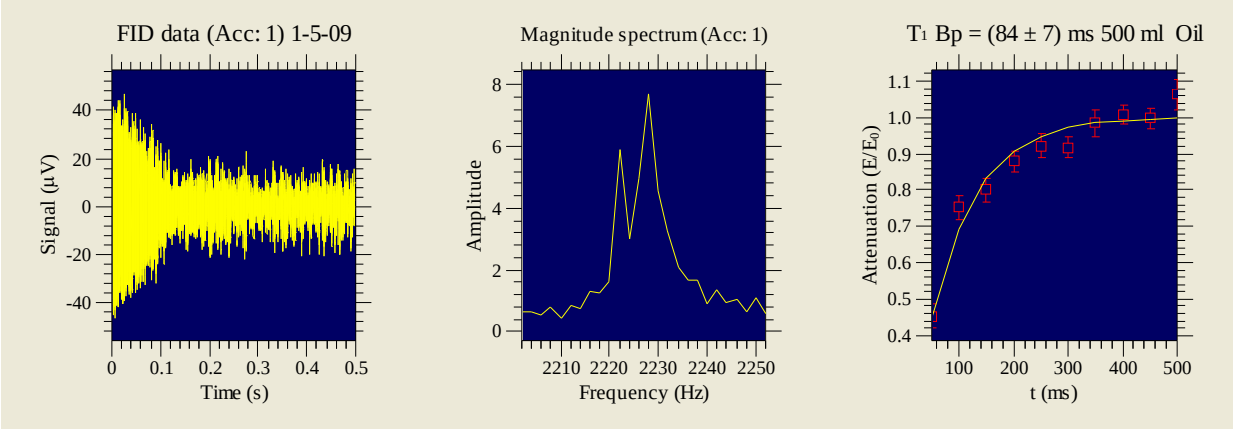

Figure A.26 T_1-B_p plots of 500 ml bottle of oil

A.4 Spin Echoes and Spin-spin Relaxation (T_2)

T_2 is the loss of spin coherence (synchronization) of the spin precession in the transverse plane.

FIDs decay exponentially, and this decay is determined by the transverse or spin-spin relaxation time, T_2. However, in-homogeneity in the local field produces a rapid decay with a time constant known as T_2*. So the decay time of FID is referred to as T_2*. Equation A.5 shows the correlation between T_2* and T_2 where ΔB_0 presents magnetic field in-homogeneity.

Equation A.5: $$\frac{1}{T_2 *} = \frac{1}{T_2} + \gamma \Delta B_0$$

T_2 is a consequence of irreversible de-phasing via spin-spin relaxation resulting from the random motion of the spins. However, T_2* combines the irreversible spin-spin relaxation effects with reversible magnetic field in-homogeneity causing de-phasing effects. The spin echo amplitude depends on T_2 and not T_2* meaning that in-homogeneity reduces T_2* but has no effect on T_2. The spin echo pulse sequence known as a 180° pulse could refocus the de-phasing magnetization caused by the in-homogeneous detection field to allow T_2 to be measured accurately. This pulse sequence (Figure A.27) uses two B_1 excitation pulses; the 90° pulse that rotates the magnetization about the X-axis by a tip angle of 90° followed by a delay time called the echo time (Tε) in which the spins diphase during this time due to in-homogeneity as well as spin-spin relaxation effect. Then a 180° pulse is applied causing refocusing of the de-phased spins while producing another echo time (Tε) which is the time between the 90° pulse and the 180° pulse as shown in Figure A.27. The center of the spin echo occurs after a time, Tε, after the 180° pulse. So, an echo with reduced amplitude due to only spin-spin relaxation is generated.

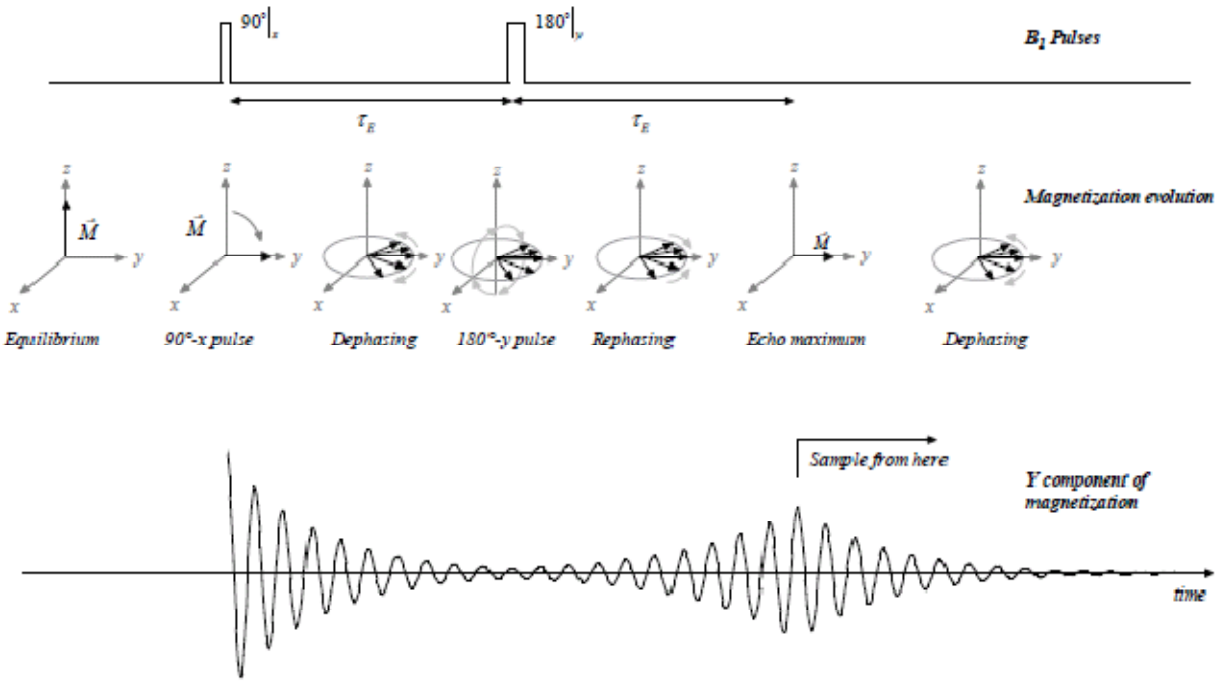

Figure A.27 The Spin Echo pulse sequence diagram for measuring T_2 relaxation (Polarizing pulse not shown) (Magritek, Terranova-MRI User Manual 2005)

The echo time should be chosen (Figure A.28) long enough to accommodate the entire echo, meaning Tε should allow for the complete relaxation of the signal excited by the 90° pulse. So the echo time should be longer than the signal persistence in the FID, and this could be accomplished through a PC experiment. Also, in order to observe the entire echo, the echo should fall in the center of the acquisition window by fulfilling Equation A.6.

Equation A.6: $T_{acqu} = 2\,(T\varepsilon - T_{acqu\ delay})$

Figure A.29 demonstrates different Spin Echo experiments by fulfilling Equation A.6 meaning that most of the echoes obtained are in the center of the acquisition window.

However, in experiment (a) acquisition time must be less than 0.4 second while it is 1 s, and as a result, the echo is not centered in the widow. Also purposely de-shimming is applied to create in-homogeneity in order to observe that the sides of the echo are decayed more rapidly. This is determined by T_2*, and the greater the de-shimming, the slimmer the echo. For example in experiment (a) a much greater de-shimming is applied compare to experiment (f). However,

the echo amplitude in the time domain and the spectrum is not changed significantly. Figure A.30 depicts the Spin Echo for a 500 ml bottle of oil. Since hydrogen nuclei in the oil sample are not mobile, T_2 value for this sample is very low. Also with the Terranova instrument it was not possible to acquire T_2 for oil due to the fact that T_2 less than 100 ms is not possible to be measured. Figures A.31 and A.32 present the case when the FID is optimized, so magnetic in-homogeneity is the minimum or does not exist. Therefore there is no echo acquired and the time domain window resembles an FID window.

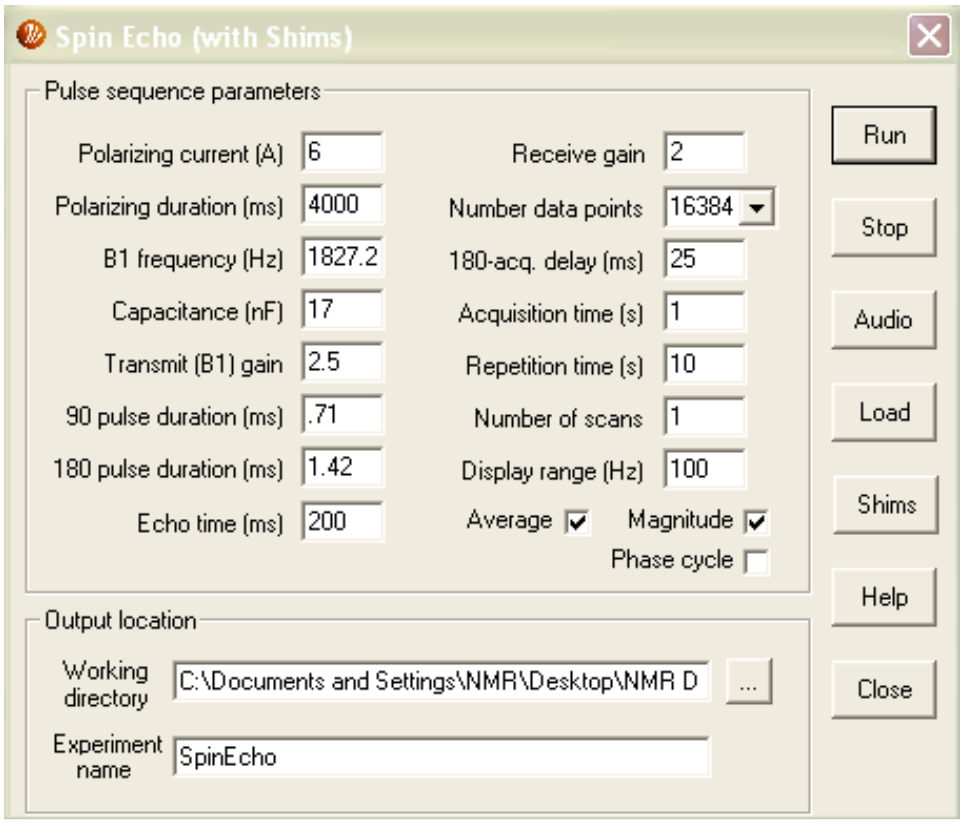

Figure A.28 Spin Echo macro corresponding to data set a

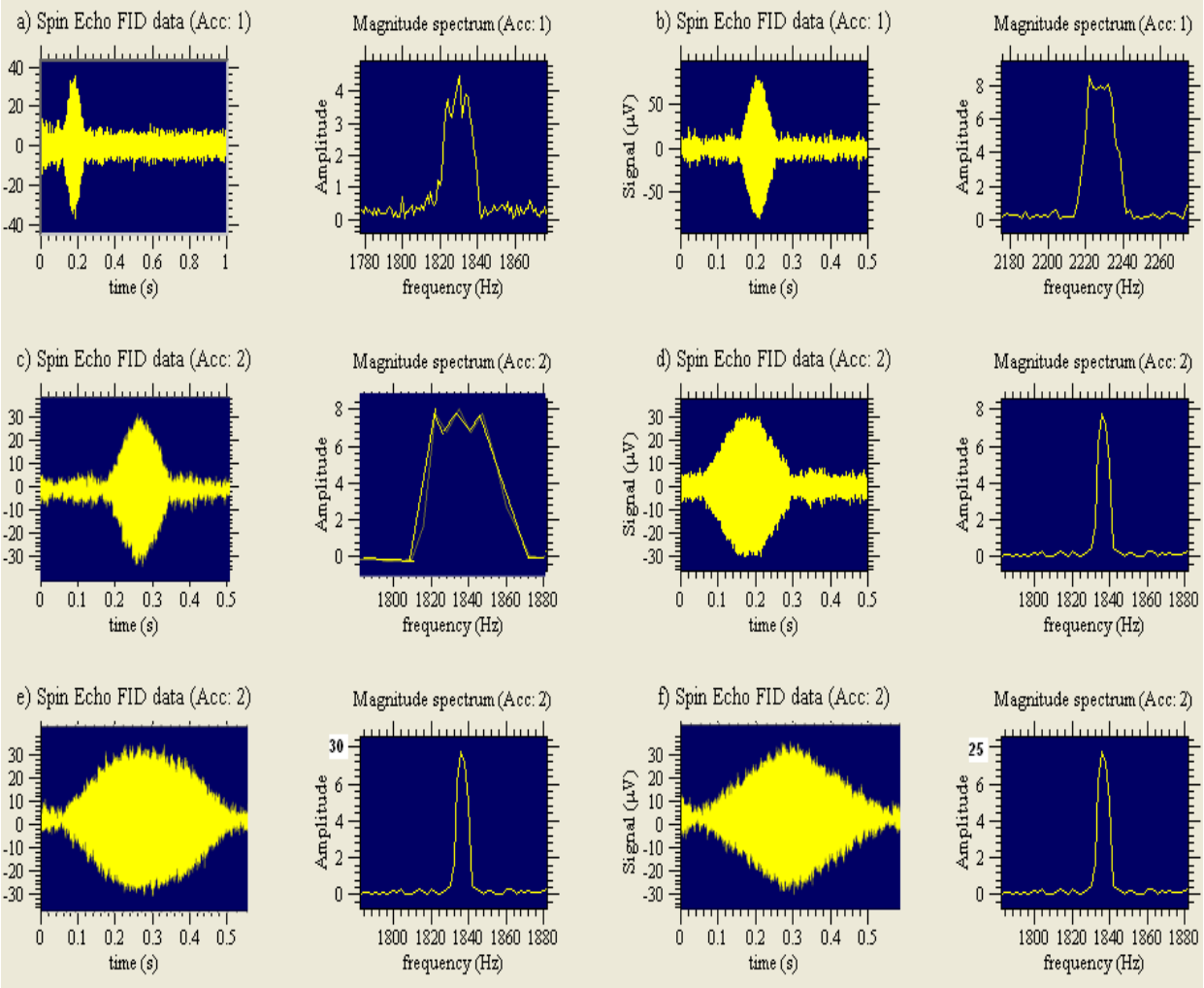

Figure A.29 Various plots of Spin Echo Experiments

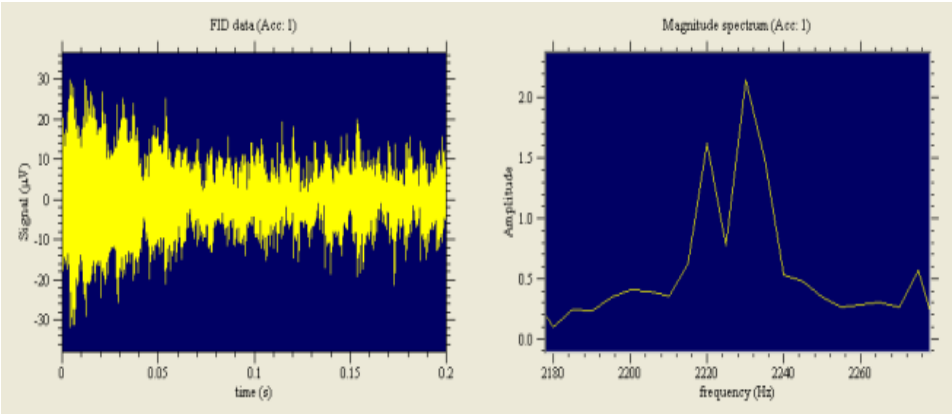

Figure A.30 Spin Echo plot of oil

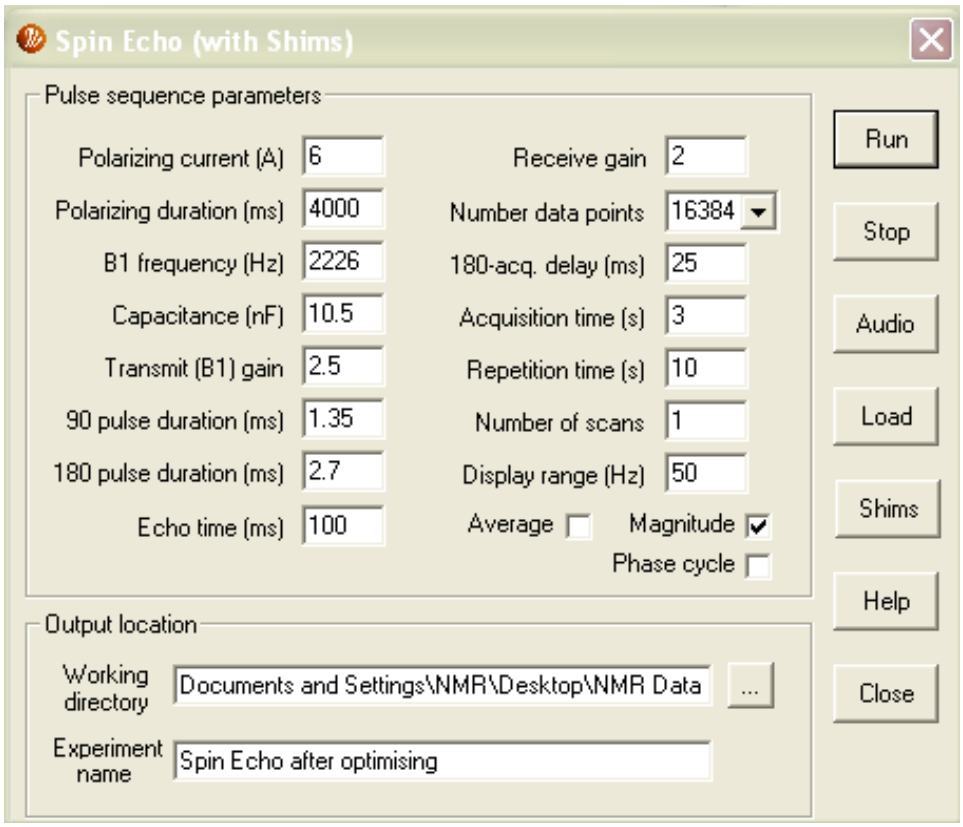

Figure A.31 Spin Echo macro after optimizing

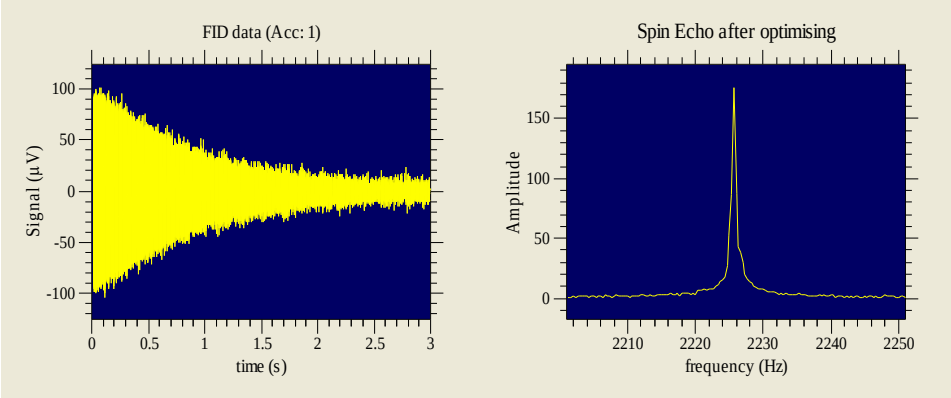

Figure A.32 Plots of Spin Echo after optimizing

The T_2 experiment is just a succession of Spin Echo experiments with incrementally longer echo times. In a T_2 experiment data is collected only from the peak of the echo onward. The echo amplitude (as well as FID amplitude) is determined by integrating the area under the spectral peak. If the echo time is short or T_2* is long, the excited signal from the 90° pulse may not relax to zero before the application of the 180° pulse which causes problems to view the

echo. However, if deliberately the magnetic field gets disrupted by de-shimming, or if phase cycling is used, a better T_2 will be acquired.

Further, an echo should persist around 100 ms while the minimum echo time should be 100 ms to allow for the ring down of the B_1 coil. The echo amplitude can be measured via equation A.7 where E is the amplitude of the echo and E_0 is the amplitude of the echo in the absence of T_2 decay.

Equation A.7: $E = E_0 \exp(-2\,T\varepsilon/T_2)$

E decays as a function of echo time with T_2 time constant. The relative echo amplitude (E/E_0) is determined for each Tε, and is plotted in the far right of Figures A.34 and A.35.

The T_2 macro repeats the Spin Echo experiment for an array of echo times. A range of echo times for T_2 experiment is 10-20 steps of 50-100 ms starting at 50 ms (Figure A.33). The output of the macro is the echo amplitude at each echo time. The echo amplitude is determined by integrating the sample peak in the spectrum. The integration is defined in the T_2 macro. Sampling starts at the center of the echo, so the full echo will not be observed.

Figures A.34 and A.35 demonstrate the T_2 values for 500 ml water bottles doped with different concentrations of cupric sulfate. As depicted, the higher the copper concentration of the solutions, the lower the T_2 values are due to copper being a paramagnetic contrasting agent. Also, T_2 for plain water has different values due to environmental and parameter changes. Chapter 4 of the STUDENT GUIDE explains T_2 relaxation very clearly.

A.4.1 Filtering

Filtering the time domain data means that the incoming FID is multiplied by an exponential filter indicated in the FID window as a red curve. The filter has already been applied to the FID in yellow. Many of the NMR and MRI macros contain a filter check box.

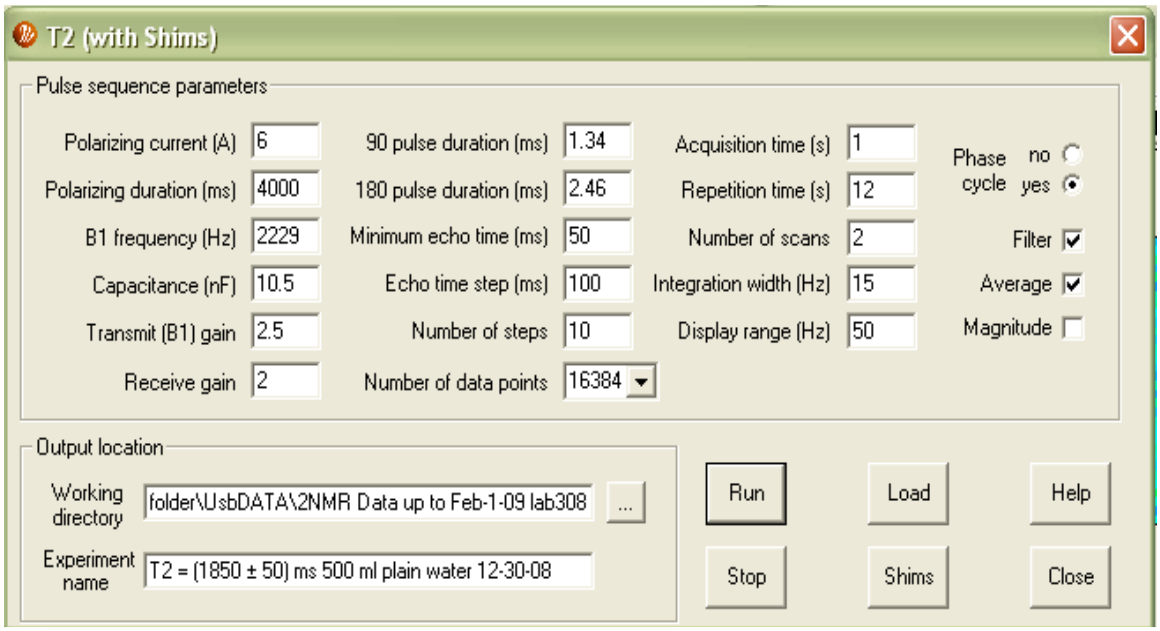

Figure A.33 T_2 of a 500 ml bottle of water (The Gui is related to the first series of T_2)

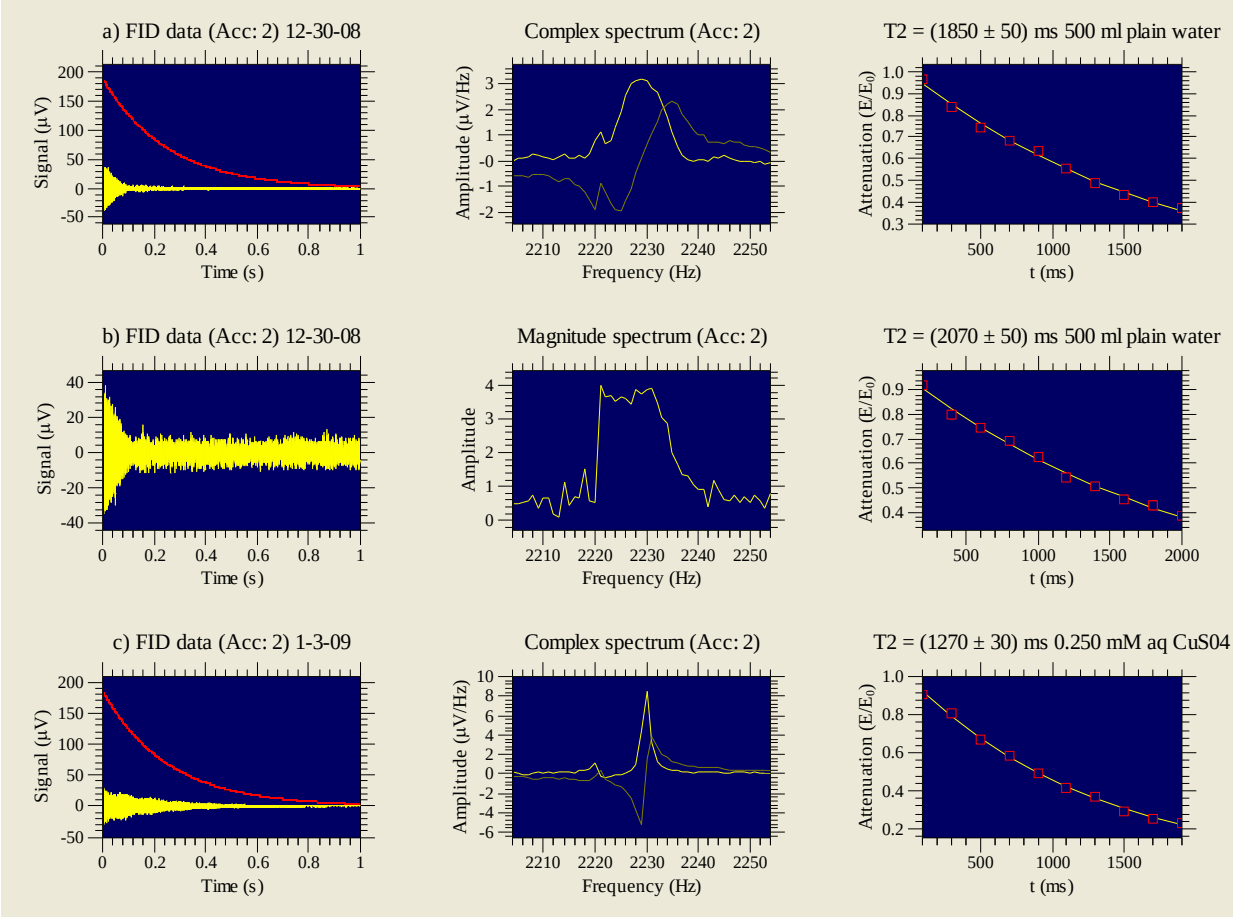

Figure A.34 T_2 plots of 500 ml water doped with various concentrations of cupric sulfate

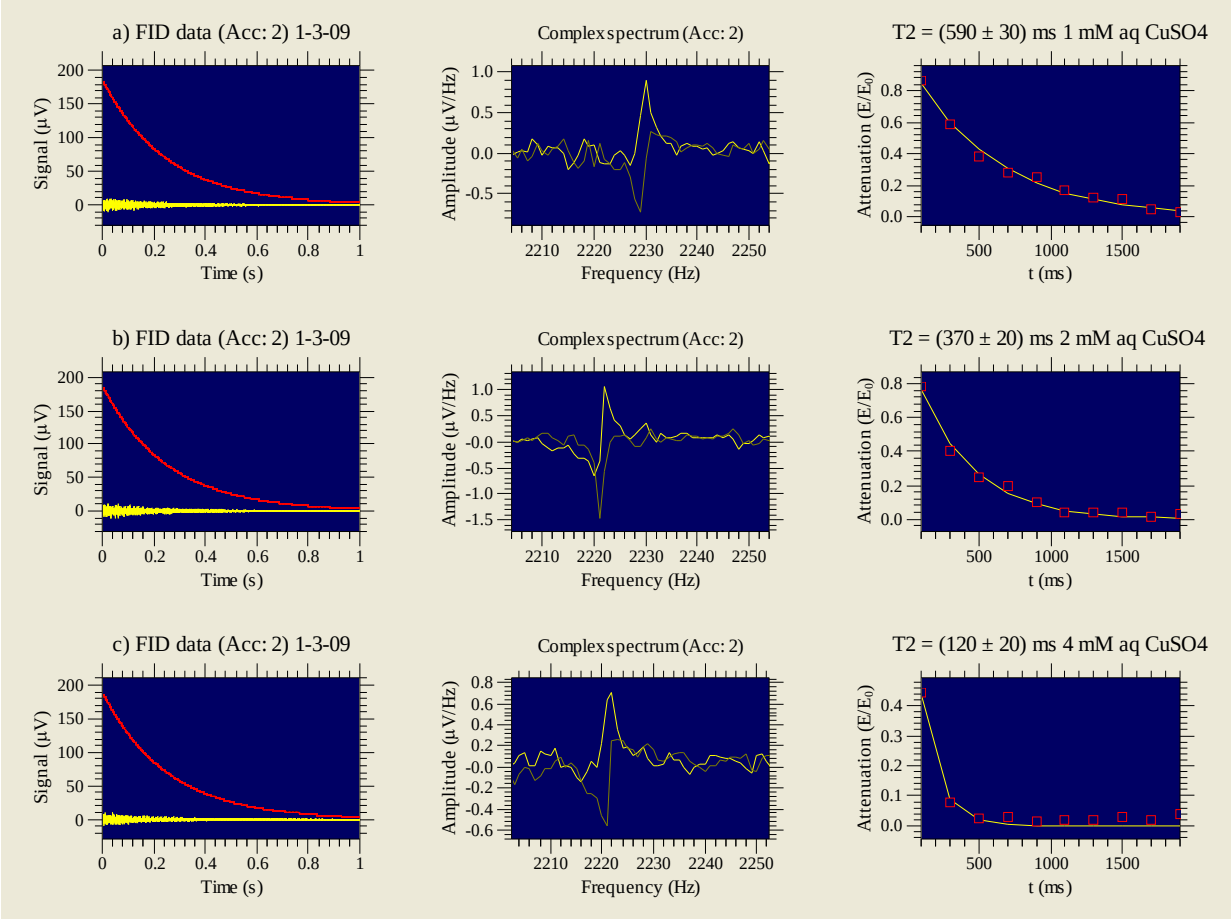

Figure A.35 T_2 plots of 500 ml water doped with various concentrations of cupric sulfate

A.5 Pulsed Gradient Spin Echo Experiment (PGSE)

PGSE is used to measure the molecular self diffusion coefficient and fluid flow. Two gradient pulses are applied after each RF pulse. Section 4.4 of the USER MANUAL covers this experiment in detail. The diffusion coefficient for water is determined as depicted in Figure A.36.

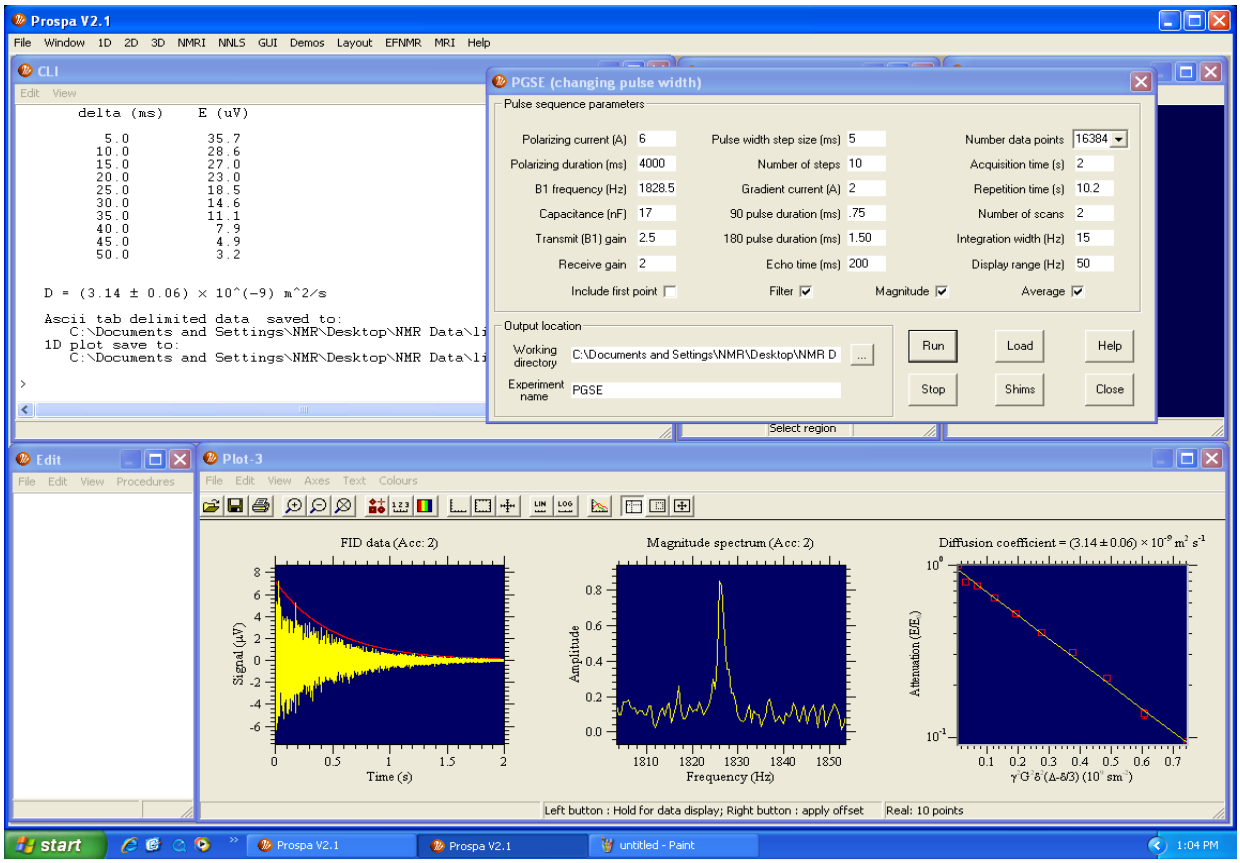

Figure A.36 Pulse Gradient Spin Echo Experiment

A.6 Multiple Echo Experiment (CPMG)

The Carr-Purcell-Meiboom-Gill (CPMG) experiment is a single shot spin-spin relaxation time constant measurement. The CPMG pulse sequence is applied to a sample to measure its T_2. This experiment introduces the principles of multiple echo experiments and the effects of various pulse phases on echo amplitude. Chapter 5 of the STUDENT GUIDE explains about this experiment. Figures A.37 and A.38 are examples of this experiment. As depicted in Figure A.38.c, the best T_2 is obtained through the use of refocusing 180° pulses having phases alternating by 180°, while the relative phase between the excitation 90° and refocusing (180°) pulses is 0.

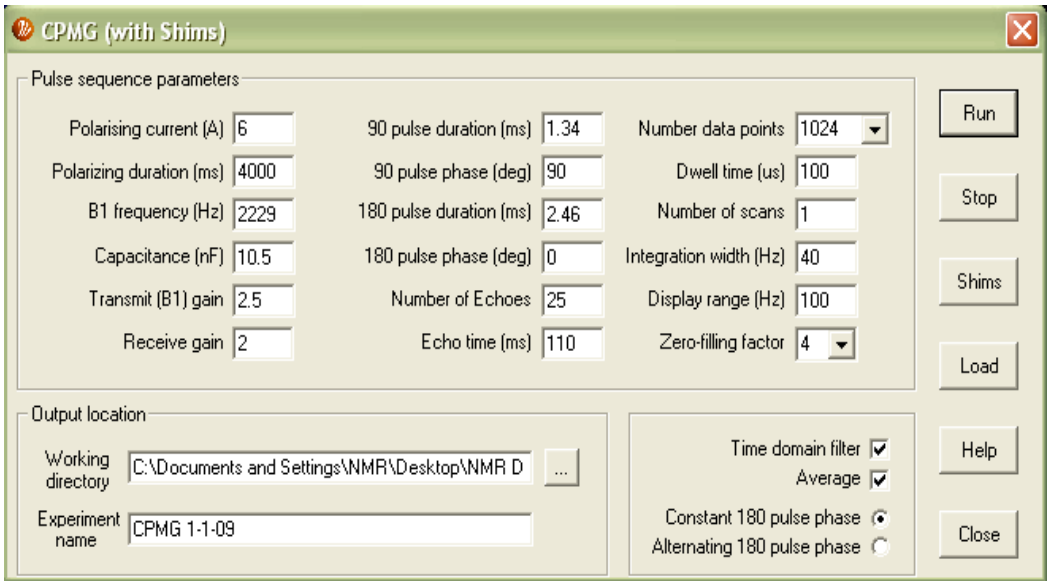

Figure A.37 CPMG macro of 500 ml bottle of water

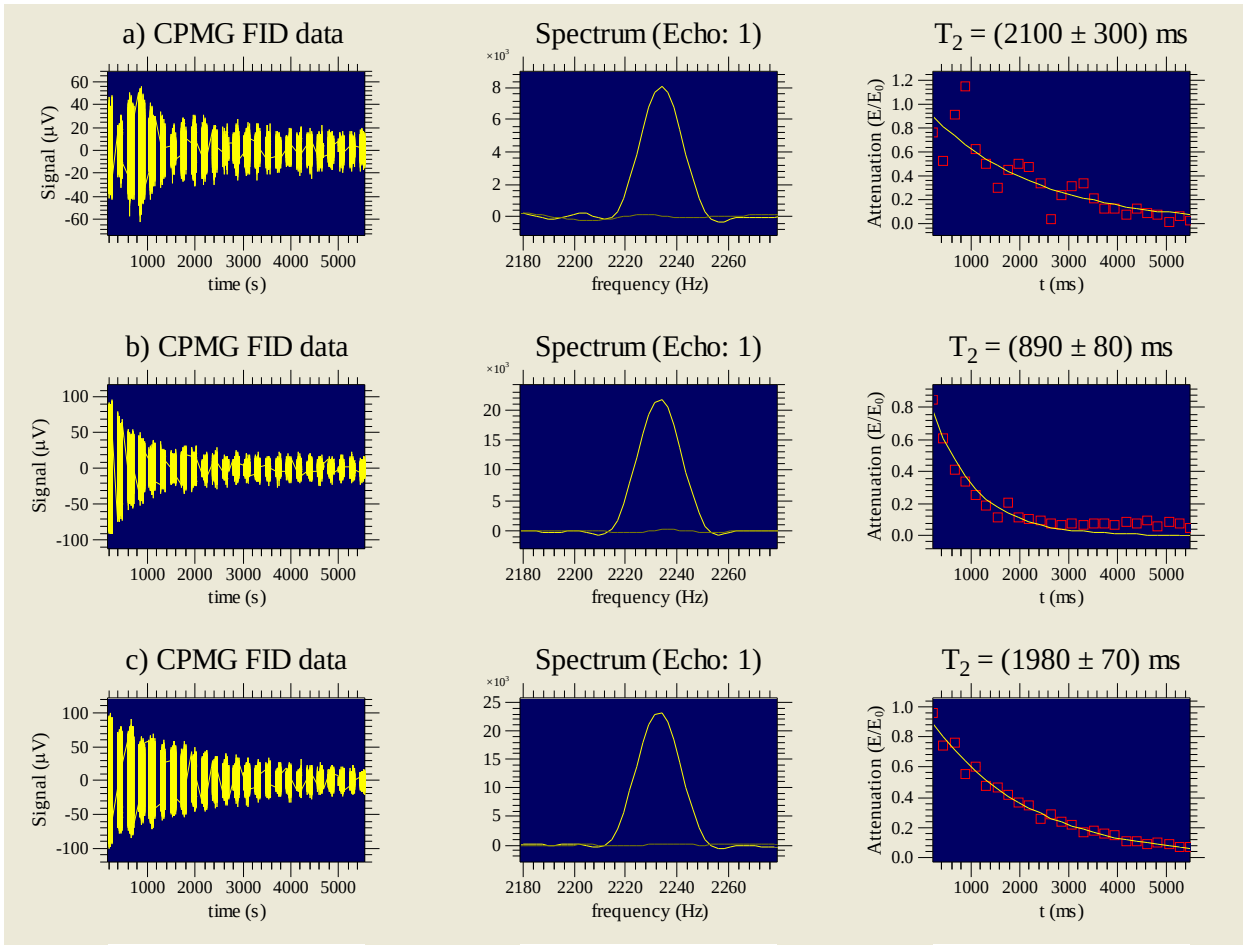

Figure A.38 Plots of CPMG of 500 ml bottle of water

A.7 Gradient Echo Magnetic Resonance Imaging in 1D

In MRI, a magnetic field gradient or simply gradient is applied before data collection to give each voxel (volume element) a unique NMR tag. MRI is an NMR experiment in which by applying gradients, information about the position of spins is encoded into signal. The gradients change the magnitude of the static magnetic field, B_0, as a function of position across the sample. Therefore spins in different regions of the sample experience difference magnetic field strengths, and will resonate at different frequencies. The direction of this magnetic field is always the same and points along the Z axis, but the magnitude of the field changes (Figure A.39). So, the Larmor frequency of the sample shows spatial dependence called spatial encoding.

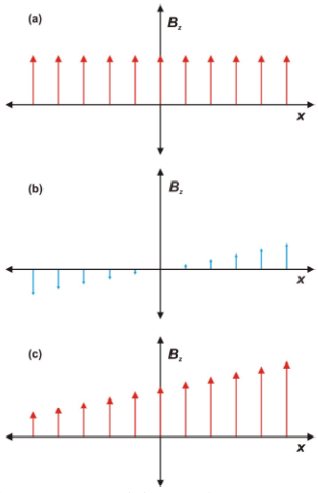

Figure A.39 (a) Static magnetic field in the Z direction. (b) Field gradient in the X direction. (c) Combined (a) and (b) gives a magnetic field in the Z direction that alters in magnitude as a function of X. (Magritek, Terranova-MRI Student Guide 2006)

Further, the term isochromat means localized group of spins all precessing at the same frequency. A single isochromat in the presence of a linear gradient at position, X, within a sample generates a signal; the NMR signal from the entire sample is the sum of the signal from all isochromats weighted by the spin density at each point in space. The spin density is the spatial representation of an ensemble of spins in a sample called image, and image information is extracted from the NMR signal.

The NMR data in the presence of a gradient is called k-space, Fourier space, angular spatial frequency or reciprocal space. It is called k-space because it is the space covered by the phase and frequency encoding data. K-space is a temporary memory for spatial frequency information, so a data acquisition matrix contains raw image data before image processing. Once k-space data is Fourier transformed, image data is obtained. In two dimensional Fourier transform imaging, a line of data corresponds to the digitized MRI signal at a particular phase encoding level. The position in k-space is directly related to the gradient across the object being imaged. By changing the gradient over time, the k-space data are sampled in a trajectory through Fourier space at each point until it is filled (DatabaseMRI, k-space 2003-2009).

EFMRI is performed via two methods: Gradient Echo (GE) or Spin Echo (SE) imaging. In Gradient Echo imaging the way to sample k-space is acquiring data by reversing the sign of the gradient meaning to reverse the k-space direction. First, the net magnetization vector is constant when the gradient is absent. However, when a gradient is present, each spin precesses at a frequency depending on position. In Figure A.39 this is shown by several magnetization vectors corresponding to each isochromat within the sample in which it rotates at an offset frequency. So, the spins precess at different rates dependent on the local field, some faster and some slower. When the gradient is reversed, meaning that the amplitude of the gradient is reversed from $-G/G_r$ (gradient read) to $+G/G_{ro}$ (gradient readout), the fast spins become slow and the slow spins become fast. The now fast will catch up with the now slow. When they catch up, the signal will be the highest which is called an echo. Stronger gradients result in shorter echoes because the slow spin slower and fast spin faster catch up with the slow spin and pass them, then the spins loose coherence quickly as well. This gradient reversal reverses the offset frequency of each isochromat causing the spins to re-phase to form an echo.

In terms of k-space, the k-space encoding vector decreases linearly as a function of time in the direction of *G* until gradient reversal. At the time of gradient reversal, it means that the evolution of the k-space vector is reversed from a linear decrease with time to a linear increase with time. So, after the gradient pulse inversion from $+G/G_r$ to $-G/G_{ro}$, sampling the signal as a function of time will cover an entire line of k-space from -k to +k. In summary, k-space is traversed during a gradient echo as follow: as the spins evolve in the gradient -G, the k-space vector decreases linearly with time from 0 to -kx. Then, reversal of the polarity of the gradient inverts the spin evolution, and the k-space vector increases linearly with time from –kx to 0 and to +kx. Acquisition of the entire line in k-space occurs during the G_{ro} phase, not G_r.

This technique is called Gradient Echo because refocusing the signal like Spin Echo creates an echo. The center of this echo occurs at k = 0, and the time to the center of the echo is marked T_{echo}.

In MRI the axis in which the image is formed is determined by the gradient. For example, an image along X means the gradient is directed along the X axis (the long axis) of the probe. The Z axis is directed along the blue arrow on the end of the probe which is aligned with the Earth's field during the set up process (orientation). This alignment is very important for imaging because the gradients will not be orthogonal if the probe is not aligned properly. Finally the Y axis is orthogonal to both the Z and X axes.

An object dimension must be measured for imaging; this is called the field of view (FOV) of the image. Also, a pixel is defined as the smallest unit of an image on a computer screen. Equation A.8 describes the correlation between FOV and the number of pixels in the image, the matrix size (N), with the image resolution, also called the size of a pixel (ΔX).

Equation A.8: $\Delta X = FOV/N$

The higher the size of a single pixel, the lower the resolution will be, and the higher the number of pixels, the higher the resolution will be. ΔX is called nominal resolution because blurring between pixels may cause the actual resolution to be worse. Also, FOV should be large to encompass the entire sample, yet small enough so that the sample occupies most of the FOV. A large matrix size improves the resolution of an image, but causes a low SNR and long experiment time, so, a compromise should be considered. The frequency spread across the image (Δf) is called the bandwidth and measured in Hz. For a FOV and bandwidth, the gradient strength is calculated by Equation A.9.

Equation A.9: $$Gx = \frac{2\pi\Delta f}{\gamma FOV}$$

The procedure for running a GE experiment includes running an Auto shim with the sample to ensure a narrow line-width. These parameters are not visible in the imaging macros, yet they are used. Then, T_1-B_p and T_2 experiments should be run to determine proper polarizing duration and echo time. Polarization duration should be considered as twice to three times as T_1 to compromise between a short imaging time and best SNR while echo time should be considered 1/3 of T_2 in case of SE experiment and in case of GE as follow:

Equation A.10: $T_{echo} = 2\ (T_{acqu\text{-}delay}) + T_{acqu}\ (N/\Delta f = 32/64 = 0.5s) = (2 \times 20\ ms) + 500\ ms = 540\ ms$

It should be noted that an echo-time of less than 100 ms causes image distortion. For GE and SE imaging, the phase gradient duration (T_{grad}) should be as short as possible (50 ms). These values should be inserted in the GE imaging macro (Figure A.41).

Next, common parameters located under the MRI menu which are determined during the instrument setup (Figure A.40) should be checked. Then, GE imaging under the same menu is selected (Figure A.41) which contains image parameters, pulse sequence parameters, and output location. Image parameters are number of dimensions, orientation, FOV, and number of the

pixels in the image.

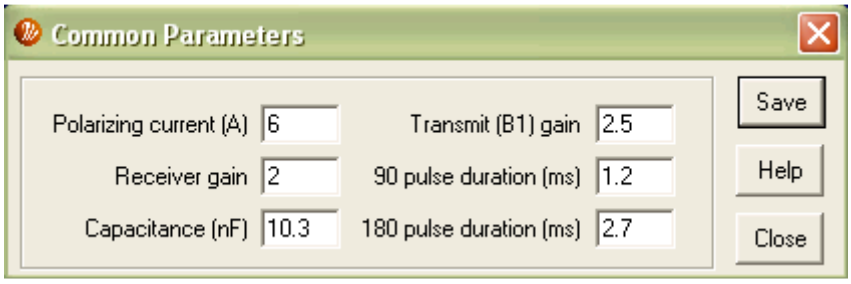

Figure A.40 Common Parameters

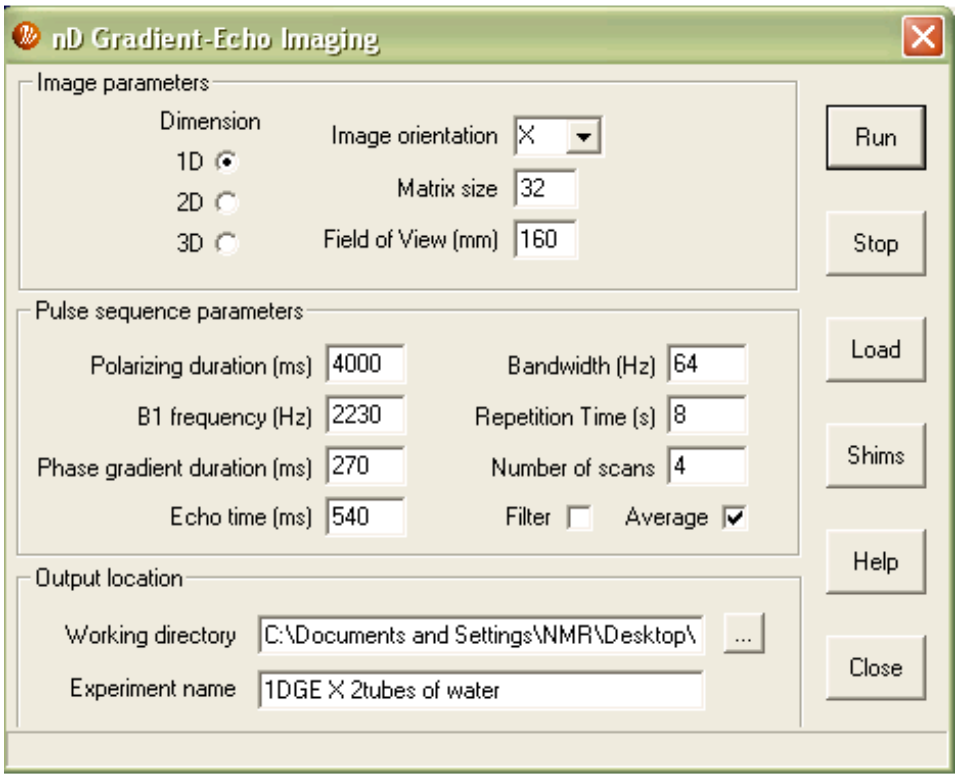

Figure A.41 1D GE X macro for 2 phantom tubes of water

The GE pulse sequence (Figure A.42) includes the polarization and RF pulses in which at the end of the RF pulse the magnetic field gradient, called the read gradient or encoding gradient ($-G/G_r$), is switched on. The read gradient changes the strength of the magnetic field as a function of position, causing the spins to precess at different frequencies according to their location. This causes a loss of phase coherence as a function of time causing the decay of the FID signal corresponding to a progression with time of the k-space vector from zero (at time = 0)

to –k. After T_{grad} time, called phase gradient duration, the gradient is switched to a positive value called gradient read out (+G/G_{ro}). The change in gradient polarity causes re-phasing of the spins and forming a GE. Therefore, G_{ro} is the opposite of the encoding gradient which causes the spins to rephase and form an echo. G_{ro} is left on for the duration of acquisition, no matter how long that may be. The time from the excitation pulse to the center of the echo is called the echo time (T_{echo}). In terms of k-space, the positive gradient results in a linear increase in the k-space vector as a function of time, so that the k-space vector evolves from –k to 0 to +k as a function of time.

In general, echo is a term for re-phasing (and not de-phasing) of the spins in case of the 180° pulse. However, in GE imaging the time between the gradient switch and the center of the echo is called echo time. Although in GE imaging the procedure includes reversing the gradient polarity and refocusing of the de-phased signal which results in the formation of an echo, this procedure neither refocuses the de-phasing due to underlying magnetic field in-homogeneity, nor spin-spin relaxation.

Based on Figure A.42, the echo time, is the time from the RF pulse to the center of the echo. The phase gradient duration, T_{grad}, is the time from the RF pulse to the gradient switch. The delay between the gradient switch and the beginning of the acquisition is called $T_{acqu\text{-}delay}$ and the acquisition time, T_{acqu} is the time data is acquired. The acquisition delay is considered 20 ms to allow for any B_1 coil ring-down caused by switching gradients.

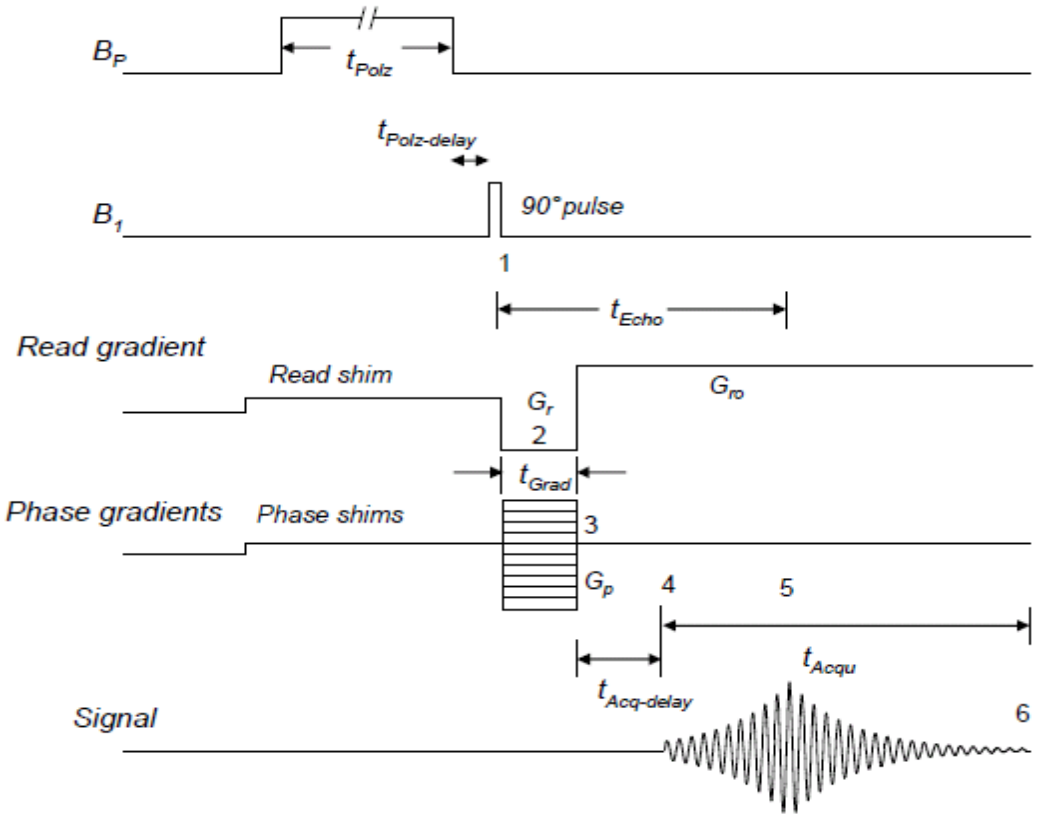

Figure A.42 Pulse sequence for GE imaging
(Magritek, Terranova-MRI Student Guide 2006)

After clicking run on GE imaging macro, a dialog called Confirm Parameters appears (Figure A.43). It shows the field of view, gradient strength, gradient current, and shim current for the three axes. In the one-dimensional case the second and third gradients are zero while there is shim currents used on these axes. The two gradient values for the read dimension (G_r and G_{ro}) are of equal magnitude but opposite sign. The polarizing coil duty cycle should be 50% or less to prevent overheating and is calculated as the ratio of the polarizing duration to the repetition time. The total experiment time for 1D imaging is equal to the repetition time times the number of accumulations. The acqu.par file listed at the bottom of the confirm parameters contains all the experimental parameters, the data.1d file contains the raw k-space data, and data.pt1 contains the final plot of the k-space data and the image.

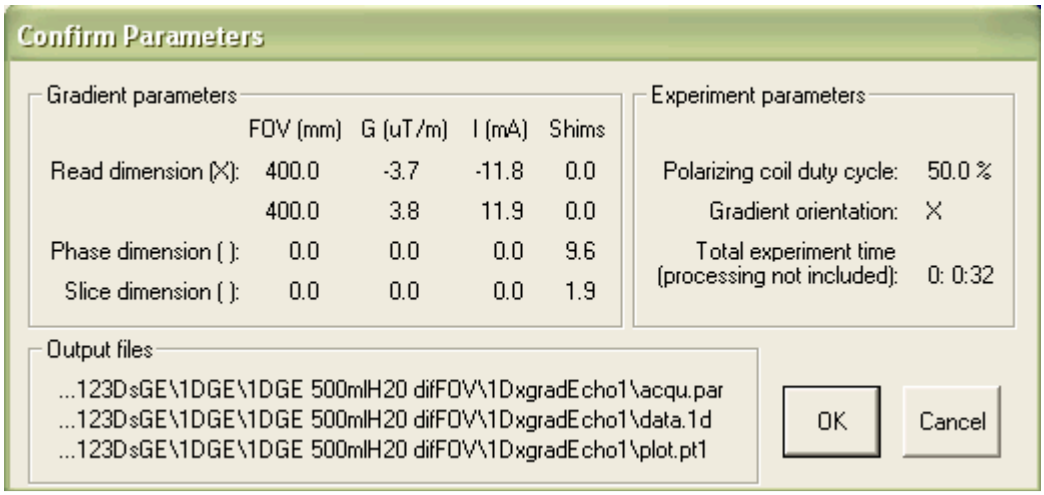

Figure A.43 Confirm parameters window

In Terranova-MRI imaging, data is obtained via a large number of data points (16384). Following the acquisition, the data being sampled are converted in Prospa from the Larmor frequency to zero and then encountered with a filter that eliminates all frequencies outside the chosen bandwidth. Therefore only frequencies within the bandwidth being centered about the B_1 frequency remain. The output of the filtering process is the k-space signal with real and imaginary components which include no noise over the chosen bandwidth. The number of points in the filtered signal is equal to the number of pixels in the image. The filtered k-space signal is displayed in the left-hand plot of the 1D plot window (Figure A.44). The Y-axis for the k-space as well as the image is the signal intensity. These values are arbitrary and a function of the voltage induced in the probe.

Figure A.44 demonstrates that the echo is in the center of the acquisition window. All image information is retrieved in the form of an echo. The amplitude of the echo decays as a function of the echo time with a time constant of T_2. So, the longer the echo time, the less intense the echo will be. It should be noted that the echo time should be well below the T_2 value since at time T_2 only about 37% of the FID signal is left.

Also, Figure A.44 demonstrates the application of two phantom tubes where “phantom” in MRI refers to a sample that is constructed to mimic a target sample. The length of the probe cavity is 28.5 cm, the length of the tubes is 11.5 cm, the diameter of the tubes is 28 mm, and the separation between the tubes is 7 mm. These tubes are used to provide an image with the difference between nominal and actual resolution. In case of the X direction (part a of Figure A.44) neither the edges are sharp nor is the top flat. This is due to blurring in the image and effects of the long length of the sample bottle compared to the region of gradient linearity. This causes the signal to roll off at the edges instead of having sharp edges. The projection along the X and Y axes contains one peak in the image (parts a and b of Figure A.44). However, the projection of the sample magnetization onto the Z axis contains two peaks which represents the two tubes (part c of Figure A.44).

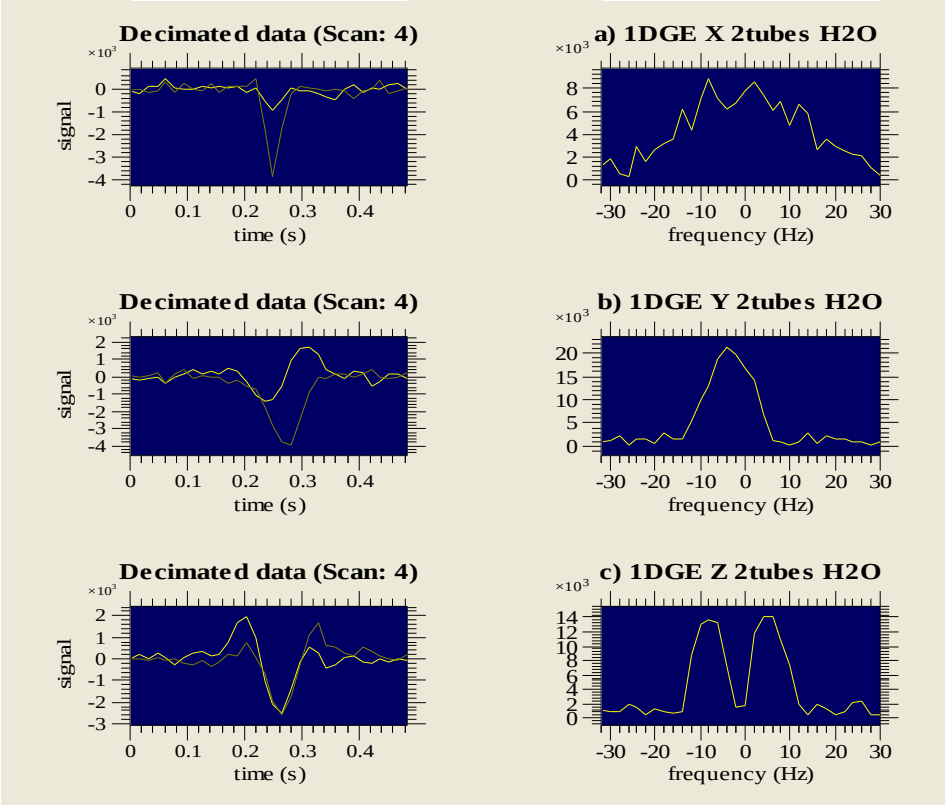

Figure A.44 Plots of 1D GE X for 2 phantom tubes of water

Until now the magnitude of the signal has been visualized while in the k-space plot the

complex data is presented as well. The complex data contains a set of imaginary (pale line) and real numbers (solid line). The phase is determined from these numbers, and as the phase changes the real and imaginary cycle through positive and negative numbers. The image plot is in magnitude, which is the magnitude of the real and imaginary parts.

The next attempt is to explore 1D imaging parameters in terms of frequency. Figure A.45 illustrates the macro for the first experiment of 1D GE X orientation of 500 ml water with a FOV equal to 150 mm. From the plot window in Figure A.46, the width of the sample in frequency units, the applied gradient strength and current (either by calculating or via the confirm parameter dialog window) along with the width in space of the sample were determined and collected as Table A.1. Figure A.46 illustrates 1D GE imaging of a 500 ml water bottle in X, Y, and Z orientations along with FOV of 150, 200, and 400 mm for each orientation. The length of the bottle is 14 cm while the diameter is 7 cm. So, considering the length of the cavity, by inserting the bottle, 7.25 cm of the cavity is empty on each side. As depicted in Figure A.46 by increasing the FOV the frequency spread across the sample (bandwidth) is decreased which means by increasing the FOV the object appears smaller because with a larger FOV the sample takes up less of the available space.

Table A.1 A comparison of the object width in space versus the acquired width in Hz

$G_r = 2\pi\Delta f/\gamma FOV$	Width of the sample from the plot (Hz)	Gradient Strength (μT/m)	Gradient Current (mA)	Width of the sample (cm)
FOV=150 mm	X=60	-10	-31.5	14
FOV=150 mm	Y=35	-10	-36.2	7
FOV=150 mm	Z=35	-10	-36.2	7
FOV=200 mm	X=42	-7.5	-23.7	14
FOV=200 mm	Y=28	-7.5	-27.2	7
FOV=200 mm	Z=28	-7.5	-27.2	7
FOV=400 mm	X=28	-3.7	-11.8	14
FOV=400 mm	Y=16	-3.7	-13.6	7
FOV=400 mm	Z=16	-3.7	-13.6	7

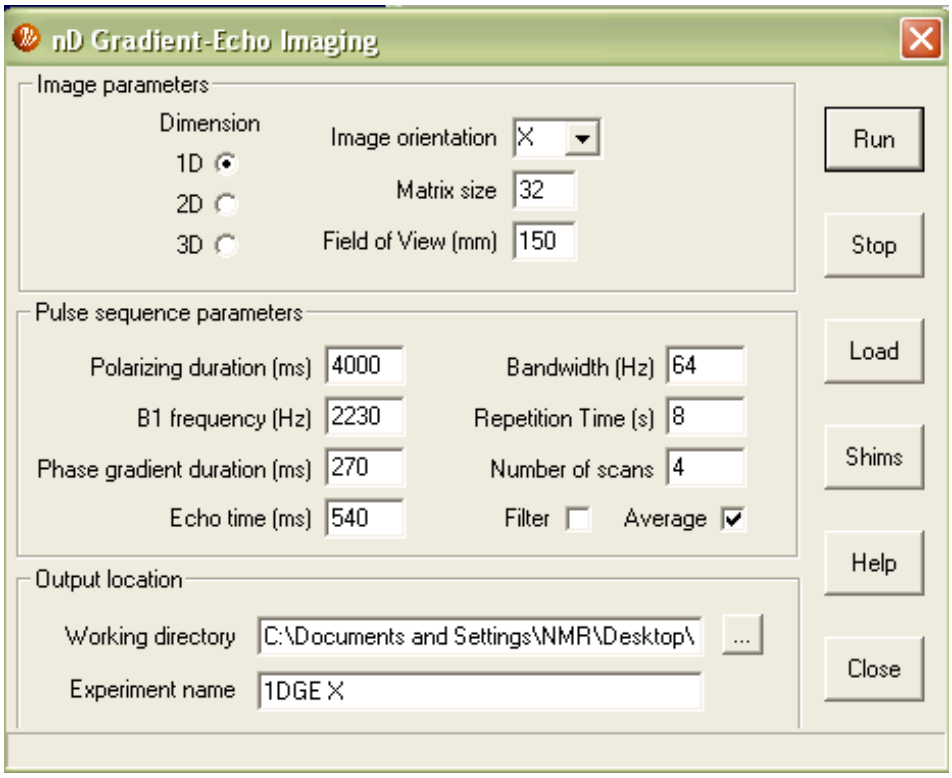

Figure A.45 1D GE X orientation macro for a 500 ml water with a FOV of 150 mm

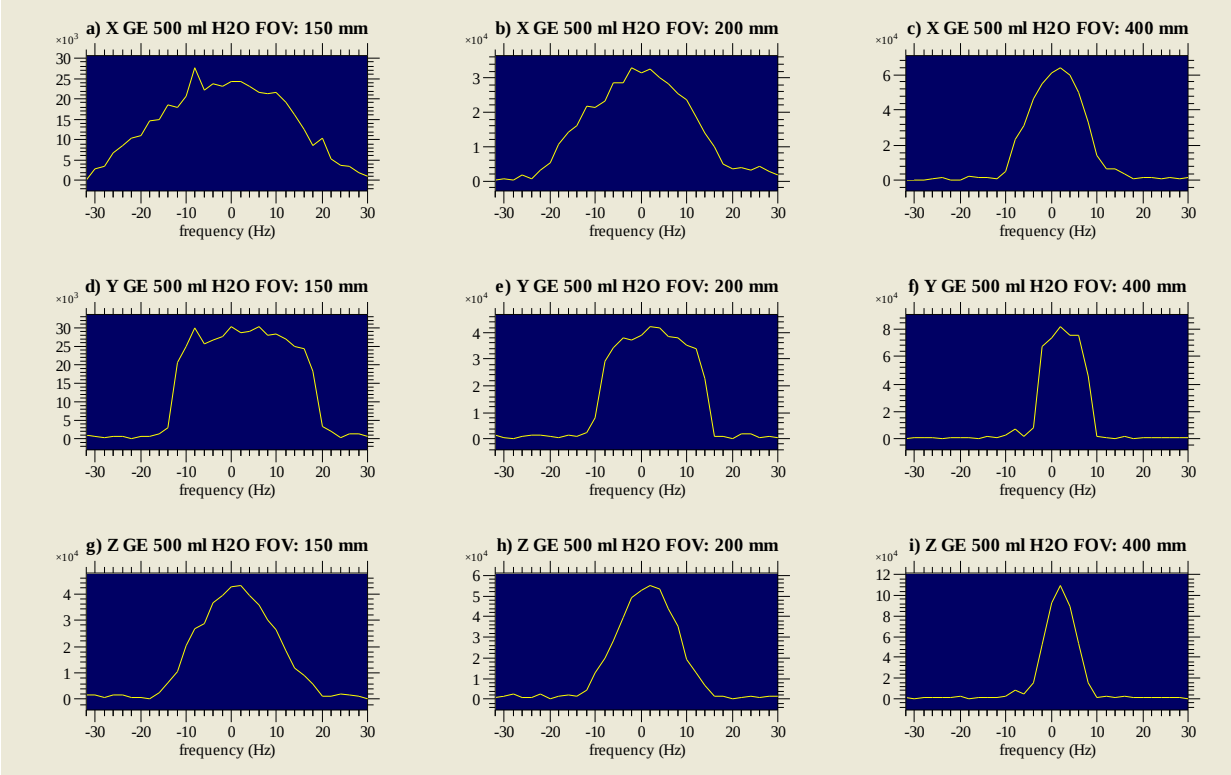

Figure A.46 Plots of 1D GE X orientation of 500 ml water with various FOV

The bandwidth of the signal corresponds to the FOV of the image. Line width in Hz is defined as spectral resolution or frequency resolution designated as Δf, and narrow line width means more resolution and better SNR. So, with a 500 ml water bottle a PC was done and an FID with an acquisition time of 3 seconds was acquired. To properly measure the line width, the magnitude option should be turned off. The line width of a single pixel is measured as follow: Δf/N = 64/32 = 2 Hz while the spectral line width of the peak is 42/32 = 1.3 Hz (FOV = 200mm). So, blurring in the image (Figure A.46) is present. Figure A.47 demonstrates the same plots as Figure A.46 along with the obtained k-space plots.

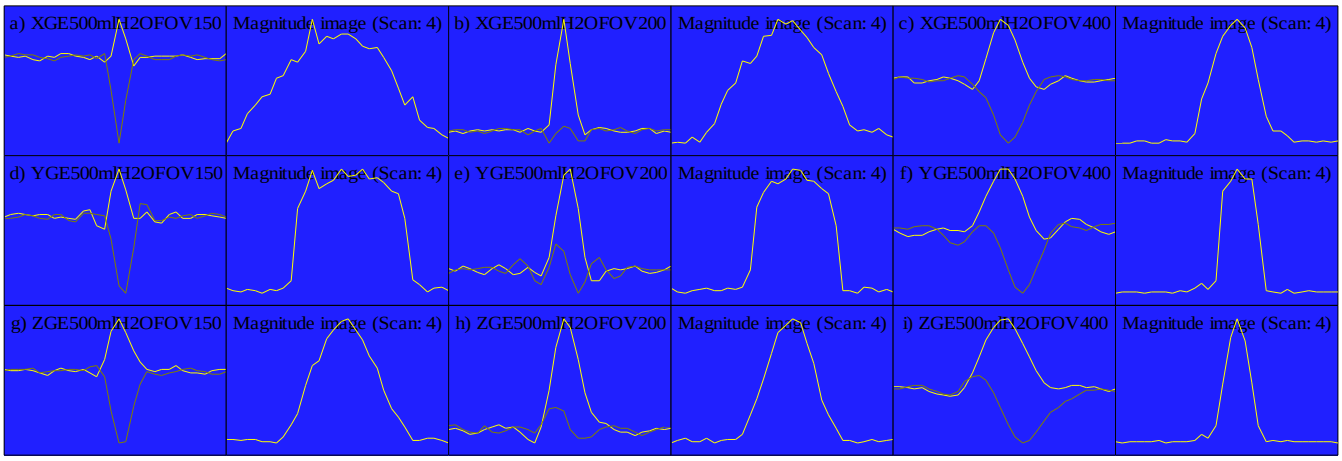

Figure A.47 Plots of 1D GE X orientation of 500 ml water (K-Space and various FOV)

A.8 Gradient Echo Magnetic Resonance Imaging in 2D and 3D

1D MRI, the method of sampling k-space as a function of time in the presence of a constant gradient G is covered. In this method magnetic field gradients are used to encode the spatial position of the spins by changing the Larmor frequency of the spins as a function of position during signal acquisition, also referred to as frequency encoding. However, in order to acquire 2D MRI, a combination of frequency encoding and phase encoding is required. In frequency encoding, the gradient is kept fixed while k-space is sampled as a function of time, whereas in phase encoding the time is kept fixed and data is acquired for discrete values of G.

The reason it is called phase encoding is because over a fixed time period, T_{grad}, in which the gradient is applied, the spins acquire a phase offset correlated to position. And an entire line in k-space in the phase dimension is obtained by acquiring data for a range of gradients from $-G_{max}$ to $+G_{max}$. In 2D MRI, frequency encoding is applied in the read dimension (first dimension) while phase encoding is applied in the phase dimension (second dimension). So, frequency change and phase change are both a function of position.

According to Figure A.42, the pulse sequence for 2D GE imaging is as follow: The polarizing pulse (B_p) is switched on to magnetize the sample for the duration of at least twice the sample's T_1 to get a reasonable signal level. Then, there is a short delay ($T_{polz\text{-}delay}$ = 50 ms in which limits T_1 of samples to more than 100ms.) to allow the current to switch off and the magnetization to rotate along the Earth's field direction. Next, the 90° B_1 pulse excites the sample followed by the application of $-G/G_r$ in the read dimension which spatially encodes one dimension of the image. At the same time, in the phase dimension, a gradient pulse is switched on following the excitation pulse which has a duration denoted by T_{grad} (phase gradient time). During this pulse, the spins acquire a phase offset that is proportional to their position (The gradient echo does not refocus this phase offset since the direction of the phase gradient, G_p, is orthogonal to the direction of the read gradients, G_r and G_{ro}). The read, G_r, and phase gradients, G_p, are switched on for a time T_{grad} to move the sampling into k-space. These gradients cause a rapid de-phasing of the magnetization. Following the phase and read gradient pulses, the read-out gradient, G_{ro}, is switched on and the receiver starts digitizing the signal induced by the precessing magnetization. The readout gradient has the reverse sign to the shorter read gradient so that the spins re-phase producing an echo. Again, there is a short delay *(*$T_{acq\text{-}delay}$ = 20 ms) between the end of the phase gradient pulse and the start of data acquisition to allow for coil

ring-down. The encoding means encoding in both directions (T_{grad} encoding time of phase and T_{grad} encoding time of read/G_r). They are generally the same time for each gradient but not necessarily the same strength. This pulse sequence is repeated N_p times for values of G_p from $-G_{pmax}$ to $+G_{pmax}$ in order to sample all 2D k-space.

Moreover, in terms of k-space sampling, it includes the signal excitation by the RF pulse and the magnetization vector rotating into the transverse plane. Then the read gradient (G_r) and the phase gradient (G_p) are switched on followed by evolution as a function of time in the presence of these two gradients leading to a movement in the read and phase dimensions in k-space. Next the phase gradient is switched off, so there is no more evolution in the phase dimension. Then the read gradient is switched in polarity so that the evolution in the read dimension is reversed, and the spins precess as a function of time in the positive read gradient. In k-space this is a progression from negative k-read, to zero on the read axis to positive k-read. Data is sampled as a function of time during this evolution along one line in k-space, and, the read gradient is switched off while acquisition of one line in k-space is complete. The entire process is repeated for different values of the phase gradient G_p, so each line in k-space is sampled. Finally a 2D image is acquired from the k-space via employing a Fourier transform. The Fourier transform is implemented automatically while the data is collected, however in case of 3D, k-space data is not Fourier transformed until all data has been collected.

The phase gradients are zero in 1D imaging, so k-space is one dimensional; for 2D imaging, there is a phase gradient producing 2D k-space, while for 3D imaging there are 2 phase gradients producing 3D k-space data. In all three experiments a single read gradient is used.

At this point it is important to describe ways of improving imaging efficiency. Obtaining 2D and especially 3D images are time consuming because an echo signal for each step of the

phase encoding gradient should be acquired. Therefore it is necessary to make the acquisition as efficient as possible in order to acquire fast 2D or 3D images. The goal in imaging is to acquire the best SNR in a short time. Also, it is known that by signal averaging *N* images, the SNR of an image can be increased by a factor of $\sqrt{N}$ at a cost of a factor of *N* in imaging time. Based on this, to improve imaging efficiency, we have to decrease the imaging time and increase the SNR of a single acquisition.

It is known that the polarizing pulse applied to maximize the signal for a water sample is the most time consuming pulse of the imaging process. Also, the implemented delays between the polarizing pulses to prevent overheating in the coil take time. As explained earlier, the time required to obtain a sufficient polarization in the sample during the polarizing pulse is known as the spin-lattice relaxation time constant T_1. So the optimal polarizing time depend on the T_1 of the sample and can be estimated to be 2-3 T_1.

Therefore, it is beneficial to use a sample with a short T_1 in order to minimize the polarization time. As explained in the introduction, the relaxation properties of water can be modified through the use of a paramagnetic contrast agent such as $CuSO_4$. The local magnetic fields generated by a paramagnetic contrast agent, due to its positive magnetic susceptibility, decrease the T_1 and T_2 relaxation times of nearby hydrogen nuclei (neighboring spins). For example, a solution of 3 mM copper sulfate in a 500 ml bottle has a T_1 and T_2 of 200 ms. Therefore, by using this sample, the polarization time reduces from 4000 ms to 400 ms.

(2 × T_1 = Polarization time; 2 × Polarization time = Repetition time, TR)

So, if a 2D imaging with a matrix size (N_p) of 32 and 8 scans (N_{scan}) is run with and without the contrast agent, the experiment time would be:

With the agent: Experiment time = TR × Np × Nscan = 800 ms × 32 × 8 = 204.8 s = 3.4 min

Without the agent: Experiment time = TR × Np × Nscan = 8 s × 32 × 8 = 2048 s = 34 min

By applying a greater matrix sixe, a higher number of accumulations or by running a 3D image; the difference in the experiment time will be more profound. Therefore, it is possible to improve the efficiency by shortening imaging time via the application of a contrast agent.

In addition, in the GE pulse sequence if the echo time is long and T_2^* is short, then the SNR of the image will be low. So, it is wise to use a short echo time to improve the SNR in order to increase the efficiency of imaging. There are two ways to decrease the echo time in a GE pulse sequence: by increasing the gradient (G_r) amplitude or by asymmetric echo sampling.

The center of the echo occurs at the center of k-space, k = 0 and $G_r = G_{ro}$ (Figure A.42). So echo occurs at a time, T_{grad}, following the gradient switch, where T_{grad} is the duration of the first pulse. In order to maintain a large acquisition time and have a high frequency resolution image, the duration of the second gradient pulse cannot be shortened. However, it is possible to increase the amplitude of the first gradient pulse and decrease its duration to cause a decrease in the echo time without decreasing the acquisition time. For example, G_r amplitude could be increased from 7.5 μT/m to 40.5 μT/m to shorten the echo time (Figure A.42) from 540 ms to 320 ms based on the following Equations:

Equation A.11: $T_{echo} = 2\,(T_{acqu\text{-}delay}) + T_{acqu} = 2 \times 20\text{ ms} + 500\text{ ms} = 540\text{ ms}$

Equation A.12: $T_{acqu} = \frac{Nread}{\Delta f} = \frac{32}{64} = 0.5\text{ s} = 500\text{ ms}$

where N_{read} is the number of pixels in the read dimension (matrix size) and Δf is the bandwidth. (Longer T_{acqu} means more resolution)

Equation A.13: $T_{echo} = T_{grad} + T_{acqu\text{-}delay} + \frac{1}{2} T_{acqu} = 50\text{ ms} + 20\text{ ms} + \frac{500ms}{2} = 320\text{ ms}$

The $\frac{1}{2}$ factor that appears before T_{acqu} in the above expression for the echo time constrains the echo to the center of the acquisition window which means that negative and positive k-space are

sampled equally. However, the echo time can be reduced more by allowing the echo to appear early in the acquisition window meaning negative k-space is not sampled as fully as positive k-space. This method is called asymmetric echo sampling.

The noise level usually is higher than the signal level at negative k-space, so new information is not obtained by sampling this data. Also, the magnitude of the image will not be affected by only sampling positive k-space. However, in practice it is wise to choose an echo time to encompass the negative k-space sampling such that both sides of the echo are present in the acquisition window. Therefore echo time should be reduced from 0.5 to 0.25 for the T_{acqu} as follow:

Equation A.14: $$T_{echo} = T_{grad} + T_{acqu\text{-}dealy} + \frac{1}{4} T_{acqu} = 50 \text{ ms} + 20 \text{ ms} + \frac{500}{4} \text{ ms} = 195 \text{ ms}$$

As a result, by decreasing the echo time through the use of higher G_r amplitude or the asymmetric echo sampling a better SNR and a higher efficiency in imaging is possible. For example, by considering the three obtained T_{echo} as 540 ms, 320 ms, and 195 ms, the relative echo amplitude are 0.165, 0.344, and 0.522 respectively. Therefore, by comparing the first two echo times, the SNR shows an improvement by a factor of two while by comparing the first and the last echo times, the SNR shows an improvement by a factor of three.

The procedure for running a 2D GE imaging of 500 ml doped water is similar to 1D GE imaging. Just like 1D MRI, a 2D MRI is only a projection of the entire 3D sample into a given plane and it is not a slice through the object along the imaging plane as is the case with medical imaging. The image orientation menu provides six permutations for the read and phase gradients as XY, XZ, YX, YZ, ZX, and ZY. The first letter in a pair addresses the direction of the read gradient and the second denotes the direction of the phase gradient. As an example, in XY image the read direction represents the long axis of the probe and the phase direction represents

the axis orthogonal to both the long axis of the probe and the direction of the Earth's field. Further more, the ZY or YZ plane is the plane perpendicular to the long axis of the coil and a 2D image of the long bottle in this orientation will be circular.

The matrix sizes for the read and phase dimensions are chosen separately, as is the case for FOV in each direction. It is possible to have different matrix sizes in the two dimensions, but it is recommended to maintain an isotropic FOV, meaning FOV should be the same in all directions. A chosen FOV should encompass the entire sample but should not be much larger than the dimensions of the sample (180-200 mm). A matrix size of 32 in the read dimension and 16 in the phase dimension is recommended to avoid a long experiment time. The optimal polarizing duration for the 500 ml doped water sample (3 mM) is 600 ms as a compromise for a short imaging time and a good SNR.

It is recommended to run a PC right before acquiring an image in order to determine the correct B_1 frequency (Larmor frequency) of the sample. The optimal values for the following are: phase gradient duration = 50 ms, echo time = 200 ms, bandwidth = 64 Hz and repetition time = 1.5 s. Four signal averages leads to achieving a good SNR.

Figure A.48 depicts a macro for part a) of Figure A.49, and it should be noted that the parameters on this macro are somewhat different than what is described above. Figure A.49 illustrates the images of the doped water in six possible orientations while in each case the image parameters such as FOV or matrix size are different from the rest. On the left side k-space data is presented while on the right the 2D Fourier transform of k-space (image) is present. Also, in parts a) and b) in the X dimension, d) in the Y dimension, and f) in the Z dimension of this figure there is a vertical streak of noise hence it is repeated in every single scan at the same point even though there is no signal at the beginning or end. It can be removed sometimes by decreasing

the bandwidth until it is no longer visible, but this reduces the image resolution. However if the noise peak appears within the image, repositioning the probe is the solution.

The image plot is in magnitude and the red is the most intense while the k-space is complex data and only the real component is plotted in the 2D window (Figure A.49). If the most intense regions of k-space data are desired, plotting the magnitude of the k-space should be acquired. Then, a cone instead of line ripples moving away from a drop of water is observed.

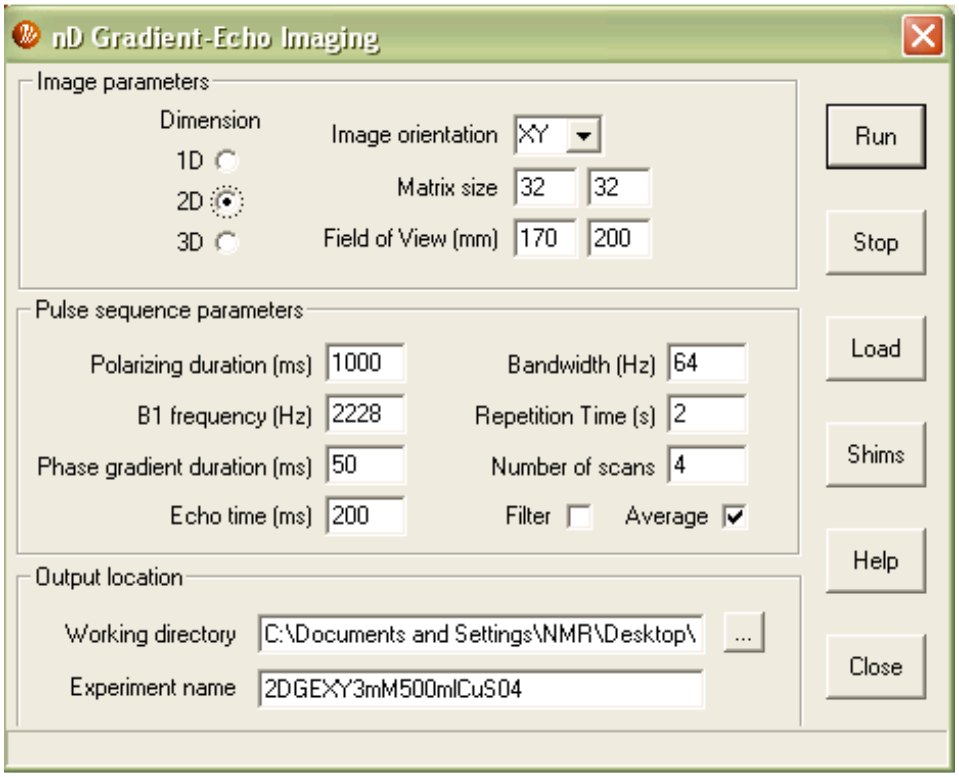

Figure A.48 2D GE macro (XY imaging orientation) of 500 ml doped water

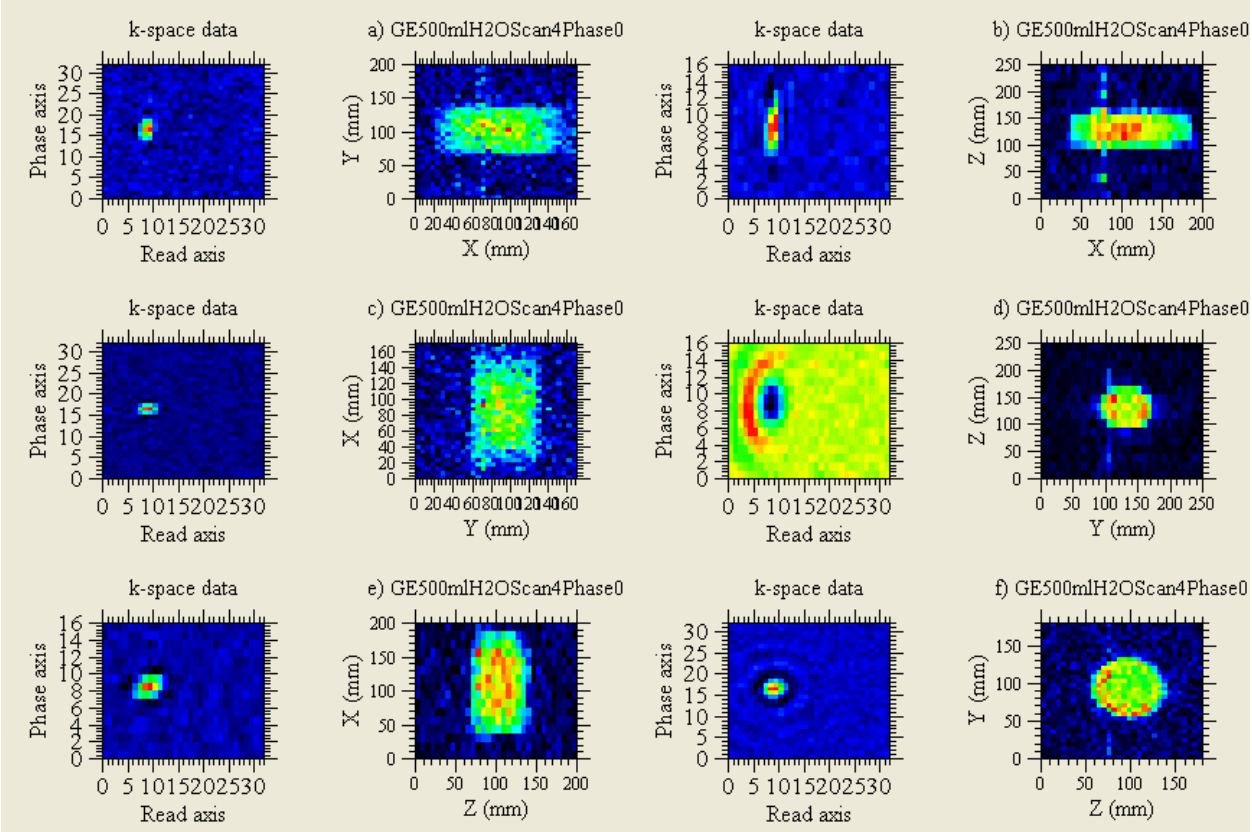

Figure A.49 Plots of six possible orientations via 2D GE imaging of 500 ml doped water

As the acquisition proceeds the 2D plot windows will be updated with newly obtained data. The phase gradient steps are implemented such that the center of k-space is acquired first while the outer lines of k-space are acquired last. The low spatial frequencies equivalent to the center lines of k-space (low values of k) provide a low-resolution image whereas the high spatial frequencies equivalent to the outer lines of k-space (large values of k) provide high-resolution image information. Therefore, as k-space is sampled from the center out, the image will become more defined meaning the acquisition of high k-space data adds more definition to the image which results a high-resolution image. As a result, the edges of the image become crisper as higher k-space data is acquired. However, for large numbers of pixels in the phase dimension, N_p, there will be a point where additional lines in k-space are mostly noise resulting in no increase in image resolution.

More specifically, when a spectrum in both directions is taken; one direction is using the echo, and the other direction is using the phase. And when transforming a short FID such as 0.25s a broad peak will be obtained while the resolution will be determined by how long the FID is collected. On the other hand, if a 2 seconds FID is collected, a much narrower peak will be obtained meaning a higher resolution is achieved. The same scenario is true for an echo. If the ends of an echo are chopped off, a broad peak is acquired. Where as if far beyond the echo peak is collected; it will narrow and produce a more resolution signal.

It should be noted that because of the acquisition delay ($T_{acq\text{-}delay}$) it is not possible to sample all the k space data. Even if this delay were zero, sampling a whole row of k-space requires a long echo time which may result in significant signal reduction if the sample T_2 is short. To minimize incomplete sampling of k-space, the echo time should be selected long enough so that data acquisition begins well to the left of the echo peak.

By performing a 2D experiment, collecting an echo one point at a time in the phase direction and the entire echo in the read direction is accomplished. In the phase direction, the middle points of the echo are collected first because those will be the most intense spectra. However, to get the resolution needed to fill out the echo on either side, it is obtained by going to higher phases while not much information is acquired, yet higher resolution is obtained.

Figures A.50-53 relates the presence of contrasting agent enhancing the MRI signals while reducing the experiment time to improve the imaging efficiency as explained earlier.

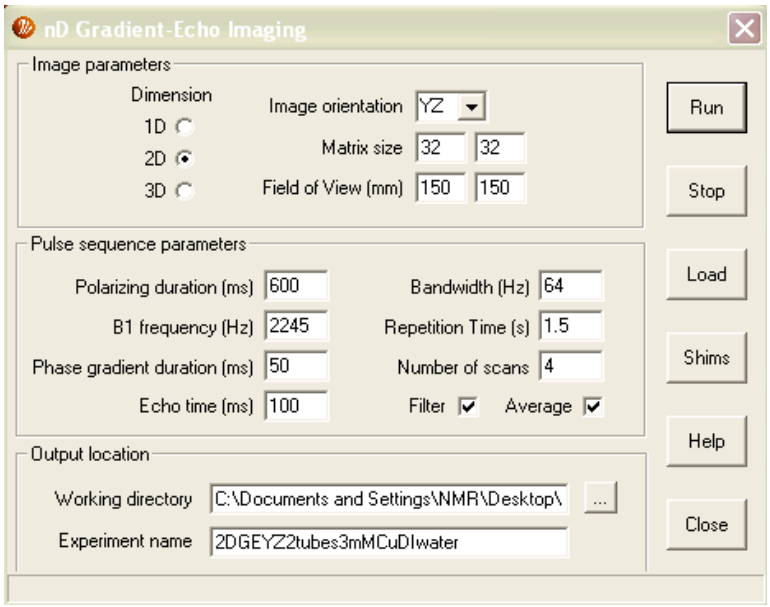

Figure A.50 Macro of 2 tubes: water versus doped water (contrast)

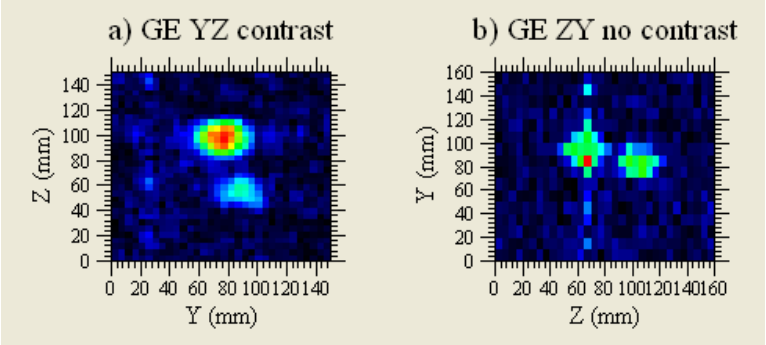

Figure A.51 Plots of Figure A.50 and A.52
a) Water (bottom)/doped water (top) b) Doped water (left and right)

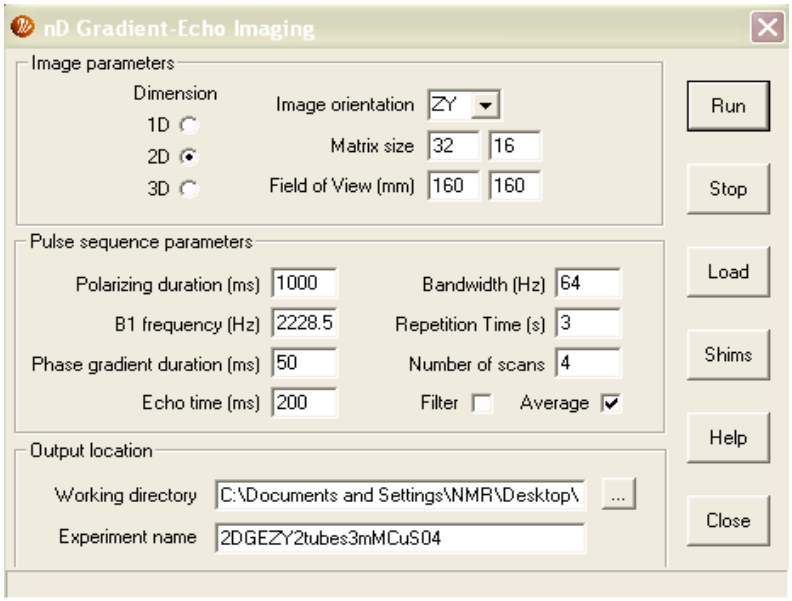

Figure A.52 Macro for 2 tubes of doped water (no contrast)

If the object does not appear in the center of the FOV, it is possible that the sample is not located in the center of the magnetic field gradient coil. Also, the object may not appear in the center of the read dimension if the B_1 frequency parameter is not the Larmor frequency of the sample. If the object is skewed in a plane, the reason is non-orthogonality of the gradients meaning Z is not aligned with B_e.

3D image can also be obtained while imaging time is much longer if high resolution and good SNR are desired. In Figures A.53-54, a 2.3 hour 32 by 32 by 32 image of a bottle of water has been collected using 4 scans per line of k-space. At the end of the experiment, the 3D k-space data has been automatically transformed and stored in the matrix. Planes from this data set can be displayed using the plot3Dslices macro (in the 3D menu) or via the 3D surface plot option in the 3D plot window's contextual menu.

A description of each GE macro parameter along with parameter limits are addressed on page 5-9 of the USER GUIDE.

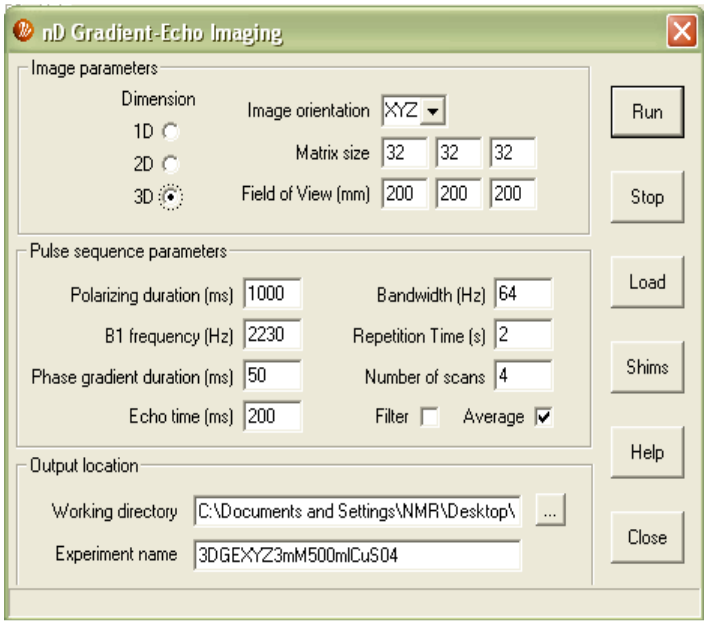

Figure A.53 3D GE XYZ orientation of a 500 ml bottle of water

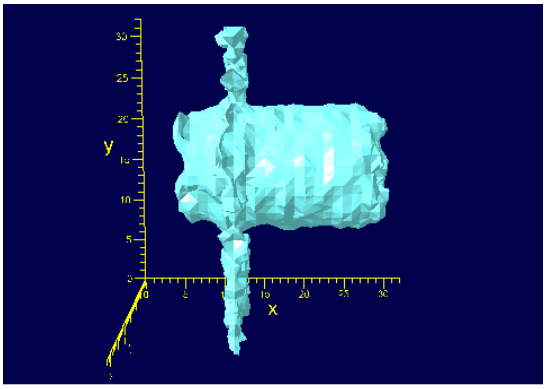

Figure A.54 3D GE XYZ of 500 ml water plot

In Figures A.55-56, a 34 minutes 32 by 16 by 16 image of two doped water phantom tubes has been collected using 4 scans per line of k-space. By comparison, the only difference in Figure A.57 is the number of pixels in the Y and Z directions being 32 by 32 resulting in a 2.3 hour imaging time while all other parameters are the same.

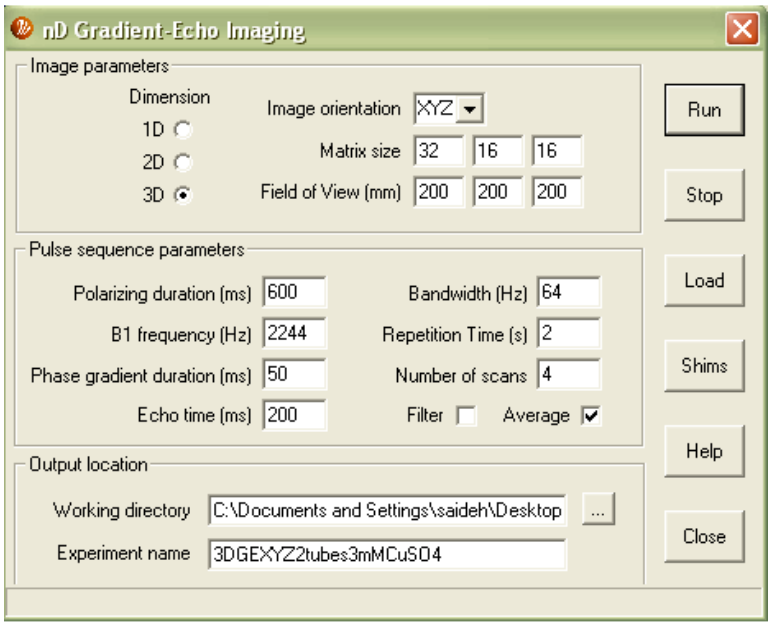

Figure A.55 3D GE XYZ of 2 doped water phantom tubes

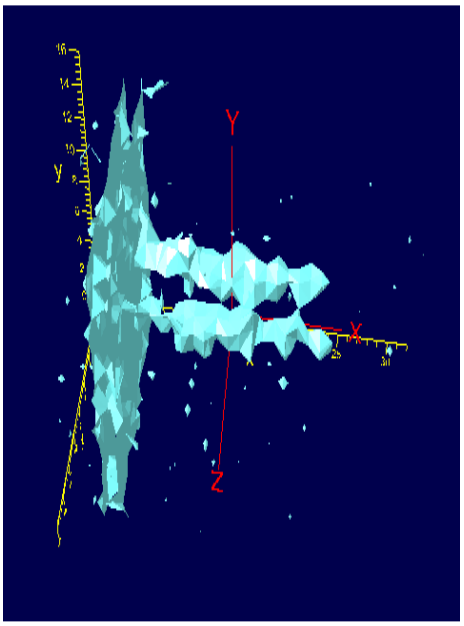

Figure A.56 A plot of 3D GE XYZ of 2 doped water phantom tubes

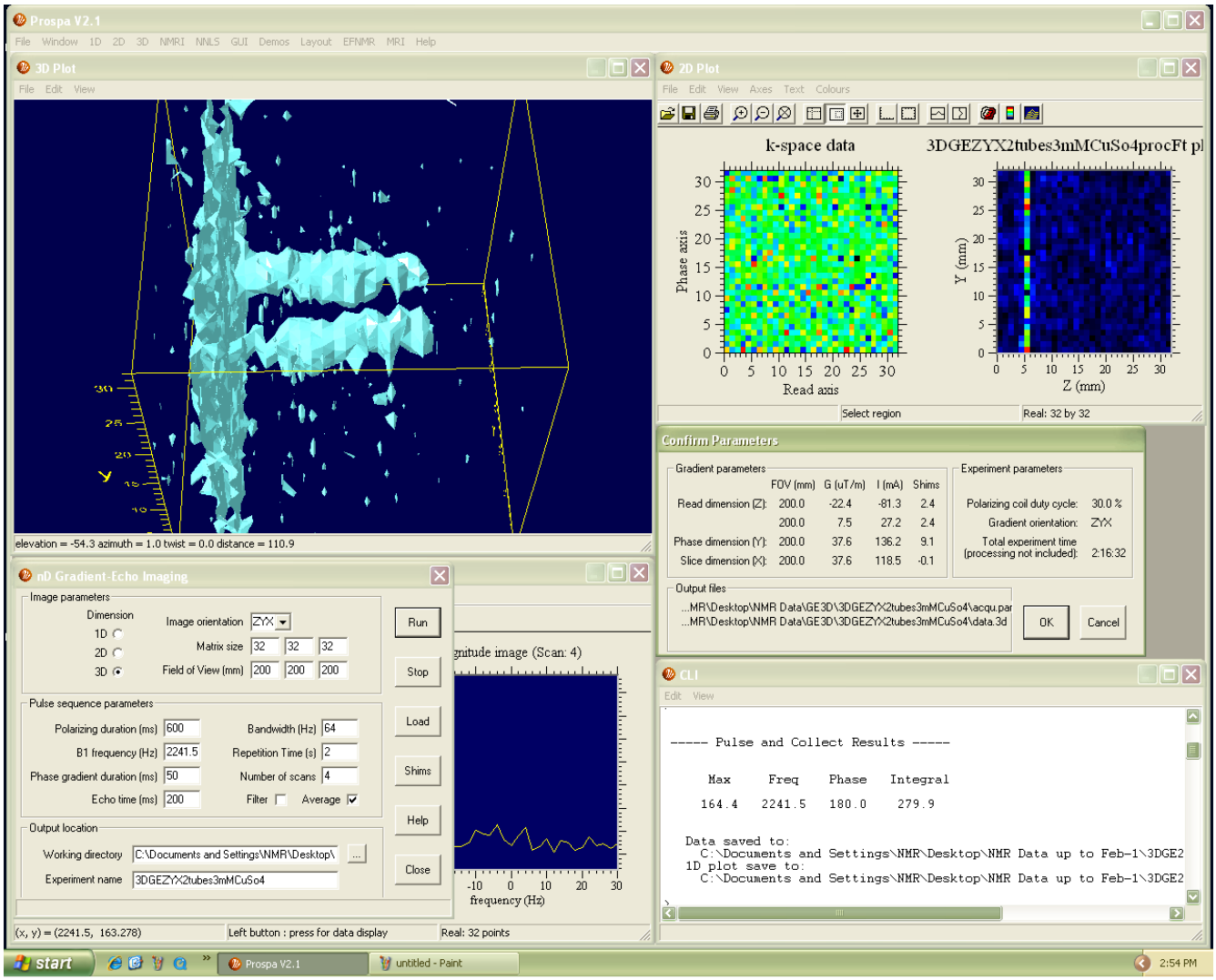

Figure A.57 3D GE ZYX orientation of 2 doped water phantom tubes

A.9 Spin Echo Magnetic Resonance Imaging in 1D

This form of imaging uses gradients in conjunction with a 90-180° pulse to traverse k-space. In SE imaging, frequency encoding in the read dimension is accomplished via the use of a method called spin echo. Also, in SE imaging the 180° pulse is used to refocus the effects of in-homogeneities in the Earth's field as well as to refocus the purposely introduced de-phasing by applying a magnetic field gradient. Therefore, an advantage of this method is that any de-phasing of the signal due to B_o in-homogeneity will also be re-focused by the 180° pulse.

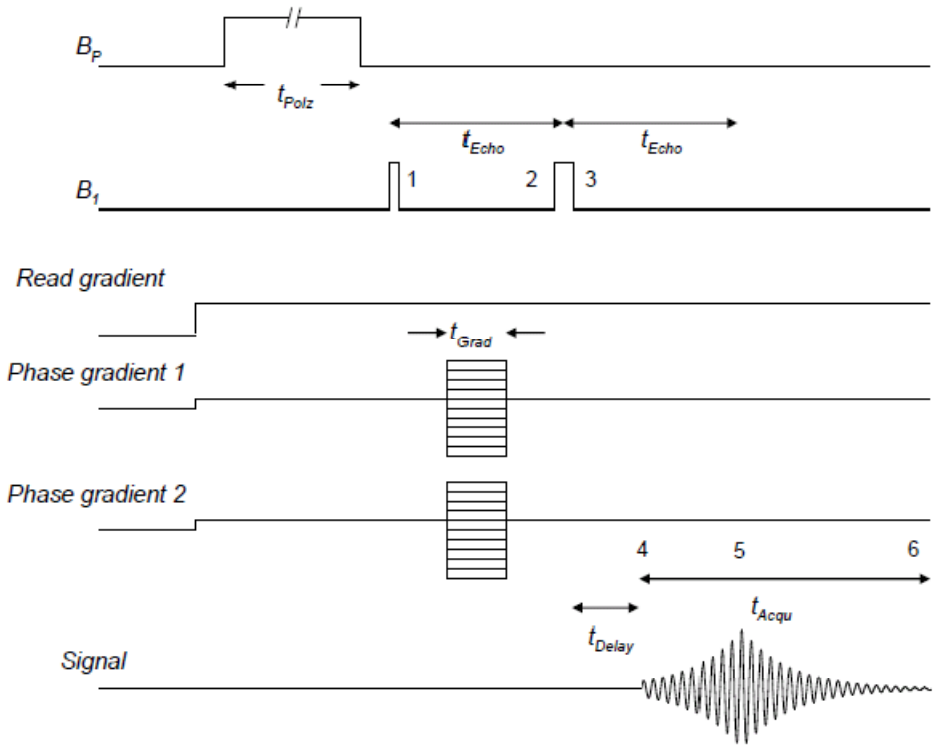

Figure A.58 Spin Echo imaging pulse sequence (Magritek, Terranova-MRI Student Guide 2006)

According to Figure A.58, the polarizing pulse (B_p) is switched on, and the 90° pulse in the presence of a constant read gradient, G_r, excites the nuclei of the sample. The read gradient is switched on before the polarizing pulse but has no effect until the 90° pulse is started. Also, the B_1 and read gradient pulses make a 1D spin-echo imaging. This RF pulse rotates the bulk magnetization vector into the transverse plane. Each isochromat (group of spins that experience the same static field) resonate at the same frequency and rotate at an offset frequency correlated to their position, magnitude, and the direction of the applied gradient. Therefore, as time goes by, the net magnetization vector can be visualized as a collection of magnetization vectors, each corresponding to an isochromat within the sample precessing at a slightly different offset frequency.

Then the phase gradients are switched on for a time T_{grad} to move the sampling into k-space. These gradients result in de-phasing of the magnetization. After a time, T_{echo}, a 180°

pulse is applied causing the magnetization to refocus to produce an echo in another T_{echo} after the 180° pulse. This means that the 180° pulse rotates the magnetization vectors about the Y axis such that in the subsequent T_{echo}, the magnetization vectors realign resulting in a re-focusing of the NMR signal. During this period, the readout gradient (G_{ro}) has a constant value causing k-space to traverse in the read direction of the gradient. The position of the echo corresponds to the center of k-space along the read gradient axis. Data acquisition starts after the 180° pulse and $T_{acq\text{-}delay}$ (25 ms) to allow for probe ring down while acquisition continues for T_{acq} time.

In terms of k-space in the first step the signal is excited by a 90° pulse and the spins evolve with time in the presence of G_r. This leads to an increase in k as time evolves. In step 2, after a time period of T_{echo}, a 180° pulse inverts the signal which is a change from $+T_{echo}$ to $-T_{echo}$, so a movement takes place from kx to -kx. In step 3, after the inversion pulse, the spins again evolve in time in the presence of G_r, corresponding to a linear increase in k with time. The signal is sampled as a function of time during this time period. The re-focusing and decay of the echo is depicted at the bottom line of the pulse sequence in Figure A.58.

The height of the echo signal is weighted by 180° not T_2*. Also, the time between the 90° pulse and echo peak is two echo time which means SE imaging produce less signal than the gradient echo method for short 180° samples if both have the same echo time setting. For gradient echo imaging, instead of using a pulse to refocus the spins as in a spin echo image, the spins are refocused with a gradient in the opposite direction from the encoding gradient. So SE and GE differ in their refocusing methods. Methods for encoding and reading are different for different imaging methods.

The procedure for running a SE (1D, 2D and 3D) imaging is the same as before. The only point worth mentioning is that for 1D SE imaging even though there is no phase gradient

duration, this parameter should be set to 50 ms. Also, re-shimming is necessary whenever the sample is changed, the probe is moved, or metal objects around the room are moved.

Figure A.59 illustrates the macro for 1D SE imaging of an Erlenmeyer flask filled with water. It should be noted that the polarization time is 4 s since the sample is just water. The purpose of running this experiment was demonstrating the correspondence of an object inserted inside the cavity with its obtained image. Figure A.60 illustrates the plots for this macro while the echo time has changed from 100, to 200, 400 and 500 ms. The different plots of Erlenmeyer flask prove that as echo time increases, the shape of the flask in the image become less clear.

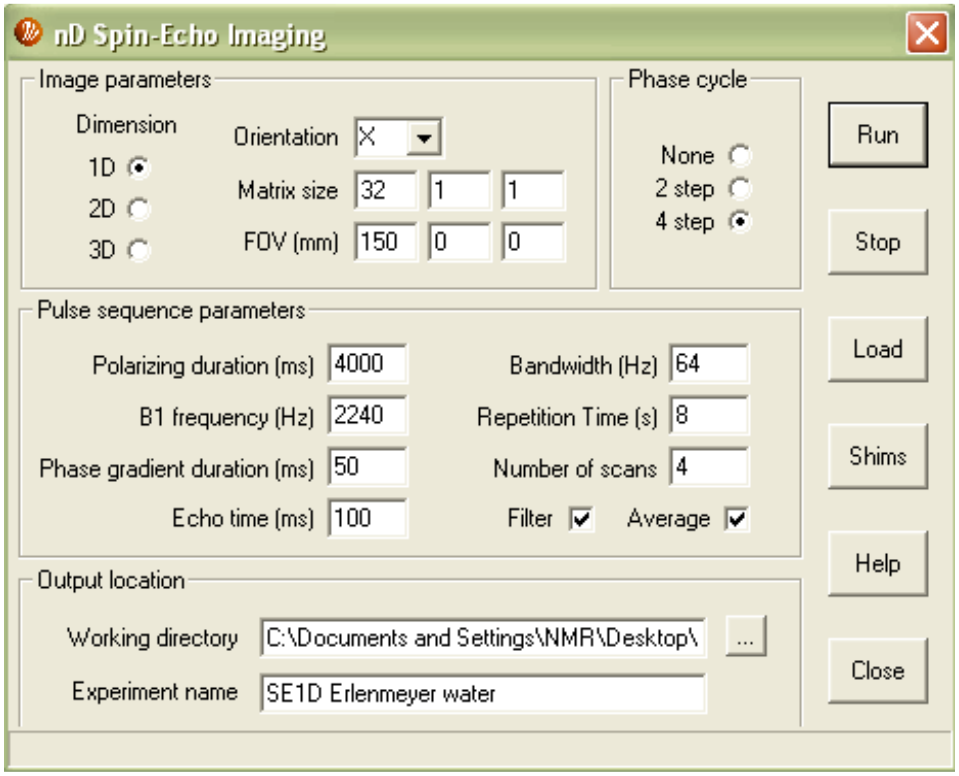

Figure A.59 1D SE macro of an Erlenmeyer flask filled with water

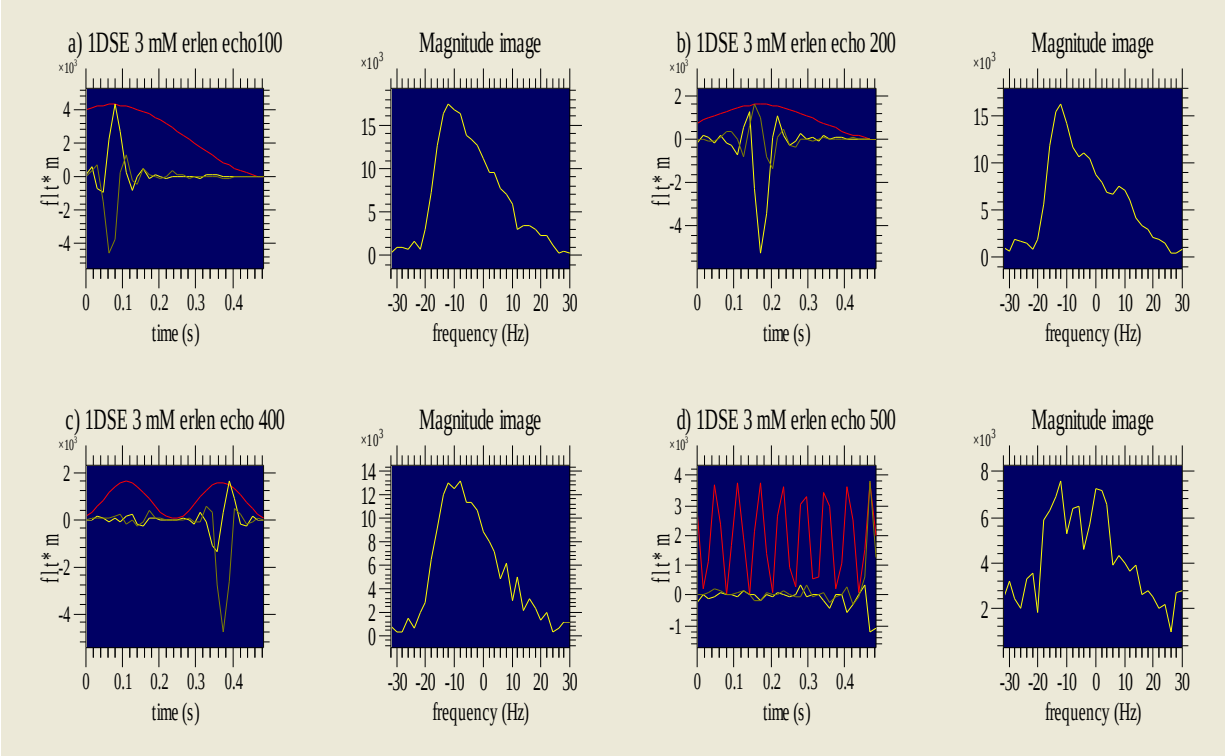

Figure A.60 Plots of 1D SE images of an Erlenmeyer flask filled with water

In this experiment (Figure A.60) the image bandwidth is 64 Hz which means with a 2 Hz line width 32 horizontally resolved points called data points or matrix size in our 64 by 32 pixel image are present. The experiment is run with filter on and 8 scans. The image appearing on the right side of the 1D window is the projection of the sample magnetization onto the X axis. On the left side is the complex k-space data with the applied filter shown in red.

As mentioned earlier, collected data is down-converted from the Larmor frequency (2240 Hz) to 0 Hz and filtered, removing all unwanted frequencies outside the desired bandwidth. This way only a few data points need to be processed.

To obtain the best image resolution when performing imaging experiments, the frequency range across the image (the bandwidth) should be greater than or equal to the line width multiplied by the number of image points (data points/N_{read}). The following are some points to remember in imaging:

- Frequency resolution = line width = spectral resolution = $1/T_{acqu} = \Delta f$
- Δf = bandwidth/$N_{read} \rightarrow 64/32 = 2 = \Delta f$
- Decreasing the bandwidth increases SNR at the expense of losing resolution
- Narrow line width, better SNR, more resolution
- Resolution is determined by how long the FID is collected/T_{acqu} determines resolution
- Polarization duty cycle decreases with increasing the TR
- The height of magnitude image increases with decreasing the T_{echo}
- The shorter the T_{echo}, the greater the SNR
- Matrix size = number of pixels = data points (Np = # of pixels in the phase dimension)
- Polarization time times 2-3 = TR
- In 1D imaging: Experiment time = number of scans times TR
- In 2D imaging: Experiment time = number of scans times TR times Np
- In 2D imaging: Experiment time = number of scans times TR times N_p^2

An MRI image quality can be improved by methods such as phase cycling and filtering.

A.9.1 Filtering in Imaging

Filtering is used to smooth an image. Filtering is an operation in which the k-space data is multiplied by a function prior to Fourier transformation. Multiplication of k-space is equal to convolution of the image. So, by applying a function to the k-space data, the image can be convolved via the Fourier transform of this known function in the image domain. In SE imaging a sine-bell-squared filter is applied to the k-space data. The center of this filter is shifted to correspond to the center of k-space which is the center of the echo signal as well. An applied filter benefits MRI imaging by increasing the SNR through reduction of noise. However, the drawback of filtering is a loss of resolution through blurring of the image. Some filters are

designed to improve SNR, others improve resolution, and some are a compromise of both.

Figure A.61 illustrates the macro for 1D SE imaging of a 500 ml solution of 3 mM doped water with copper. Since doped water is used T_1 and T_2 values are shortened, polarization time and echo time are reduced as well, resulting in a shorter experiment time. The dialog window is similar to GE macro except that phase cycle is added.

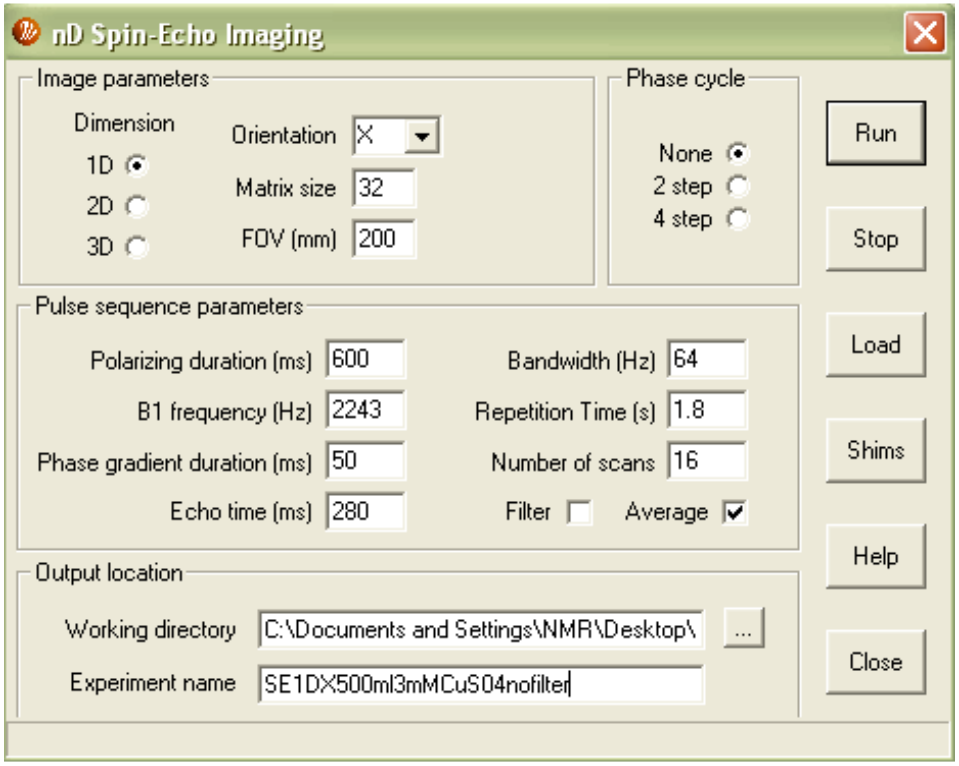

Figure A.61 1D SE macro of a 500 ml aqueous CuSO4

Figure A.62 illustrates the plots for 1D SE imaging of a 500 ml solution of 3 mM doped water with copper in X, Y, and Z orientation with and without filter. For example, part a) of Figure A.62 demonstrates the use of a filter in the X orientation while in part b) the same experiment was run without applying a filter. By comparing experiments a) and b), c) and d), or e) and f) filtering results in a smoother image. PC of 1D SE filter and no filter was 29.

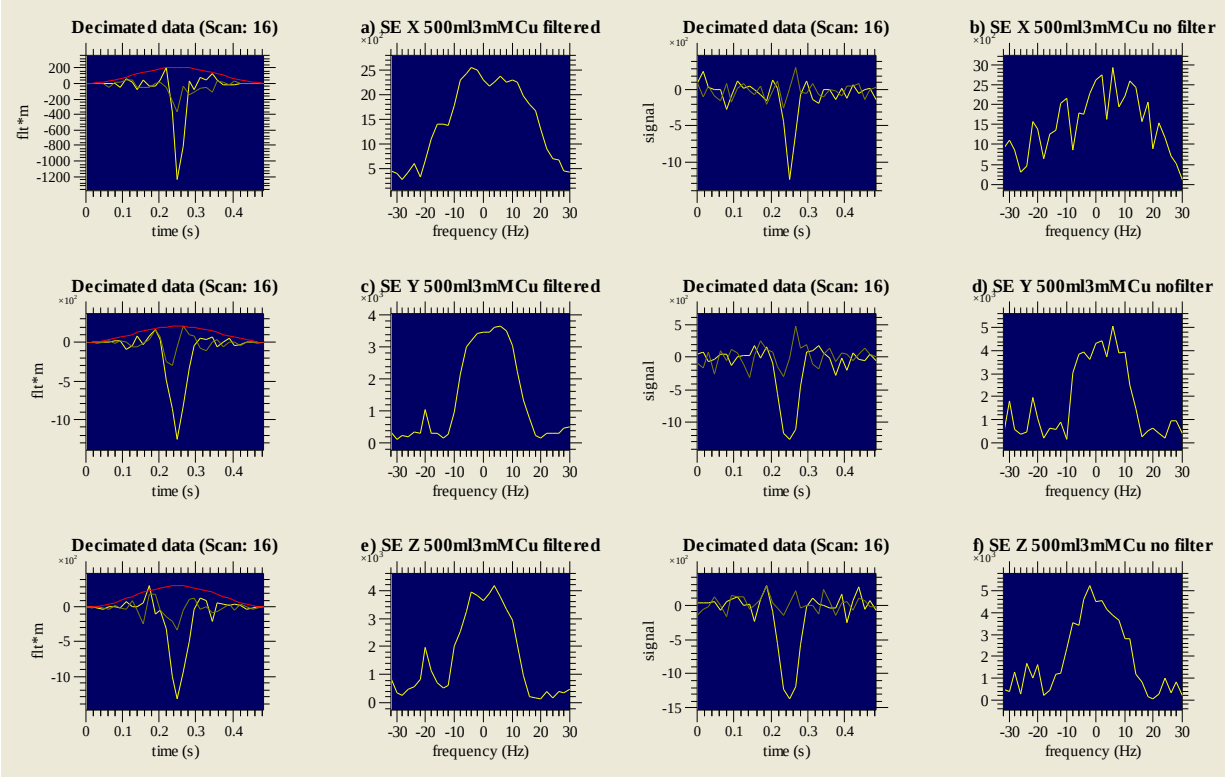

Figure A.62 Plots of 1D SE images of 500 ml aqueous CuSO4

A.10 Spin Echo Magnetic Resonance Imaging in 2D and 3D

In order to accomplish a 2D spin-echo image, a phase gradient is applied after the excitation pulse for 50 ms corresponding to the duration of T_{grad}. The phase dimension in k-space is sampled by obtaining spin-echo signals for each distinct value of the phase gradient.

Also, a lower resolution imaging is preferred to evaluate the image quality. Lower resolution helps because the signal which was in N data points in the 1D experiment is now spread over N^2, so the extra N experiments help a bit, but at the same time it introduces extra noise, so we are still $\sqrt{N}$ worse off than in the 1D case if the resolution is kept the same.

While the experiment is running, one can quickly determine whether the image will be good or not. At any time the experiment can be terminated by pressing the stop button. Additional accumulations may be required if the SNR is poor.

A.10.1 Phase Cycling in Spin Echo Imaging

Phase cycling is used in Spin Echo imaging to cancel any signal from the 90° pulse which has not decayed by the time of data acquisition. Also any signal from non-ideal 180° pulse which may act as an excitation pulse as well as an inversion pulse if it is inhomogeneous or not exactly 180° could be improved by phase cycling. Phase cycling involves the manipulation of the phase of the RF pulses in successive signal acquisitions such that desired signal is combined constructively whereas signals arising from system interference are combined destructively.

In the rotating frame the transverse plane, X'Y', rotates about the longitudinal direction (Z or the Earth's field direction) at the Larmor frequency. Also, the B_1 pulse is an oscillating magnetic field with a frequency equal to the Larmor frequency of the sample. This pulse ideally should be perpendicular to the Earth's field. So, a stationary vector in the transverse plane of the rotating frame can be used to designate this oscillating magnetic field. Figure A.63 a) illustrates a B_1 pulse oriented along the X' axis in the rotating frame which tips the longitudinal magnetization vector, M_z, into the transverse plane by a tip angle θ with a phase of 0° and 3 cycles. The relative phase between the B_1 pulse and the transverse magnetization vector, M_{xy}, is 90°. Also, as depicted in Figure A.64 a) and b) in these two PC experiments, the relative phase between these two excitation pulses is 180°. By considering the rotational frame of reference, the first B_1 pulse is oriented along the X' axis and tips the longitudinal magnetization vector to the Y' axis (Figure A.63 c). And the second B_1 pulse is oriented along the –X' axis and tips the longitudinal magnetization to the –Y' axis (Figure A.63 d). Consequently, the precession of the transverse magnetization vector, M_{xy}, about the Earth's field vector, B_e, induces the NMR signal. The relative phase between the two acquired FID signals in Figure A.63 e) and f) is 180° because

the relative phase of the transverse magnetization vectors in the rotating frame of reference is 180°. So, relative phase of an FID signal depends on phase of the excitation pulse.

Therefore, phase cycling provides a chance for distinguishing between the desired NMR signal and background interference through the manipulation of the phase of successive RF excitation pulses. For example, as seen above, by increasing the pulse phase by 180° results in an inversion of the FID signal. As a result, successive 180° RF pulse phase shifts, combined with successive addition and subtraction of the acquired signal result in cancellation of background interference. This is called coherent noise cancellation which is an example of a type of phase cycling.

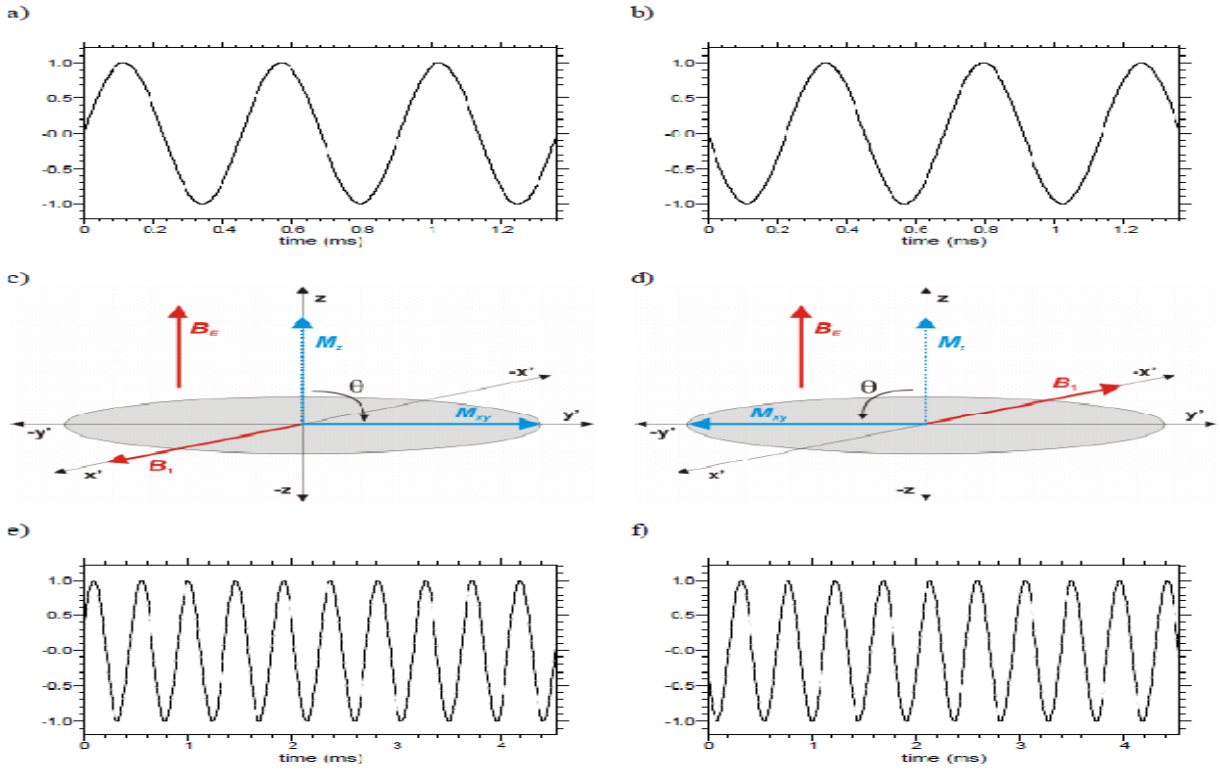

Figure A.63 a) and b) are two simulated B_1 pulses with a relative phase difference of 180°. B_1 pulses are along the X' and –X' axes in the rotating frame (c) and (d). In (c) the B_1 pulse along X' excites a transverse magnetization along Y'. In (d) the B_1 pulse along –X' excites a transverse magnetization along –Y'. The NMR signal from these two excitations is 180° out of phase relative to each other because they are 180° out of phase in the rotating frame. This is illustrated by NMR signals in (e) and (f) (Magritek, Terranova-MRI Student Guide 2006).

In the SE imaging, the phase cycle button has options none, 2 step and 4 step. For the 2 step phase cycle to be applied properly, the number of scans must be a multiple of 2, and for the 4 step phase cycle the number of scans must be a multiple of 4. This is because each step in the phase cycle corresponds to one scan, so to carry out one complete n step phase cycle, the pulse sequence must be repeated n times.

Figure A.64 demonstrates the application of the filter as well as phase cycle in a 2D SE imaging of a sample of 500 ml water doped with copper sulfate in the YZ plane. In part a) in the absence of filter and phase cycling, the signal is weak while in part b) in the presence of the filter the signal becomes much stronger. Part c) and d) present the presence of 2 and 4 step phase cycling respectively. In both cases the signals are stronger compared to a) or b). Also, PC of this series of experiments was 32.

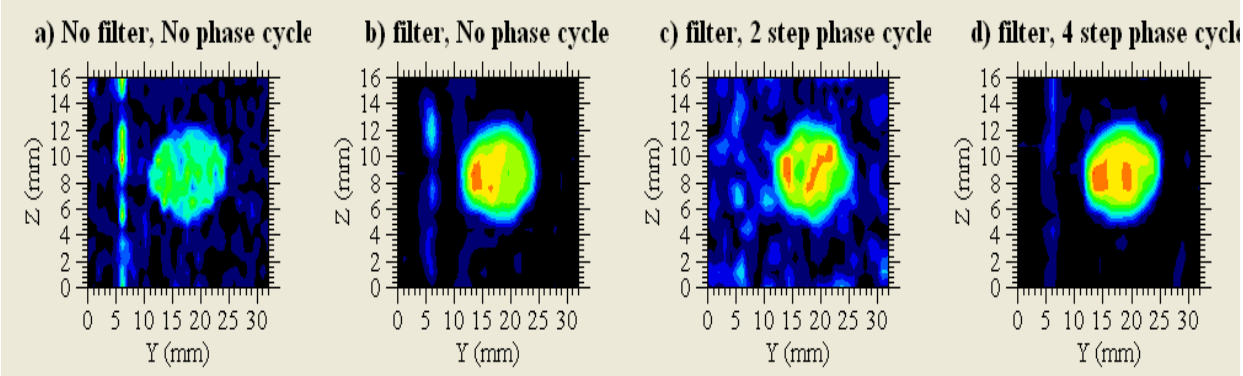

Figure A.64 2D SE images of 500 ml doped water with and without filter and Phase cycle

A.10.2 Orientation

Figure A.65 illustrates the macro for a 2D SE imaging of two phantom tubes one filled with water as the control versus the other tube filled with a solution of 4 mM $CuSO_4$ for the purpose of demonstrating the effect of contrasting agents on the signal acquisition. Figures A.66-67 illustrates the corresponding images in the Z direction (meaning the tubes were parallel to the Z axis of the probe) with 16 and 32 matrix sizes in the phase dimension in the six possible orientations. Figures A.68-69 illustrates the corresponding images in the Y direction (meaning the tubes were parallel to the Y axis of the probe) with 16 and 32 matrix sizes in the phase dimension in the six possible orientations.

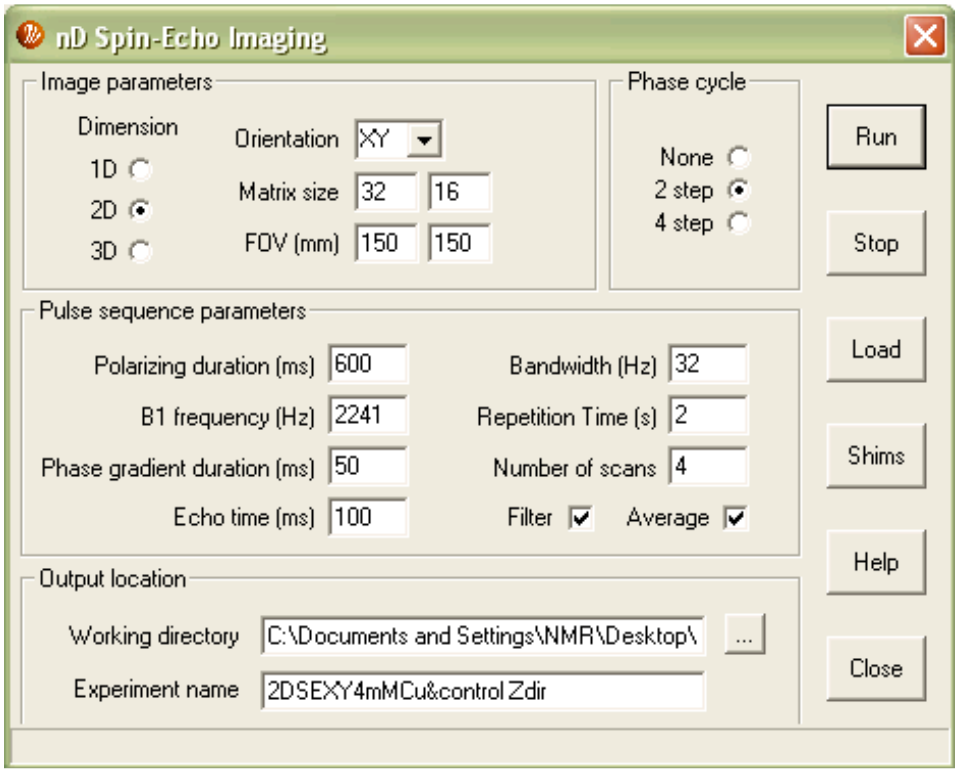

Figure A.65 SE imaging macro of 2 phantom tubes

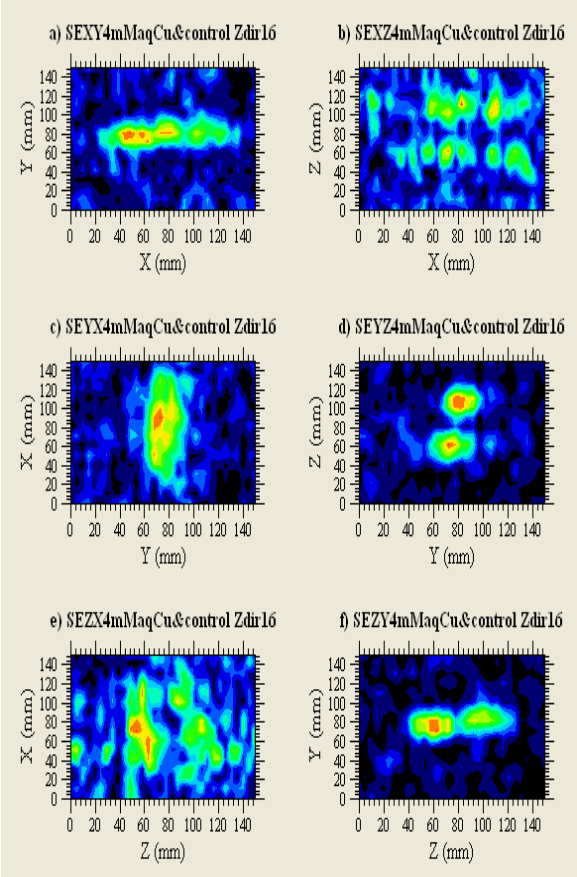

Figure A.66 SE images of 4 mM copper versus control in the Z direction with 16 matrix size

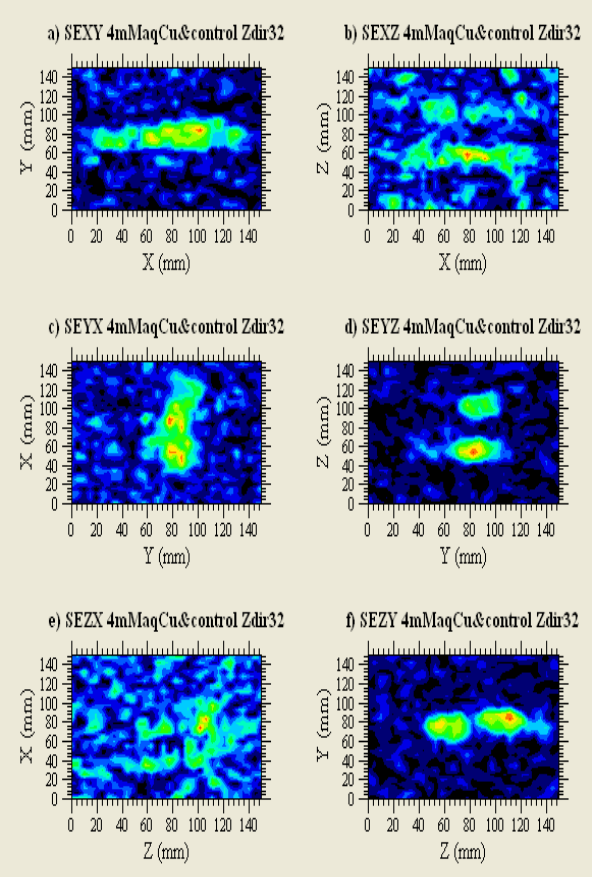

Figure A.67 SE images of 4 mM copper versus control in the Z direction with 32 matrix size

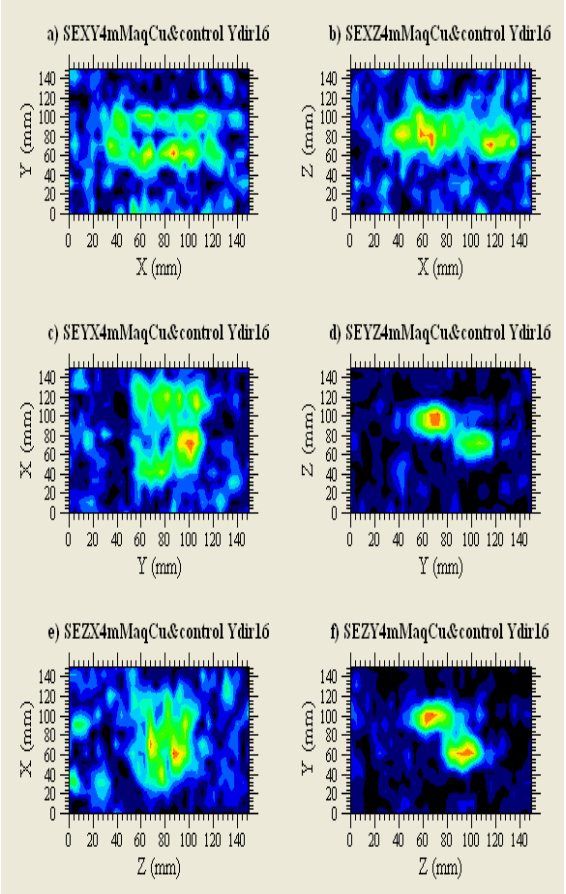

Figure A.68 SE images of 4 mM copper versus control in the Y direction with 16 matrix size

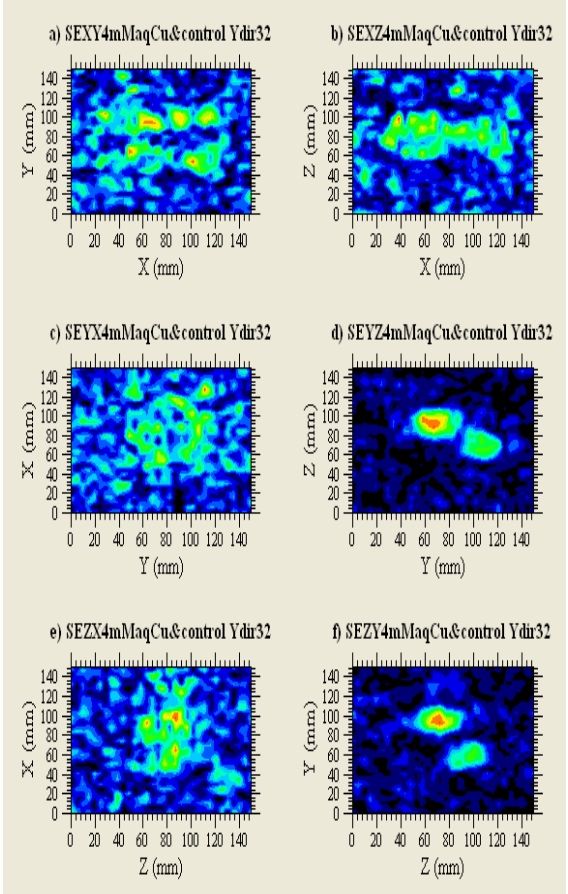

Figure A.69 SE images of 4 mM copper versus control in the Y direction with 32 matrix size

In addition, Figure A.70 illustrates 1D and 2D image orientations for a 500 ml bottle as well as phantom tubes.

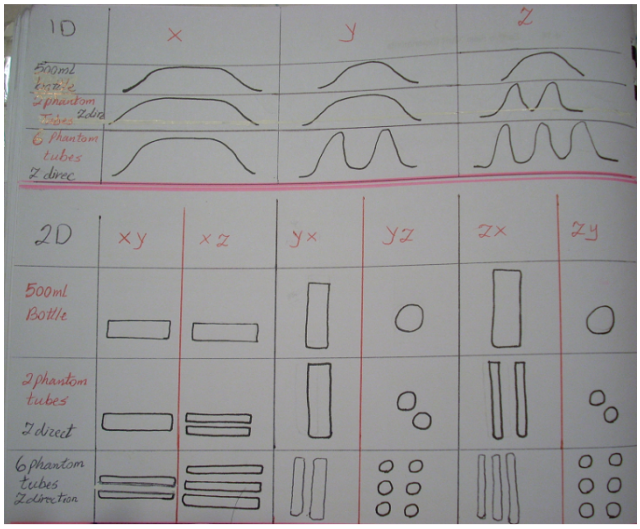

Figure A.70 1D and 2D orientations (500 ml bottle and phantom tubes)

Figure A.71 is an example of XY image while the image is being produced. The macro is written such that the most intense low frequency rows of k-space are scanned before the high frequency rows, which contain fewer signals, so image blurring is obvious. As time of imaging elapses, the image becomes less blurred.

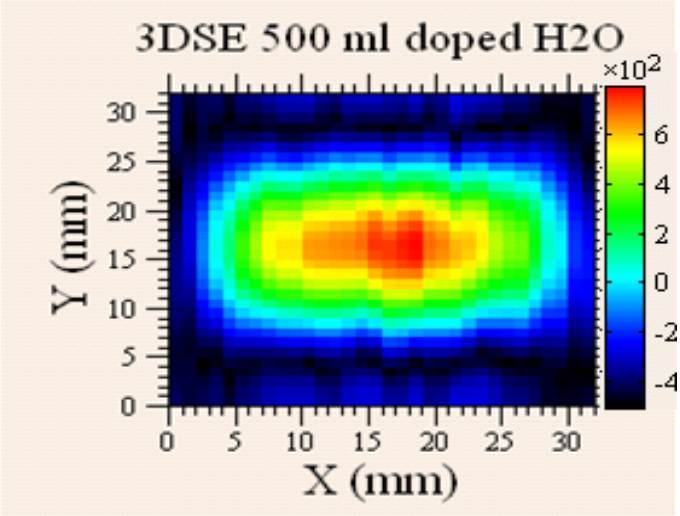

Figure A.71 2D plot of a 3D SE of 500 ml (3mM Cu) doped water (matrix size: 32x32x32)

The total 3D imaging time can be quite long if high resolution and a good SNR are desired. In the following example (Figure A.72-73) a 2.05 hour 32 by 16 by 16 image of a 500 ml doped water has been collected using 16 scans per line of k-space and 4 step phase cycling. At the end of the experiment the 3D k-space data is automatically transformed and stored in the matrix. Planes from this data set can be displayed using the "plot 3D slices" macro or by using the "3D iso-surface plot" option in the 3D plot contextual menu (refer to Appendix B).

It is possible to use a second Prospa program to view the progress of the collected data set while the pulse program is running. Also, it is possible to retrieve old data by loading the 3D data set "data.3d" stored in the data folder using the macro "import Data" in the NMRI menu, and transforming it using the macro "nD Fourier Transform" in the same menu. A view of these macros is available in Appendix B. The time domain data (k-space) is kept in "mat3d" which is a 3D data set, whereas "mat3dFt" is a matrix with the image data. Also, when re-processing the

original data set, a filter mimicking the shape of the k-space data is needed and is provided by the corresponding macro.

The image in Figure A.73 was retrieved by running the “3D iso-surface plot macro” found in the 3D plot contextual menu. In the iso-surface plot macro, the higher the surface plot number, the more clear a 3D image is, and less noise is present until it reaches a point where the image gets smaller. The lower the surface plot number, the stronger an image as well as noise is present until it reaches a point where we get a full box of flakes where the image is not recognized any more.

A description of each SE macro parameter along with parameter limits are addressed on page 5-20 of the USER GUIDE.

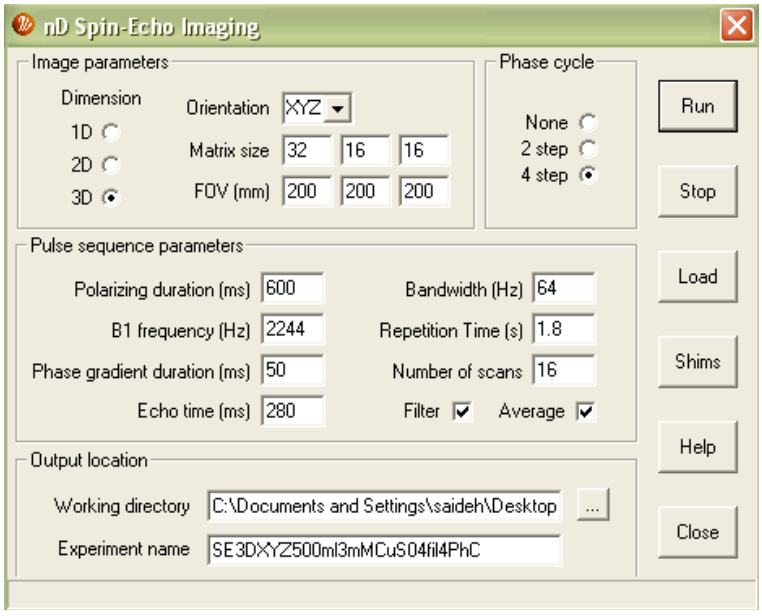

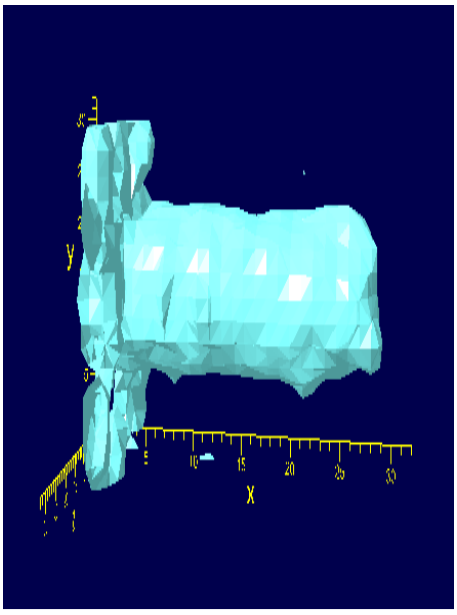

Figure A.72 3D SE macro of 500 ml water doped with Cu **Figure A.73 plot of 3D SE of the sample**

The text content of Appendix A is derived from the Terranova-MRI USER MANUAL and STUDENT GUIDE as well as several personal communications.

APPENDIX B

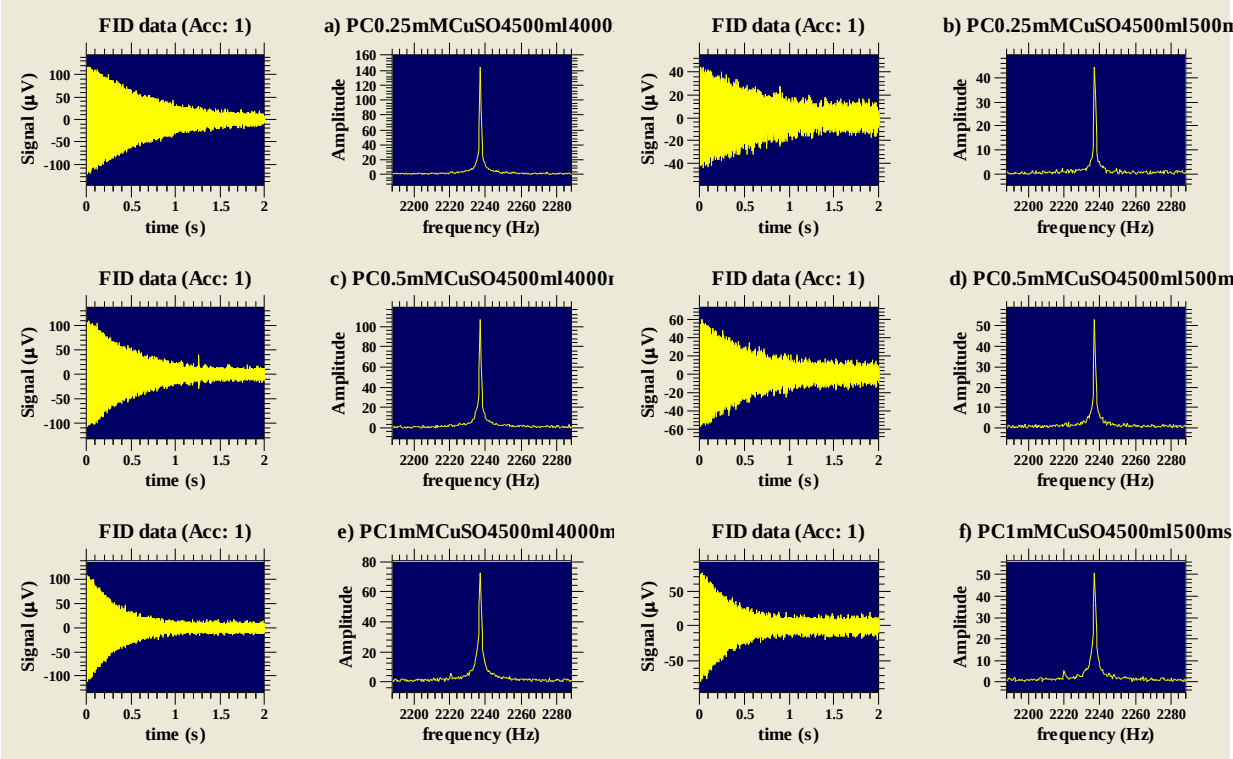

Figure B.1 Comparing FID and spectrum of 500 ml water doped with 0.25-1 mM CuSO4

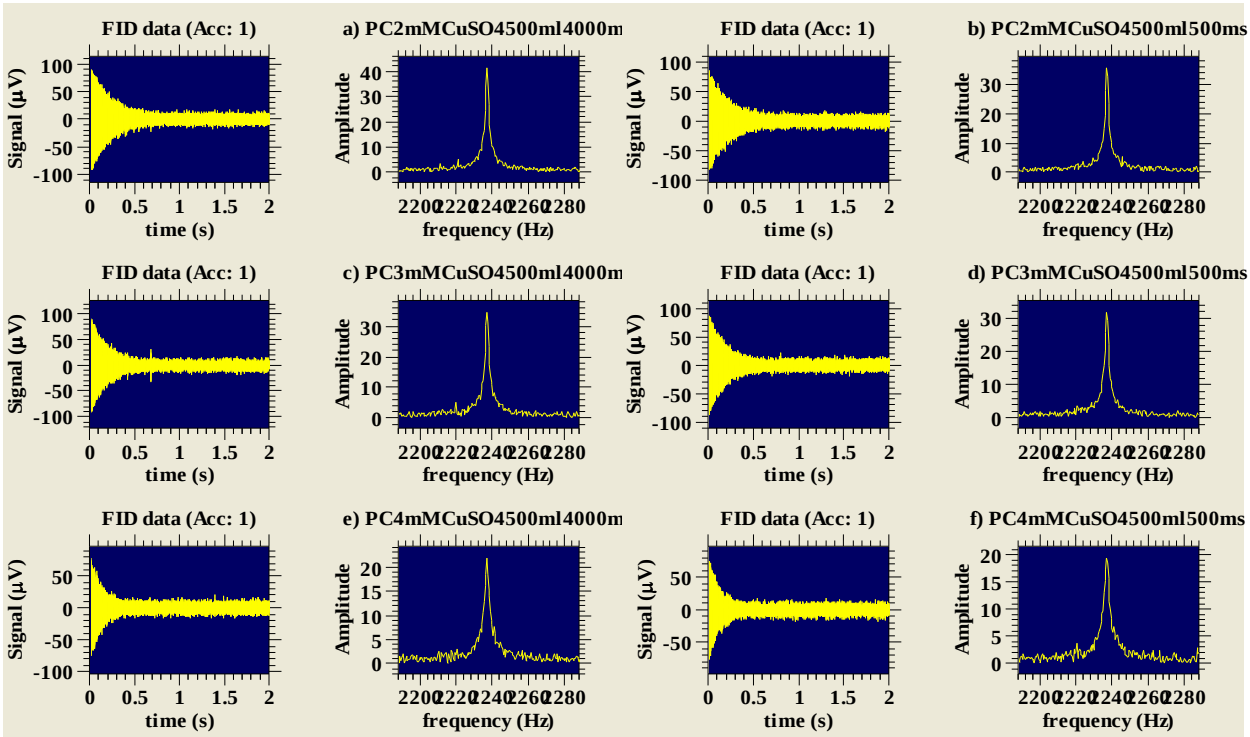

Figure B.2 Comparing FID and spectrum of 500 ml water doped with 2-4 mM CuSO4

Sample type CuSO4 (µM)	Polarization duration(ms)	FID amplitude (µv)	Spectrum amplitude (µV/Hz)
pure water	4000	100	150
pure water	500	30	28
250	4000	120	145
250	500	44	44.5
500	4000	110	107
500	500	56	53
1000	4000	100	73
1000	500	75	51
2000	4000	90	41
2000	500	80	36
3000	4000	90	34.5
3000	500	90	32
4000	4000	80	22
4000	500	70	19.5

Figure B.3 Copper (II) Concentration and Polarization Duration versus Signal Parameters

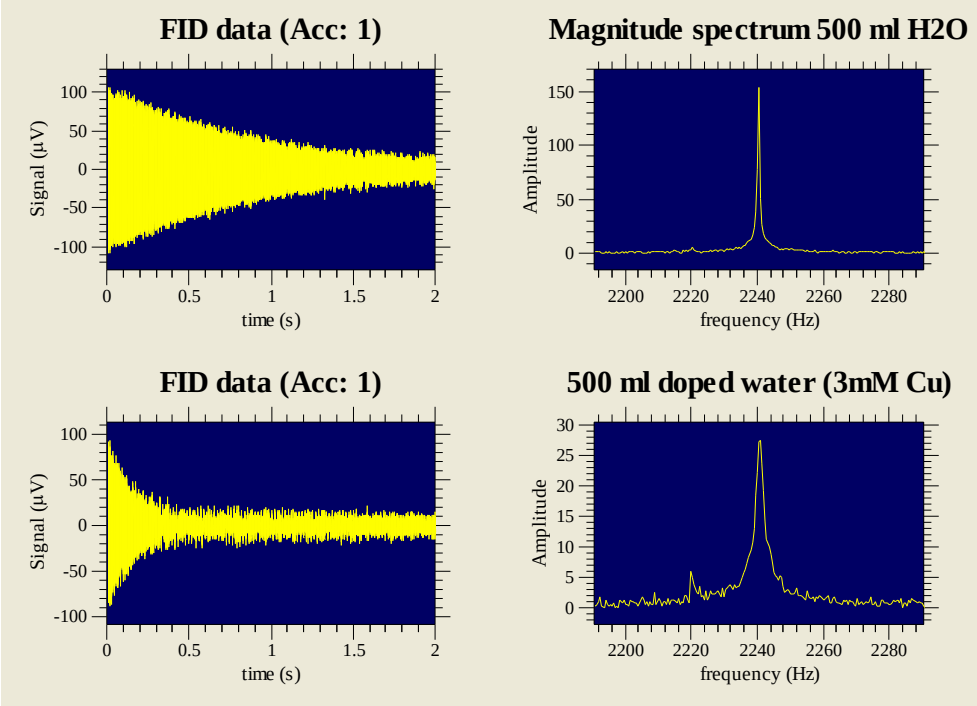

Figure B.4 A comparison of FID and spectrum of a 500 ml water and doped water

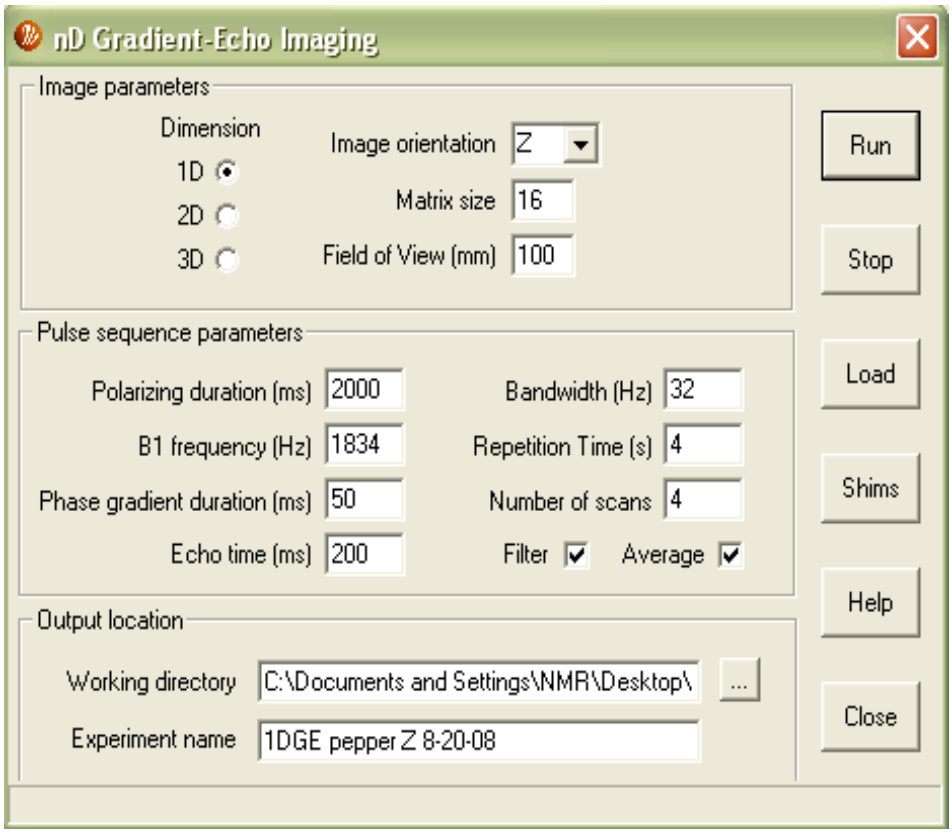

Figure B.5 1D GE macro of a green bell pepper (PC: 20)

Figure B.6 The probe in the earth direction in room 308

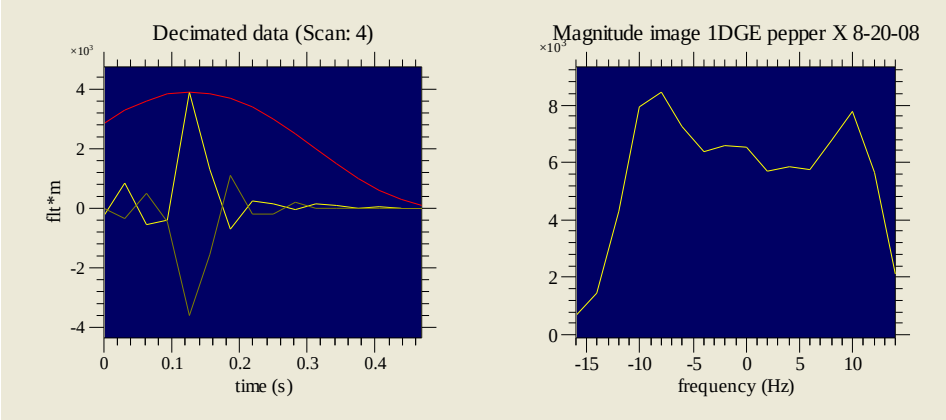

Figure B.7 1D GE X orientation plot of the pepper

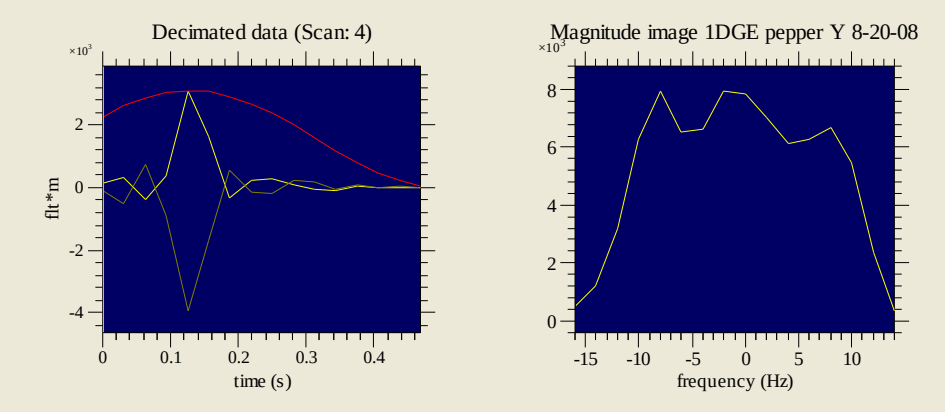

Figure B.8 1D GE Y orientation plot of the pepper

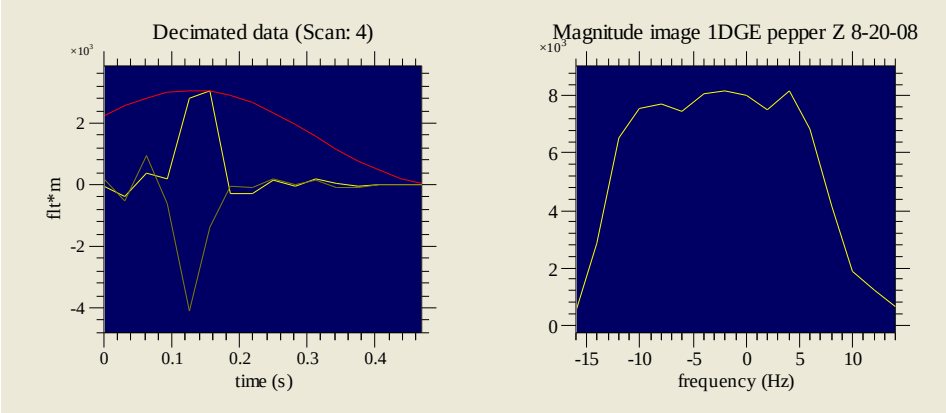

Figure B.9 1D GE Z orientation plot of the pepper

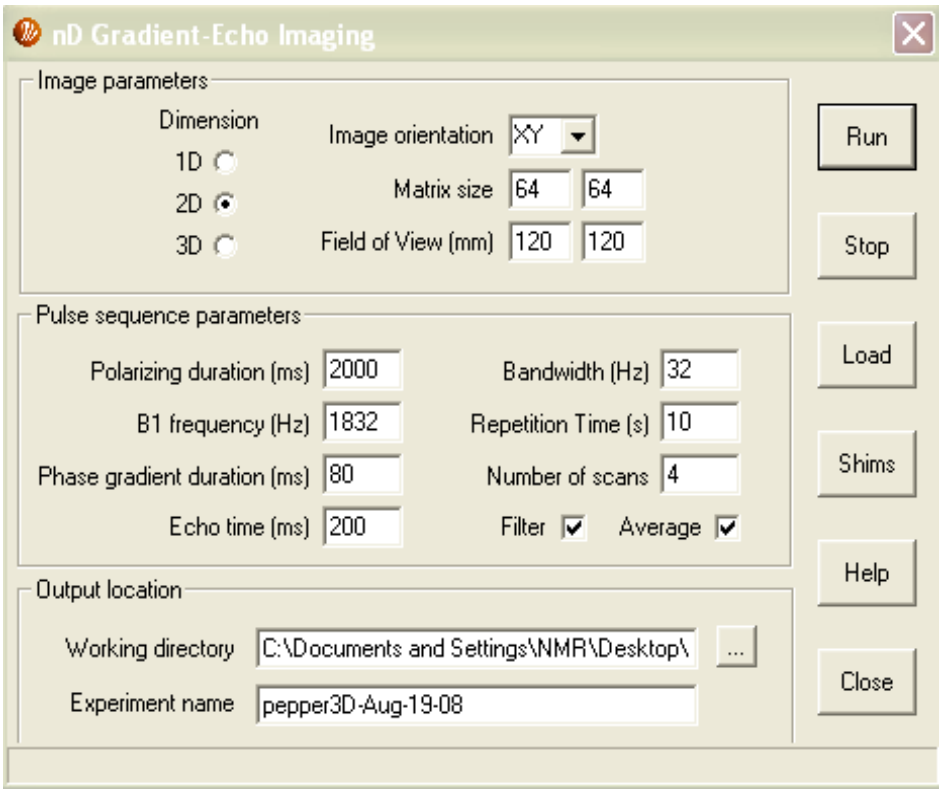

Figure B.10 2D GE macro of a bell pepper

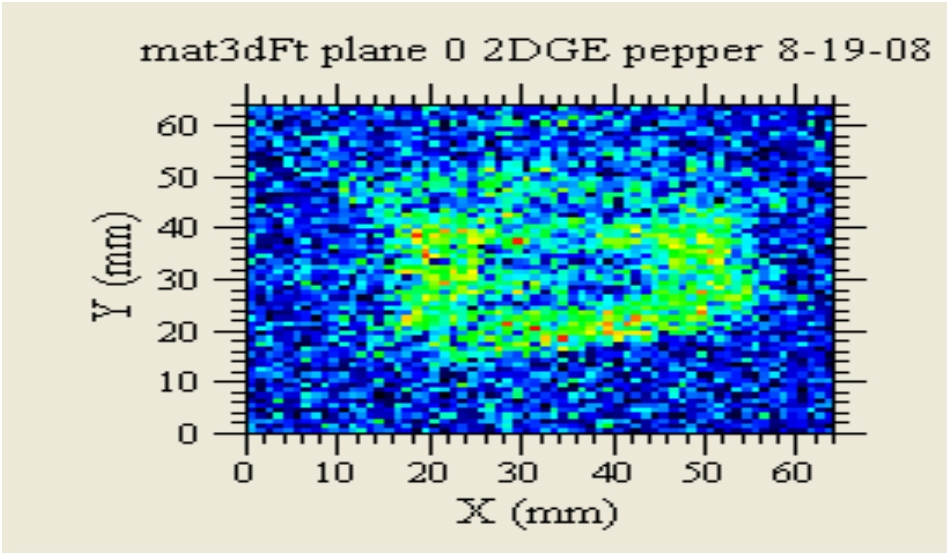

Figure B.11 2D GE image of the bell pepper

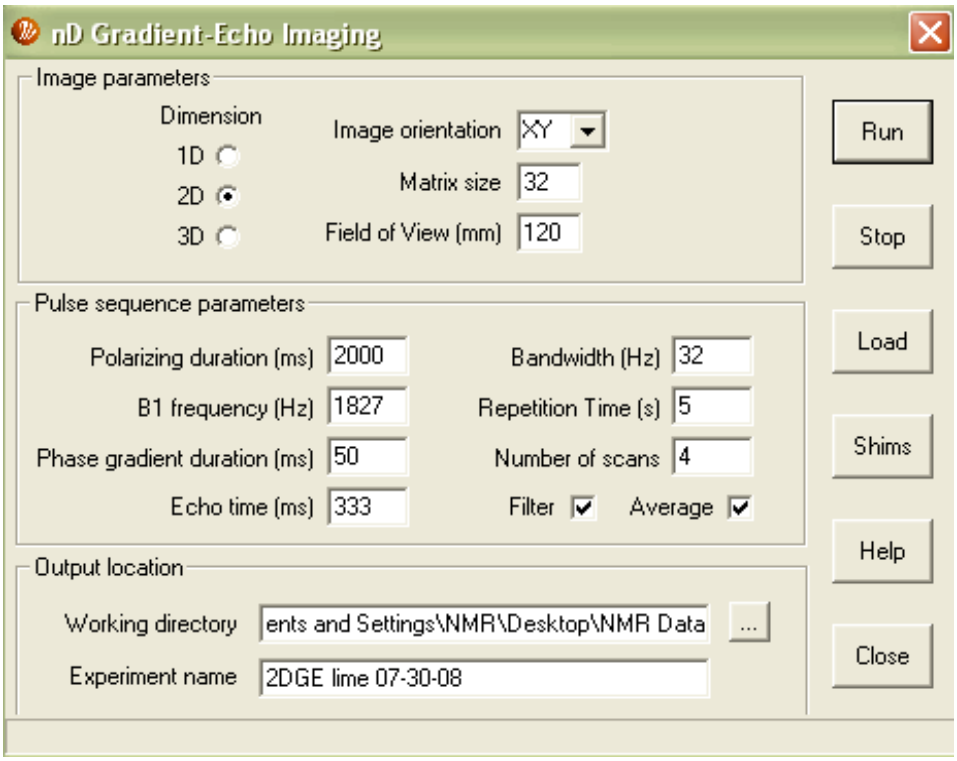

Figure B.12 2D GE macro of a lime

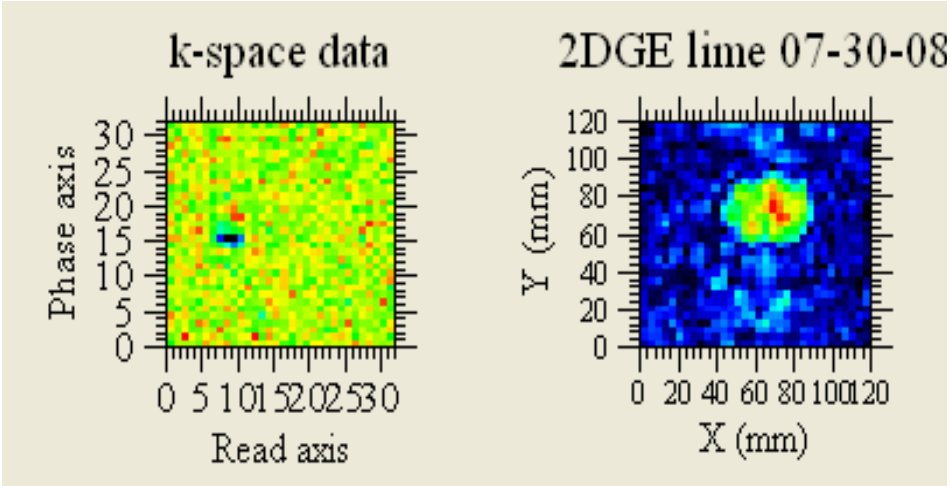

Figure B.13 2D GE image of the lime

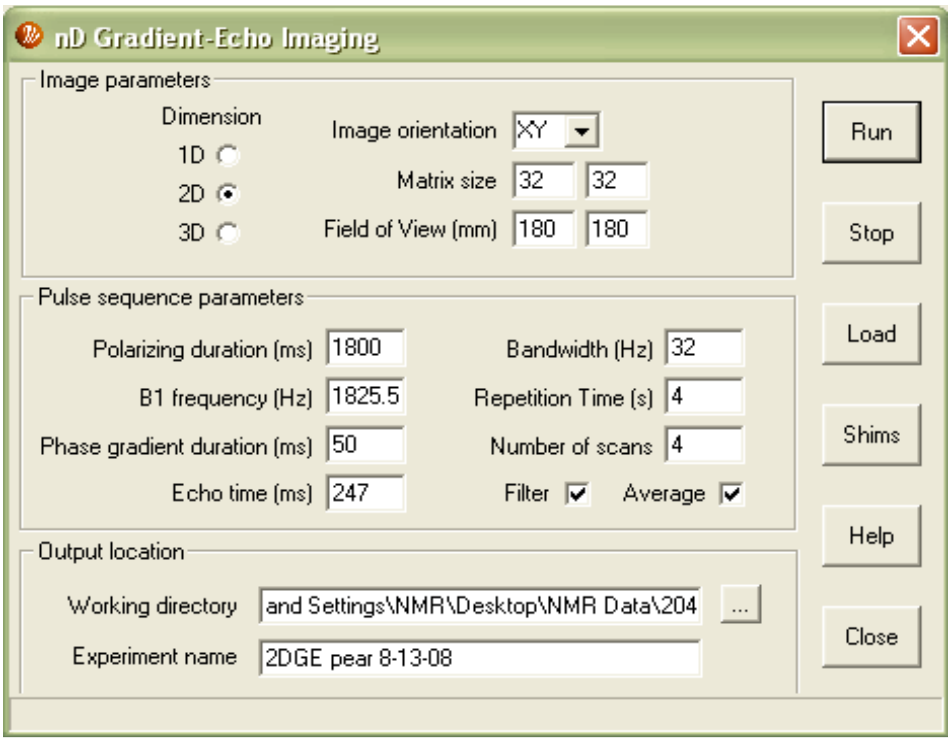

Figure B.14 2D GE macro of a pear

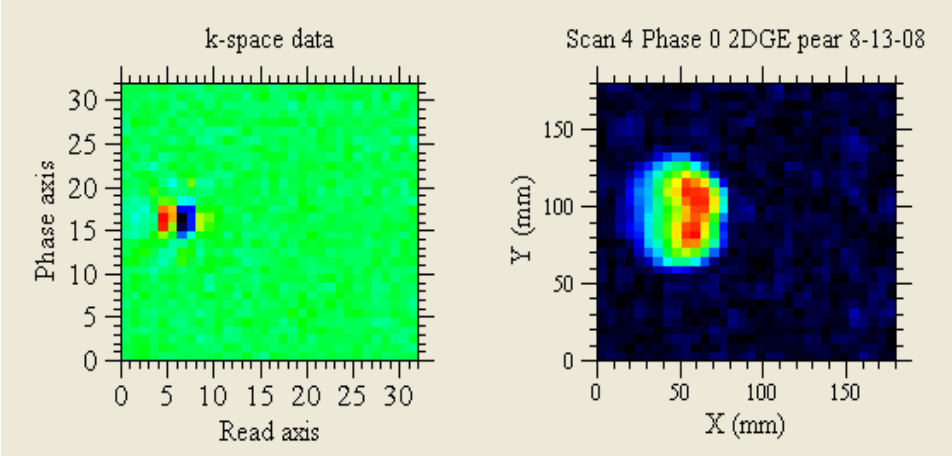

Figure B.15 2D GE image of the pear

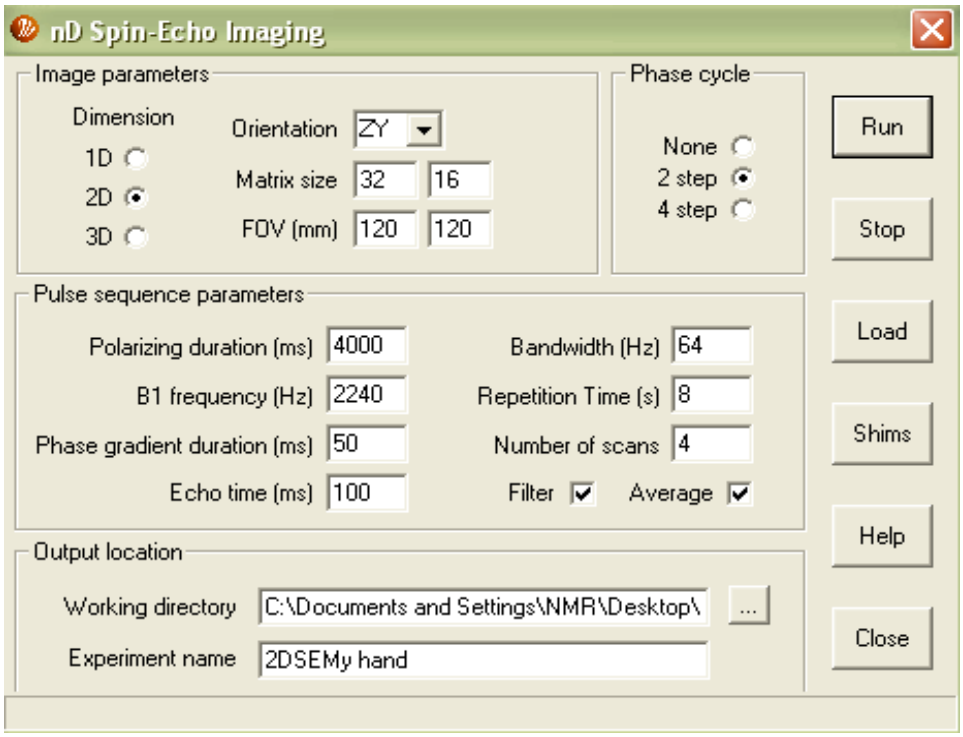

Figure B.16 2D SE macro of my hand

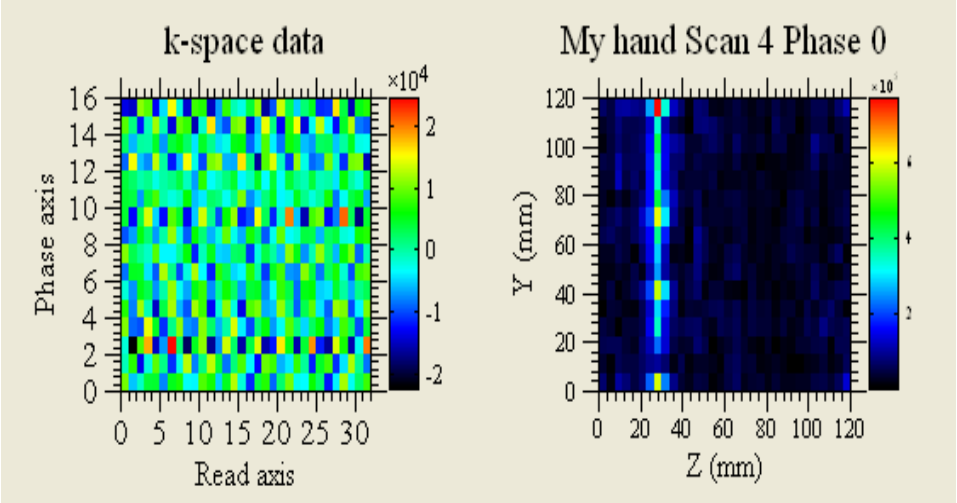

Figure B.17 2D SE plot of my hand

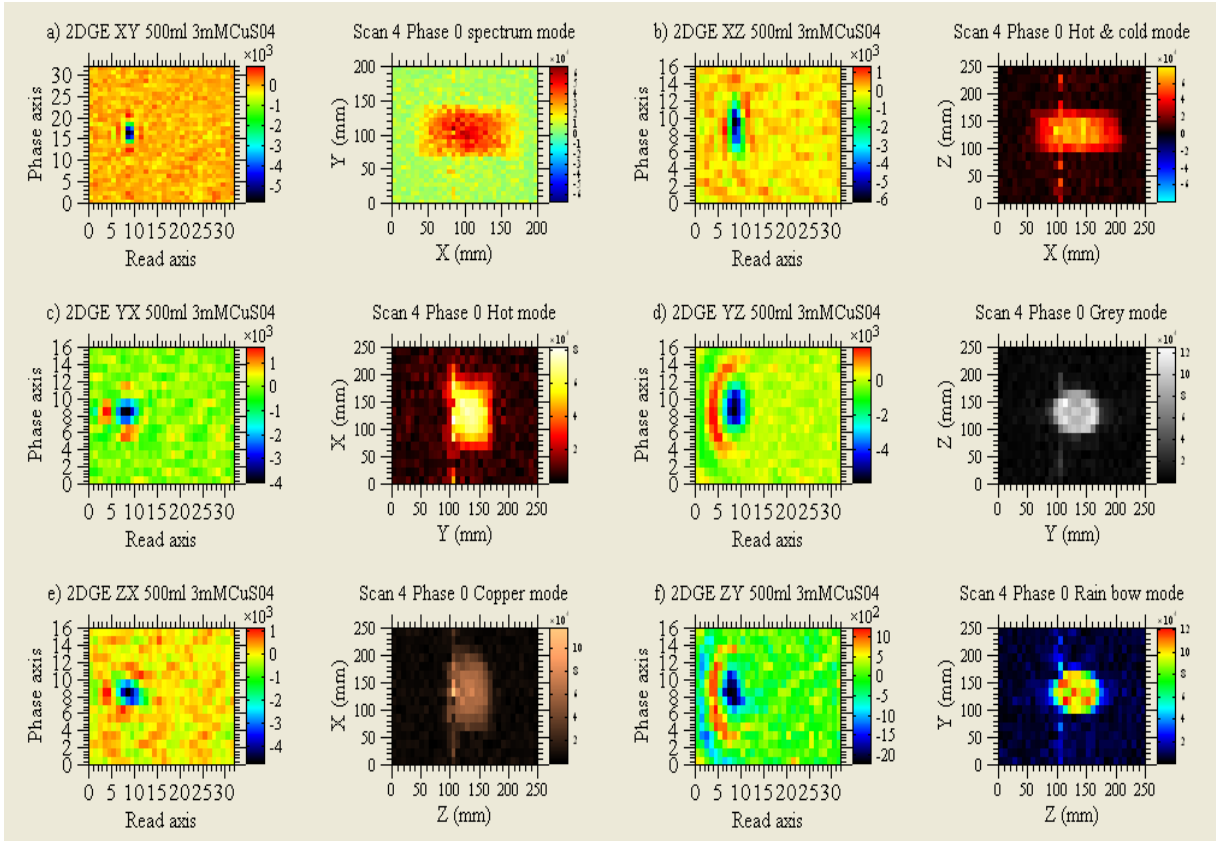

Figure B.18 Six 2D orientations of 500 ml doped water (various color modes)

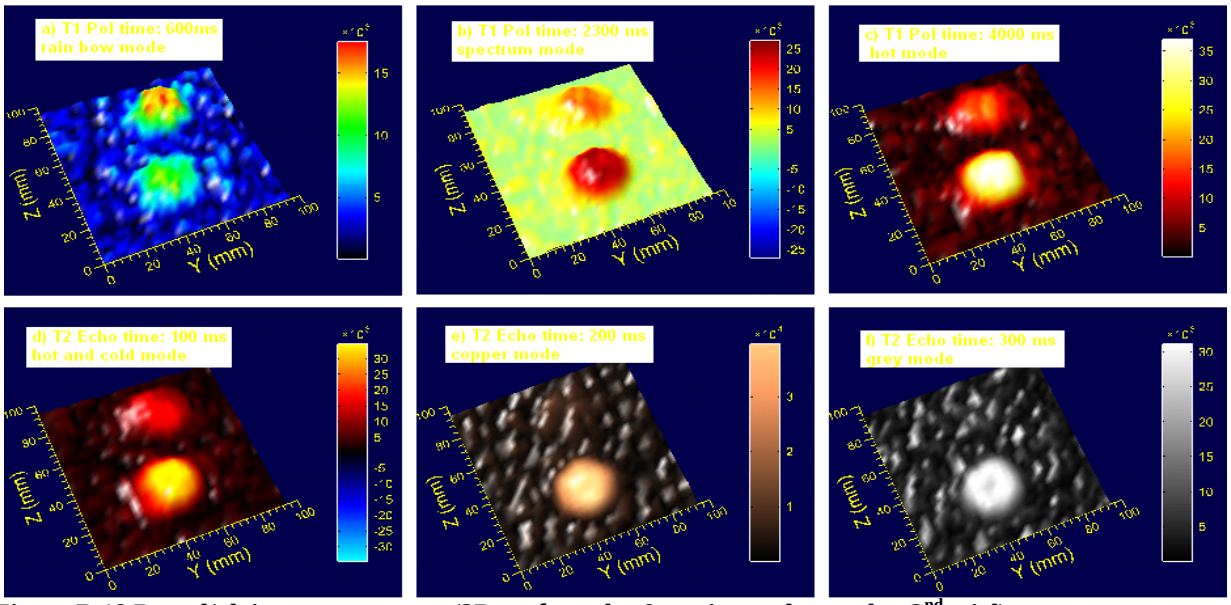

Figure B.19 Doped/plain water contrast (2D surface plot & various color modes, 2nd trial)

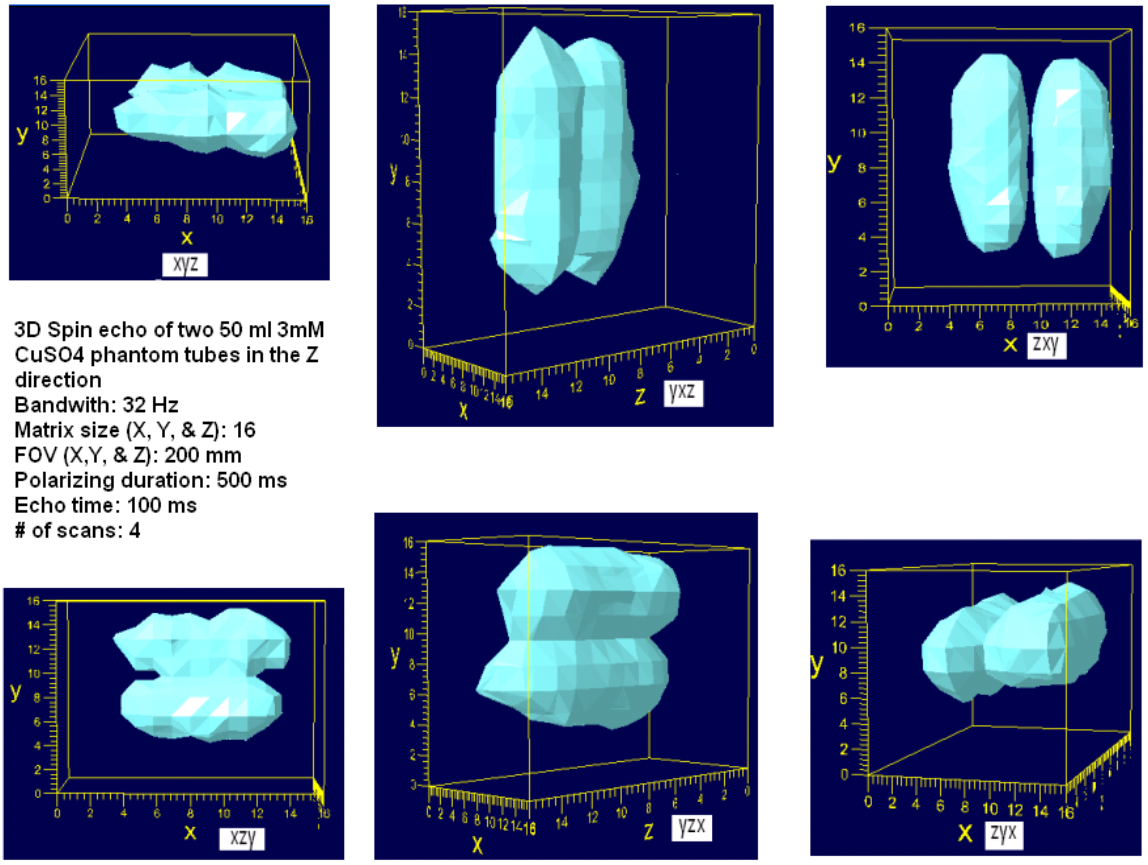

Figure B.20 Six 3D SE orientations of two phantom tubes

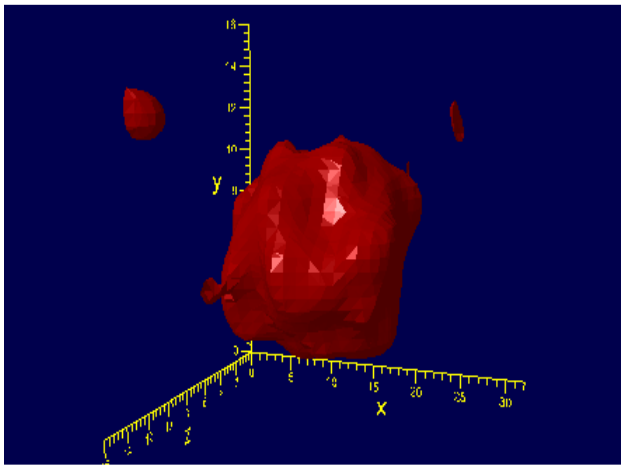

Figure B.21 3D image of a plump

Plump	3D SE/XYZ
PC	28
T_1B_p	840 ms
T_2	830 ms
Matrix size	32 (16)
Field of view	100 mm
Pol time	1,000 ms
Echo time	200 ms
Bandwidth	32 Hz
# of scans	4
Filter	Yes/gaussian
Surface level	15,000

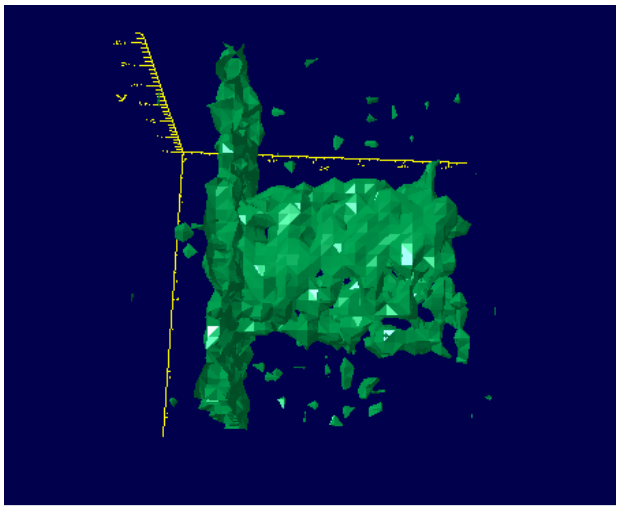

Figure B.22 3D image of a green pepper

Pepper	3D SE/XYZ
PC	35
T_1B_p	1130
T_2	820
Matrix size	32
Field of view	150 mm
Pol time	2,000 ms
Echo time	200 ms
Bandwidth	64 Hz
# of scans	4
Filter	yes/sinebellsquared
Surface level	28,000

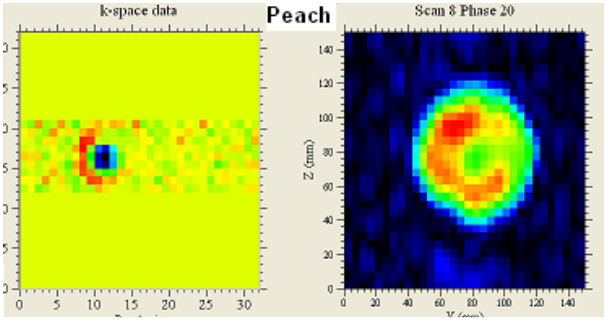

Figure B.23 2D image of a peach

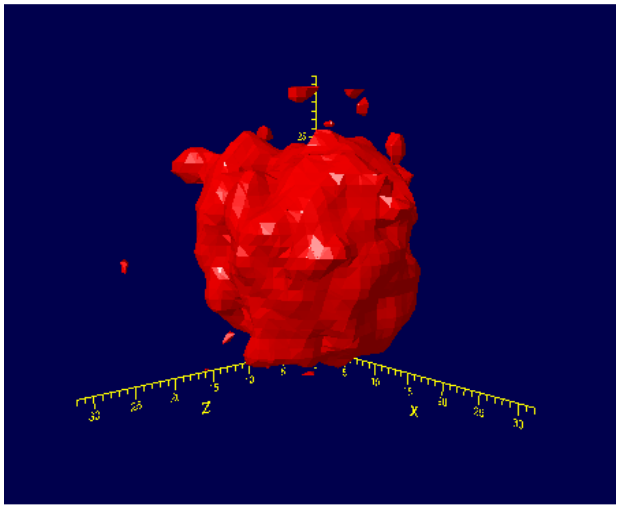

Figure B.24 3D image of the peach

Peach	3D SE/XYZ
PC	44
T_1B_p	890
T_2	660
Matrix size	32 (16)
Field of view	120 mm
Pol time	1,000 ms
Echo time	200 ms
Bandwidth	64 Hz
# of scans	4
Filter	yes/exponential
Surface level	13,000

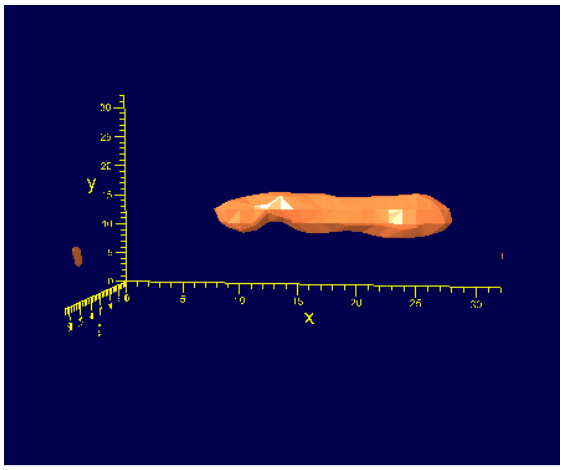

Figure B.25 3D image of a carrot

Carrot	3D SE/XYZ
PC	8
T_1B_p	380
T_2	720
Matrix size	32.16.16 (/2)
Field of view	200 mm
Pol time	1,000 ms
Echo time	200 ms
Bandwidth	64 Hz
# of scans	4
Filter	yes/sinebell
Surface level	20,000

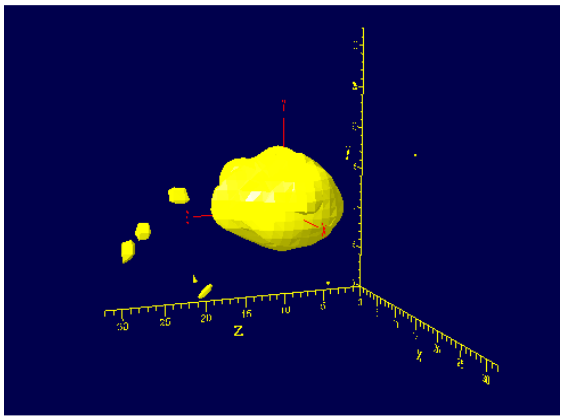

Figure B.26 3D image of a lemon

Lemon	3D SE/ZYX
PC	4.3
T_1Bp	330
T_2	470
Matrix size	32.32.32 (16,8,8)
Field of view	140 mm
Pol time	4,000 ms
Echo time	100 ms
Bandwidth	32 Hz
# of scans	2
Filter	yes
Surface level	40,000

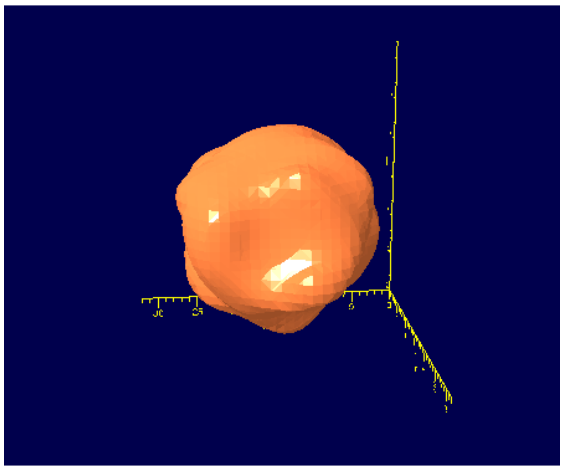

Figure B.27 3D image of an orange

Orange	3D SE/XYZ
PC	42
T_1B_p	1,130
T_2	1,000
Matrix size	32.16.16 (/2)
Field of view	200 mm
Pol time	1,000 ms
Echo time	200 ms
Bandwidth	32 Hz
# of scans	4
Filter	yes/shsinebellsquared
Surface level	15,000

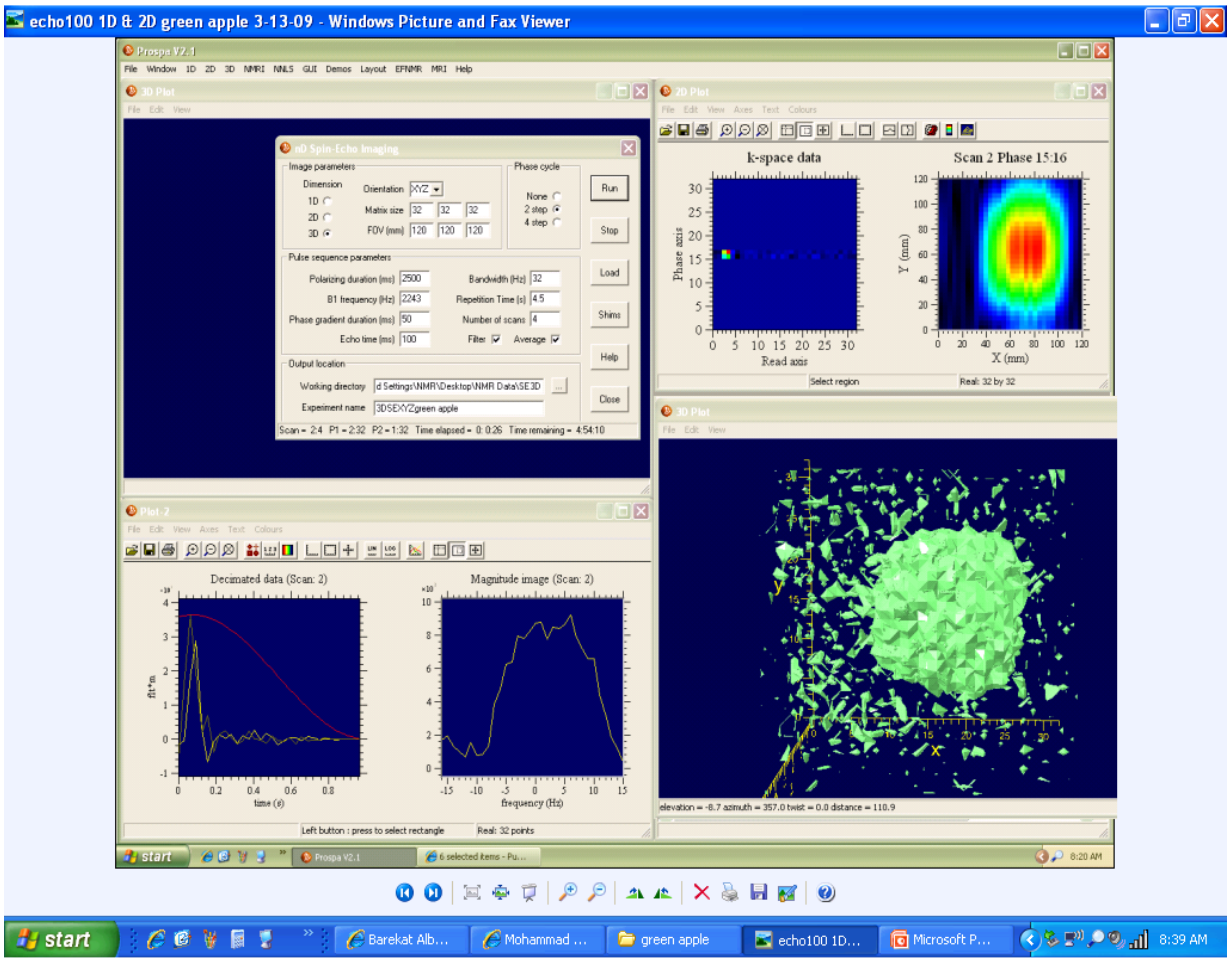

Figure B.28 1D, 2D, and 3D image of an apple

Same apple after being kept in the probe for hours turned brown.

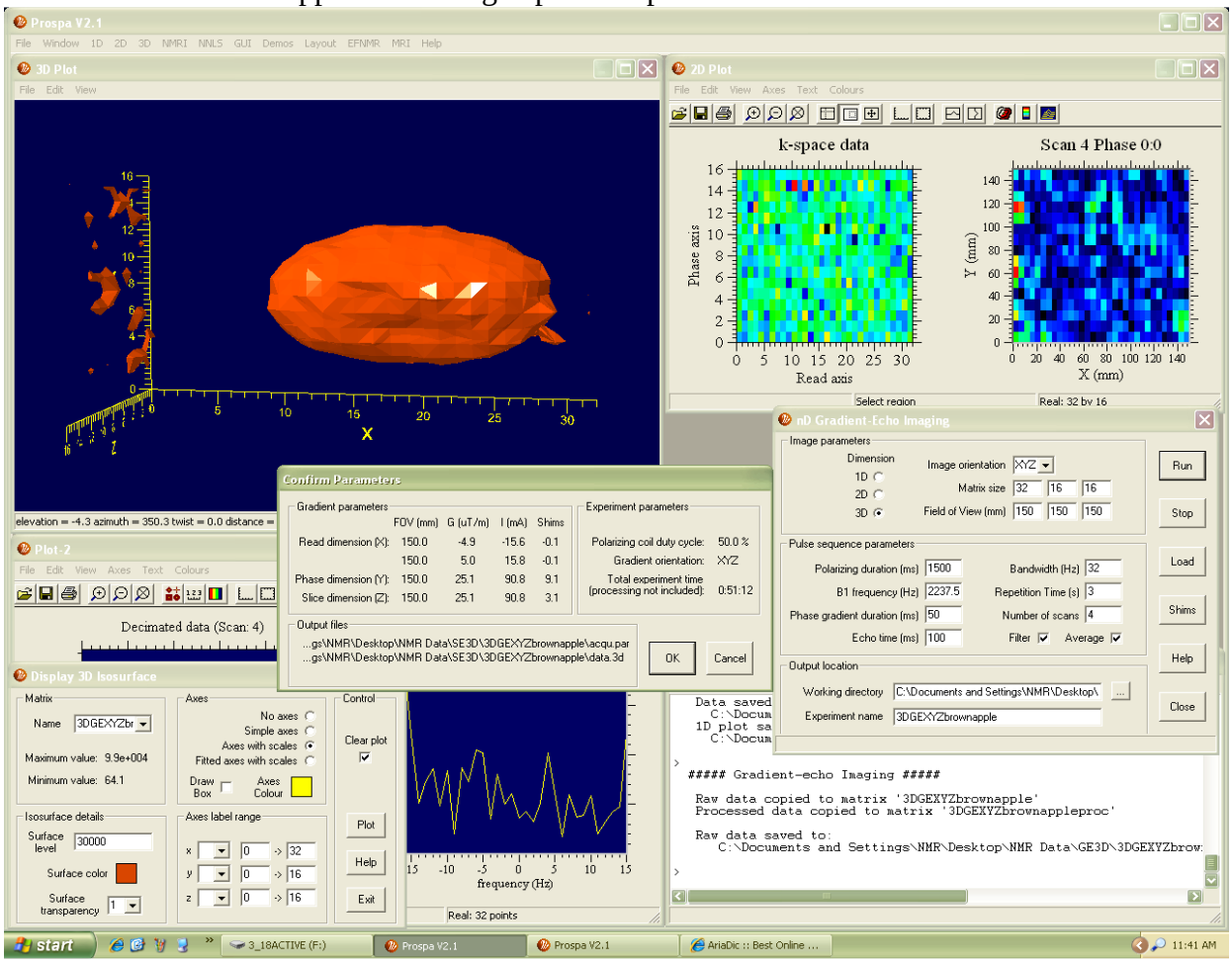

Figure B.29 3D image of a heated apple

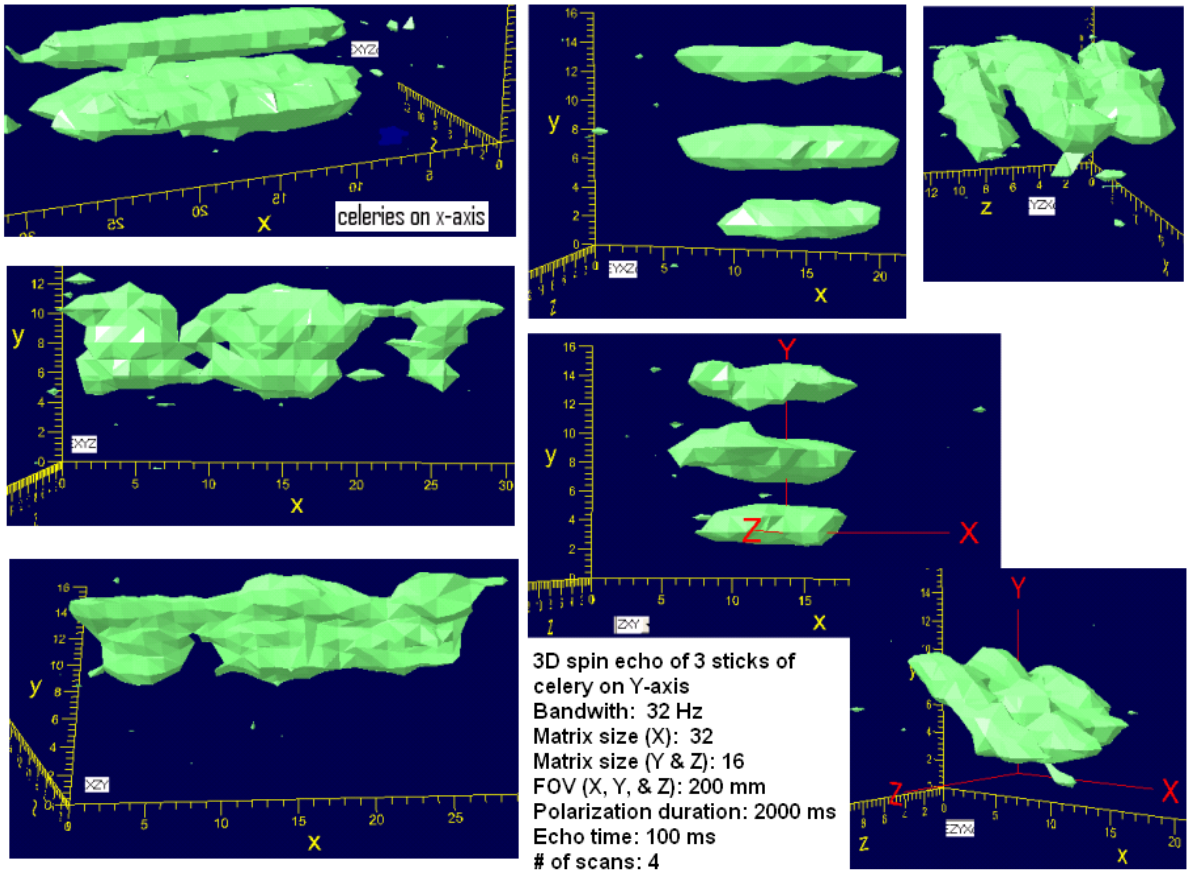

Figure B.30 Six 3D SE orientations of 3 sticks of celery

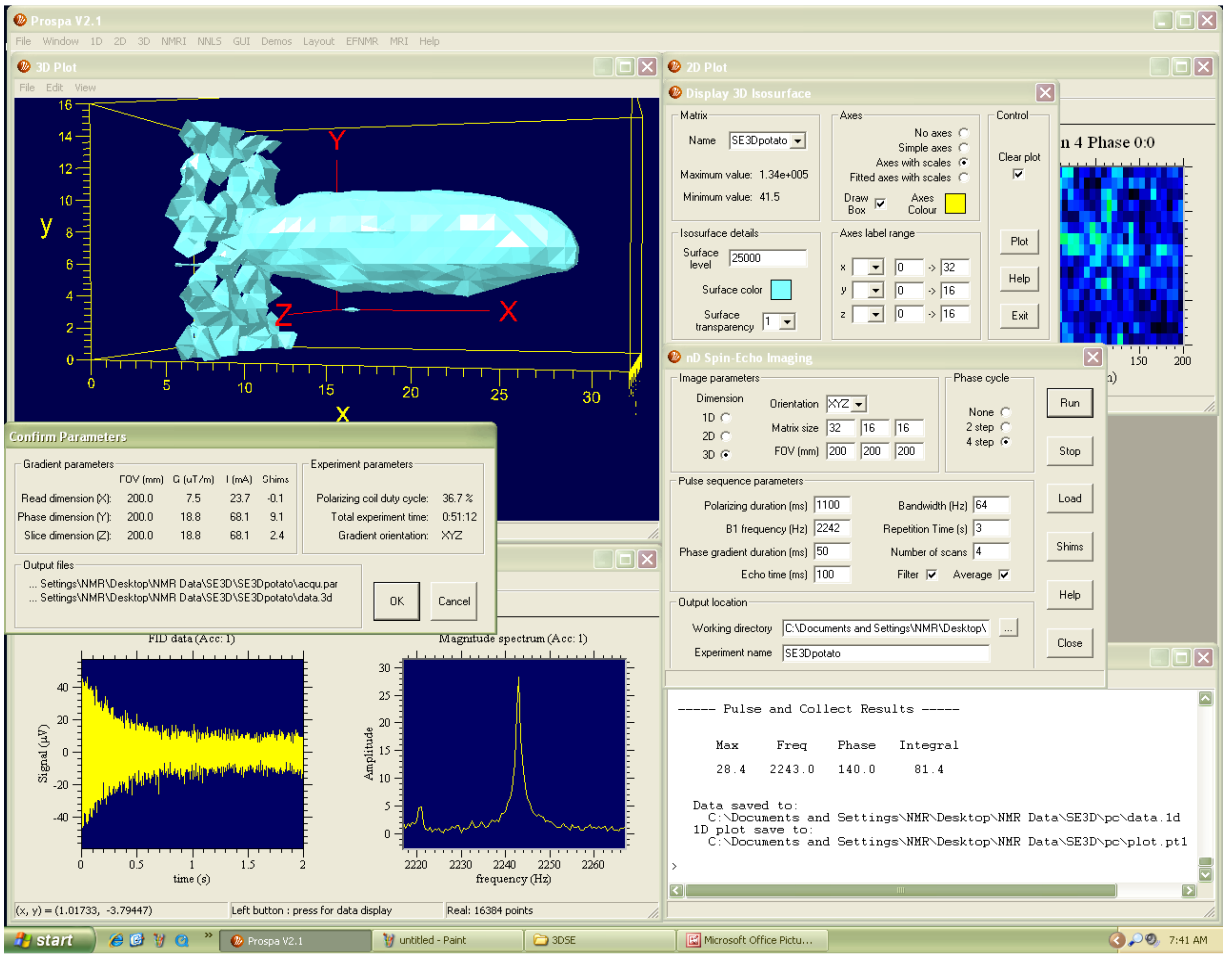

Figure B.31 3D SE of a potato along with its pulse and collect

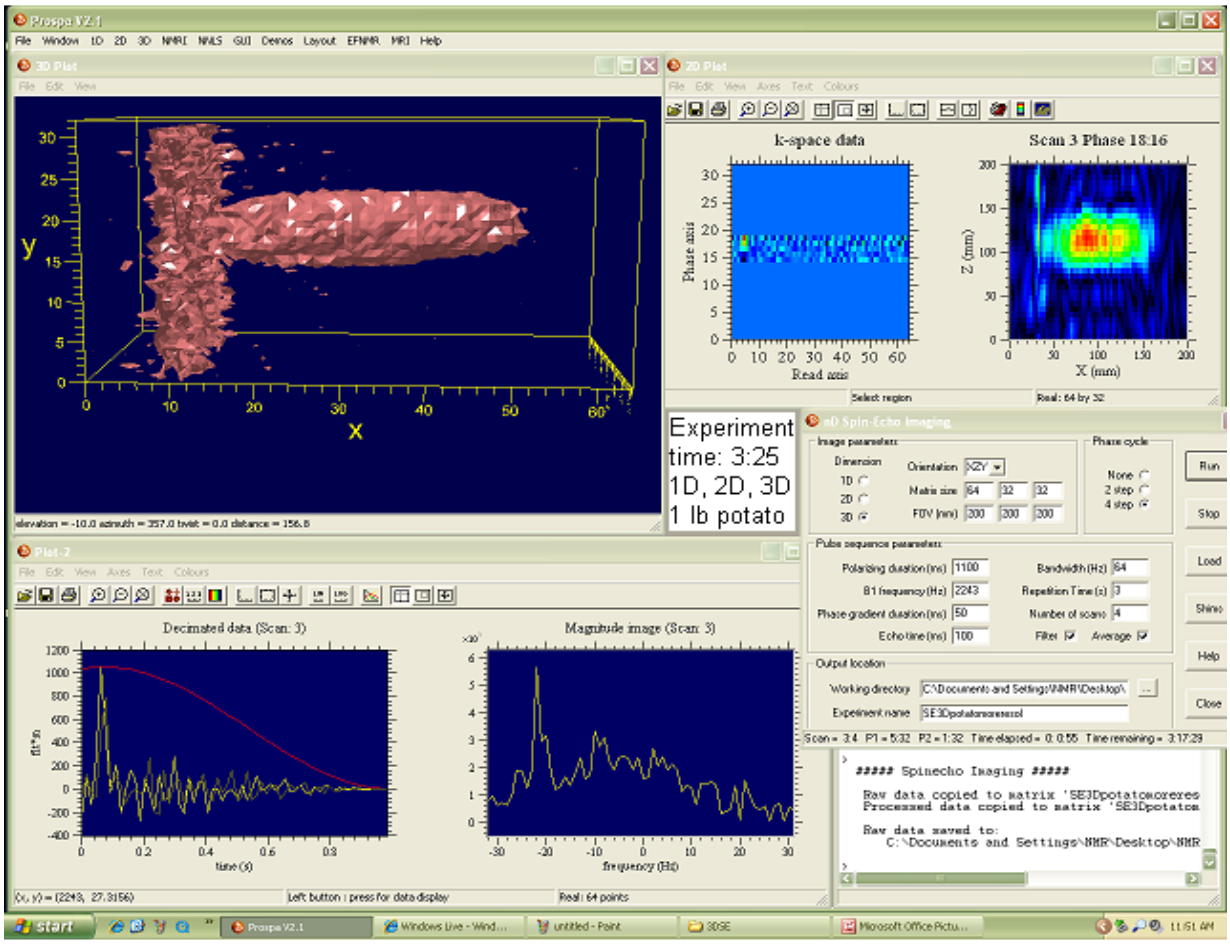

Figure B.32 1D, 2D, and 3D SE of the potato

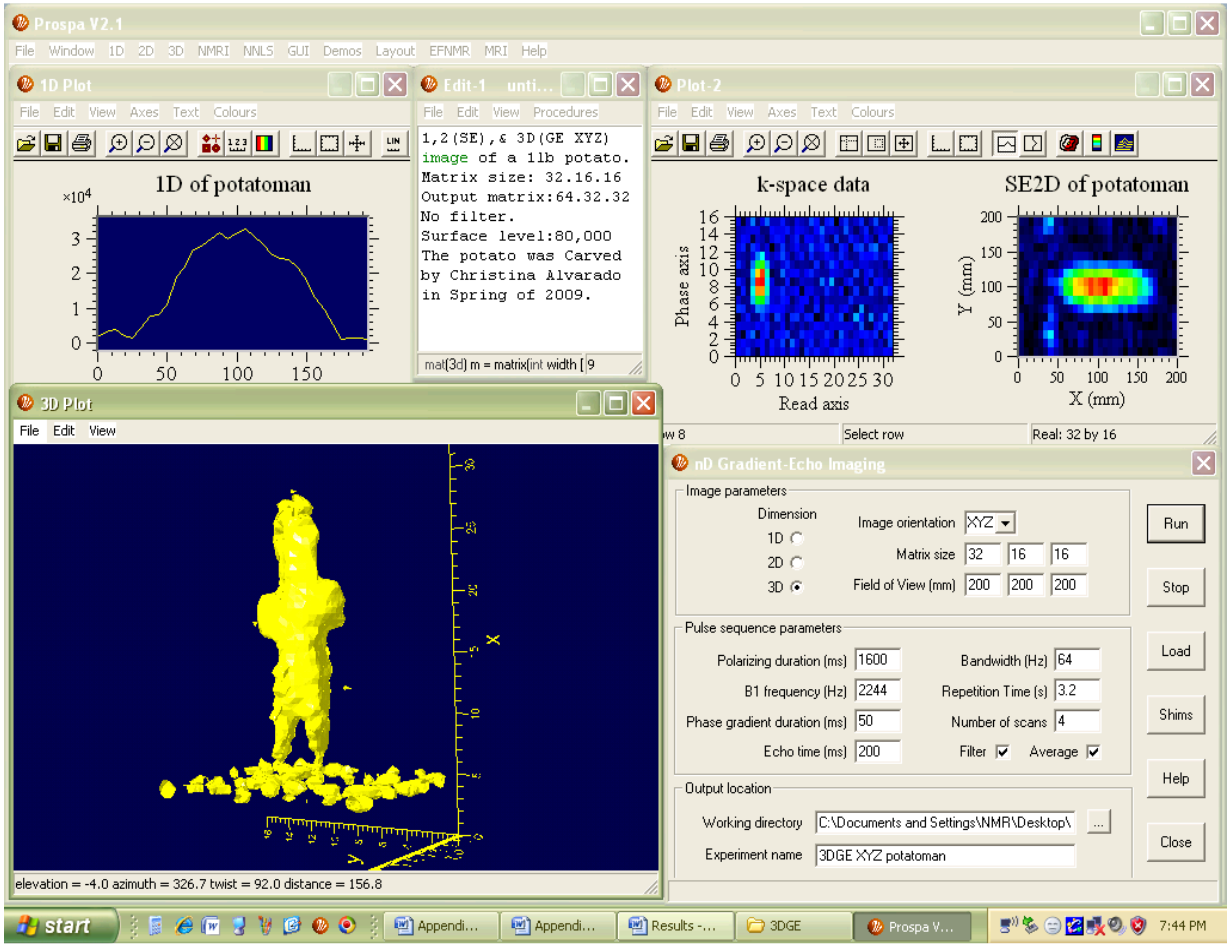

Figure B.33 1D, 2D, and 3D GE of a potatoman

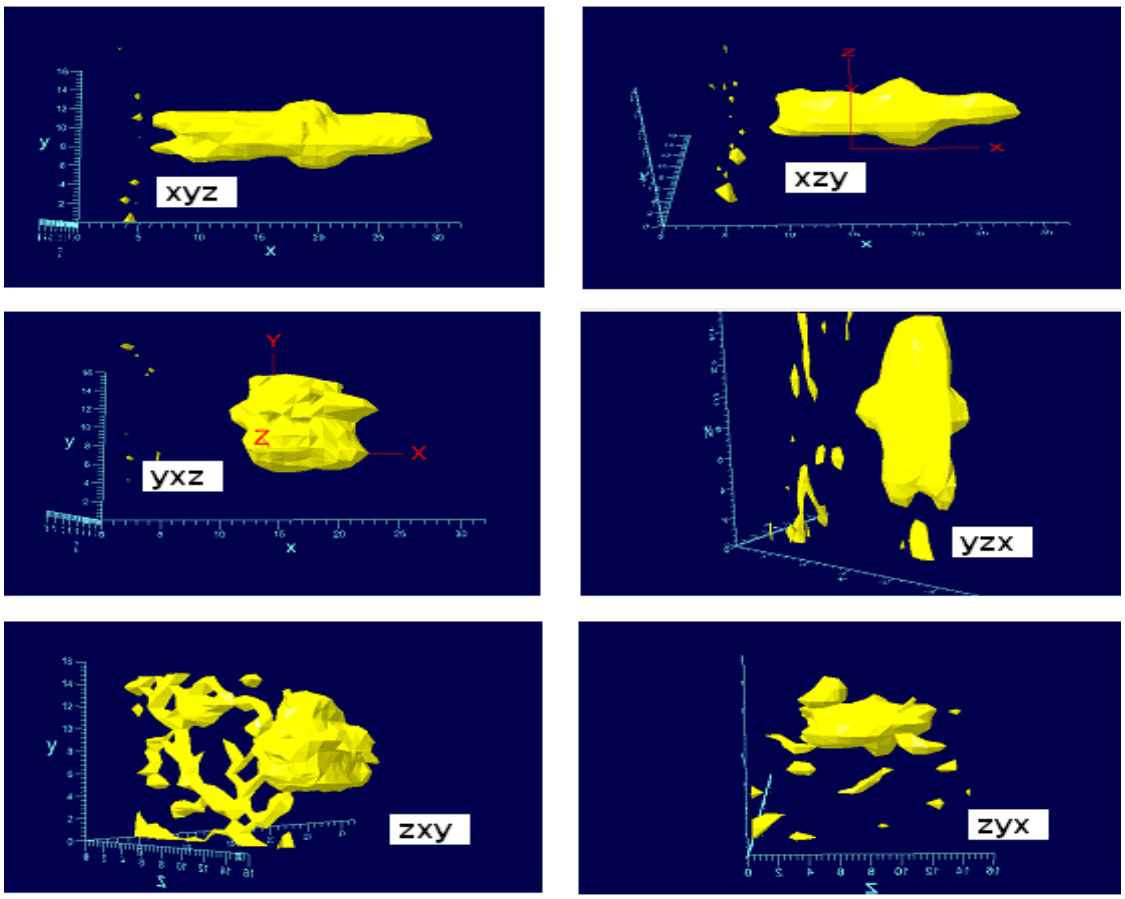

Figure B.34 Six orientations of potatoman right after imaging

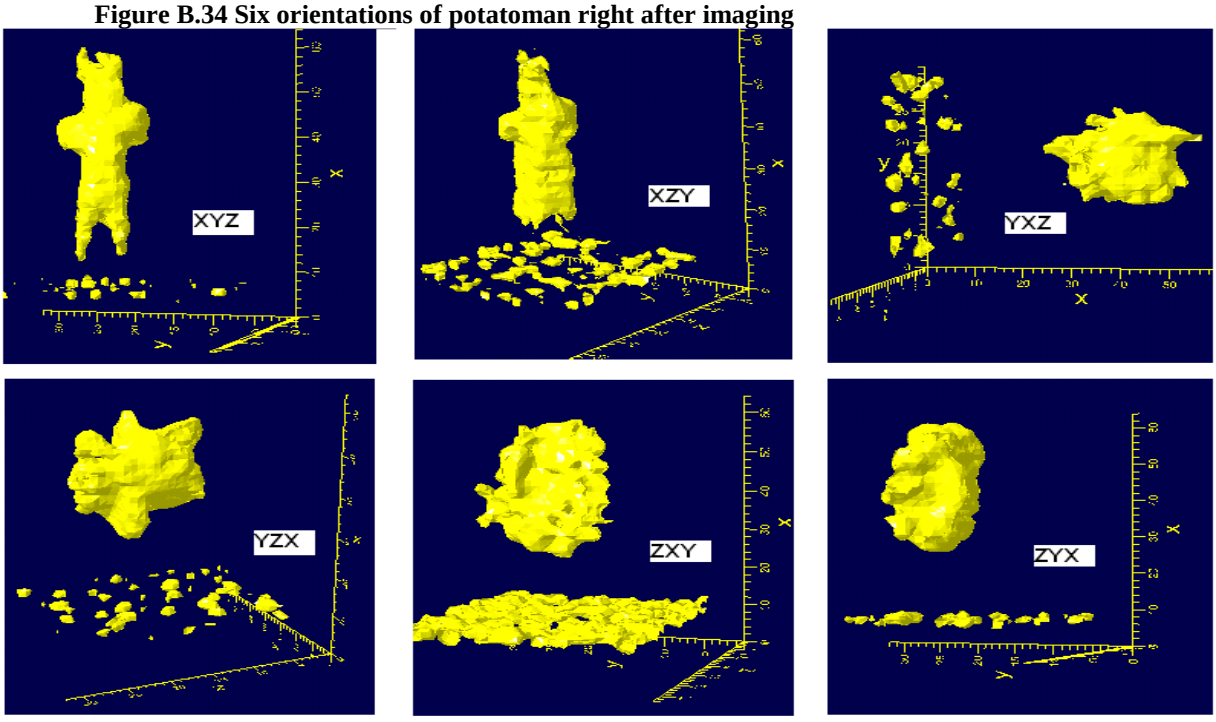

Figure B.35 Six orientations of potatoman from retrieved data

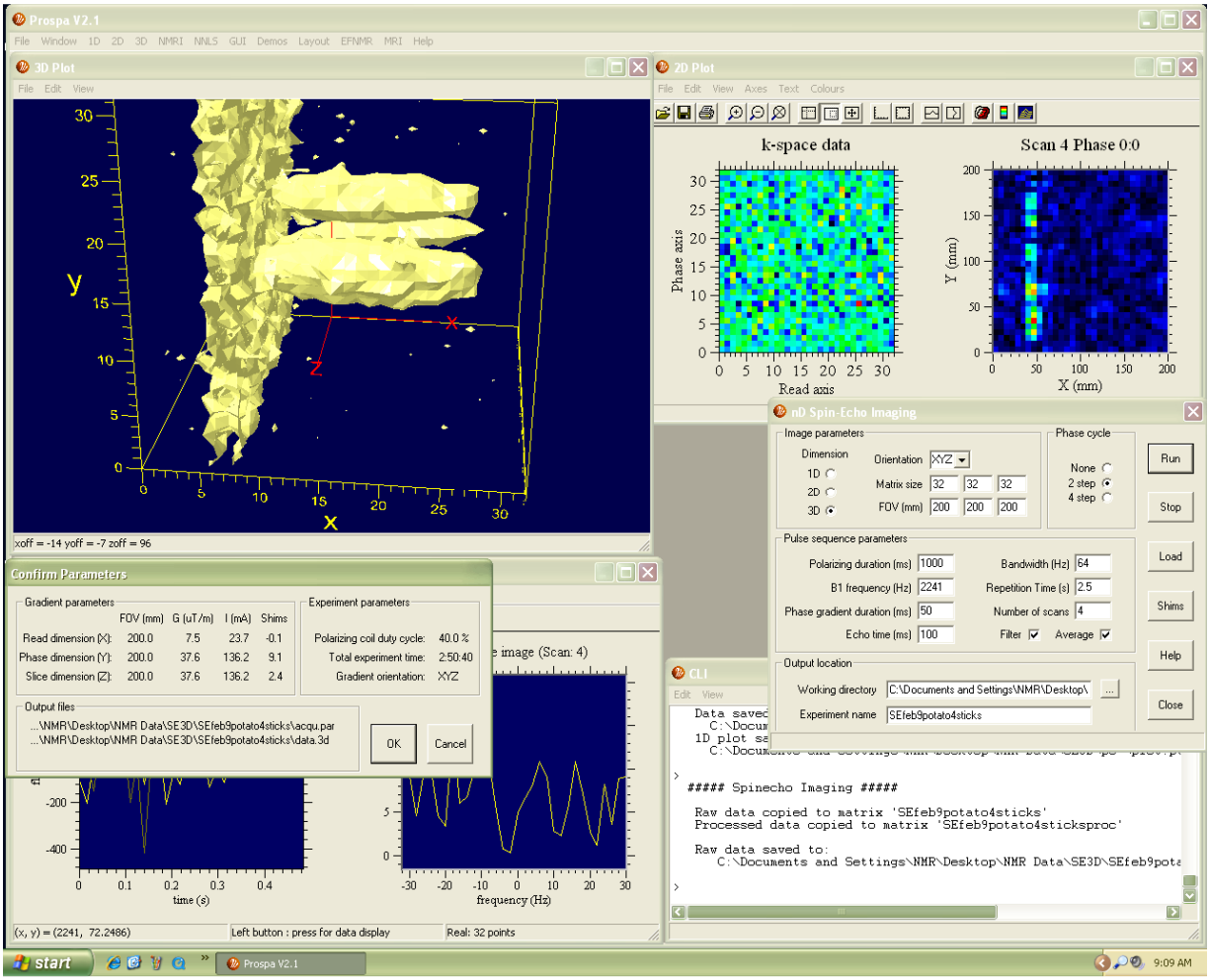

Figure B.36 3D SE of four sticks of a potato

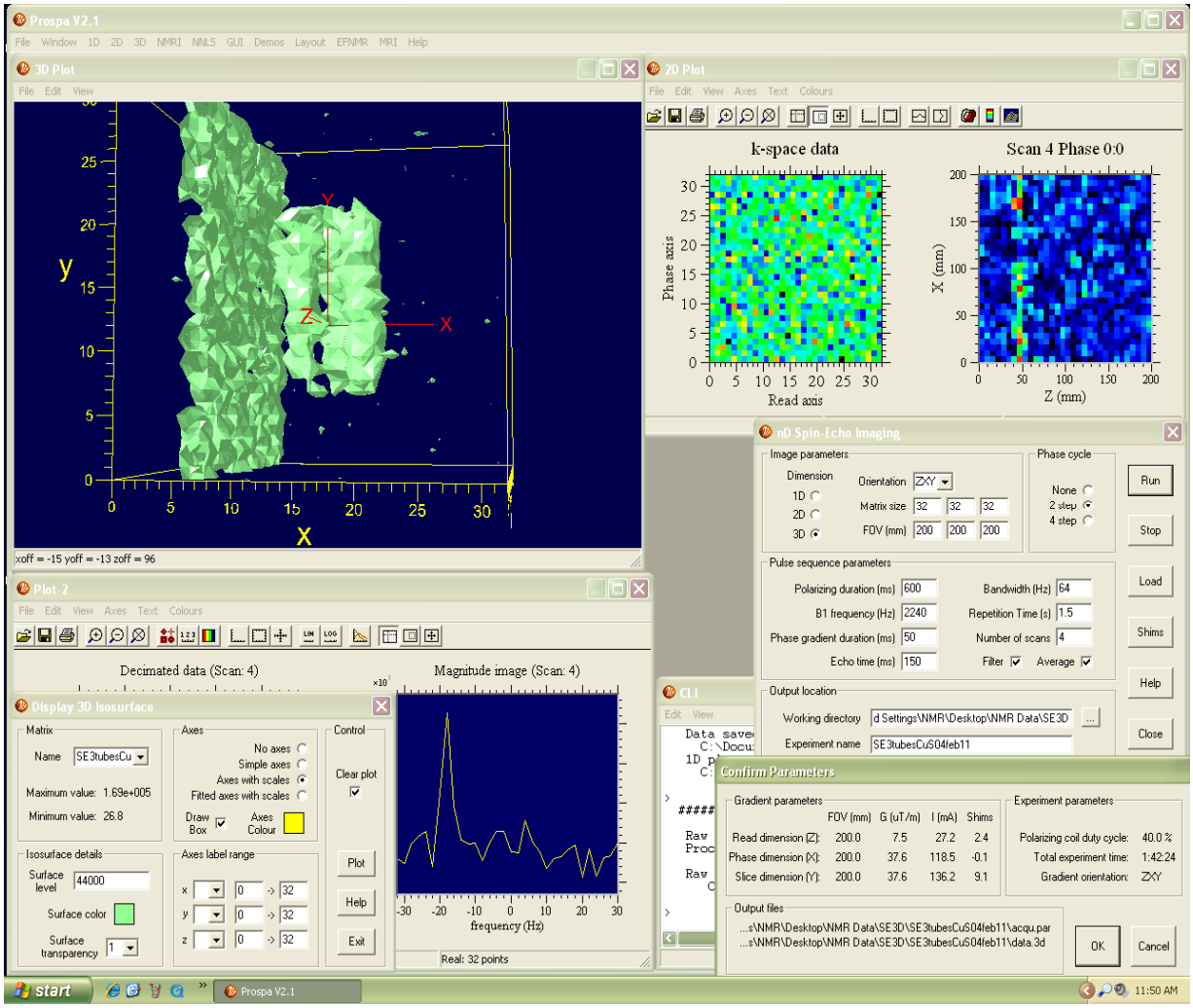

Figure B.37 3D SE of 3 phantom tubes of doped water

No filter, surface level: 40,000

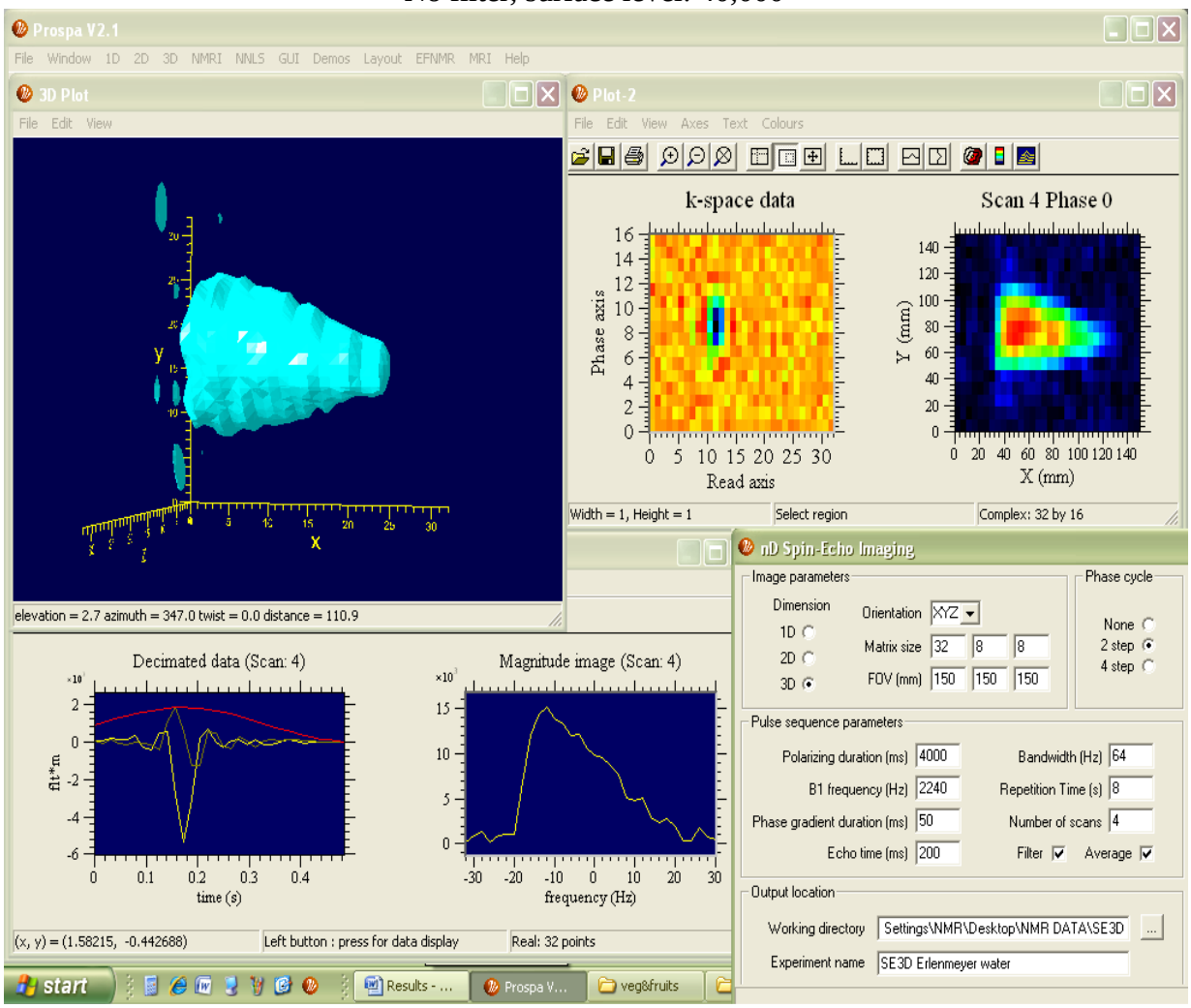

Figure B.38 1D, 2D, and 3D SE of an Erlenmeyer flask filled with water

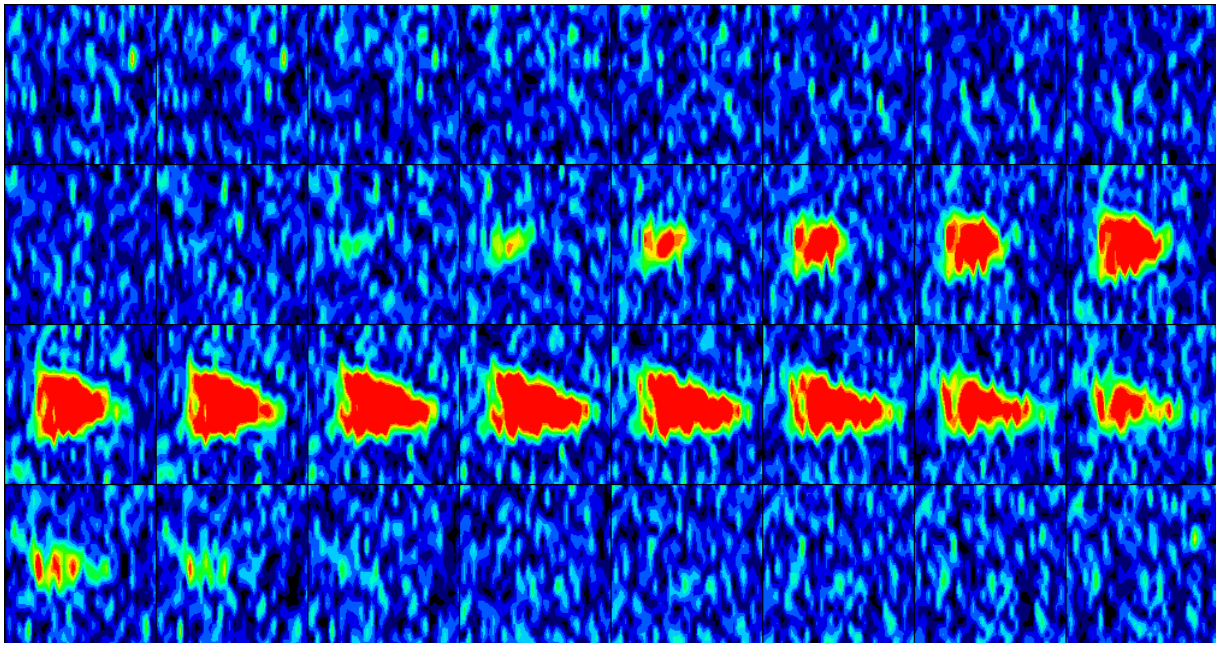

Figure B.39 2D multiplot of the Erlenmeyer filled with water in the XY direction

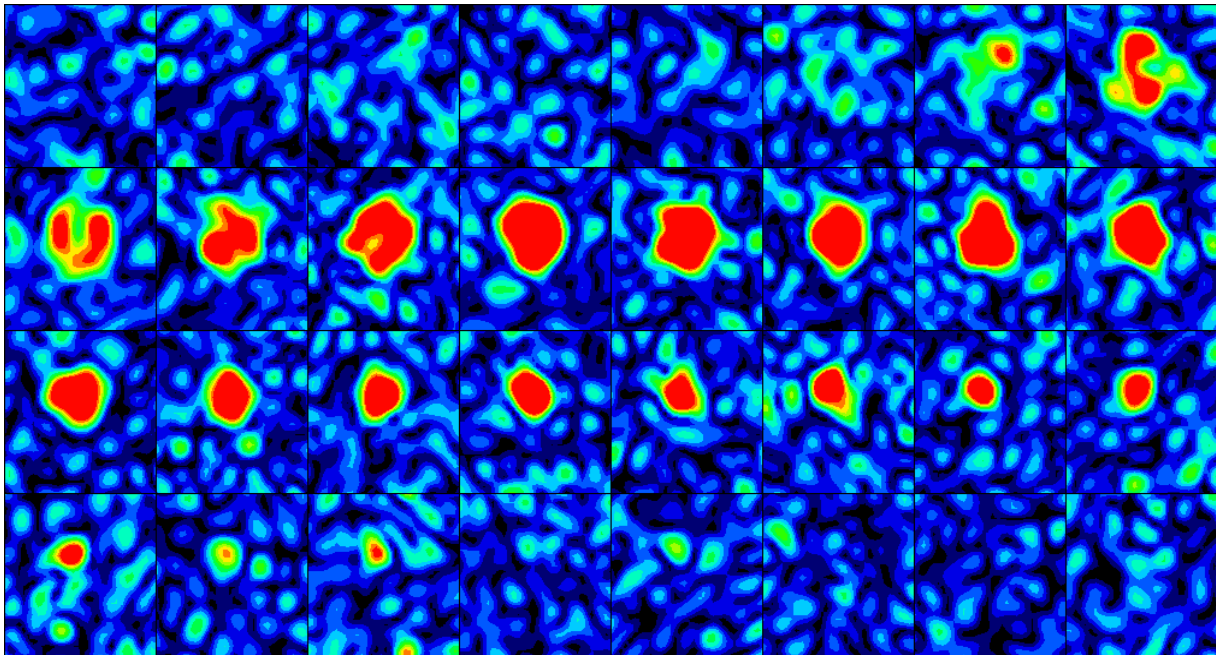

Figure B.40 2D multiplot of the Erlenmeyer filled with water in the YZ direction

No filter, surface level: 25,000

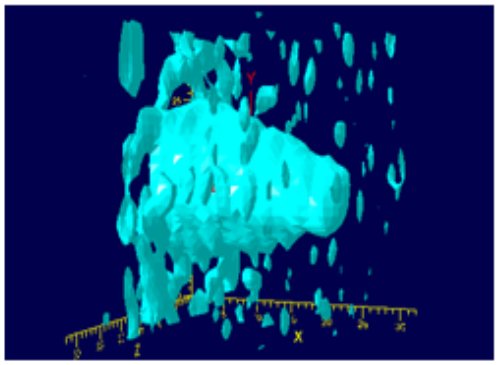

Exponential filter, surface level: 8,000

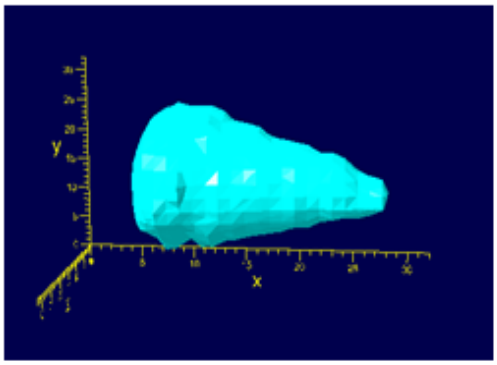

Sinebellsquared filter, surface level: 12,000

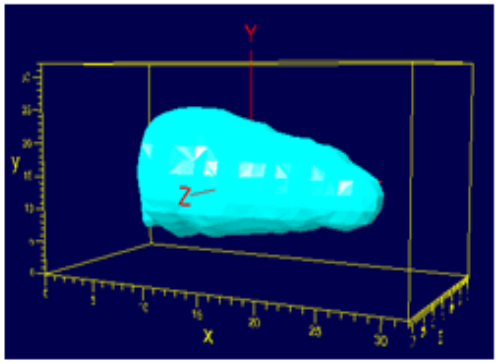

Sinebell filter, surface level: 20,000

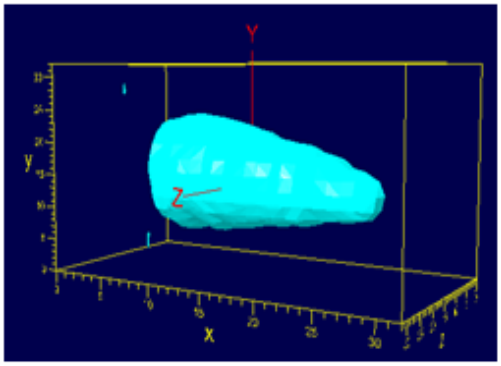

Gaussian filter, surface level: 9,000

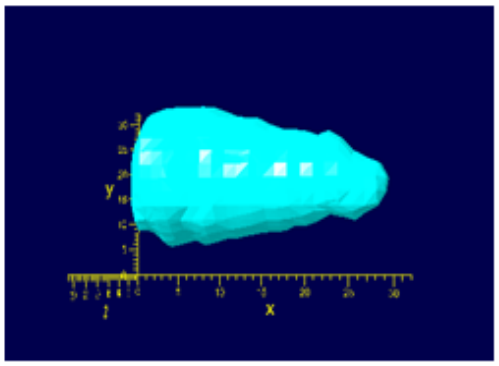

Shsinebellsquared filter, surface level: 14,000

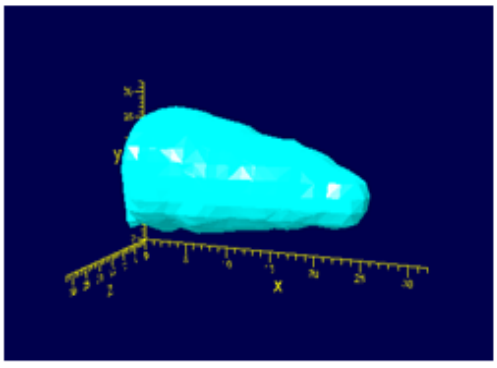

Figure B.41 Same Erlenmeyer flask with different filters

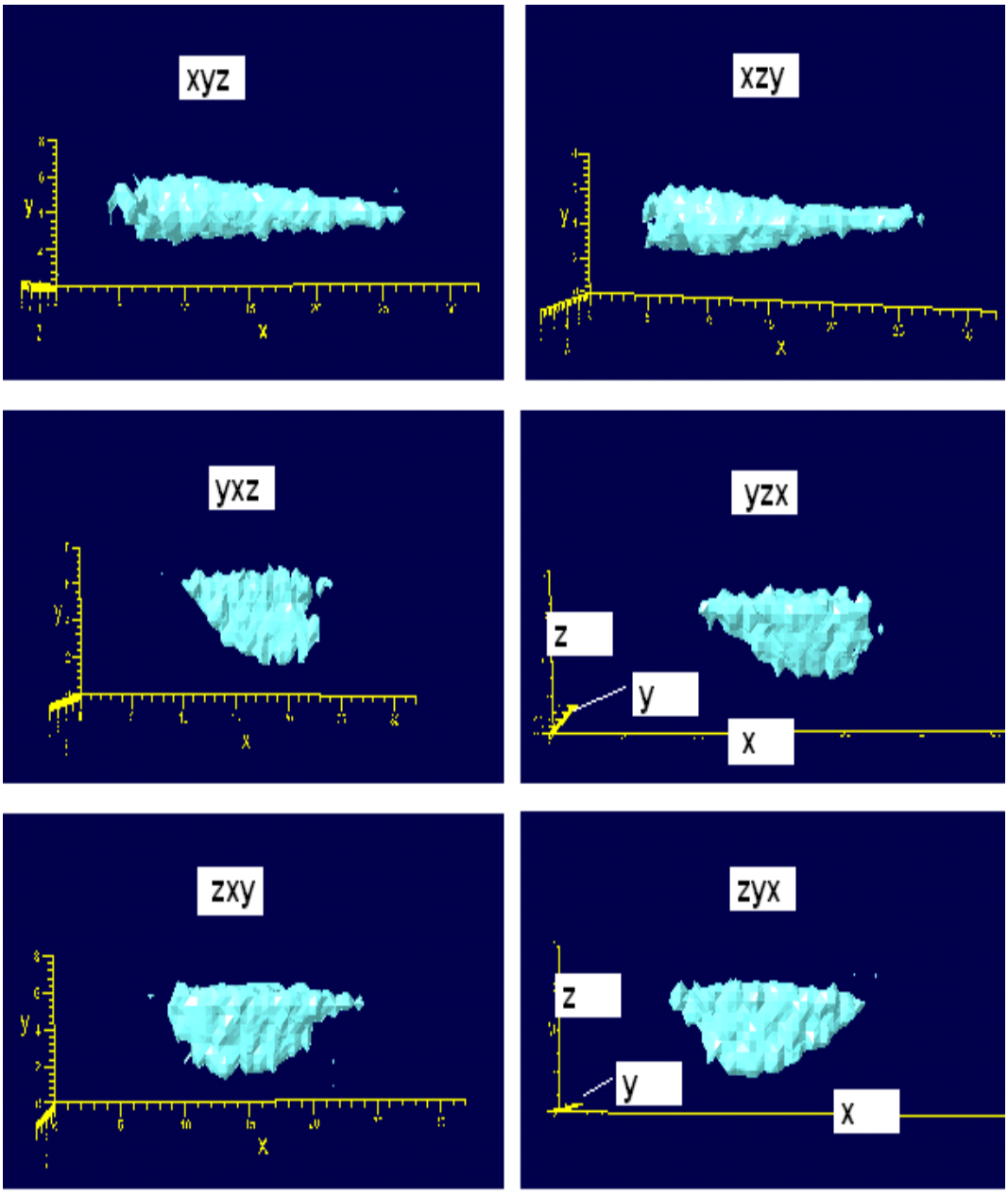

Figure B.42 Six orientations of Erlenmeyer flask from retrieved data

APPENDIX C

Pulse and collect plus relaxation time constants of some samples:

Sample	PC (μV/Hz)	T1 B_e (ms)	T1 B_p (ms)	T2 (ms)
500 ml water 4000 ms	100-150	≈ 2000	≈ 2000	≈ 2000
500 ml water 500 ms	28			
500 ml aq 0.25 mM CuSO4 4000&500 ms	150&50	1320 ± 30	1360 ± 30	1270 ± 30
500 ml aq 0.5 mM CuSO4 4000&500 ms	98&45	840 ± 40	860 ± 30	870 ± 30
500 ml aq 1 mM CuSO4 4000&500 ms	70&50	530 ± 20	560 ± 10	590 ± 30
500 ml aq 2 mM CuSO4 4000&500 ms	40&36	290 ± 20	320 ± 30	370 ± 20
500 ml aq 3 mM CuSO4 pol time 4000&500 ms	28&26	185 ± 7	185 ± 7	192 ± 9
500 ml aq 3mM CuS04 pol time 1000-ms	27-28	178 ± 4	178 ± 4	170 ± 10
500 ml aq 4 mM Cu pol time 4000&500 ms	17.5&17.5	124 ± 5	124 ± 5	120 ± 20
2 tubes of water	37			
2 tubes of aq 3 mM CuSO4 4000 ms&600 ms	7.5&7.7			
2 tubes of aq 3 mM Cu & water 4000 ms	23			
2 tubes of aq 3 mM Cu & water 4000&600 ms	14.4&8			
500 ml oil	9	190 ± 20	84 ± 7	not possible
2 tubes of aq 3mM Cu & mesquite	5.6			
2 tubes of aq 3 mM Cu & parsley	5			
2 tubes of aq 3 mM Cu & soybean	7			
Celery tubes 4 mM Cu & control after 3days	5			
Soybean tubes 0.25 mM Cu & control (stems)	7			
Soybean tubes 0.5 mM&control (leaves&roots)	4			
	3.6			
mesquite tubes 0.25 mM Cu & control	4.5			
Cilantro tubes 4mM Cu & control 20hrs	5			
green apple	42		1200 ± 30	1120 ± 20
green apple after autoshim	49			
brown apple	25		690 ± 30	460 ± 20
peach	44		890 ± 30	660 ± 40
plump	28		840 ± 40	830 ± 60
orange	42		1000 ± 100	1130 ± 60
peeled orange	25		1010 ± 70	1000 ± 60
lemon	4.3		330 ± 20	470 ± 60
carrot	6.6		380 ± 30	720 ± 100
pepper	39		1130 ± 40	820 ± 60
potato	20-30		360 ± 50	490 ± 10
little person	21.5		780 ± 40	700 ± 20
500 ml packed parsley	barely 1		430 ± 40	640 ± 60
500 ml packed celery	13		680 ± 60	900 ± 100

BIBLIOGRAPHY

1. Barik, K. C., and A. S. Chandel. "Effect of copper fertilization on plant growth, seed yield, copper and phosphorus uptake in soybean (Glycine max) and their residual availability in Mollisol." *Indian Journal of Agronomy* 46, no. 2 (2001): 319-326.
2. Bernal, M., M. V. Ramiroa, R. Casesb, R. Picorela, and I. Yruela. "Excess copper effect on growth, chloroplast ultrastructure, oxygen-evolution activity and chlorophyll fluorescence in Glycine max cell suspensions." *Physiologia Plantarum* 127 (2006): 312-325.
3. Bernal, M., R. Cases, R. Picorel, and I. Yruela. "Foliar and root Cu supply affect differently Fe- and Zn-uptake and photosynthetic activity in soybean plants." *Environmental and Experimental Botany* (Elsevier) 60 (2007): 145-150.
4. Blumich, B. *NMR Imaging of Materials.* New York: Oxford University Press, 2000.
5. Bushberg, J. T., j. A. Seibert, E. M. Leidholdt, and J. M. Boone. *The Essential physics of Medical Imaging.* 2nd. California: Lippincott Williams & Wilkins, 2002.
6. Callaghan, P. T., C. D. Eccles, and J. D. Seymoura. "An EFNMR apparatus suitable for pulsed gradient spin echo measurements of self-diffusion under Antarctic Codnition." 1997.
7. Coy, A., Halse, M. E., R. Dykstra, C. Eccles, M. Hunter, R. Ward, and P. T. Callaghan. "A practical and flexible implementation of 3D MRI in the Earth's magnetic field." *Journal of Magnetic Resonance (JMR)* (Elsevier Inc.) 182 (2006).
8. Database MRI. *k-space.* 2003-2009. http://www.mr-tip.com/serv1.php?type=db1&dbs=K-Space.
9. Database MRI. *T1.* 2003-2009. http://www.mr-tip.com/serv1.php?type=db1&dbs=T1.

10. Database MRI. *T2.* 2003-2009. http://www.mr-tip.com/serv1.php?type=db1&dbs=T2.
11. De La Rosa, G., J. R. Peralta-Videa, and Gardea-Torresday J. L. "Production of Low-molecular weight thiols as a response to cadmium uptake by tumbleweed." *Plant Physiology and Biochemistry* (Elsevier) 43 (2005): 491-498.
12. El-Mashad, A. "Differential responses of two cultivars of soybean to different levels of Cu stress." 32, no. 2 (2003): 125-143.
13. Fernandes, J. C., and F. S. Henriques. "Biochemical, Physiological, and Structural Effects of Excess Copper in Plants." *The Botanical Review* 57, no. 3 (1991).
14. Fukushima, E., and S. B. W. Roeder. *Experimental Pulse NMR A Nuts and Bolts Approach.* 1st ed. London-Tokyo: Addison-Wesley Publishing Company, Inc., 1981.
15. Gardea, J. L., J. R. Peralta-Videab, G. De la Rosaa, and J. G. Parsonsb. "Phytoremediation of heavy metals and study of the metal coordination by X-ray absorbtion spectroscopy." *Coordination Chemistry Reviews* 249 (2005): 1797–1810.
16. Gardea-Torresdey, J. L., E. Rodriguez, J. G. Parsons, J. R. Peralta-Videa, G. Meitzner, and G. Cruz-Jimenez. "Use of ICP and XAS to determine the enhancement of gold phytoextraction by Chilopsis linearis using thiocyanate as a complexing agent." *Anal Bioanal Chem* 382 (2005): 347–352.
17. Halse, M. E., and P. T. Callaghan. "A dynamic nuclear polarization strategy for multi-dimensional Earth’s field NMR spectroscopy." *Journal of Magnetic Resonance* (Elsevier) 195 (2008): 162-167.
18. Haque, N. "Dissertation." *Screening The Phytoremediation Potentail of Native Plants Growing on Mine Tailings in Arizona, USA.* Dec. 2008.
19. Health, U.S. Depr. of. "Health Consultation." Colorado, 2003.

20. Jakubovics, J. P. *Magnetism and magnetic materials.* 2nd ed. London: The University Press, Cambridge, 1994.

21. Jurgonski, L. J., and D. J. Bugbee, B. Nielsen, S.S. Smart. "Controlled Environments Alter Nutrient Content of Soybeans." 20, no. 10 (1997): 1979-1988.

22. Keeler, J. *Understanding NMR Spectroscopy.* Wiley, 2005.

23. Kuperman, V. *Magnetic Resonance Imaging.* Academic Press, 2000.

24. Levitt, M. H. *Spin Dynamics.* 2nd. Wiley, 2008.

25. Magritek. *Prospa Software Manual.* version 2.1. 2004-2006.

26. Magritek. *Terranova-MRI Student Guide.* 2006.

27. Magritek. *Terranova-MRI User Manual.* 2005.

28. Melton, B. F., and V. L. Poliak. "Instrumentation for the Earth's Field NMR Technique." *The review of scientific instruments* 42, no. 6 (1971): 769-773.

29. Mohoric, A., G. Planinsic, M. Kos, A. Duh, and J. Stepisnik. "Magnetic Resonance Imaging System Based on Earth's Magnetic Field." *Instrumentation Science & Technology* (Taylor & Francis), 2004: 655- 667.

30. Peralta-Videab, J. R., E. Gomez, K. J. Tiemannb, M. Duarte-Gardeac, and J. L. Gardea-Torresdey. "Alfalfa growth promotion by bacteria grown under iron limiting conditions." *Advances in Environmental Research* (Elsevier) 6 (2002): 391-399.

31. Planinsic, G., J. Stepisink, and M. Kos. "Relaxation-Time Measurement and Imaging in the Earth's Magnetic Field." *Journal of Magnetic Resonance* (Academic Press, Inc.), 1994: 170-174.

32. Qui, L., Z. Yi, M. Burghoff, and L. Trahms. "NMR in the earth's magnetic field using a nitrogen-cooled superconducting quantum interference device." *Applied Physics Letters* 91 (2007): 1-3.

33. Research, Machines. "The Free Dictionary by Farlex." Helicon Publishing. 2009. http://encyclopedia.farlex.com/soybean+plant.

34. Robinson, J. N., A. Coy, Dykstra R., Eccles, and C. D. "Two-dimensional NMR spectroscopy in Earth's magnetic field." *Journal of Magnetic Resonance* (Elsevier) 182 (2006): 343-347.

35. Senthilkumar, P., W.SPM. Prince, S. Sivakumar, and C.V. Subbhuraam. "Prosopis juliflora—A green solution to decontaminate heavy metal (Cu and Cd) contaminated soils." *Chemosphere* (Elsevier) 60 (2005): 1493-1496.

36. Sias, S. "Thesis." *Survey of Northern Chihuahuan Desert Plants for Phytoremediation potential.* 1998.

37. Thiele, C. M. "Magnetic Resonance at or below the Earth's Magnetic Field." *Angew. Chem. Int.* (Wiley-VCH Verlag GmbH & Co. KGaA, Weinheim) 46 (2007): 4820 – 4824.

38. Victor, R., A. Pillay, and S. Al-Minj. "Copper Tolerance to Germination in Mesquite, a Potential Tree Species for Restoring Mined-lands in Oman." *Journal of Agricultural, Food, Environmental Sciences* 1, no. 1 (2007).

39. Vlaardingerbroek, M. T., and Boer J. A. *Magnetic Resonance Imaging, Theory and practice.* 3rd ed. New York: Springer, 2003.

40. Weishaupt, D., V. D. Kochli, and Marincek. *How Does MRI Work?* 2nd. Springer, 2006.

41. Xu, S., C. W. Crawford, S. Rochester, V. Yashchuk, and D., Pines, A. Budker. "Submillimeter-resolution MRI at the EMF with an atomic magnetometer." *PHYSICAL REVIEW* 78 (2008).

42. Zhi-Pei, L., and Paul C. L. *Principles of Magnetic Resonance Imaging.* New York: IEEE Press, 2000.

VITAE

Saideh Sadat Mortazavi, the daughter of Dr. Seyed Hosein Mortazavi and Naheed Rahmani, was born in Tehran, Iran January 20th, 1965. After graduating from High School in 1983, she started her B.S. at California Poly Technique State University in San Luis Obispo in January of 1985. While pursuing her bachelor's degree in Chemistry, she worked as a teaching assistant. She completed her B.S. in Chemistry at the University of Shaheed Beheshty, in Tehran, Iran in 1993. From 1998 to 2007, she held an administrative and teaching position at Tehran International School in Tehran, Iran. She started her Master's in Chemistry at the University of Texas at El Paso in August of 2007 while working as a teaching assistant. She joined Dr. James Salvador's research group in December of 2007. At present, she is pursuing a doctoral degree in Chemistry.

This thesis has been typed by Saideh Sadat Mortazavi.